

https://dspace.org/

Synthesis and study of carbon nanotubes and carbon spheres

Mhlanga, Sabelo Dalton

2009-09-10T06:17:48Z
http://hdl.handle.net/10539/7224

Downloaded from a DSpace repository. https://dspace.org/

Chapter 1

Introduction

1.1 Background and rationale

Since the synthesis of carbon nanotubes (CNTs) by Iijima in 1991 [1] methods to make these materials have been extensively investigated [2]. The synthesis of CNTs has sparked a worldwide escalation of interest within the scientific community focussing on the synthesis, modification or functionalization and application of these nanomaterials. The applied and potential applications of CNTs are due to their outstanding mechanical and unique electrical properties, which have been thoroughly described in the literature [3-10]. Such applications include their use as biosensors for harmful gases and chemical analyses, biomedical applications, catalyst supports, coatings of all sorts, conducting composites/plastics, controlled drug release applications, electronic nanocomponents and material protection applications, energy storage, field emission sources, fuel cell membranes, hydrogen storage, microscope probes, nanotube reinforced composites, nano-conveyors, sporting goods and in water purification [11-26].

The synthesis of CNTs can be achieved using arc discharge [27], laser ablation [28], chemical vapour deposition (CVD) [29], and most recently in closed systems (e.g. in an autoclave or sealed quartz tube) under pressure [30]. The CVD method is generally classified into two categories namely, the floating catalyst process, a gas phase process; and the substrate CVD process, involving the use of a thermally stable material to support metal particles that are responsible for the molecular decomposition of carbon to form the CNTs [29h, 31a]. While all the CNT production processes have their disadvantages in terms of purity and cost, the CVD process is generally the most widely used because it is a low cost process that is industrially scaleable, versatile, and it allows for the controlled growth of high purity CNTs under optimized reaction conditions (**Table 1.1**) [31b].

Table 1.1: A comparison of CNT synthesis methods

Method	Space time yield	Amorphous carbon	Carbon purity
Arc discharge	Low	High	High
Laser ablation	Low	High	High
Floating catalyst or gas phase	Medium	Low	Medium
CVD and CCVD	High	Low	Medium – High*

* High carbon purity can be attained after purification [31b].

The most widely used metals for the fabrication of CNTs are iron (Fe), cobalt (Co) and nickel (Ni) as well as the alloys of these nanoparticles. The metals are usually supported on materials that are stable at high temperatures. The support used in the substrate CVD process plays an important role in influencing the activity of the catalyst. Several factors need to be taken into consideration when choosing a support. These include

(i) the decomposition temperature of the support and hence its useful reaction range,

(ii) the surface area of the support and

(iii) the metal catalyst-support interaction that controls the size of the catalyst particle and the sintering potential of the catalyst.

High surface area materials such as SiO_2, Al_2O_3, TiO_2 and zeolites provide excellent supports for catalytic CNT production [32-42]. However, the nature of these materials does not allow for their easy removal and thus purification of CNTs produced on these supports remains a challenge and often requires several acidic/oxidation steps that result in damage to the CNT graphitic structures as well as compromised thermal stability of the CNT. This damage affects the work function of the CNTs. Environmental aspects also need to be taken into consideration when selecting the support because the solvents used

during the purification process have to be disposed off [43-70]. To circumvent these environmental problems, the use of readily removable supports has been studied both by ourselves and others [71-78].

Calcium carbonate ($CaCO_3$), albeit used in relatively few studies, has proven to be an excellent support for mono- and bimetallic transition metal particles (typically Fe, Ni and Co) because it satisfies both the catalyst activity and environmental aspects for the synthesis of CNTs. Previous studies have revealed the advantages of using this material as a support for CNT synthesis [71-77]. At 700°C, $CaCO_3$ changes to CaO (lime), which is an environmentally friendly material that can readily be dissolved in dilute acids such as HNO_3 and HCl. As a result, this support together with the metal catalyst particles can be removed from the produced CNTs with ease, resulting in clean materials that are relatively free of contaminants. Besides this characteristic feature; it is also a cheap material that is readily available. A limitation is that the decomposition point of $CaCO_3$ leads to low surface area CaO. However, the chemistry involved during the decomposition of $CaCO_3$ has advantages that make $CaCO_3$ a more suitable support over other materials. The chemistry involved is discussed in detail in the literature review of supported metal catalysts in Chapter 3. The CNTs produced on $CaCO_3$ have been used as supports for catalysts in the Fischer-Tropsch reactions [73] and for the thermal decomposition of hydrocarbons [79].

In this thesis, we report on the use of Fe, Co and Fe-Co bimetallic catalysts supported on $CaCO_3$ prepared by 'wet' impregnation, deposition-precipitation and reverse micelle methods for the synthesis of 'clean' multi-walled carbon nanotubes (MWCNTs) in large quantities with near 100% selectivity. The use of a novel material; calcium pyrophosphate, $Ca_3(PO_4)_2$, as an alternative support is also presented. $Ca_3(PO_4)_2$ has a high melting point (1670°C), high surface area of 42.4 m^2/g (compared to $CaCO_3$, 10 m^2/g), is insoluble in water and alcohols, and highly soluble in weak acids [80]. These properties would thus render this material highly suitable for the CVD synthesis of CNTs. The CNTs produced from the former and latter substrates have been studied using a range of techniques thus providing new information on the properties of these materials.

Another form of carbon, which is graphitic in nature, has been described in the literature. Earlier studies referred to this material as nanosized carbon spheres [81] or carbon nanobeads while more recent studies have called them carbon spherules [82-84] nanoballs [85], carbon pearls [86] or carbon microspheres [87]. These are all spherical in shape. This form of carbon has not received as much interest (compared to CNTs) because in most cases it forms accidentally as a by-product in the synthesis of CNTs by chemical vapour deposition (CVD) methods. Since microscopic techniques have become readily available, recent work has been carried out on these carbon spheres (CSs) focusing on their microscopic structural properties, as well as their fabrication using catalytic synthesis and the direct pyrolysis of hydrocarbons [88,89]. In this thesis, we also present some results on the synthesis of CSs using acetylene (C_2H_2) as a carbon source in the absence of a catalyst and their potential application as a support for cobalt catalysts [90]. Again, the procedures used for the synthesis of CSs are motivated by the fact that they do not impact negatively on the environment and can readily be scaled up for industrial application.

The search for new synthetic strategies for generating nanostructured carbon or carbon-hybrid materials is topical in materials chemistry, motivated by the natural abundance of carbon and therefore the cost effectiveness of carbon precursors and the promising applications of the resulting materials. Due to the intrinsic properties of the carbon materials such as their high strength, high thermal resistance and light weight, CSs can be used in the manufacture of high strength composites, as catalyst carriers, lubricants and as wear-resistant materials [91-94]. An alternative is to use these materials as catalyst supports. While much information has been generated in this area; to our knowledge, no report has appeared that systematically relates CS particle size (as determined by electron microscope studies) to reaction conditions as described in this thesis.

1.2 Objectives

The project was primarily undertaken to elucidate and optimize the synthesis of high purity CNTs using environmentally friendly supports via chemical vapour deposition. Under this umbrella, the objectives of the research project are then described as follows:

(i) To determine the optimum conditions for the reproducible fabrication of CNTs using $CaCO_3$ as a support. This involved identifying the appropriate transition metal catalyst, methods for preparation of the metal-support mixtures (the catalysts) and appropriate catalyst pre-treatment conditions (e.g. ageing time, calcination, drying).

(ii) To characterize the catalysts by mere inspection of physical appearance and also by a detailed analysis using Brunauer-Emmett-Teller (BET) surface area, temperature programmed reduction (TPR), powder X-ray diffraction (PXRD), high resolution transmission electron microscopy (HRTEM), energy dispersive X-ray (EDX) spectroscopy and by thermogravimetric analysis (TGA). Information obtained here allowed for the study of the metal particle morphology, dimension and dispersion. Consequently, this provided an understanding of the metal-support interactions and its impact on the catalytic activity and selectivity of the catalysts.

(iii) To synthesize and evaluate new catalysts using other supports, which have not to date been used [e.g. $Ca_3(PO_4)_2$]. Environmental and cost aspects were considered in the selection of these supports and their efficiency was compared with $CaCO_3$.

(iv) To synthesize and characterize tailored CNTs produced from the synthesized catalysts i.e. CNTs with uniform structural morphology such as diameter and distribution. This was achieved by controlling the parameters that determine catalytic activity and selectivity. Such parameters include synthesis temperature, type of carbon source, gas flow rates and synthesis time.

(v) To study the physico-chemical properties of the CNTs using a range of techniques such as transmission electron microscopy (TEM), scanning

electron microscopy (SEM), EDX, TGA, Raman spectroscopy, PXRD spectroscopy, BET surface area and porosity analysis, X-ray photoelectron spectroscopy (XPS) and high resolution scanning tunnelling electron microscopy (HRSTEM).

The synthesis of the carbon spheres mentioned in Section 1.1 incidentally emanated as the research on CNT synthesis progressed. As a consequence, detailed studies involving the CVD synthesis of the CSs were undertaken. The results obtained on the synthesis of the CSs are also presented and form a major part of the thesis.

1.3 Thesis outline

Chapter 1 gives a motivation of the work presented in the subsequent chapters. Although each chapter briefly introduces itself, the information contained in this chapter is general and gives a justification to the problems presented and briefly what measures were undertaken to address them and how that was achieved. The main objectives of the study are also presented in this chapter.

Chapter 2 is a general literature review. The chapter will be brief and will give a description of nanotechnology today and its significance in revolutionary trends associated with this technology. Emphasis will be on carbon nanotechnology. The commonly used CNT synthesis procedures, important properties of the CNTs as well as their characterization techniques will be discussed briefly to reveal their role in carbon nanotechnology.

Chapter 3 reviews the literature of CNTs synthesized from supported metal catalysts. Since the work presented in this thesis mainly focussed on supported catalysts for the CVD synthesis of CNTs, it then suffices to explain the role of supported metal catalyst with reference to previous studies and literature reports. The catalyst preparation methods, types of supports, sources of carbon as well as the types of CNTs obtained will

be discussed from a literature perspective. The purification of CNTs will be reviewed and crucial aspects of purification will be presented.

Chapter 4 is a literature review of the use of *organometallic transition metal complexes* in the synthesis of shaped carbon nanomaterials. This chapter is dedicated to the role of organometallic precursors in the synthesis of carbon nanomaterials; presented separately to give a better understanding of the gas phase conditions that lead to the formation of various carbon nanomaterials including CNTs. This chapter was published as a review in the *Journal of Organometallic Chemistry* in 2008.

Chapter 5: The results and discussion of work done on the "**Catalytic CVD synthesis of multiwalled carbon nanotubes using Fe, Co, and Fe-Co/$CaCO_3$ catalysts"** is presented. A part of this work has been published in the *South African Journal Chemistry*, 2009.

Chapter 6: The results and discussion of work done on "**Iron-cobalt catalysts synthesized by a reverse micelle impregnation method for controlled growth of carbon nanotubes"** is presented. This work was published in *Diamond and Related Materials*, 2008.

Chapter 7: The results and discussion of work done on "**A new $Ca_3(PO_4)_2$-$CaCO_3$ support mixture for the CVD synthesis of roughened multiwalled carbon nanotubes"** is presented. This work has been submitted for publication in *Materials Chemistry and Physics*, 2009.

Chapter 8: The results and discussion of work done on the **"The effect of reagent residues on the stability and structure of CVD carbon nanotubes"** is presented. This work has been submitted for publication in the *Journal of Nanoscience and Nanotechnology*, 2009.

Chapter 9: A review of the literature surrounding the synthesis of carbon spheres using catalytic and non-catalytic chemical vapour deposition is presented. This chapter will serve as an introduction to the subsequent chapters where the results obtained during our synthesis of carbon spheres are discussed. It discusses briefly the main procedures of CS synthesis using catalytic as well as non catalytic methods. The proposed CS growth mechanisms are also described. Lastly, the precursor effects on CS morphology are reviewed. This chapter will be published as a review in *Materials Science and Engineering Research* in 2009.

Chapter 10: The results and discussion of work done on the **"Synthesis and study of carbon microspheres for use as catalyst support for cobalt"** is presented. This work was accepted for publication in the *South African Journal of Science*, 2009.

Chapter 11: The results and discussion of work done on the **"Controlled syntheses of carbon spheres in a swirled floating catalytic chemical vapour deposition (SFCCVD) vertical reactor"** is presented. The work will be published in part an international accredited journal.

Chapter 12 presents a general summary and conclusion of the work presented in this thesis. The chapter highlights the successes of the project and the usefulness of its outcomes.

1.4 References

1. S. Iijima, Nature **354** (1991) 55.
2. S. Iijima, Physica B **323 (**2002) 1.
3. B.M. Endo, T. Hayashi, Y.A. Kim, M. Terrones, M.S. Dresselhaus, Phil. Trans. R. Soc. Lond. A **362** (2004) 2223.
4. J. Hone, M.C. Llaguno, M.J. Biercuk, A.T. Johnson, B. Batlogg, Z. Benes, J.E. Fischer, Appl. Phys. A: Mater. Sci. Process. **74** (2002) 339.

5. A. Krishnan, E. Dujardin, T.W. Ebbesen, P.N. Yianilos, M.M.J. Treacy, Phys. Rev. B **58** (1998) 14013.
6. B.G. Demczyk, Y.M. Wang, J. Cumings, M. Hetman, W. Han, A. Zettl, R.O. Ritchie, Mater. Sci. Eng. A: Struct. Mater. Properties Microstruct. Process. **334** (2002) 173.
7. B.Q. Wei, R. Vajtai, P.M. Ajayan, Appl. Phys. Lett. **79** (2001) 1172.
8. T. Durkop, S.A. Getty, E. Cobas, M.S. Fuhrer, Nano Lett. **4** (2004) 35.
9. M. Burghard, Surf. Scie. Reports **58** (2005) 1.
10. P. Ball, *Made to measure: New materials for the 21st Century*, USA: Princeton University Press, 1997.
11. M. Terrones, A. Jorio, M. Endo, Y.A. Kim, T. Hayashi, H. Terrones, J-C. Charlier, G. Dresselhaus and M.S. Dresselhaus, Mater. Today **7 (**2004) 30.
12. M. Trojanowicz, Trend. Anal. Chem. **25** (2006) 480.
13. L.M. Dai, P. Soundarrajan, T. Kim, Pure Appl. Chem. **74** (2002) 1753.
14. P.M. Ajayan, L.S. Schadler, C. Giannaris, A. Rubio, Adv. Mater. **12** (2000) 750.
15. S.J. Tans, R.M. Versucheren, C. Dekker, Nature **393** (1998) 49.
16. C.N.R. Rao, B.C. Satishkumar, A. Govindaraj, M. Nath, Chemphyschem **2** (2001) 78.
17. M.S. Dresselhaus, G. Dresselhaus, A. Jorio, Annu. Rev. Mater. Res. **34** (2004) 247.
18. M. Meyyappan, *Carbon nanotubes - science and applications*, CRC Press, Boca Raton, 2004.
19. L. Dai, *Carbon nanotechnology*, University of Dayton, Dayton, Ohio 45469-0240, USA, Elsevier. 2006.
20. J. Robertson, Mater. Today **10** (2007) 37.
21. M. Trojanowicz, Trend. Anal. Chem. **25** (2006) 480.
22. A. Bianco, K. Kostarelos, C.D. Partidos, M. Prato, Chem. Commun. (2005) 571.
23. P. Serp, M. Corrias, P. Kalck, Appl. Catal. A: General **253** (2003) 337.
24. M. Paradise, T. Goswami, Materials & Design **28** (2007) 1477.
25. V. Ivanov, A. Fonseca, J.B. Nagy, A. Lucas, P. Lambin, D. Bernaerts, X.B. Zhang, Carbon **33** (1995) 1727.
26. K.L. Salipira, B.B. Mamba, R.W. Krause, T.J. Malefetse, S.H. Durbach. Environ. Chem. Lett. **5** (2007) 13.

27. (a) T.W. Ebbesen, P.M. Ajayan, Nature **358** (1992) 220; (b) H. Huang, H. Kajiura, S. Tsutsui, Y. Hirano, M. Miyakoshi, A. Yamada, M. Ata, Chem. Phys. Lett. **343** (2001) 7; (c) Ph. Redlich, M, J. Loeffler, P. M. Ajayan, J. Bill, F. Aldinger, and M. Ruhle, Chem. Phys. Lett., **260** (1996) 465; (d) M. Terrones, W. K. Hsu, S. Ramos, R. Castillo, and H. Terrones, Fullerene Sci. Technol, **6** (1998) 787; (e) W. K. Hsu, S. Firth, P. Redlich, M. Terrones, H. Terrones, Y. Q. Zhu, G. Grobert, A. Schilder, R. J. H. Clark, H. W. Kroto, and D. R. M. Walton, J. Mater. Chem. **10** (2000) 1425; (f) H. Zeng, L. Zhu, G. Hao, R. Sheng, Carbon **36** (1998) 259; (g) Z.J. Shi, Y.F. Lian, X.H. Zhou, Z.N. Gu, Y. Zhang, S. Iijima, L. Zhou, K.T. Yue, Carbon **37** (1999) 1449.

28. (a) A. Thess, R. Lee, P. Nikolaev, H. Dai, P. Petit, J. Robert, C. Xu, Y.H. Lee, S.G. Kim, A.G. Rinzler, D.T. Colbert, G.E. Scuseria, D. Tománek, J.E. Fischer, R.E. Smalley, Science **273** (1996) 483; (b) S. Bandow, S. Asaka, Y. Saito, A.M. Rao, L. Grigorian, E. Richer, P.C. Eklund, Phys. Rev. Lett. **80** (1998) 3779; (c) J. Liu, A.G. Rinzler, H. Dai, J.H. Hafner, R.K. Bradley, P.J. Boul, A. Lu, T. Iverson, K. Shelimov, C.B. Huffman, F. Rodriguez-Macias, Y. Shon, T.R. Lee, D.T. Colbert, R.E. Smalley, Science **101** (1998) 1253.

29. (a) A. Govindaraj, C.N.R. Rao, Pure Appl. Chem. **74** (2002) 1571; (b) C.N.R. Rao, A. Govindaraj, Acc. Chem. Res. **35** (2002) 998; (c) C.J. Lee, J. Park, Y. Huh, J.Y. Lee, Chem. Phys. Lett. **343** (2001) 33; (d) M.S. Mohlala, X-Y. Liu, N.J. Coville, J. Organometal. Chem. **691** (2006) 4768; (e) S.E. Iyuke, A.B.M. Danna, Microp. Mesop. Mater. **84** (2005) 338; (f) L. Tapaszto, K. Kertész, Z. Vértesy, Z.E. Horváth, A.A. Koós, Z. Osváth, Zs. Sárközi, Al. Darabont, L.P. Biró, Carbon **43** (2005) 970; (g) L.P. Biró, Z.E. Horváth, A.A. Koós, Z. Osváth, Z. Vértesy, Al. Darabonta, K. Kertésza, C. Neamtub, Zs. Sárközia, L. Tapasztóa, J. Optoelectro. Adv. Mater. **5** (2003) 661; (h) A-C. Dupuis, Prog. Mat. Scie. **50** (2005) 929; (i) M. Joseyacaman, M. Mikiyoshida, L. Rendon, J.G. Santiesteban, Appl. Phys. Lett. **62** (1993) 657; (j) M. Endo, K. Takeuchi, K. Kobori, K. Takahashi, H.W. Kroto, A. Sarkar, Carbon **33** (1995) 873; (k) S. Amelinckx, X.B. Zhang, D. Bernaerts, X.F. Zhang, V. Ivanov, J.B. Nagy, Science **265** (1994) 635; (l) J.B. Park, G.S. Choi, Y.S. Cho, S.Y. Hong, D. Kim, S.Y. Choi, J.H. Lee, K.I. Cho, J. Cryst. Growth **244** (2002) 211; (m) K.B.K.

Teo, C. Singh, M. Chhowalla, W.I. Milne, Encyclopaedia of Nanoscience and Nanotechnology, **X** (2003) 1.

30. (a) V.O. Nyamori, N.J. Coville, Organometallics **26** (2007) 4083; (b) D. Jain, A. Winkelm, R. Wilhelm, Small **2** (2006) 752; (c) J. Liu, M. Shao, Q. Xie, L. Kong, W. Yu, Y. Qian, Carbon **41** (2003) 2101; (d) M. Laskoski, W. Steffen, J.G.M. Morton, M.D. Smith, U.H.F. Bunz, J.Am. Chem. Soc. **124** (2002) 13814; (e) B.El Hamaoui, L. Zhi, J. Wu, U. Kolb, K. Müllen, Adv. Mater. **17** (2005) 2957; (f) L. Zhi, T. Gorelik, R. Friedlein, J. Wu, U. Kolb, W.R. Salaneck, K. Müllen, Small **1** (2005) 798; (g) J. Wu, B. El Hamaoui, J. Li, L. Zhi, U. Kolb, K. Müllen, Small **1** (2005) 210; (h) S. Liu, X. Tang, Y. Mastai, I. Felner A. Gedanken, J. Mater. Chem. **10** (2000) 2502; (i) C. Wu, X. Zhu, L. Ye, C. Yang, S. Hu, L. Lei, Y. Xie, Inorg. Chem. **45** (2006) 8543; (j) P.I. Dosa, C. Erben, V.S. Iyer, K.P.C. Vollhardt, I.M. Wasse, J. Am. Chem. Soc. **121** (1999) 10430; (k) V.S. Iyer, K.P.C. Vollhardt, R. Wilhelm, Angew. Chem. Int. Ed. **42** (2003) 4379.
31. (a) K. Hernadi, Z. Kónya, A. Siska, J. Kiss, A. Oszkó, J.B. Nagy, I. Kiricsi, Mat. Chem. & Phys. **77** (2002) 536. (b) M. Bierdel, S. Buchholz, V. Michele, L. Mleczko, R. Rudolf, M. Voetz, A. Wolf, Phys. Stat. Sol. B **244** (2007) 3939.
32. C.J. Lee, J. Park, J.A. Yu, Chem. Phys. Lett. **360** (2002) 250.
33. C.J. Lee, J. Park, Carbon **39** (2001) 1891.
34. J.E. Herrera, D.E. Resasco, J. Catal., **221** (2004) 354.
35. W. Qian, F. Wei, T. Liu, Z.W. Wang, Solid State Commun. **126** (2003) 365.
36. R.L. Vander Wala, T.M. Ticichb, V.E. Curtisb, Carbon **39** (2001) 2277.
37. S. Inoue, Y. Kikuchi, Chem. Phys. Lett. **410** (2005) 209.
38. S. Inoue, T. Nakajima, Y. Kikuchi, Chem. Phys. Lett. **406** (2005) 184.
39. K. Hernadi, A. Fonseca, J.B. Nagy, D. Bernaerts, J. Riga, A. Lucas, Synthetic Metals **77** (1996) 31.
40. A.L. Balch, M.M. Olmstead**,** Chem. Rev. **98** (1998) 2123.
41. K. Hernadi, A. Fonseca, J.B. Nagy, A. Fudala, D. Baenaerts, A. Lucas, Zeolites **17** (1996) 416.
42. P. Francesco, Catal. Today **41** (1998) 129.

43. T. W. Ebbesen, P. M. Ajayan, H. Hiura and K. Tanigaki, Nature (London) **367** (1994) 519.
44. P. M. Ajayan, T. W. Ebbesen, T. Ichihashi, S. Iijima, K. Tanigaki and H. Hiura Nature (London) **362** (1993) 522.
45. Sc. Tsang, P. J. F. Harris and M. L. H. Green, Nature (London) **362** (1993) 520.
46. H. Hiura, T. W. Ebbesen and K. Tanigaki, Adv. Mater. **7** (1995) 275.
47. K. C. Hwang, J. Chem. Soc., Chem. Commun. (1995) 173.
48. A.K. Sinha, D.W. Hwang, L.P. Hwang, Chem. Phys. Lett. **332** (2000) 455.
49. X. Song, Y. Fang, Spectrochimica Acta Part A **67** (2007).
50. K. Hernadi, A. Fonseca, J.B. Nagy, A. Fudala, D. Baenaerts, A. Lucas, Synthetic Metals **77** (1996) 31.
51. G.S. Duesberg, W. Blau, H.J. Byrne, J.Muster, M. Burghard, S. Roth, Synthetic Metals **103** (1999) 2484.
52. R. Engel-Herbert, H. Pforte, T. Hesjedal, Mater. Lett. **61** (2007) 2589.
53. J.-F. Colomer, P. Piedigrosso, A. Fonseca and J. B.Nagy, Synthetic Metals **103** (1999) 2482.
54. M. Chen, H.-W. Yu, J.-H. Chen, H.-S. Koo, Diam. Rel. Mater. **16** (2007) 1110.
55. Kuo Chu Hwang, J. Chem. Soc., Chem. Commun., 1995.
56. P.X. Hou, S. Bai, Q.H. Yang, C. Liu, H.M. Cheng, Carbon **40** (2002) 81.
57. S.-H. Su, W.-T. Chiang, C.-C. Lin, M. Yokoyama, Physica E **40** (2008) 2322.
58. L. Vaccarini, C. Gaze, R. Aznar, V. Micholet, C. Journet, P. Bernier, Synthetic Metals **103** (1999) 2492.
59. A. Bougrine, A. Naji, J. Ghanbaja and D. Billaud, Synthetic Metals **103** (1999) 2480.
60. J-F. Colomer, P. Piedigrosso, I. Willems, C. Journet, P. Bernier, G. Van Tendeloo, A. Fonseca, J. B.Nagy, J. Chem. Soc., Faraday Trans. **94** (1998) 3753.
61. E. Salernitano, L. Giorgi, Th. Dikonimos Makris, R. Giorgi, N. Lisi, V. Contini, M. Falconieri, Diam. Rel. Mater. **16** (2007) 1565.
62. Z. Shi, Y. Lian, F. Liao, X. Zhou, Z. Gu, Y. Zhang, S. Iijima, Solid State Commun. **112** (1999) 35.
63. K.B. Shelimov, R.O. Esenaliev, A.G. Rinzler, C.B. Huffman, R.E. Smalley, Chem. Phys. Lett. **282** (1998) 429.

64. F. Li, H.M. Cheng, Y.T. Xing, P.H. Tan, G. Su, Carbon **38** (2000) 2041.
65. K.L. Strong, D.P. Anderson, K. Lafdi, J.N. Kuhn, Carbon **41** (2003) 1477.
66. Y. Zhang, Z. Shi, Z. Gu, S. Iijima, Carbon **38** (2000) 2055.
67. M. Yumura, S. Ohshima, K. Uchida, Y. Tasaka, Y. Kuriki, F. Ikazaki, Y. Saito, S. Uemura, Diam. Rel. Mater. **8** (1999) 785.
68. Y. Mackeyev, S. Bachilo, K.B. Hartman, L.J. Wilson, Carbon **45** (2007) 1013.
69. K. Shen, H. Xu, Y. Jiang, T. Pietraß, Carbon **42** (2004) 2315.
70. H. Ago, Th. KugIer, F. Caciaili, K. Petritsch, R.H. Friend, W.R. Salaneck, Y. Ono, T. Yamabe, K. Tanaka, Synthetic Metals **103** (1999) 2494.
71. E. Couteau, K. Hernadi, J.W. Seo, L. Thiên-Nga, Cs. Mikó, R. Gaá1, L. Forró, Chem. Phys. Lett. **378 (**2002) 9.
72. H. Kathyayini, N. Nagaraju, A. Fonseca, J.B. Nagy, J. Mol. Catal. **223 (**2004) 129.
73. (a) M.C. Bahome, L.L. Jewell, D. Hildebrandt, D. Glasser, N.J. Coville, Appl. Catal. A: General **287 (**2005) 60; (b) A. Tavasoli, K. Sadagiani, F. Khorashe, A.A. Seifkordi, A.A. Rohani, A. Nakhaeipour, Fuel Process. Technol. **89** (2008) 491.
74. J. Cheng, X. Zhang, Z. Luo, F. Liu, Y. Ye, W. Yin, W. Liu, Y. Han, Mat. Chem. Phys. **95 (**2006) 5.
75. A. Magrez, J.W. Seo, C. Mikó, K. Hernádi, L. Forro, J. Phys. Chem. B, **109 (**2005) 10087.
76. A. Magrez, J. W. Seo, V.L. Kuznetsov, L. Forró, Angew. Chem. Int. Ed. **46 (**2007) 441.
77. (a) S.D. Mhlanga, N.J. Coville, Diam. Rel. Mater. **17** (2008) 1489; (b) T.C. Schmitt, A.S. Biris, D.W. Miller, A.R. Biris, D. Lupu, S. Trigwell, Z.U. Rahman, Carbon **44** (2006) 2032.
78. W.Z. Li, J.G. Wen, M. Sennett, Z.F. Ren, Chem. Phys. Lett. **368** (2003) 299.
79. P. Serp, M. Cossias, P. Kalck, Appl. Catal. A: General **253 (**2003) 337.
80. R.C. Weast, M.J. Astle, W.M. Beyer, *CRC handbook of Chemistry and Physics*, CRC Press, Inc., Boca Raton, Florida, 65th Ed., (1984-1985).
81. Z.C. Kang, Z.L. Wang, J. Phys. Chem. **100** (1996) 5163.
82. Q. Wang, H. Li, L. Chen, X. Huang, Carbon **39** (2001) 2211.

83. V.G. Pol, M. Motiei, A. Gedanken, J. Calderon-Moreno, M. Yoshimura, Carbon **42** (2004) 111.
84. F. Li, Q. Qian, F. Yan, G. Yuan, Carbon **44** (2006) 128.
85. X. Liu, B. Huang, N.J. Coville, Carbon **40** (2002) 2791.
86. L.P. Biró, G.I. Márk, Z.E. Horváth, K. Kertész, J. Gyulai, J.B. Nagy, Ph. Lambin Carbon **42** (2004) 2561.
87. A. Ma, X. Wang, T. Li, X. Liu, B. Xu, Mat. Sci. and Eng. A **443** (2007) 54.
88. H. Qian, F. Han, B. Zhang, Y. Guo, J. Yue, B. Peng, Carbon **42** (2004) 761.
89. Y.Z. Jin, C. Gao, W.K. Hsu, Y. Zhu, A. Huczko, M. Bystrzejewski, M. Roe, C.Y. Lee, S. Acquah, H. Kroto, D.R.M. Walton, Carbon **43** (2005) 1944.
90. S.D. Mhlanga, K.C. Mondal, N. Naidoo, N. Kunjuzwa, M.J. Witcomb, Neil J. Coville, SAJS (2009). Accepted for publication.
91. Y.Z. Jin, C. Gao, W.K. Hsu, Y.Zhu, A. Huczko, M. Bystrzejewski, M. Roe, C.Y. Lee, S. Acquah, H. Kroto, D.R.M. Walton, Carbon **43** (2005) 1944.
92. S. Kohjiya, A. Katoh, T. Suda, J. Shimanuki, Y. Ikeda, Polymer **47** (2006) 3298.
93. A.I. Medalia, L.W. Richards, J. Colloid Interf. Scie. **40** (1972) 233.
94. F.E. Dolle, J. Lahaye, S. Misono, Carbon **32** (1994) 1363.

Chapter 2

General literature review

2.1 Nanotechnology

Nanotechnology 'the fourth industrial revolution' has been defined in many ways. Most definitions revolve around the study and control of materials at length scales below 100 nm. The most appealing definitions to us, taken from different sources are given below:

Nanotechnology is the creation of functional materials, devices and systems (of any useful size) through control/manipulation of matter on the nanometer length scale and exploitation of novel phenomena and properties which arise because of the nanometer length scale [1].

Nanotechnology is the design, characterization, production, and application of structures, devices, and systems by controlled manipulation of size and shape at the nanometer scale (atomic, molecular, and macromolecular scale) that produces structures, devices, and systems with at least one novel/superior characteristic or property [2].

The concept of nanotechnology was first introduced by a Nobel Prize winner Richard Feynman in 1959 in his lecture entitled "*There is plenty of room at the bottom*" [3]. This lecture triggered the "*nano revolution"* as manifested by the explosion of research on the nanoscale [4-6]. The enthusiasm in nanoscale research resulted in the birth of the scanning tunnelling microscope (STM) in 1981 [7], the atomic force microscope (AFM) [8] and other new materials (nanomaterials) including the C_{60} molecule (fullerene) in 1985 [9] and carbon nanotubes in 1991 [10].

The definition of nanomaterials is broad. However, nanomaterials are generally categorised as materials that have structured components with at least one dimension less

than 100 nm. Nanomaterials can be created by *'top down*' techniques, producing very small structures from larger pieces of material; for example by etching to create circuits on the surface of a silicon microchip. They may also be constructed by '*bottom up*' techniques, atom by atom or molecule by molecule. This can be done by self-assembly, in which the atoms or molecules arrange themselves into a structure due to their natural properties. Crystals grown for the semiconductor industry provide an example of self assembly. Another approach is to use tools to move each atom or molecule individually. Although this 'positional assembly' offers greater control over construction, it is currently very laborious and not suitable for industrial applications [3a,11].

The advantages of nanomaterials can be observed from their size and surface effect properties. Quantum size effects result in unique mechanical, electronic, photonic, and magnetic properties of nanoscale materials. The chemical reactivity of nanoscale materials is greatly different from the macroscopic form (e.g. the colour of bulk gold is yellow yet gold nanoparticles are black). As the size of materials decreases, the ratio of surface atoms increases. Due to the high surface-to-volume ratio associated with nanometer sized materials, a tremendous change in chemical properties is also achievable [12,13].

2.2 Carbon nanotechnology

The discovery of the buckminsterfullerene C_{60}, "bucky ball" by Kroto *et al* [9] and the studies on carbon nanotubes (CNTs) by Iijima [10] has resulted in carbon nanotechnology becoming the building block of the entire field of nanotechnology [3a].

Carbon has long been known to exist in various structures (e.g. diamond, graphite, amorphous carbon). However other forms are now known (e.g. fullerenes, carbon fibers, carbon onions, carbon spheres or balls, carbon nanotubes etc) that emanate from the unique ability of carbon to achieve various forms of sp, sp^2 and sp^3 electronic configurations (Fig. 2.1). While much attention has been paid to these carbon nanostructures, CNTs have in recent times received greater attention.

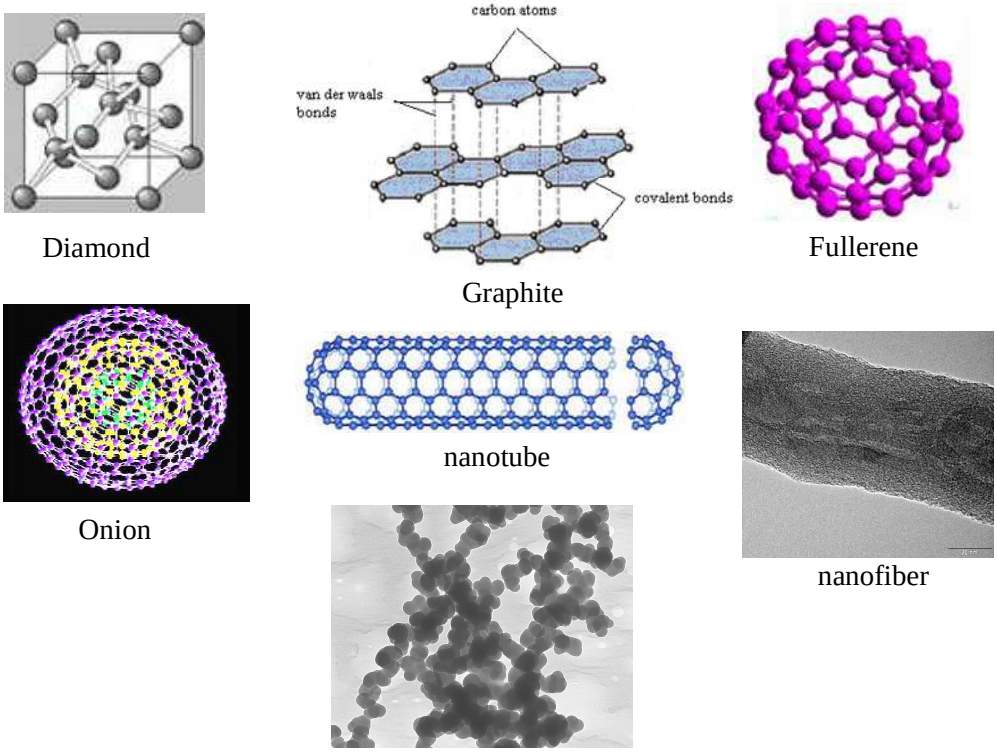

Fig. 2.1: Carbon allotropes.

Carbon nanotubes exist in two major categories: single walled carbon nanotubes (SWCNTs) and multiwalled carbon nanotubes (MWCNTs). A single walled carbon nanotube is a one-atom thick sheet of graphite (called graphene) rolled up into a seamless cylinder. When an additional graphene tube exists around a central SWCNT, a double walled carbon nanotube (DWCNT) is formed. Additional layers of the graphite sheets result in the formation of a MWCNT. They are called 'nanotubes' because they possess diameters in the order of the nanometer (i.e. 10^{-9} m) and they are usually a few micrometers in length. Such cylindrical carbon molecules have novel properties that make them potentially useful in many applications in nanotechnology as mentioned in the introduction. Physically, CNTs appear as black soot and they are chemically inert at standard room temperature and pressure (Fig. 2.2).

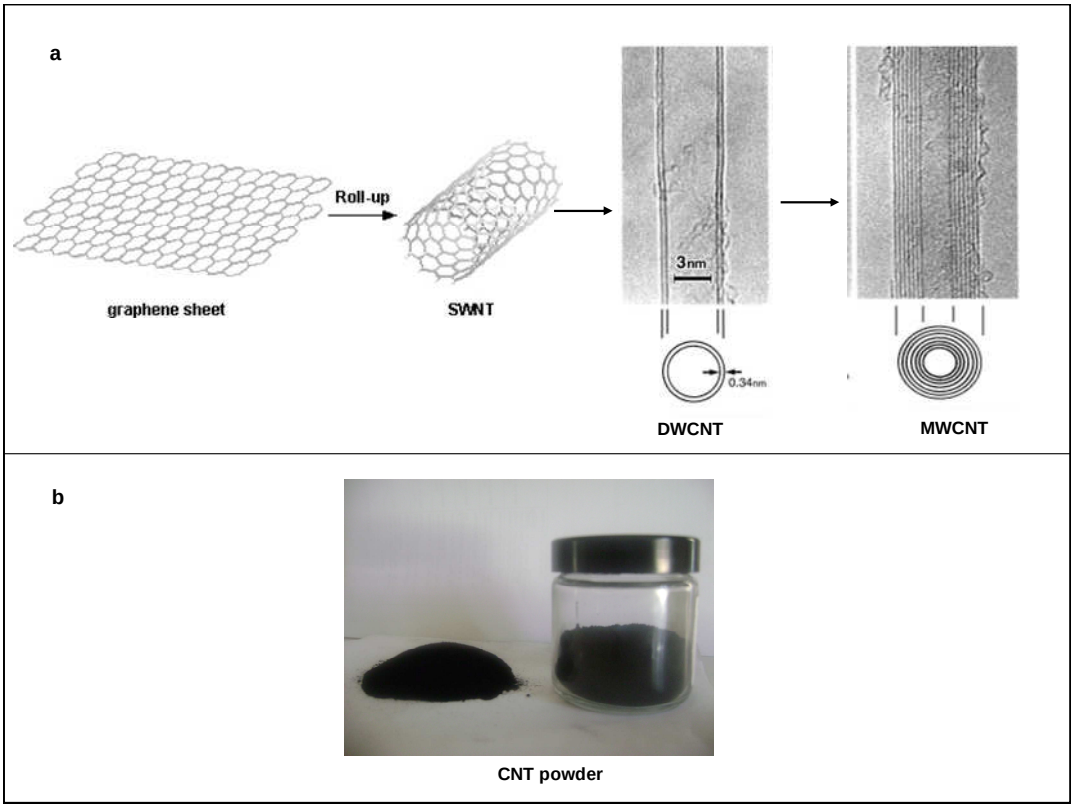

Fig. 2.2: (a) Types of CNTs as defined by the rolling of graphite sheets [2,10]; (b) A picture of CNT powder.

2.3 CNT synthesis methods

The synthesis of CNTs is certainly one of the most prevailing aspects of carbon nanotechnology and new synthesis methods are still being reported. This prevalence is driven by the outcome of scientific research, which is continuously finding new applications for CNTs in today's world. Several techniques have been used to synthesize CNTs namely; the arc discharge, laser ablation and chemical vapour deposition (CVD) methods.

(i) Arc discharge

The arc discharge method was the first method used to produce CNTs [10]. Typically, nanotubes synthesized by this method are formed through arc-vaporisation of two carbon

rods placed end to end, separated by approximately 1 mm, in an enclosure that is usually filled with inert gas (He, Ar) at low pressure (between 50 and 700 mbar). A direct current of 50 to 100A driven by approximately 20V creates a high temperature discharge between the two electrodes. The discharge vaporises one of the carbon rods and forms a small rod shaped deposit on the other rod. The production of SWCNTs or MWCNTs depends on the uniformity of the plasma arc and the temperature of the deposit formed on the carbon electrode [14-18].

(ii) Laser ablation / Laser vapourization

This method was reported by Smalley's group in 1995 at Rice University [19]. A pulsed or continuous laser is used to vapourize a graphite target in an oven at 1200°C. The main difference between a continuous and pulsed laser, is that the pulsed laser demands a much higher light intensity (100 kW/cm^2) compared to a continuous laser (12 kW/cm^2). The oven is usually filled with He or Ar gas so as to keep the pressure at 500 Torr. A very hot vapour cloud forms, then expands and cools rapidly. As the vaporised species cool, small carbon molecules and atoms quickly condense to form larger clusters, possibly including fullerenes [18].

(iii) Chemical vapour deposition (CVD)

CVD synthesis is achieved by decomposing a carbon source in the gas phase by using an energy source, usually a high temperature furnace, to transfer energy to a gaseous carbon molecule. Commonly used gaseous carbon sources include methane, acetylene, ethylene, carbon monoxide, benzene, toluene, and short chain alcohols. The energy source is used to "crack" the molecule into reactive atomic carbon. The carbon then diffuses towards the substrate, which is heated and coated with a catalyst (e.g. Ni, Fe, Co, Ru) where it will form CNTs. Carbon nanotubes are formed if the proper parameters are maintained such as temperature and gas flow rates. Excellent alignment, as well as positional control on a nanometre scale, can be achieved by using CVD. Control over the diameter, as well as the growth rate of the nanotubes can also be maintained. If an appropriate metal is used,

the catalyst can preferably grow SWCNTs rather than MWCNTs. The reaction temperatures for the synthesis of nanotubes by CVD are generally within the 600 – 900°C range [20-22].

As mentioned earlier (Section 1.1), the CVD process can be classified into two commonly used processes; the substrate/supported catalyst CVD and the vapour phase/ pyrolysis/floating catalyst CVD. Both techniques require the use of a transition metal, a high temperature zone, and a carbon source for the fabrication of CNTs. Due to the significance and relevance of these techniques to our research, carbon nanomaterials obtained via these processes are reviewed extensively in Chapters 3 and 4 of this thesis.

(iv) Autoclave processes

The autoclave process is another type of CNT synthesis method developed in recent years that does not use a gas flow system. Rather the reaction to produce CNTs takes place in a closed container (e.g. autoclave or sealed quartz tube), at elevated pressures. Typically, in this method, organometallic complexes (sometimes containing an external carbon source) are used as starting materials to synthesize CNTs [23].

2.4 CNT characterization

Characterization of carbon nanostructures can be ascertained using a variety of techniques. The most widely used techniques are the electron microscopy techniques (TEM and SEM), Raman spectroscopy, thermogravimetric analysis (TGA) and X-ray diffraction (XRD). The usefulness of these techniques for the characterization of CNTs is described below in view of the fact that they have been used extensively in this study. Other advanced techniques such as scanning tunnelling microscopy (STEM), atomic force microscopy (AFM), X-ray photoelectron spectroscopy (XPS), secondary ion mass spectrometry (SIMS) and electron energy loss spectroscopy (EELS) have been used for evaluation of CNTs and other nanomaterials. These characterization techniques have been reviewed in detail by Belin *et al* [24].

(i) Electron microscopy (EM)

Electron microscopic techniques such as transmission electron microscopy (TEM) and scanning electron microscopy (SEM) are very useful tools for characterizing substances at the nanometer level. EM is used to determine the size and shape of nanomaterials. The main difference between SEM and TEM is that SEM sees contrast due to topology and composition of a surface (e.g. length, diameter, uniformity and density) whereas the electron beam in TEM projects all information on the mass it encounters in a two dimensional image (e.g. wall structure and crystallinity) as well as length and diameter [10,25-28]. TEM is particularly important in showing the inner cavity of the CNTs and thus distinguish tubes from fibers. High resolution TEM (HRTEM) is particularly important in evaluating the quality of CNTs as this technique can view samples at higher magnifications. Both TEM and SEM techniques can be coupled with an energy dispersive X-ray (EDX) spectrometer which allows for the determination of the elemental compositions of the materials.

(ii) Raman spectroscopy

Raman spectroscopy has been widely used to investigate both vibrational and electronic properties of solids. CNTs are generally characterized by looking at the response in three spectral regions namely the radial breathing mode (RBM), the tangential mode (G-band) and the disorder-induced mode (D-band) corresponding to the excitation of related vibrational modes [29-31]. The RBM Raman peaks appearing in the range 120 - 250 cm^{-1} (for diameters 1 - 2 nm) provide essential information on SWCNTs and they correspond to the atomic vibrations of the C atoms in the radial direction. The G-band, characterized by multi-peak features around 1580 cm^{-1} indicates original graphitic features. Spectra in this frequency range can be used for SWCNT characterization, independent of the RBM examination. Finally, the D-band at around 1345 cm^{-1}, is characteristic of disordered features in graphitic sheets. The structural quality of a CNT sample can be measured by the ratio I_D/I_G between the intensities of peaks D and G [29].

(iii) Powder X-Ray diffraction (PXRD)

X-ray diffraction is one of the oldest and most frequently used techniques in catalyst characterization. It is used for the identification of bulk crystalline phases of catalysts by means of lattice structural parameters, to monitor the kinetics of bulk transformations, and to obtain information on the particle sizes. PXRD can also be used to study structural and morphological features of the as-synthesized and treated CNT samples [32]. From the X-ray diffractograms, one can infer whether the purification processes were effective, by monitoring the carbon, support, as well as metal catalyst particles used.

(iv) Thermogravimetric analysis (TGA)

TGA is a thermal analysis technique used to measure changes in the mass of a sample as a function of temperature and/or time. TGA is commonly used to determine polymer degradation temperatures, residual solvent levels, absorbed moisture content and the amount of inorganic (non-combustible) filler in polymer or composite material compositions [33,34]. It can be used to determine the thermal stability of carbon nanomaterials under oxidizing and inert atmospheres. The amount of impurities in carbon nanomaterials can be determined using TGA under an oxidizing atmosphere.

(v) Brunauer-Emmet-Teller (BET) measurement

The BET method is the most popular model used to determine total surface area of materials. Surface area is a measure of the exposed surface of a solid sample on the molecular scale. Knowing the surface area helps predict how materials will burn, dissolve, adsorb, or react with other materials. The BET method can also be used in the sizing of nanoparticles [35,36].

2.5 Properties of CNTs and applications

Knowledge of the Young's modulus (*E*) of a material is the first step towards its use as a structural element for various applications [37]. CNTs exhibit extraordinary mechanical properties: a Young's modulus of over 1 Tera Pascal has been reported [37-42]. Their stiffness is comparable to that of diamond and they possess an estimated tensile strength of 200 Giga Pascal, which is one hundred times higher than the value displayed by steel while weighing six times less. While theory and experiments show that the Young's modulus of CNTs is at least as high as graphite and can be even higher for small SWCNTs, Salvetat *et al.* [37] have shown that Young's moduli for MCWNTs are dependent on the degree of order of the tube's graphitic walls. The Young's modulus decreases as the disorder increases, however their resistance will still be very high. Also, it has been shown that the structure of CNTs is not easily changed by pressure [40]. These properties are ideal for reinforced composites and nanoelectromechanical systems (NEMS) [43].

Besides the extraordinary mechanical properties of CNTs, they have unique electrical and heat conductivity properties that are not debatable. CNTs can either be electrically conductive or semiconductive, depending on their helicity; leading to nanoscale wires and electrical components. These one-dimensional fibers exhibit electrical conductivity as high as copper and thermal conductivity as high as diamond [44]. They are probably the best electron field-emitters possible. The CNTs can be branded as polymers of pure carbon and can be reacted and manipulated using the tremendously rich chemistry of carbon. This provides opportunity to modify their structure and to optimise their solubility and dispersion during application (e.g. for use in biomedical applications). Most considerably, CNTs are molecularly perfect, which means that they are free of property-degrading defects in the nanotube structure [45].

Another fascinating property of CNTs is their high aspect ratio of about 1000:1, which provides reliable imaging of deep trenches, while good resolution is retained due to their nanometer-scale diameter [46]. It has also been said that the higher the aspect ratio of the

filler particles (e.g. in conductive plastics), the lower the loading required to achieve a given level of conductivity. CNTs have the highest aspect ratio of any carbon fibrous material.

CNTs also possess good thermal properties. Thus they are expected to be very good thermal conductors along the tube, exhibiting a property known as "ballistic conduction," but good insulators laterally to the tube axis. It is predicted that carbon nanotubes will be able to transmit up to 6000 $W \cdot m^{-1} \cdot K^{-1}$ at room temperature. Copper on the other hand is a metal well-known for its good thermal conductivity but it only transmits by contrast 385 $W \cdot m^{-1} \cdot K^{-1}$ [47]. The thermal stability of CNTs can be evaluated using TGA. CNTs are more stable to oxidation than activated carbon but more reactive than graphite [48]. The studies conducted on the thermal behaviour of CNTs have shown different behaviours for SWCNTs and MWCNTs. SWCNTs were found to be more stable than MWCNTs because of the changes associated with their surfaces [49].

CNTs have proven to be a promising material in heterogeneous catalysis and interest in their use as catalyst supports in increasing tremendously. According to a review by Serp *et al.* [48], carbon materials (e.g. graphite-like nanofibers and CNTs) attract a growing interest due to their specific characteristics which are mainly: (i) resistance to acid/basic media, (ii) possibility to control, up to certain limits, the porosity and surface chemistry of the materials and (iii) easy recovery of precious metals by support burning resulting in a low environmental impact. Interestingly, CNTs are in the forefront of today's research in heterogeneously catalysed reactions because of their superior properties explained above. As a result, the focus of our group was to synthesize CNTs for application as catalysts (metal) supports.

Below is a list of some real and potential applications of CNTs [14,50,51].

- Batteries
- Biosensors for harmful gases and chemical analyses
- Biomedical applications
- Capacitors
- Cathodes for microwave tubes
- Catalyst supports
- Chemical factory-on-a-chip applications
- Coatings of all sorts
- Computers and TVs (with nano circuits)
- Conducting composites / plastics
- Conductors for micro electronic devices
- Controlled drug release applications
- DNA chips
- Electronic applications
- Electronic rectification, ballistic switching, and logic functions
- Electronic nanocomponents and material protection applications
- Energy storage
- Fibres and fabrics
- Field effect transistors
- Field-emission flat panel displays
- Filter applications
- Fuel cell membranes
- Heat pipe
- Hydrogen storage
- Light emitting diodes (LEDs)
- Microscope probes
- Molecular pumps
- Nanometric test tubes
- Nanotube reinforced composites
- Nano-data storage
- Quantum wires
- Single electron transistors
- Sporting goods
- Water desalinators
- Water purification
- Wireless devices

2.6 The nanotube market and commercial availability

The past few years have seen a considerable increase in the number of companies in the US and Europe producing industrial-scale quantities of CNTs and major growth has been witnessed in only a few years [52]. Increase in information coupled with theoretical and experimental work going on in the area of nanotechnology, suggests that nanotubes are one of many nanoscale technologies that are set to transform our lives today [51]. Thus, growth in the market will help reduce the cost of consumer products, increase our standard of living world-wide and increase our health and wellbeing.

In a report published in NanoNews (US), the global market for CNTs was worth $50.9 million by the end of 2006 and reached $79.1 million by 2007. It is expected that the world demand for CNTs will expand to $200 million in 2009. This obviously shows an exponential growth over a period of 4 years. However, a number of issues, including high costs, inadequate purity levels, and insufficient product yields in manufacturing, still need to be addressed. According to the report, as these issues are resolved, growth in global nanotube demand is expected to accelerate and surpass $9 billion by 2020 [53]. Our research reveals that, in this global market SA is expected to account for approximately 3 % of the global market. **Table 2.1** is an estimate for the CNT market globally [54].

Table 2.1: An estimate of the carbon nanotube market world-wide.

Millions (Rands)	**2004**	**2009**	**2014**
Total demand	42	1 505	4 049
By type			
Single-walled nanotubes	0	665	4 200
Multiwalled nanotubes	42	840	3 290
By end use			
Electronics	0	630	2 765
Automotive	7	217	1 155
Aerospace/defense	0	70	455
Other	35	588	3 115
By Region			
U.S.	14	399	2 030
Western Europe	7	224	1 260
Asia/Pacific	21	791	3 500
Other	0	91	700

Currently research reveals that basic advancement in technology comes about twice a century and leads to massive wealth creation. Fig. 2.3 reveals that this century will be dominated by nanotechnology and by 2020 there will be widespread adoption of this new technology. There is a great drive for the production of CNTs at large scale. Clearly there exists great potential and opportunity for growth in the CNT market. This growth is largely driven by the passion to develop new materials that will sustain economic development.

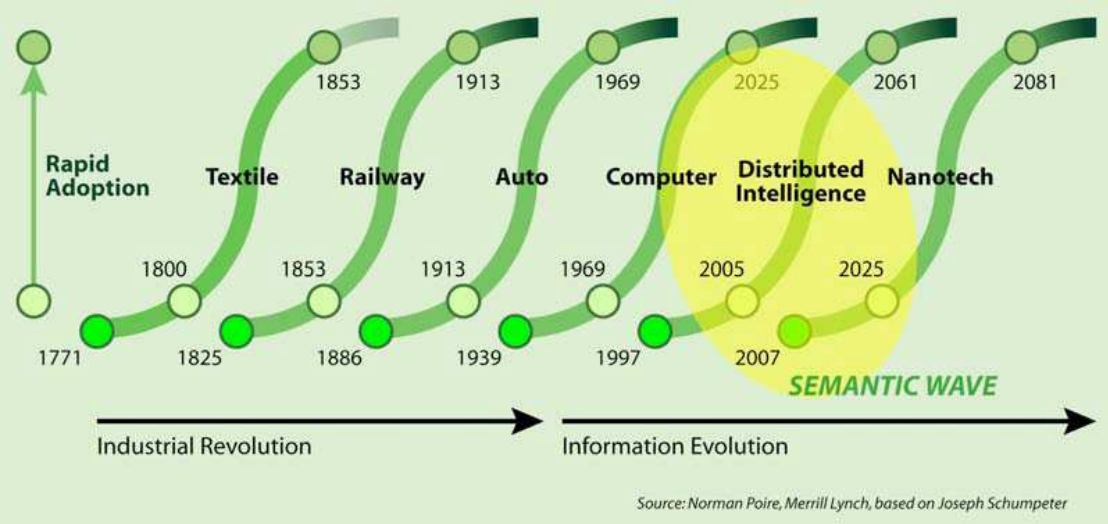

Fig. 2.3: Advances in science and technology over centuries [55].

2.7 References

1. http://www.nano.gov/html/facts/whatIsNano.html (accessed on 1st June 2008).
2. http://www.nanowerk.com/nanotechnology/introduction/introduction_to_nanotechnology_1.html (accessed on 1st June 2008)
3. (a) L. Dai, *Carbon nanotechnology*, University of Dayton, Dayton, Ohio, USA, Elsevier B.V., 2006; (b) R.P. Feyman, A lecture in engineering science, California Institute of Technology, 1960.
4. E.K. Drexler, Proc. Natl. Acad. Sci. USA **78** (1981) 5275.
5. E.K. Drexler, *Engines of creation - the coming era of nanotechnology*, Anchor Press/Doubleday, Garden City. N.Y., 1986.
6. http://www.kheper.net/topics/nanotech/nanotech-history.htm (accessed on 1st June 2008).

7. (a) G. Binning, H. Rohrer, Ch. Gerber, E. Weibel, Phys. Rev. Lett. **49** (1982) 57; (b) G. Binning, H. Rohrer, Rev. Mod. Phys. **59** (1987) 615; (c) G. Binning, H. Rohrer, Angew. Chem. Intl. Ed. Engl. **26** (1987) 606.
8. R. Howard, L. Benatar, *A practical guide to scanning probe microscopy*, Park Scientific Instruments, Sunnyvale, CA, USA.
9. H.W. Kroto, J.R. Heath, S.C. O'Brien, R.F. Curl, R.E. Smalley, Nature **318** (1985) 162.
10. S. Iijima, Nature **354** (1991) 56.
11. (a) A. Aggeli, N. Boden, S. Zhang, *Self-assembling peptide systems in biology, medicine, and engineering*, Kluwer Academic Publishers, Dordrecht, 2001; (b) A.N. Golden, *Handbook of nanophase materials*, Marcel Derker, Inc., New York, 1997; (c) G.A. Ozin, A.C. Arsenault, *Nanochemistry: a chemical approach to nanomaterials*, Cambridge: Royal Society of Chemistry, 2005.
12. G. Cao, *Nanostructures and nanomaterials - synthesis properties and applications*, London: Imperial College Press, 2004.
13. G.A. Mansoori, *Principles of nanotechnology: molecular-based study of condensed matter in small systems*, University of Illinois at Chicago, USA; World Scientific pub. Co., 2005.
14. M. Paradise, T. Goswami, Mater. Design **28** (2007) 1477.
15. H. Zheng, L. Zhu, G. Hao, R. Sheng, Carbon **36** (1998) 259.
16. Y.S. Park, K.S. Kim, H.J. Jeong, W.S. Kim, J.M. Moon, K.H. An, D.J. Bae, Y.S. Lee, G.S. Par, Y.H. Lee, Synth. Metal. **126** (2002) 245.
17. Z. Shi, Y. Lian, F.H. Liao, X. Zhou, Z. Gu, Y. Zhang, S. Iijima, H. Li, K.T. Yue, S. Zhang, J. Phys. Chem. Solid. **61 (**2000) 1031.
18. A. Huczko, Appl. Phys. A **74** (2002) 617.
19. T. Guo, P. Nikolaev, A. Thess, D.T. Golbert, R.E. Smalley, Chem. Phys. Lett. **243** (1995) 49.
20. A.C. Dupuis, Progr. Mater. Scie. **50** (2005) 929.
21. C. Perrego, P. Villa, Catal. Today **34** (1997) 281.
22. F. Pinna, Catal. Today **41 (**1998) 129.
23. (a) V.O. Nyamori, N.J. Coville, Organometallics **26** (2007) 4083; (b) D. Jain, A. Winkelm, R. Wilhelm, Small **2** (2006) 752; (c) J. Liu, M. Shao, Q. Xie, L. Kong, W. Yu, Y. Qian, Carbon **41** (2003) 2101; (d) M. Laskoski, W. Steffen, J.G.M. Morton, M.D. Smith, U.H.F. Bunz, J.Am. Chem. Soc. **124** (2002) 13814; (e) B.El

Hamaoui, L. Zhi, J. Wu, U. Kolb, K. Müllen, Adv. Mater. **17** (2005) 2957; (f) L. Zhi, T. Gorelik, R. Friedlein, J. Wu, U. Kolb, W.R. Salaneck, K. Müllen, Small **1** (2005) 798; (g) J. Wu, B. El Hamaoui, J. Li, L. Zhi, U. Kolb, K. Müllen, Small **1** (2005) 210; (h) S. Liu, X. Tang, Y. Mastai, I. Felner A. Gedanken, J. Mater. Chem. **10** (2000) 2502; (i) C. Wu, X. Zhu, L. Ye, C. OuYang, S. Hu, L. Lei, Y. Xie, Inorg. Chem. **45** (2006) 8543; (j) P.I. Dosa, C. Erben, V.S. Iyer, K.P.C. Vollhardt, I.M. Wasse, J. Am. Chem. Soc. **121** (1999) 10430; (k) V.S. Iyer, K.P.C. Vollhardt, R. Wilhelm, Anew, Chem. Int. Ed. **42** (2003) 4379.

24. T. Belin, F. Epron, Mater. Scie. Eng. B **119** (2005) 105.
25. J.W. Niemantsverdriet, *Spectroscopy in Catalysis: An Introduction*, 2nd ed., Wiley-VCH, p. 137, 2000.
26. Z.L. Wang, P. Poncharal, W.A. de Heer, J. Phys. Chem. Solid. **61** (2000) 1025.
27. S. Xie, W. Li, Z. Pan, B. Chang, L. Sun, J. Phys. Chem. Solid. **61** (2000) 1153.
28. C. Gommes, S. Blacher, N. Dupont-Pavlovsky, C. Bossuot, M. Lamy, A. Brasseur, D. Marguillier, A. Fonseca, E. McRae, J.B. Nagy, J.-P. Pirard, Colloids and Surfaces A: Physicochem. Eng. Aspect. **241** (2004) 155.
29. A. Jorio, M.A. Pimenta, A.G.S. Filho, R. Saito, G. Dresselhaus, M.S. Dresselhaus, New J. Phys. **5** (2003) 139.
30. J. Maultz, S. Reich, C. Thomsen, Phys. Review B. **65** (2002) 233.
31. M.S. Dresselhaus, G. Dresselhaus, R. Saito, A. Jorio, Phys. Reports **409** (2005) 47.
32. R.K. Rana, Y. Koltypin, A. Gedanken, Chem. Phys. Lett. **344** (2001) 256.
33. M.E. Brown, *Handbook of thermal analysis and calorimetry vol.1, principles and practice.* Elsevier: Amsterdam, 1998.
34. P.J. Haine, *Thermal methods of analysis. Principles, applications and problems.* Chapman and Hall: London, 1995.
35. Micromeritics TriStar 3000 Operating Manual, 2007.
36. G. Thiele, M. Poston, R. Brown, Micromertics Analytical Services and MVA Scientific consultants, www.particletesting.com. (accessed on 2nd April 2008).
37. J.-P. Salvetat, J.-M. Bonard, N.H. Thomson, A.J. Kulik, L. Forr´o, W. Benoit, L. Zuppiroli, Appl. Phys. A **69** (1999) 255.
38. R. Pagani, C&EN, **1** (1999) 31.
39. M. M. J. Treacy, T. W. Ebbesen, J. M. Gibson, Nature, **381** (1996) 678.

40. J. Tang, A. Matsushita, T. Tikegawa, M. Yudusaka, S. Bandow, S. Iijima, Mater. Rec. Soc. Symp. Proc., **593** (2000).
41. Y.Q. Zhang, G.R. Liu, X. Han, Phys. Lett. A **349** (2006) 370.
42. R.B. Pipes, P. Hubert, Compos. Scie. Technol. **62** (2002) 419.
43. http://www.phys.psu.edu/people/display/index.html?person_id=202;mode=research;research_description_id=419 (accessed on 3rd June 2008).
44. http://mmptdpublic.jsc.nasa.gov/jscnano/background.htm (accessed on 3rd June 2008).
45. http://www.nanoten.com/ntyp.html (accessed on 3rd June 2008).
46. http://cmliris.havard.edu/ (accessed on 3rd June 2008).
47. http://en.wikipedia.org/wiki/Carbon_nanotube (accessed on 4th June 2008).
48. P. Serp, M. Corrias, P. Kalck, Appl. Catal. A **253** (2003) 337.
49. J. M. Moon, K. H. An, Y. H. Lee, Y. S. Park, D. J. Bae, D. S. Park, J. Phys. Chem. B **105** (2001) 5677.
50. R.H. Baughman, A.A. Zakhidov, W.A. de Heer, Science **297** (2002) 787.
51. M.J. Pitkethly, Nano Today, (2004) 20.
52. http://www.nanoten.com/ntyp.html (accessed on 13th March 2008).
53. http://www.netcomposites.com/netcommerce_features.asp?1485 (accessed on 13th March 2008).
54. http://en.wikipedia.org/wiki/Carbon_nanotube#_ref-24 (accessed on 13th March 2008).
55. http://d.scribd.com/docs/1skmz11asidk3q2rro4q.pdf (accessed on 15th January 2009).

Chapter 3

Carbon nanotubes from supported catalysts: a literature review

3.1 Introduction

The CVD synthesis of CNTs basically involves two main steps; the preparation of the catalyst in the first step followed by the actual synthesis of the CNTs as the second step. The catalyst preparation step is crucial since it determines the properties and quantities of carbon materials produced. Therefore, while this chapter aims to discuss the types of carbon materials produced using different metals, supports/substrates as well different sources of carbon; the role of these are discussed first to state their significance in CNT synthesis.

The ***metal*** (catalyst) is the key component in the synthesis of CNTs. It serves as the active (nucleation) site for the growth of CNTs. Several studies have shown that without the metal particle, the CVD synthesis of CNTs is not possible [1a]. However, a recent study by Liu *et al*. [1b] has shown that CNTs (in this case single-walled CNTs) could be efficiently be synthesized from Al_2O_3 ceramic nanoparticles without any metal catalyst particle. The CNTs were grown using alcohol chemical vapour deposition using ethanol as a carbon source. The parameters determining the catalytic properties in the CVD synthesis of CNTs have been reviewed by Dupuis in 2005 [1]. According to Dupuis and others [2-6], the catalytic properties of the metal are determined by:

(i) the composition e.g. electronic structure and carbon solubility;
(ii) the morphology e.g. size and crystallographic orientation;
(iii) the preparation method, which affects the metal particle size and dispersion (Fig. 3.1);
(iv) the support e.g. metal-support interactions and
(v) pre-treatment conditions e.g. effect of electronic structure and catalyst morphology.

Therefore during the preparation of metal particles on substrates, the effect of these properties should not be ignored since they influence the activity of the catalyst in the decomposition of the carbon.

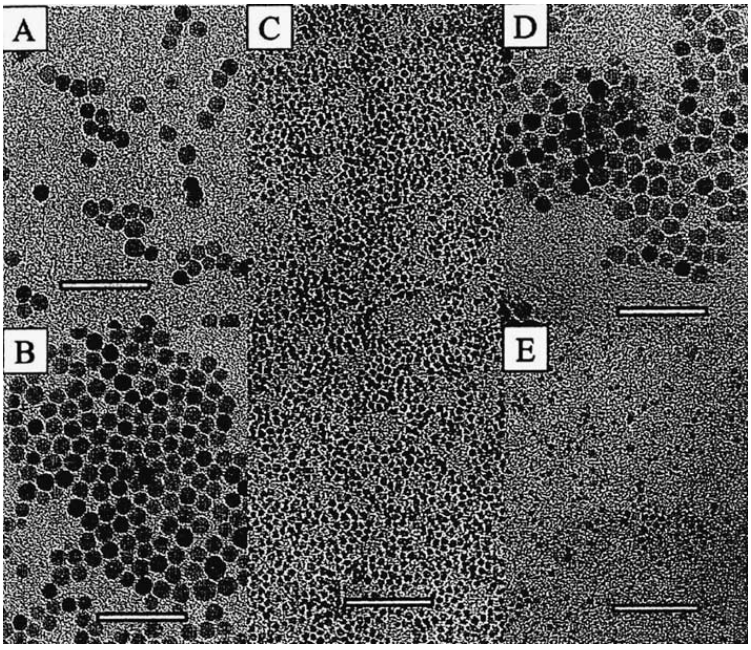

Fig. 3.1: Iron-molybdenum nanoparticles synthesized with different protective agents. A: 1 mmol of octanoic acid. B: 2.5 mmol of octanoic acid. C: 1 mmol of octanoic acid and 1 mmol of bis(2-ethylhexyl)amine. D: 1 mmol of bis(2-ethylhexyl)amine. E: 2.5 mmol of bis(2-ethylhexyl)amine. The scalebars in all figures are 100 nm [1].

The ***support*** (substrate) is usually an inorganic material with high thermal stability and it plays an important role in the dispersion of the metal particles [1,2]. Studies have shown that the use of a support to disperse a chosen metal is not only of economic benefit (lower preparation costs/longer productive lifetime) but the substrate can also influence catalyst performance through electronic interaction(s), spillover, and migration effects [4,8-11].

It has been observed that unsupported metal particles are not suitable for the decomposition of hydrocarbons to form CNTs [12]. A wide range of materials have been used as supports for various metals i.e. both monometallic and bimetallic systems. **Table 3.1** gives some of the physical characteristics of the materials commonly used as supports for catalysts. The use and influence of these supports in CNT synthesis will be described in Section 3.4. The choice of support is largely driven by the end use

(application) of the materials as the support is usually found in the product and becomes an impurity. In addition, the metal-support interaction also plays a role in determining the efficiency of the catalyst in CNT formation [1-6].

Table 3.1: Some important properties (general) of commonly used commercial substrates for CNT synthesis [7].

Supporting material	**Meting point (°C)**	**Solubility in H_2O (at 20 - 25°C)**	**Solubility in other solvents**
SiO_2	1650 (±75)°C	insoluble	sol in HF
TiO_2	1870°C	insoluble	sol in conc H_2SO_4 & alkali
Al_2O_3	2054°C	insoluble	very slightly sol in acid & alkali
Zeolite (e.g Y-types, HZSM-5)	varies with type	insoluble	-
MgO	2800°C	0.00062 g/100ml	sol in acid & NH_4 salts, insol in alcohol
La_2O_3	2300°C	0.0004 g/100 ml	Sol in acid & NH_4Cl
CeO_2	2100°C	insoluble	sol in conc H_2SO_4 & HNO_3, insol in dilute acid
Si	1410°C	insoluble	Sol in HF+HNO_3
$CaCO_3$	825°C	0.000153 g/100 ml	sol in acid & NH_4Cl
CaO	2572°C	dissolves	sol in acid
$Ca(OH)_2$	512°C (decomposes)	0.185 g/100 ml	sol in NH_4 salts & acid
$MgCO_3$	350°C (decomposes)	10.6 mg/100 ml	sol in acid
$Mg(OH)_2 \cdot 4H_2O$	350°C	0.0012 g/100 ml	Sol in acid & NH_4 salts
$BaCO_3$	811°C	0.0022 g/100 ml	sol in acid & NH_4Cl
NaCl	801°C	35.9 g/100 ml	Slightly sol in alcohol, liquid, NH_3; sol in glycerium, insol in HCl
$CaCl_2$	772°C (anhydrous)	74.5 g/100 ml (20 °C)	Sol in alcohol, acetone & acetic acid

* sol = soluble; insol = insoluble

While most of the materials may be suitable for use as supports, their choice is also influenced by their cost and availability. Low cost materials are usually preferred especially if production of the nanomaterials at large scale is desired. Also, as will be

shown in Section 3.4, the materials with melting temperatures below 600°C are generally not suitable for CNT synthesis.

3.2 Catalyst preparation methods

In order to have metal-support mixtures (hereafter to be referred to as the catalysts) with large specific surface area and consequently a maximum specific activity, the active metal component is usually deposited on the surface of a support, preferably a highly porous and thermostable material (with a high surface area and suitable mechanical strength) which is not only able to disperse the metal, but also to increase its thermal stability and hence the catalyst life [2]. Catalysts can be prepared using different methods and these have been described in the literature [1-3,5a]. Some commonly used methods for the preparation of catalysts for CNT synthesis are listed below:

(i) Impregnation ("incipient wetness" and "wet" impregnation)
(ii) Deposition-precipitation
(iii) Reverse micelles
(iv) Co-precipitation
(v) Sol-gel
(vi) Ion-exchange precipitation

The first three methods have been used in this study. The procedures involved for each of the methods will be explained in the experimental sections. Generally, the preparation of catalysts involves a combination of some or all of several unit operations/steps that determine the catalytic properties (**Table 3.2**) [3].

Table 3.2: Unit operations in catalyst preparation.

1. Precipitation	7. Calcination
2. Gelation	8. Impregnation
3. Ageing	9. Crushing and grinding
4. Decantation, filtration, centrifugation	10. Mixing
5. Washing	11. Activation, Reduction
6. Drying	

3.3 CNT growth mechanism on supported catalysts

A number of studies have reported on the growth mechanism of CNTs synthesized on supported catalysts [1,13-26]. The overall description of the growth mechanism varies from one report to the other, but they all postulate that the mechanism can occur in two different ways depending on the position of the catalyst with respect to the substrate (metal-support interactions). When weak interactions between the metal and the support exist, then the tip-growth mechanism is observed. When strong interactions exist then the extrusion/root/base-growth mechanism is observed (Fig. 3.2) [27]. It is believed that the mechanisms can occur simultaneously since both interactions can exist in the same catalyst. In general, the carbon filament growth mechanism is based on the concepts of the vapour-liquid-solid (VLS) theory developed by Wagner and Ellis [14].

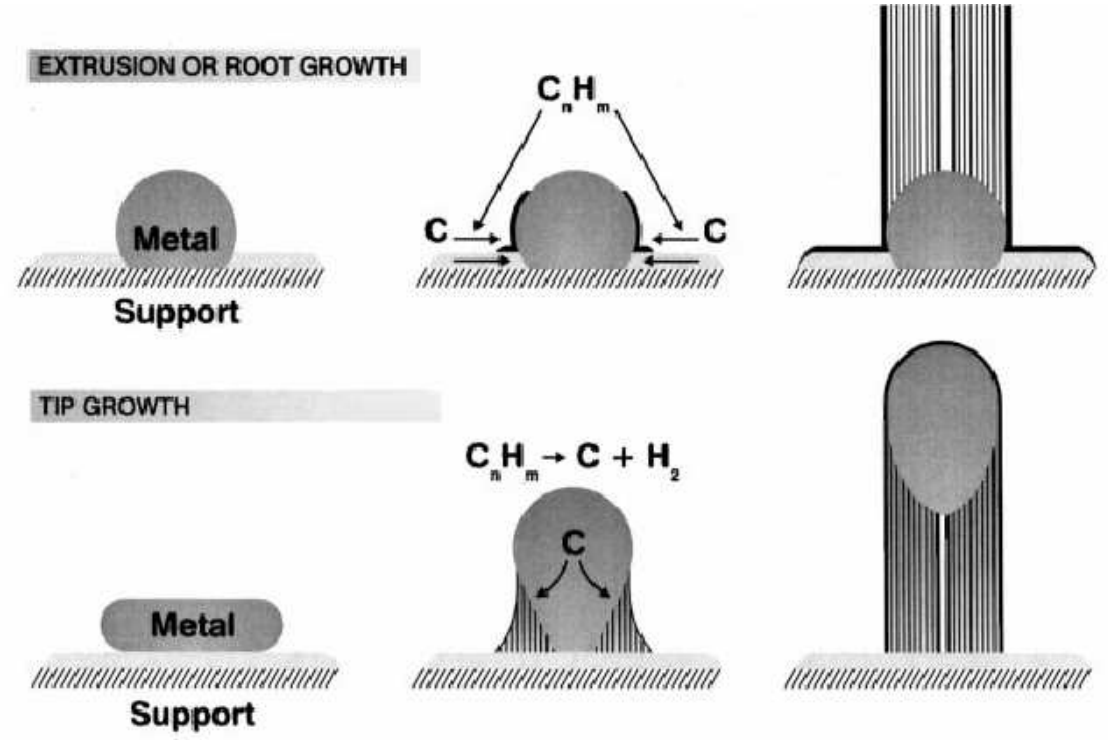

Fig. 3.2: The two types of CNT growth mechanisms [27].

Seidel and co-workers [20] reported on the effect of the interaction between the support and the catalyst on the SWCNT growth. It was observed that a weak interaction inhibits SWCNT growth since the catalyst particles become too large, a moderate interaction gives particles with the right size and shape for SWCNT growth, whereas a strong interaction prevents formation of suitable particles. Other studies have tried to explain the processes that occur during the gas phase pyrolysis of hydrocarbons to form CNTs [28]. Brukh *et al.* [24] studied the self-assembly and reaction pathways leading to CNT formation using a tubular plug flow reactor and used a kinetic simulation to predict the reaction pathways. In their study, the CVD precursor (C_2H_4) decomposed to form elemental carbon via a sequence of free radical reactions (Fig 3.3), which then assembled as CNTs or non tubular carbon (NTC). A similar observation can be expected for other linear hydrocarbons.

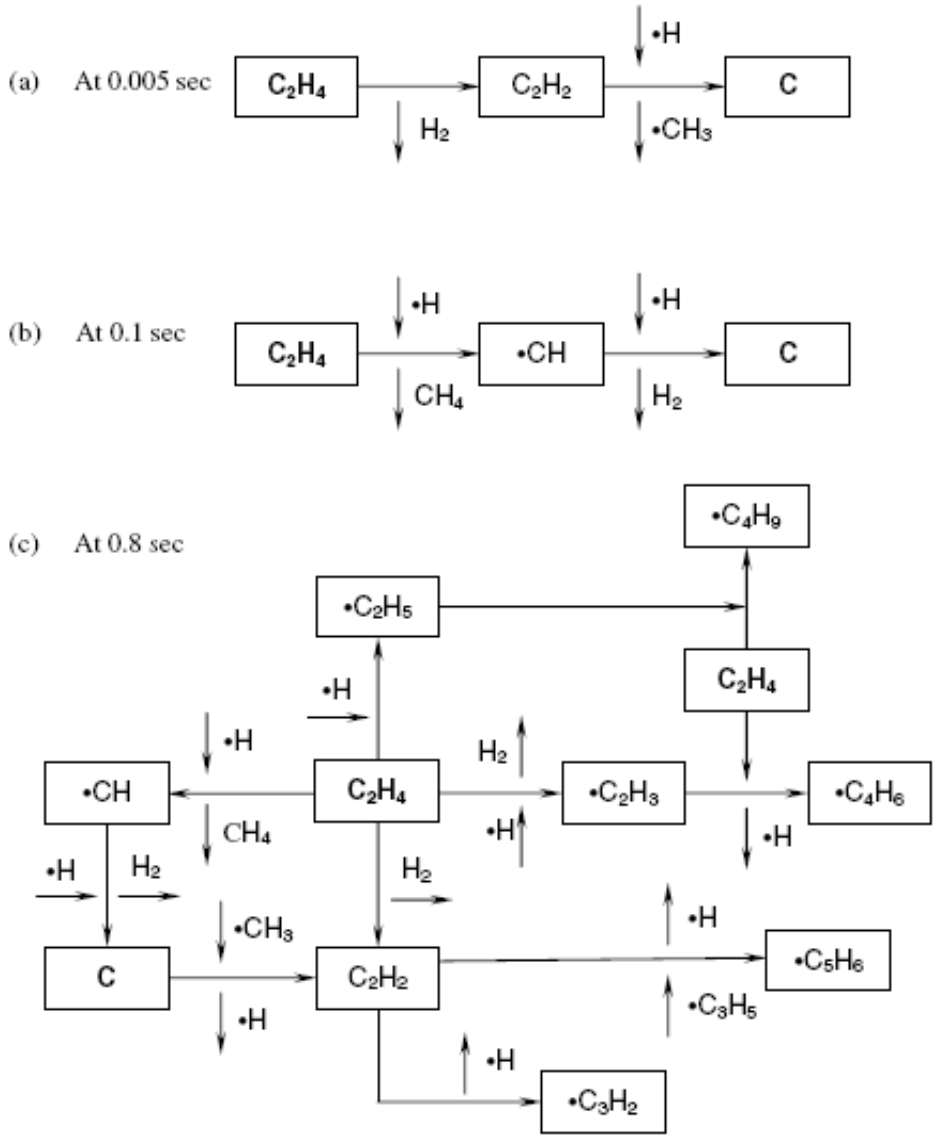

Fig. 3.3: Major pathways to consumption of C_2H_4 and production/consumption of C at different residence time [24].

3.4 Transition metal elements as catalysts for the CVD synthesis of CNTs

Transition metal elements (e.g. Fe, Co, Ni, Ru, Cu, Mo, V, Rh, Au etc) have been used extensively as catalysts for the CVD synthesis of CNTs (i.e. SWCNTs, DWCNTs and MWCNTs) and other carbon nanomaterials. Here, a literature review of the use of these metals is presented. Whilst most of the work done since the discovery of CNTs is presented, we acknowledge the fact that some papers may unintentionally be left out but the information gathered should sufficiently cover the key literature to date.

In this literature review, the information on the use of transition metal elements as catalysts for the CVD synthesis of CNTs has been presented in the form of tables to facilitate a quick evaluation of key information. The information presented in each table includes the *catalyst* used, the *support*, the *carbon source*, *reaction conditions* (e.g. temperature and gas flow rates), reactor design and the *distinct properties* of the CNTs obtained. A summary of key factors is given in the last column of each table. Whilst there are numerous forms of carbon that can be produced by the CVD technique, the focus will be on MWCNTs (**Table 3.3**), SWCNTs (**Table 3.4**) and DWCNTs (**Table 3.5**). Studies involving the use of $CaCO_3$ as a support in the CVD synthesis are presented separately (**Table 3.6**) in view of the fact that this is the support used in this study.

Transition metals have also received extensive attention in the form of organometallic complexes for the CVD synthesis of CNTs. The most widely used organometallic complexes are those of Co, Fe, Ni and Ru. The organometallic complexes have become important metal precursors especially for the *continuous production* of CNTs and can lead to formation of other forms of shaped carbon materials besides CNTs. An enormous amount of research has been done using organometallic complexes as catalysts for the synthesis of CNTs using the *floating catalyst process and autoclave processes*. For a better understanding of the chemistry involved during the CNT synthesis using organometallic complexes in the floating catalyst and autoclave processes, the literature has been reviewed extensively in Chapter 4.

Table 3.3: The use of supported transition metal elements as catalysts for the CVD synthesis of **MWCNTs**.

Catalyst	Support/substrate	Carbon source	CNT synthesis conditions	Distinct properties of CNTs and summary	Reference
Fe	Y-Zeolite (Na-Y)	C_2H_2	CNTs were produced by using 10% C_2H_2 in N_2 with flow rate of 60 m1/min for 30 min at 700°C in a horizontal fixed bed reactor.	MWCNTs diameters were controlled by using zeolite supports with different pore sizes. The larger the diameter of the zeolite pore support, the larger the size of the nanoparticles deposited and the larger the size of the CNTs produced.	29
Fe	Silicon wafer	C_2H_2	A gas mixture of C_2H_2 (18 sccm), H_2 (100 sccm); $Fe(CO)_5$ was used with an excess of Ar (500 sccm) as diluter and carrier gas was used at 750°C in a horizontal furnace with a water cooled injector.	Large arrays of aligned MWCNTs were obtained using a cheap single-furnace method.	30
Fe	SiO_2/Ti	C_2H_2	CNTs synthesis entailed the passage of C_2H_2 at 30 sccm for 10 min at 850 and 950°C in a fixed bed reactor. The deposited Fe film was pre-treated by NH_3.	Bamboo shaped MWCNTs were grown and characterized by AFM. Greater diameters and compartment distances of the bamboo structures were observed for the BS-MCWNTs grown at 950°C than for those grown at 850°C.	31
Fe	ammonium-exchanged zeolite	acetonitrile	An alumina boat with 0.2 g of ferric nitrate impregnated zeolite (Na or NH_4 containing) was placed in a flow through tube furnace, which was then heated to the required temperature (in the range 700 - 900°C) under a flow of Ar. The temperature of the furnace was maintained at the target temperature for a specific duration (1, 10, or 20 h) under a flow of Ar saturated with acetonitrile.	Bundles of aligned N-doped carbon nanotubes were prepared by a simple CVD method. The nitrogen content of the nanotubes varied between 6 and 9 wt % depending on the CVD temperature at which they were prepared.	32
Fe (or Co, Ni)	SiO_2	C_2H_2	The catalyst films were etched by introducing NH_3 gas into the quartz reactor at 750 - 950°C. CNTs were sequently grown	The respective growth rate of CNTs shows that the performance of catalysts is in the order of Ni > Co > Fe. Bamboo-like structured CNTs were exclusively	33

Table 3.3 continued

			using C_2H_2 with a flow rate of 30 sccm for 10 min at the same temperature.	produced irrespective of the catalyst used.	
Fe	SiO_2	C_2H_2	CNTs were synthesized over several Fe/SiO_2 catalysts, by the decomposition of $^{13}C_2H_2$ (99% ^{13}C isotopic purity) using a pulsed method at 700°C.	^{13}CMAS-NMR technique was revealed as a powerful tool, not only to characterize the carbon species generated during CNTs synthesis, but also to detect a new signal near 75 ppm, ascribed to small superparamagnetic carbide particles, as it was also supported by ^{57}Fe Mössbauer spectroscopy. A tip growth CNT growth mechanism was observed.	34
Fe	SiO_2	C_2H_2	A C_2H_2/NH_3 mixture gas was introduced over the catalyst at a flow rate of 30 and 60 sccm, respectively, for 10 min at 900°C.	MWCNTs with bamboo partitions were obtained. The Fe nanoparticles are easily oxidized to Fe_2O_3 after the synthesis, but the nanoparticles during the CNT synthesis are shown to be in the liquid iron phase due to the reducing force of NH_3. This is revealed by cross-sectional transmission electron microscopy examinations of the nanoballs and the Fe inclusions along with relevant chemical analyses.	35
Fe	SiO_2	C_2H_2	The catalyst was fluidized initially for 20 min, at room temperature, in N_2 (flow rate 600 ml/min). Then H_2 was also introduced into a mixture of N_2/H_2 (540/60 ml/min) heating from room temperature to 723 K, with a heating ramp of 10 K/min. After 10 min longer at this temperature, the reactor was heated to 973 K at 10 K/min in N_2 (600 ml/min). Once a temperature of 723 K was achieved, acetylene was introduced into a reaction mixture of $N_2/C_2H_2/H_2$ (580/15/10 ml/min) over 60 min.	The results presented indicate that catalysts become more active in acetylene decomposition at higher iron contents, but this activity results in lower selectivity to homogeneous and well-defined CNTs, yielding high proportion of CNFs, capsules of carbon, and amorphous carbon.	36
Fe, Ni, Co	montmorillonite	C_2H_2	The metal ion exchanged or metal salt impregnated clay precursors were then	The successful growth of MWCNTs on montmorillonite surfaces has been attained via CVD	

Table 3.3 continued

			inserted into a fixed bed flow reactor furnace and degassed at 80°C with Ar for 20 min. The temperature was raised to 700°C and then a mixture of Ar/C_2H_2 15% in C_2H_2 was introduced. A total flow rate of 45 mL/min was kept constant for various periods of time.	of acetylene and studied by means of electron microscopy, XRD, Mössbauer spectroscopy, and thermal analysis measurements.	37
Fe	Mesoporous silica	C_2H_4	MWCNTs were grown by thermal CVD in a tube furnace using pure ethylene at atmospheric pressure. Growth time was typically 30 min, and the ethylene flow rate was 300 or 900 sccm.	Well-aligned CNTs were obtained with C16EO10 films at relatively high Fe loading levels (Fe:Si molar ration 1.80). Similar CNTs were grown on P123 mesoporous silica films. On CTAC mesoporous silica films, CNTs grew only parallel to the substrate in cracks. It was also demonstrated that CNT diameters can be controlled by changing the Fe loading level in the mesoporous silica substrates.	38
Fe	Si and Al substrates	C_2H_2	The furnace was then purged with 100 ml/min nitrogen for 5 min before a mixture of 2 ml/min C_2H_2 and 98 ml/min N_2 was introduced at 0.5 bar for 0.5 - 3 h. The overall gas pressure of 0.5 bar (2% C_2H_2 and 98% N_2 was kept constant for the time of deposition. The temperature of the substrate was chosen according to the substrate material - 700°C and 750°C for Si, 630°C and 650°C for the Al substrate.	Multiwall type CNTs with a length in the range of 1 - 10 nm and a diameter of 5 - 100 nm were produced. It was observed that the size and the density of the nucleation centres on a substrate determine the diameter and the density of nanotubes. The CNTs grow well aligned only for very high nucleation densities.	39
Ni, Co and Fe	glass substrate with Cr buffer layers	C_2H_2, C_3H_4 and CO	The CNT growth was performed at the temperature at approximately 550°C by the PECVD method at various gas flow rates and pressures.	The study showed that as the flow rate ratio of NH_3/C_3H_4 increased, the growth rate of CNTs was enhanced and the average diameter became smaller. Ni was more efficient for the field emission of CNTs than any other catalyst metal when using the C_2H_2 gas, and in case of C_3H_4 as the carbon source, Co played an important role as the catalyst. When using	40

Table 3.3 continued

				the CO gas, Fe was the most activated catalyst for the CNTs growth under the flow rate ratio of CO/NH_3 of 18.	
Fe	SiO_2, Al_2O_3, ZrO_2 and TiO_2	CH_4	Catalysts were tested in a fluidized bed at 600 - 800^oC in a quartz reactor. Methane consumption was preset at 12 cm^3/min in all the cases.	The maximal carbon yield, 45 g per g of iron, was obtained with the Fe/SiO_2 catalyst comprising silica in amounts of 15 wt%. Carbon nanotubes with thin walls built up by coaxial cylindrical graphene layers were formed in large amount over the Fe/Al_2O_3 catalyst. Centres of growth of *octopus*-like nanotubes were observed.	41
Fe	SiO_2	Ferrocene and cyclopentadienyl iron dicarbonyl dimer	The deposition experiments were performed at 830 °C and with Ar (120 sccm) in a dual zone furnace. The precursor was transfered to the hot zone with a rate of 5 mg/min (ferrocene) or 2 mg/min (cyclopentadienyliron dicarbonyl dimer). The deposition time was set to 10 min.	A CVD synthesis route of Fe-filled CNTs is presented and how to control the diameter distribution by utilizing defined multi-layered substrates. It was shown that beside ferrocene, cyclopentadienyliron dicarbonyl dimer is also an ideal source of carbon and iron for the synthesis of aligned Fe-filled CNTs.	42
Fe and Fe/Ni	Al_2O_3	C_2H_4	A mixture of N_2 and C_2H_4 (99.99% purity; N_2 /C_2H_4 1:1; total flow rate 1.5l /min) is fed into the reactor and the ethylene decomposed on the catalyst at 823 K and normal pressure. The reaction is carried out for about 5 h and then the reactant flow is stopped and the reactor cooled in a nitrogen flow.	A small amount of Ni introduced into the catalyst can significantly increase the yield of CNTs, but the CNTs change from straight tubes with concentric parallel carbon sheets to helical tubes of the fish-bone type. Raman characterization of CNTs prepared at 823 and 1023 K and CNTs annealed at 2473 K shows that CNTs deposited on the Fe/Ni /Al_2O_3 catalyst have poor crystallinity, as compared with that on the Fe/Al_2O_3.	43
Fe	SiO_2	CO	The CNT synthesis was performed in a vertical quartz reactor. For a given reaction, the catalysts were reduced in 100 ml/min H_2/He (25 vol.%) at 600^oC for 6 h. Subsequently, synthesis gas (CO/H_2 = 40:10	It was shown that CNT growth rate depends strongly on the catalyst particle size. An optimum particle size exists for the maximum growth rate, which has been demonstrated at two different temperatures.	44

Table 3.3 continued

			ml/min) was introduced, and the reaction was carried out for 9.5 h at 600°C and 6.5 h at 650°C.		
Fe	graphite flakes, silica, NaY, and ZSM-5	cetylene, ethylene and propylene	The gas decomposition temperature range was 650-800°C. The gas feeds applied during the reactions were the following: 8 ml/min acetylene (or other hydrocarbon) (Alpha gas, 99.5% purity) in nitrogen flow of 75 ml/min in the fixed bed flow reactor, and the same amount of acetylene in nitrogen flow of 30 ml/min in the fluidized bed reactor.	By using Fe/silica, the highest activity ever observed in catalytic nanotube formation can be reached. Concerning purification, despite the lower formation of carbon deposit on Fe/zeolite Y (impregnation), when compared to Fe/silica (ion-adsorption precipitation), the isolation of nanotubes is easier when the support is zeolite. In fact, zeolite catalysts being soluble in aqueous HF, the isolation of nanotubes with some amorphous carbon from Co/zeolite Y has already been reported with 76% yield.	45
Fe	MgO	C_5H_{12} and C_2H_2	Typically 1.5 g of precursor powder was filled in the quartz tube and the atmosphere was purged with 410 scm^3 argon for 5 min. Then the furnace was heated to the synthesis temperature (450 - 850°C). The synthesis was started with the introduction of 42 scm^3 acetylene mixed with 368 scm^3 argon for 20 min.	It has been shown that the fluidised-bed CVD synthesis of CNTs on a Fe_2O_3/MgO precursor powder is very well suited to produce large quantities of nanotubes. Depending on the synthesis temperature both MWCNT and SWCNT could be synthesised with acetylene as the carbon source. For temperatures of 500-650°C MWCNT and for higher temperatures of 700 - 850°C SWCNT were synthesised.	46
Fe	Al_2O_3	C_2H_6	The catalyst was first treated in hydrogen under the conditions stated. After this treatment the hydrogen flow was replaced by a mixture of ethane and hydrogen (60:60 ml/min) and the temperature of the furnace was rapidly increased (20°C/min) to 750°C. The synthesis was carried out at 750°C for 2 h.	According to the observed results ethane is an active carbon source for growing MWCNTs with high yield and selectivity. The reaction temperature should be kept ≤750°C as synthesis carried out at 800°C under similar reaction conditions led to the formation of amorphous soot and carbon nanoparticles mixed with nanotubes.	47
Fe	SiO_2	C_2H_2	The Fe-deposited SiO_2 substrates were pre-	The CNTs produced have bamboo structure, closed	

Table 3.3 continued

			treated using NH3 flow at 350 sccm prior to growing the CNTs. The CNTs were grown using a two stage furnace at 550°C using C_2H_2 flowing at 120 sccm for 20 min. The first zone was maintained at 850°C to activate the reactant gas.	tip, and defective graphite sheets.	48
Fe	SiO_2 and zeolite Y	C_2H_2	Decomposition of C_2H_2 was studied in a fixed-bed flow reactor at 700°C with a time of contacting with C_2H_2 (reaction time) of 30 min. Each reaction was carried out using the same flow of acetylene (8 ml/min) and nitrogen (75 ml/min) and a catalyst amount of approx. 30 mg.	Co/silica catalysts produced from a Co solution of pH 8, can produce carbon nanotubes of well-graphitized structure with high activity. Straight nanotubes as well as bent and helically wound nanotubes were observed. Using the zeolite Y as support, it was possible to optimize the method for the deposition of almost all carbon in the form of tubular filaments.	49
Fe	SiO_2	C_2H_4	CNT synthesis was carried out in a fluidized bed reactor at 550°C - 700°C. The catalyst was activated at 650°C for 120 min by flowing a mixture of H (50 sccm) and He (100 sccm). The flow of C_2H_4 was set to 22.4 sccm for all of the reactions performed.	The materials produced from C_2H_4-H_2 mixtures on Fe-SiO_2 catalysts is mainly composed of MWCNTs homogeneously distributed on the support, with small amounts of encapsulated particles, depending on the processing conditions. This process allowed an homogeneously distributed deposition of nanotubes (10-20 nm diameter), that remain anchored to the support.	50
Ni	Al_2O_3	ethylene or pyrene	The ethylene or pyrene was used in the CVD process with reactor temperatures of 545°C for Ni-catalyzed CVD and 900°C for the uncatalyzed process.	The resultant carbon nanostructures were uniform hollow tubes with open ends. Increasing the deposition time converted the carbon nanotubes into carbon nanofibers.	51
Ni	Ni grids	C_2H_4	Ethylene was introduced at a flow rate of 50 sccm, while the flow rate of H_2 was adjusted to 800 sccm. After a period time of growth (2 min, unless otherwise stated),	At lower temperature, nickel nanoparticles formed from fragmentation of nickel are the nucleation sites for carbon nanotubes; however, at higher temperature, carbon nanotubes only nucleate from	52

Table 3.3 continued

			ethylene was shut off and the whole system was cooled down to room temperature under hydrogen protection. CVD growth was carried out at 650°C, 700°C, 750°C, and 850°C, respectively.	grain boundaries and defective sites. Based on the growth mechanism of nanotubes, small amounts of Fe nanoparticles were deposited on the nickel substrate to introduce more nucleation sites at elevated temperature, and the density of nanotubes on the surface of the substrate was greatly improved.	
Fe	Si, porous Si, SiO_2, Si_3N_4, Al_2O_3, and Cr.	C_2H_2	Ar gas flowed into the quartz reaction tube while the furnace was heated. Ammonia (NH_3) was then introduced into the quartz reaction tube at a flow rate of 300 sccm for 20 min without introducing acetylene (C_2H_2) gas. After NH_3 treatment, acetylene gas was introduced into the quartz tube at a flow rate of 40 sccm for 5 - 20 min, and carbon nanotubes were grown on Fe-coated Si substrates by pyrolysis of acetylene at 800°C for 5 to 20 min.	The study showed that the pulsed laser deposition (PLD) technique is very useful for the deposition of Fe films playing a catalytic role in CNT growth. The Fe film deposited by PLD adhered well to the substrates because of high kinetic energies of ablated particles from a metal target. Using a PLD and a lift-off method, we developed a selective growth of CNTs on a patterned Fe-coated Si substrate. The vertical alignment of carbon nanotubes is due to the appropriate density of Fe nanoparticles formed from the thermal annealing of the film deposited by PLD and van der Waals interactions between neighbouring CNTs.	53
Fe, Ni, and Fe-Ni	Al_2O_3	C_2H_2	CNTs were synthesized at 600°C by flowing 10:100 sccm C_2H_2/H_2. In order to understand the growth rate of CNTs as well as to increase the carbon yield, the growth reactions were carried out for 5, 15, 30, 45, 60, 75, and 90 min. The effect of growth temperature on the carbon yield was also examined by carrying out the reaction at 600 - 700°C.	High density CNTs of 20 nm diameter were grown over the 20Fe:20Ni:60Al_2O_3 catalyst, whereas low growth density CNTs of 40 and 50 nm diameter were found over 40Fe:60Al_2O_3 and 40Ni:60Al_2O_3 catalysts. The carbon yield and the quality of CNTs increased with increasing temperature.	54
Fe	SiO_2	C_2H_2	The catalyst (100 mg) was heated, in a mixture N_2/H_2 (100/100 ml/min), from room temperature to 700°C, with a heating ramp of 10°C/min. After 120 min more	The paper showed that the CVD method with iron catalysts produces homogeneous CNTs in general, but their structure seem to be highly dependent on the metal content, the iron precursor employed (e.g.	

Table 3.3 continued

			under these conditions, acetylene was introduced in a reaction mixture of 7% of C_2H_2 in N_2, total gas flow of 500 ml/min, during 120 min. After this time the reactor was cooled down to room temperature in N_2 atmosphere.	iron-nitrates, iron-phthalocyanines) and the preparation conditions (i.e. impregnation, or deposition-precipitation) of the silica supported catalysts. Here the iron-nitrates produced the highest activity in acetylene decomposition; the iron-phthalocyanine produced the best quality CNTs, in high quantity, size homogeneity and absence of amorphous carbon. The impregnation method seemed to allow more homogeneous metallic dispersion on the silica support than the Deposition-precipitation method.	21
Fe	Al_2O_3	C_2H_2	A mixture of 2-6 sccm (0.4 - 1.2%) C H and 500 sccm N_2 is introduced at 1 bar for 15 - 180 min. The temperature of the substrate is varied between 600 and 650^oC, the upper limit being determined by the melting point of the aluminium at 660^oC.	The study revealed that the density and the length of the CNTs were greatly influenced by the precursor concentration, the time of deposition, the temperature and the ratio of C_2H_2:N_2. A growth mechanism of the CNTs is proposed.	55
Fe-Mo	Al_2O_3	propylene	Catalytic pyrolysis of propylene was performed in a nano-agglomerate fluidized-bed reactor (NAFBR) of 196 mm I.D. Propylene and N_2 were fed into the reactor through a gas pre-heater. The flow rate of propylene and N_2 gas mixture was selected to ensure turbulent operation at the reaction temperature of 700^oC.	The structure and formation mechanism of CNT agglomerates in an NAFBR involves initial CNT growth destroying the structure of the catalysts, sub-agglomerate formation and expansion of agglomerates due to CNT growth. The microstructure of CNTs produced in an NAFBR can be adjusted by controlling the catalyst structure and the level of agglomerate development.	56
Co-Mo, Co-V and Co-Fe	Zeolite (NaY) and corundum alumina (CA).	C_2H_2	The syntheses of the CNTs were performed in a fixed-bed reactor consisting of a furnace with a quartz tube in which the decomposition of acetylene is carried out. The acetylene is passed over the catalyst, spread on a quartz boat, for 1 h at a temperature of 700°C. The flows of the	When Fe or V is added to Co, the carbon deposit increased. From histograms representing the outer diameter distributions, it is clear that the outer diameter of the nanotubes can be controlled by choosing the appropriate catalyst. Thin nanotubes, in the range of 7.5 to 9.2 nm, in high yields could be synthesized using a mixture of Co and V supported	57

Table 3.3 continued

			carrier gas (nitrogen) and of the reacting gas (acetylene) were set to 300 and 30 ml/min, respectively.	on zeolite NaY. Co-Mo catalysts favoured quality tubes.	
Co	$CaCl_2$	C_2H_2	The CCVD reaction was performed in a horizontal quartz tube furnace by passing a mixture of 1:1:10 C_2H_2:H_2:N_2 for 30 min at 700^oC.	The high-yield synthesis makes it unnecessary to carry out subsequent treatment for removing the remaining catalyst. In other words, the metallic impurity is about 5%, which is quite common even in commercial samples (at least low-cost samples). In this work it was possible to remove a part of the metallic impurity by washing in HNO_3 to obtain carbon product with only 2% metallic impurity.	58
Co, Fe, Cu	SiO_2	C_2H_2	A ceramic boat containing 20-50 mg of the catalyst was placed in a quartz tube. The reaction mixture of 2.5% - 10% C_2H_2 (Alpha gas, 99.6%) in N_2 (Alpha gas, 99.99%) was passed over the catalyst bed at a rate of 0.15-0.59 mol C_2H_2 $g^{-1}h^{-1}$ over several hours at temperatures in the range 773 - 1073 K.	Cobalt on silica was found to be the best catalyst-support combination for the production of graphitic tubules. Straight and coiled carbon tubules were obtained with inner and outer diameter of 3 - 7 and 15 - 20 nm, respectively, and up to 30 pm in length. These nanotubules were not coated by amorphous carbon. Traces of amorphous carbon could be removed by hydrogen. High resolution electron microscopy images and electron diffraction patterns of the straight nanotubules were similar to those obtained by the arc-discharge method.	59
Fe-Co	MCM-48 Silica	benzene	Synthesis was carried out in a fixed bed reactor. Typically *ca* 20 mg catalyst was spread in a small quartz tube laid in the middle of the furnace. The furnace was firstly heated to 650°C in N_2, then the flowing gas was switched to the saturated steam of benzene at 25°C carried by the N_2 with the flow rate of 140 sccm for 1 h. After that, the reactor was cooled down to room temperature in N_2 ambient.	Well-graphitized curved CNTs ranging from 10 to 45 nm in diameter could be formed out of the pores of the M41S materials. The maximum yield of CNTs per hour was greater than 200% the weight of the catalyst. Quite a few helix-shaped CNTs (about 10%) were obtained with the structures clearly demonstrated by high-resolution electron microscopy.	60

Table 3.3 continued

Fe and Co	Silica, Zeolite NaY, Zeolite MCM-41, alumina	C_2H_2	A fix bed flow reactor was used in the temperature range 900-1100 K. The catalyst samples were placed in a silica boat that was placed into a horizontal tube reactor. Before introducing the reactant mixture (10% C_2H_2, 90% N_2, with a flow rate of 300 ml/min) the catalysts were purged in a nitrogen stream (300 ml/min) in order to remove water and pre-treat the catalyst at 999 K. The reactions were carried out for different reaction times (1 - 60 min) to get some approximate information on the rate of nanotube formation.	It was proven that both Co- and Fe-containing samples are good catalysts in the generation of MWCNT from acetylene *via* CCVD. The activity differences found for the various supports could be explained by the necessary localisation of the catalytically active components on the outer surface, at those places of support where a MWCNT can easily accommodate, i.e., in the big pores like the silica has.	6
Fe	SiO_2	C_2H_2	The general growing conditions were: 110 cm^3/min of the acetylene/nitrogen gas mixture, 690°C synthesis temperature, 180 Torr over pressure and two gas compositions: 2.5% and 10% C_2H_2/N_2.	The concentration of acetylene has an important influence on the characteristic of the CNTs synthesized by CVD. CNTs synthesized with low acetylene concentration were more regular and with a lower amount of amorphous carbon than those synthesized with high concentration. During the synthesis of CNTs, amorphous carbon nanoparticles nucleate on the external wall of nanotubes. At high acetylene concentration carbon nanoparticles grow, covering all the surface of CNTs, in the form of a compact coating.	61

Table 3.4: The use of supported transition metal elements as catalysts for the CVD synthesis of **SWCNTs**.

Catalyst	Support/substrate	Carbon source	CNT synthesis conditions	Distinct properties of CNTs and summary	Reference
Fe-Mo	Al_2O_3 aerogel	CH_4	For CNT synthesis methane gas flow ~1000 sccm at 850 -1000^oC was introduced over the catalyst in a horizontal reactor.	High quality SWCNTs were produced with a total amount greater than 200% the weight of the catalysts.	62
Fe-Mo	MgO	CH_4	Typically 200 mg catalyst was uniformly distributed in the centre of a quartz tube while the N_2 flow was maintained for 5 min. Subsequently, a mixture of CH_4:H_2 = 75:300, v/v at a flow rate of 375 ml/min or a mixture of CH_4:N_2 = 50:300 v/v at a flow rate of 350 ml/min was introduced and the reaction was maintained for 30 min.	High-quality SWCNTs were synthesized in gram amounts. Raman data revealed that the as-prepared SWCNTs have a diameter of about 0.74 - 1.29 nm. It was found that the diameter of the as-prepared SWCNTs can be controlled mainly by adjusting the molar ratio of Fe-Mo versus the MgO support.	63
Ni	Silica gel	CH_4	After the catalysts had been fed in and treated with appropriate conditions stated, the carrier flow was stopped and replaced by the up-flow of methane and argon in fixed proportions ranging from CH_4/Ar) = 1 to CH_4/Ar = 3, with the combined flow rate being set in the range of 0.5 - 2.4 L/min. The syntheses were conducted at atmospheric pressure, and the typical reaction time was 20 min.	The growth of SWCNTs was initiated by the rapid injection of the catalyst precursor into the preheated furnace, providing the small catalyst particles required. Without such a hot-injection procedure, no SWCNTs were formed; instead, only amorphous carbon was observed. For the hot-injection synthesis, the highest yield of SWCNTs was obtained using a nickel loading of 2.4 - 5.0 wt% on the silica support, while low (<0.2 wt %) and high (>10 wt%) nickel loadings generated amorphous carbon and carbon particles, respectively.	64
Au	Si/SiO_2 substrates	C_2H_4 and C_2H_2	Typically, substrates with Au nanoparticles (after O_2 plasma treatment) were loaded into the quartz tube and heated to growth temperature (800 or 900°C) under Ar flow. At the growth temperature, the flow of Ar was replaced by a flow of 440 sccm H_2 and maintained for 15 min to reduce the nanoparticles. Subsequently, the synthesis	The growth of SWCNTs using gold nanoparticle catalysts was successfully demonstrated.	65

Table 3.4 continued

			was initiated by introducing a flow of 20 sccm C_2H_4, 30 sccm CH_4, and 440 sccm H_2 for 10 min.		
Fe/Ru and Fe/Pt	SiO_2	CH_4	Growth of SWCNTs was carried out in a quartz tube (~ 4 cm diameter) heated by a programmable horizontal furnace. MgO-supported iron oxide catalyst powder was placed in front of the silica substrate to act as a "promoter". The furnace temperature was ramped up to 900°C at a flow rate of 300 sccm argon (99.1%), and methane (99.9%) was then added at a flow rate of 200 sccm for a further 30 min. The system was then allowed to cool to room temperature under Ar at a flow rate of 300 sccm.	The study reveals that when compared with single-component catalysts such as Fe, Ru, and Pt of similar size, bimetallic catalysts Fe/Ru and Fe/Pt produced at least 200% more SWCNTs, as measured by atomic force microscopy (AFM). Possible reasons for the high efficiency of bimetallic catalysts are discussed in this study such as the the fact that synergistic effect of bimetallic nanoparticles may result from their enhanced ability in decomposing methane and in dissolving carbon atoms, their improved wetting ability of bimetallic nanoparticles on SiO_2 surfaces, and the strong binding energy between bimetallic nanoparticles and graphene sheets.	66
Mo-Fe	Al_2O_3	CH_4	The substrate was loaded in a quartz tube CVD reactor, followed by heating to 900^oC in Ar atmosphere (1000 sccm) with a heating rate of 63^oC/min. After the temperature is stabilized at 900^oC, Ar gas flow was replaced by CH_4 (500 sccm) and H_2 (500 sccm) for the synthesis of Y-junction SWCNTs. CH_4/H_2 flow is maintained for 10 min, then only H_2 gas (500 sccm) is flowed for 5 min at the same temperature in order to increase the purity of nanotubes.	Most of the synthesized SWCNTs possessed branches forming Y-junctions. TEM images confirmed that some of the synthesized Y-junction SWCNTs consist of three individual SWCNTs with different diameters. Raman spectra showed that our sample has both semiconducting and metallic SWCNTs. The results of TEM and Raman measurements are indicative of the formation of Y-junction SWCNTs with different electrical properties. The mechanism for the growth of Y-branching was proposed.	67
Fe-Mo	Al_2O_3	CH_4	A mixture of Ar and CH_4 was introduced into the quartz tube for the production of nanotube materials. The synthesis of nanotubes was conducted at 950^oC for 30	HRTEM observation showed that the produced carbon materials consisted of about 70% SWCNTs and about 30% DWCNTs. The diameters of SWCNTs were in the range of 0.8 - 1.5 nm while the outer and inner	

Table 3.4 continued

			min in atmospheric pressure. The flow rate of CH_4 and Ar was 100 and 500 sccm, respectively. The flow of Ar/CH_4 was maintained for 30 min before the furnace was cooled to room temperature in Ar atmosphere.	diameters of DWCNTs were in the range of 1.75 - 3.1 and 0.95 - 2.3 nm, respectively. Raman analysis indicated that the synthesized SWCNTs and DWCNTs have high-quality graphite structure.	68
Fe and Mo as co-catalyst	spun-on alumina film	CH_4	The catalyst utilized was a 1 nm blanket film of Fe that was deposited on the substrate by electron beam evaporation. The CVD was performed for 10 min at 950°C. Argon gas flow was used at 0.1 slpm and methane gas was introduced into the system at a flow rate of 0.5 slpm.	It was determined here that the substrate employed as the supporting material for the Fe thin film catalyst has a strong effect on controlling the growth of either SWCNTs or MWCNTs, with clear trends noticeable. The ideal substrate for SWNT growth was a spun-on alumina film, while, single crystal substrates promoted the growth of mixed SWCNTs and MWCNTs. All remaining substrates (e.g. "over-etched" (0 0 1) silicon, poly-silicon on (0 0 1) silicon, PECVD silica, fused-silica, 30% aerogel, 50% aerogel, and 80% aerogel) grew primarily MWCNTs.	69
Re	MgO	CH_4	A quartz boat containing the prepared catalyst material was placed in the hot zone of the horizontal reactor tube. At first, the reactor (fixed bed) was exposed to a flow of Ar (~250 sccm) to remove the oxidizing atmosphere; afterward, the catalyst reduction was performed at 650°C for 30 min in a hydrogen medium (~150 sccm). The temperature was increased by 6°C/min, up to the desired growth temperature between 950 and 1100°C, during the injection of CH_4 into the reactor.	Diamagnetic single-, double-, and multiwalled CNTs were synthesized. The paper showed that rhenium is a suitable catalyst for the synthesis of such diamagnetic nanotubes with uniform diameter and a defined numbers of shells. Scanning and transmission electron microscopy investigations, Raman spectroscopy, and magnetic measurements showed the tubular structure, the high crystallinity, and the diamagnetic character of the grown nanotubes.	70
Fe-Co	USY-zeolite powder	Ethanol	Ethanol vapor was introduced from a temperature-controlled reservoir, keeping the ethanol pressure measured just before	High purity single-walled carbon nanotubes (SWCNTs) were synthesized from ethanol by catalytic CVD method. The SWCNT yield of more than 40%	

Table 3.4 continued

			the entrance of the quartz tube constant. The pyrolysis temperature was 800-850°C. Finally, the ethanol supply was stopped and the furnace was turned off before bringing the system back to room temperature with flowing 100 sccm of Ar.	was achieved over the weight of zeolite support powder with Fe/Co catalyst, which corresponded to more than 800% yield over the weight of the catalytic metal, within the CVD reaction time of 120 min assuring as-grown high quality.	71
Fe	MgO	CH_4	For the growth of CNTs, the catalyst (*ca.* 100 mg) was set in a quartz tube of 30 mm diameter and heated to the reaction temperatures, 700-850°C, with a constant heating rate of 13°C /min under an Ar flow (150 cm^3/min). At the reaction temperature, the Ar gas was switched to a mixture of CH_4 (20 vol %) and Ar with a total flow rate of 700 cm^3/min at atmospheric pressure. The reaction lasted for 10 min, unless otherwise stated. After the reaction, the system was cooled under Ar.	It was found in this study that the porous MgO support gives the SWCNTs with a narrow diameter distribution with the mean diameter and standard deviation of 0.93 and 0.06 nm, respectively, only when the Fe loading and reaction temperature are relatively low. The higher Fe loading and/or the higher reaction temperature enlarged the nanotube diameter, forming double-walled carbon nanotubes (DWCNTs) in addition to SWCNTs. This result indicates that only the diameter of Fe nanoparticles determines the growth of either SWCNTs or DWCNTs on the MgO support. The fluorescence spectra of D_2O dispersions of as-prepared nanotubes were used to identify the diameter and chirality distribution.	72
Mg/Fe-Co,Fe-Ni	Al_2O_3	CH_4	Spinel oxides of the general formula $Mg_{0.8}M_yM'_z\ Al_2O_4$ (M, M' = Fe, Co, Ni, y+z=0.2 y or z = 0.05, 0.10 and 0.15) were prepared starting with a stoichiometric mixture of the metal nitrates and subjecting the nitrate mixture along with urea to the usual procedure employed in combustion synthesis. A dry mixture of H_2-CH_4 (18 mole% CH_4) was passed over the calcined oxide at 4 1070°C for 6 min at a flow rate of 250 sccm to produce the CNTs.	Good-quality SWCNTs were obtained in high yields with the Fe-Co alloy nanoparticles, as evidenced by TEM images and surface area measurements. The diameter of the SWCNTs was in the 0.8-5 nm range, and the MWCNTs, found occasionally, possessed very few graphite layers.	73

Table 3.4 continued

Fe-Co	Y-type zeolite	Ethanol gas	The catalyst (50 mg) on a quartz boat was placed in a quartz tube inside an electric furnace. After evacuating the air, Ar gas (40 kPa) was introduced and heated to 800°C. Then Ar gas was evacuated and ethanol gas (0.67 kPa) was introduced for 15 min, 1 h and 2 h to produce raw-SWNTs.	The yields of SWCNTs were estimated to be ~95% and the purities of SWCNTs thus obtained were more than 95%, as characterized by thermo-gravimetric analysis. Raman spectra of the purified SWCNTs were essentially identical with those of the corresponding raw samples. The purification of the CNTs was achieved by oxidation of raw material at 240°C or 340°C and treatment with 1% aqueous solution of hydrofluoric acid.	74
Co-Mo	quartz	Ethanol vapour	The catalyst was supported on a quartz substrate, which was dip-coated into a Co-Mo acetate solution (both 0.01 wt% in ethanol). The catalyst was oxidized by heating the dip-coated substrate in air at 400°C, and then reduced in a flowing Ar/H_2 mixture (3% H_2) during heating of the CVD chamber. When the CVD chamber reached 800°C, the Ar/H_2 mixture was stopped and ethanol vapour (99.5% dehydrated ethanol with maximum 0.005% water) was introduced at 10 Torr to initiate SWCNT growth.	Vertically aligned SWCNT films up to 5 nm thick were produced. The film thickness was observed to increase nonlinearly with CVD reaction time. An eventual decrease in the SWCNT film thickness, observed for longer growth times, was attributed to catalyst poisoning and burning of the SWCNTs due to excessive oxygen or water in the CVD chamber. Optical absorbance by SWCNT films was found to behave similarly to the film thickness as growth proceeds.	75

Table 3.5: The use of supported transition metal elements as catalysts for the CVD synthesis of **DWCNTs**.

Catalyst	Support/substrate	Carbon source	CNT synthesis conditions	Distinct properties of CNTs and summary	Reference
Fe-Mo	Al_2O_3	CH_4	A mixture of Ar and CH_4 was introduced into the quartz tube for the production of nanotube materials. The synthesis of nanotubes was conducted at 950^oC for 30 min in atmospheric pressure. The flow rate of CH_4 and Ar was 100 and 500 sccm, respectively. The flow of Ar/CH_4 was maintained for 30 min before the furnace was cooled to room temperature in Ar atmosphere.	HRTEM observation showed that the produced carbon materials consisted of about 70% SWCNTs and about 30% DWCNTs. The diameters of SWCNTs were in the range of 0.8 - 1.5 nm while the outer and inner diameters of DWCNTs were in the range of 1.75 - 3.1 and 0.95 - 2.3 nm, respectively. Raman analysis indicated that the synthesized SWCNTs and DWCNTs have high-quality graphite structure.	68
Fe-Co	Mesopourous silica [mesophase P63 = mmc (SBA-12)]	CH_4	A variety of conditions have been tried for the synthesis, including the pre-treatment heating atmosphere (Ar or air), the heating rate (room temperature to target temperature in 2-16 h), CCVD reaction gas (CH_4 vs. CH_4 + H_2), duration of the CCVD reaction (10 min to 1 h). Synthesis temperatures used were 750-870^oC.	Bundles of tubes with relatively high percentage of DWCNTs, in areas where tubular layered structures could be clearly resolved, have been observed by TEM. In other areas, crystal-like alignment of very uniform DWCNTs was observed for the first time, suggesting that mesoporous silica might play a templating role in guiding the initial nanotube growth. In addition, compatible with nano-electronics research, bridging of catalytic islands by DWCNTs has also been demonstrated.	76
Fe-Co	MgO	CH_4	The synthesis of DWCNTs was performed in a quartz tube reactor mounted in a tube furnace. 0.6 g of the Fe-Co/MgO catalyst was put into a quartz boat at the center of the reactor tube. The tube reactor was first heated to 900^oC in N_2 atmosphere, and then CH_4 (1000 sccm) was introduced into the reactor for the DWCNT preparation. After 30 min, the reactor was cooled to room	The outer diameters of the obtained DWCNT were in the range of 1.3 - 2.0 nm. The high-quality DWCNTs with a narrow distribution of diameters might be very useful in the application of nanoelectronics and the measurement of properties of DWCNTs.	77

Table 3.5 continued

			temperature in N_2 atmosphere.		
Fe-Mo	MgO	CH_4	For CVD growth, the Fe-Mo/MgO catalyst was loaded in a vertically set quartz tube for the efficient mixture of CH_4 feedstock and the catalyst. The catalyst was annealed in an Ar atmosphere at the reaction temperature for 1 h to dry the catalyst. A flow of 20 vol % CH_4 diluted with Ar was introduced to the system, together with a controlled amount of water vapour.	Introducing a small amount of water vapor in the catalytic CVD growth SWCNTs and DWCNTs extends the catalyst lifetime and increases the nanotube yield. The mechanism of this water-assisted nanotube growth over a Fe-Mo/MgO catalyst, based on analysis of the effluent gas, in terms of chemistry of the water-induced oxidation and its effects on catalytic activity was studied. Water vapour was found to etch away carbon precipitate covering the metal catalyst, based primarily on the chemical reaction $C + H_2O \rightarrow CO + H_2$, thus maintaining the catalytic activity.	78
Fe-Co Co-Ni, Co-V, Co-Cr, Co-Mn	zeolite (TS-1(Si/Ti=50)	C_2H_2	The synthesis of DWCNTs was carried out in a horizontal quartz tubular reactor. The catalyst was spread over the quartz boat and was placed in the center of the furnace. The catalyst was annealed and activated for 30 min at 300°C and finally heated up to 900°C under Ar flow at a flow rate of 250 ml/min. C_2H_2 gas was then passed through the furnace (10 ml/min) for 30 min while Ar gas flow was maintained at a 250 ml/min. After the reaction, the furnace was cooled down to room temperature by the passage of Ar gas (250 ml/min). The DWCNT sample was collected as a black powder from the quartz boat.	High-yield (>80%) of DWCNTs were obtained. The synthetic yield of DWCNTs was sensitively affected by reaction conditions of the CCVD such as zeolite support materials, the sintering of the metal particles, hydrocarbon sources and reaction temperatures. HRTEM together with Raman spectroscopy showed that the outer tube diameter varies from 3 to 6 nm with inner-outer tube separations of 0.36-0.37 nm, which is much larger than the interlayer distance of graphite (0.335 nm). Other binary catalysts such as Co-Ni, Co-V, Co-Cr and Co-Mn provided lower yields of DWCNTs. A high-temperature heat treatment of the thick-DWCNTs at 2000°C improved greatly the crystallinity (graphitization) of the thick-DWCNTs, giving rise to ideal carbon nanotube field emitters for panel display applications.	79

Table 3.5 continued

$Mg_{1-x}Co_xO$ and Co-Mo	none	CH_4	CNTs were prepared by passing a mixture of H_2 + CH_4 (18% CH_4) gas at 1000°C over nanometre sized cobalt particles generated *in situ*. The catalyst particles were produced during the selective reduction of a solid solution of $Mg_{1-x}Co_xO$ (*x* ranging from 0.01 to 0.1) powder. In some cases, the catalyst also contains additions of Mo (Co:Mo 3:1)	Narrow diameter double-walled carbon nanotubes (DWCNTs) were obtained with high yield. Inelastic light scattering shows that the tubes have a wide distribution of helicities and also shows the importance of the environment to the tube properties. The D band of the Raman spectrum was found to be absent for some tubes consistent with predicted sensitivity of this band to helicity.	80
Co	MgO	CH_4	The catalyst (50 mg) loaded onto a Mo boat was reduced at 900 - 1000°C for 1 h in flowing gases of H_2 (40 sccm) and N_2 (100 sccm) at a pressure of 200 Torr, then the N_2 was replaced with CH_4 (10 sccm) to start CNT growth. The growth period typically lasts for 1 h at T=900 - 1000°C.	Very uniform and clean DWCNTs from Co particles dispersed on porous MgO nanoparticles. Both the surface area and pore size of the MgO nanopartilces affect the growth of DWCNTs. Very uniform DWCNTs have been prepared by using catalyst of Co 2.5 - 5wt% loaded on MgO nanoparticles with pore size of 3 nm. The DWCNTs have a very narrow diameter distribution of 2 - 4 nm.	81

Table 3.6: The use of *$CaCO_3$* supported transition metal elements as catalysts for the CVD synthesis of CNTs.

Catalyst	Support/substrate	Carbon source	CNT synthesis conditions	Distinct properties of CNTs and summary	Reference
Fe, Co and Fe-Co	$CaCO_3$	C_2H_2	The decomposition of acetylene was carried out in a fixed-bed flow reactor at 720°C. Approx. 50 mg of the prepared supported catalysts (Co/$CaCO_3$, Fe(II)/$CaCO_3$, Fe(III)/$CaCO_3$, Fe(II)-Co/$CaCO_3$ or Fe(III)-Co/$CaCO_3$) was placed in a quartz boat which was inserted in a quartz tube under nitrogen flow. Keeping a continuous nitrogen flow of 70 l/h, acetylene was let through with a gas flow of 10 ml/min for 30 min.	High quality and pure MWCNTs were synthesized using the CVD procedure. The MWCNTs could be purified using dilute acids due to the nature of the support.	82
Fe, Co and Fe-Co	$CaCO_3$	C_2H_2 and C_2H_4	CNT synthesis reactions were carried out in a horizontal furnace. About 0.5 or 1.0 g of the catalyst, spread on a quartz boat was introduced into the furnace preheated to 700°C in a flow of nitrogen (300 ml/min). After 10 min the hydrocarbon gas (acetylene or ethylene) was made to pass over the catalyst bed at a rate of 30 ml/min for 60 min. The hydrocarbon gas flow was stopped; the product on the quartz boat was cooled to room temperature while nitrogen flow was on.	The quantity and quality of the tubes produced in different synthesis reactions were however, significantly different. Out of the several supported catalysts used calcium carbonate and magnesium oxide were found to give the best yield of carbon deposit when they were used as supports for a mixture of cobalt and iron. The yield of carbon deposit was found to be very poor when these supports had only Fe. Cobalt on the other hand showed better activity than iron.	83
Co, Fe and Ni, as well as their bimetallic compounds	nanocrystalline $CaCO_3$	C_2H_2	Typically, 500 mg catalyst was uniformly spread into a small quartz vessel in a fixed bed reactor. When the furnace was heated to 1023K in a continuous nitrogen flow of 300	Compared with conventional $CaCO_3$, nanocrystalline $CaCO_3$ is an improved support that can produce CNTs in a higher yield. Among all the catalysts supported on nano-$CaCO_3$, Fe-Co/$CaCO_3$ catalyst is the most active one, promising for large-scale and low-cost production of CNTs.	84

Table 3.6 continued

			ml/min, the vessel was pushed into the middle of the furnace and acetylene was let through with a flow rate of 100 ml/min, without performing any pre-reduction treatment. After 20 min of the reaction time, the flow of acetylene was stopped and the furnace was allowed to cool to room temperature in a nitrogen atmosphere.		
Fe-Co	$CaCO_3$	C_2H_2	The nanotubes were grown from acetylene on a Fe-Co: $CaCO_3$ catalyst at 720°C as described by Couteau and co-workers.	The $CaCO_3$ catalytic support thermally decomposed into CaO and CO_2 resulting in a mixture of two catalysts for growing the nanotubes, which were found to have outer diameters belonging to two main groups 8 - 35 nm and 40 - 60 nm, respectively. The influent and effluent gases were analyzed by gas chromatography and mass spectrometry at different time intervals during the nanotubes growth process in order to better understand and optimize the overall reaction. A large number of by-products were identified and it was found that the number and the level for some of the carbon by-products significantly increased over time.	85
K-doped Co and K-doped Fe-Co	$CaCO_3$	C_2H_2	The synthesis of carbon nanotubes was carried out by the decomposition of acetylene in a fixed-bed flow reactor at 720°C. Approximately 100 mg of supported transition metal catalyst was placed in a quartz boat which was inserted in a quartz tube under N_2 flow. Keeping a continuous N_2 flow of 500 ml/min, acetylene was let through with a gas flow of 20 ml/min for 30 min. After rinsing the system with nitrogen, reaction product was collected from the quartz boat.	The authors concluded from their results obtained in this study that proper doping of CVD catalysts with potassium can increase activity with keeping the original quality of carbon nanotubes.	86

Table 3.6 continued

Fe-Co	MCO_3 (where M = Mg, Ca, Sr, Ba)	C_2H_2	For CNT production, 100 mg of the as-prepared catalyst is placed in an oven, flushed with nitrogen, and finally exposed to a mixture of acetylene and nitrogen (or argon), fluxed at 1 and 70 L/h, respectively at T= 700 - 740°C.	The authors suggested an involvement of the CO_2 groups from carbonate in the CNT growth process. This was confirmed by using carbonates with different decomposition temperatures as catalyst support. $CaCO_3$ was the best support because of the good matching between the carbonate decomposition temperature and the nanotube growth. CO_2 groups originating from a carbonate react with acetylene to produce carbon for MWCNTs.	87
Fe-Co	$CaCO_3$	C_2H_2	CNTs were synthesized as described above at 700°C.	A detailed study involving the reaction between acetylene (C_2H_2) and CO_2, mixed in an equimolar ratio, to produce carbon nanotubes was performed. A dramatic enhancement of the CNT yield compared with those of previous syntheses was observed. In addition, the lifetime of the catalyst was considerably extended and the initial growth rate was enhanced compared with those of classical acetylene decomposition reactions.	28
Fe	$CaCO_3$	C_2H_2	For CNT synthesis, the catalyst (100 mg) was loaded into a quartz boat in a fixed bed reactor at room temperature. H_2 was used to reduce the catalyst for 1 h in situ (700°C, 100 ml/min). The temperature ramping rate used was 10°C min^{-1}. The H_2 gas was then replaced with acetylene and the gas was then passed through the reactor for 3 h (700°C, 100 ml/min). The reactor was then cooled to room temperature in a H_2 atmosphere.	MWCNTs were obtained with large diameters and a varied diameter distribution. The MWCNTs were used as supports for iron. It was observed that Fe supported on CNTs produces a very stable and active catalyst.	88
Ni and Co	$CaCO_3$	C_2H_2	The prepared catalysts were placed into the furnace preheated to 700°C under N_2 atmosphere. This minimal	High-quality CNTs were successfully fabricated by using the catalytic decomposition of acetylene over Ni- and Co-supported $CaCO_3$ catalysts in fluidized bed reactor. Nitrogen	

Table 3.6 continued

			fluidization velocity (U_{mf}) and minimal bed height were estimated to be *ca.* 12 cm/min and *ca.* 25 cm, respectively. The U_{mf} was found to decrease with the growth temperature. Four growth temperatures were set at 700°C, 750°C, 800°C, and 850°C, respectively. At the desired temperature, a mixed carbon precursor (N_2:C_2H_2:H_2 = 93:6:1, v/v/v) was introduced to pass over the catalyst bed at the same velocity for 0.5 h.	physisorption indicated that the CNT products are mainly mesoporous. As-grown CNTs were found to have a multi-layered structure, and their layer numbers are increasing functions of the growth temperature according to the calculation of Debye-Scherrer's equation.	89
Fe-Co	$CaCO_3$	C_2H_4	The catalyst was loaded into the reactor under 0.047 m/s of N_2. The flow rate of N_2 was gradually reduced until the superficial gas velocity was between 0.8 to 1.2 × U_{mf} as the temperature was increased to 600°C. Reduction of the bed mixture was carried out using 50% H_2 in N_2 for 1 h at 600°C. The gas was then switched to pure N_2 and purged for 10 min before changing the temperature to the desired synthesis temperature, between 600 and 850°C. The synthesis gas mixture containing ethylene, hydrogen , and nitrogen in the ratio of 50:1:450 was introduced for 60 min.	It was shown that he technical viability of using $CaCO_3$ as a soluble support material for the synthesis of CNTs via FBCVD and have shown that MWCNTs of similar quality to those synthesized via traditional CVD techniques using insoluble alumina or silica substrates, can be synthesized, in bulk. On the basis of TGA results, the carbon yield per unit weight of catalyst obtained was ~ 1100% and the overall carbon efficiency was calculated to be 280%. Of the carbon products, ~ 89% was MWCNTs between 10 and 20 nm in diameter.	90

3.5 Summary of factors impacting CNT growth

A summary of the key factors that affect the growth of CNTs synthesized *via* the substrate CVD process are summarized based on the data presented in Tables 3.3 - 3.6.

3.5.1 Carbon source

The literature survey broadly shows that the most commonly used source of carbon for MWCNT synthesis is acetylene (C_2H_2). Ethylene (C_2H_4) has also been used in many studies but to a lesser extent, while other sources of carbon such as CO, propylene (C_3H_6), benzene, ferrocene, propyne (C_3H_4) and cyclopentadiene (C_5H_5) have also been used in very few studies. The ability of C_2H_2 to decompose at low temperature (e.g. 500°C) has made C_2H_2 a carbon source of choice for MWCNT synthesis. This is because it readily forms radicals and ions necessary for the formation of CNTs.

The use of CH_4 has been revealed in a large number of studies to favour the formation of SWCNTs and DWCNTs. Ethanol vapour has also proven to be suitable for the synthesis of aligned CNT bundles under appropriate reaction conditions. The data collected in the tables reveal that there seems to be a correlation between the CNT graphite layers and the molecular structure (C/H ratio) of the hydrocarbon gas used as carbon source. The data suggests that short chain molecules (e.g. CH_4) can preferentially produce single or double layered CNTs while longer chain molecules such as C_2H_2 and C_2H_4 result in formation multi-layered CNTs.

3.5.2 Metal particle (monometallic vs bimetallic)

The data in the tables clearly indicate that the most widely used metal to catalyze the formation of CNTs is Fe. This is because Fe is cheaper than the other transition metal elements thus rendering it suitable for industrial application. Co and Ni in their monometallic state have not been used as much as Fe. However studies have revealed that the order of reactivity of the three metals is Ni > Co > Fe. The size of the metal

particles has been shown to affect the diameters of the CNTs. It can be seen in several studies that the CNT growth can be controlled precisely by manipulating the metal particle properties during the metal-support preparation as well by post treatment of the metal-support mixture [91].

For better quality and improved CNT yields, bi-metallic particles have been used, as shown in most studies using $CaCO_3$ as a support [82-90]. In summary, the bi-metallic particles used include Fe-Co, Fe-Ni, Fe-Mo and Co-Mo. The data indicates that Mo with Fe or Co favours the formation of SWCNTs or DWCNTs with high quality graphitic structure. Other metals such as Ru, Pt, V and Mg have been found to enhance the quality of CNTs when used in conjunction with Fe or Co.

3.5.3 Advantages of using $CaCO_3$ over other supports

The importance of using a support has been described earlier in this chapter. It can be seen that SiO_2 or Si has been the mostly widely exploited support, followed by Al_2O_3, zeolites and MgO. These materials have been widely used on the merits of their high surface area and porosity, cost, as well as high thermal stability. The major challenge when using these materials is that they cannot be removed easily from the products due to insolubility issues.

A study pioneered by Couteau and co-workers in 2003 [82] resulted in increased interest in the use of other suitable support materials such a CaO, $Ca(OH)_2$, $CaCl_2$, $MgCO_3$, $BaCO_3$ as well $CaCO_3$ for CNT synthesis. $CaCO_3$ has to date received increased interest from various scientists because of the good quality, high yield and high purity materials obtained from using it as a support. We commenced our studies using this support in February 2006. Earlier studies in our group had focused on floating catalyst methodologies to make CNTs [92].

After the commencement of our study, a number of key papers have appeared further discussing development of using $CaCO_3$ as a support. The chemistry involved during the CVD of C_2H_2 over $CaCO_3$ is interesting. Studies by Magrez *et al.* [28] have explained the chemical processes taking place that render $CaCO_3$ a favourable support

for CNT synthesis over others. The chemical reactions and mechanism taking place during the CNT synthesis can be summarized in the following points:

(i) $CaCO_3$ stability is governed by a dynamic equilibrium of the decomposition reaction $CaCO_3 \leftrightarrow CaO + CO_2$ that proceeds at temperatures ranging from 600°C to 820°C. Thus, CO_2 is present as a gas and in the support (as $CaCO_3$) in a ratio that depends on the temperature applied. The $CO_2(g)/C_2H_2$ ratio is constant for a given temperature as long as the carbonate supplies CO_2 by decomposition.

(ii) A small deviation in the decomposition rate of $CaCO_3$, which is controlled by lowering or raising the growth temperature, decreases the yield significantly. The $CO_2(g)/C_2H_2$ ratio, obtained over Fe_2-Co/$CaCO_3$ or Fe-Co/$CaCO_3$ under the optimum conditions (here at 660°C), was measured by quadrupolar mass spectrometry to be 1:100 and was stable over the entire period of growth [28]. The $CO_2(g)$ is assumed to act as an etching agent that prevents catalyst poisoning [87]. It is also assumed that $CO_2(g)$ limits acetylene polymerization, which occurs by a homogeneous radical chain reaction to produce more-stable oligomers along with heavy oils [85].

(iii) Two chemical processes are possible for the reaction of acetylene with CO_2 for the synthesis of CNTs [Reactions (1) and (2)].

$$C_2H_2 + CO_2 \leftrightarrow 2C + H_2O + CO \quad (1)$$

$$C_2H_2 + CO_2 \leftrightarrow C + 2CO + H_2 \quad (2)$$

(iv) The synthesis of carbon atoms occurs at the area where acetylene, $CaCO_3$, and the catalyst meet. This triple-point junction (Fe_2-Co/$CaCO_3$/C_2H_2) is illustrated in Fig. 3.4 [28]. Once generated, carbon can diffuse either on the surface or in the bulk of the metallic particles, which catalyze the growth of the CNTs. The chemical reactions taking place at the triple-point junction strongly enhance the growth efficiency of the MWCNTs.

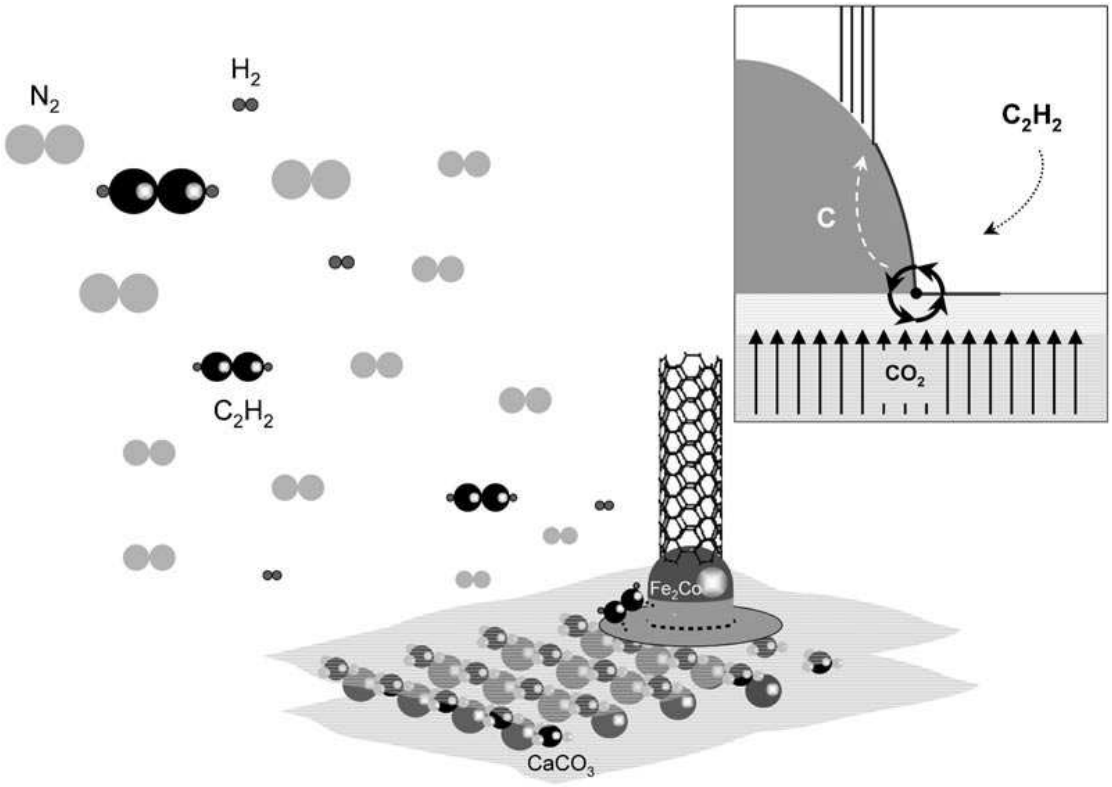

Fig. 3.4: The triple-point junction (grey area) where the reaction described by Scheme 1 takes place corresponds to the area around the metal–support interface (dashed line). The border of this area on the metallic side is considered to be the root of the CNTs and on the support side it is the carbon diffusion length. Insert: the diffusion of the carbon-containing species. In particular, carbon atoms can diffuse on the surface or in the bulk of the metallic particles from the triple-point junction towards the CNTs [28].

(v) While CO_2 is available from the bulk carbonate, it must also be generated from the products arising from Reactions (1) and (2). CO_2 regeneration is possible by the water gas shift reaction: $H_2O + CO \leftrightarrow CO_2 + H_2$ [93], or by CO disproportionation: $2CO \leftrightarrow C + CO_2$ [94]. It is believed that CO_2 regeneration takes place while H_2O and/or CO are adsorbed at the triple-point junction. CO_2 thus formed could be trapped by the support to form carbonate, which would further react with acetylene molecules. These chemical mechanisms are summarized in **Scheme 3.1** [28]. When $CaCO_3$ is employed as the support, a two step cyclic mechanism starts with the reaction of acetylene and $CaCO_3$ (CO_2) followed by CO_2 regeneration. The reaction takes place at the triple-point junction (Fe_2-Co/$CaCO_3$/C_2H_2) around the catalyst-

support interface, which strongly enhances the conversion of acetylene. Thus a *base growth mechanism* was suggested based on this concept.

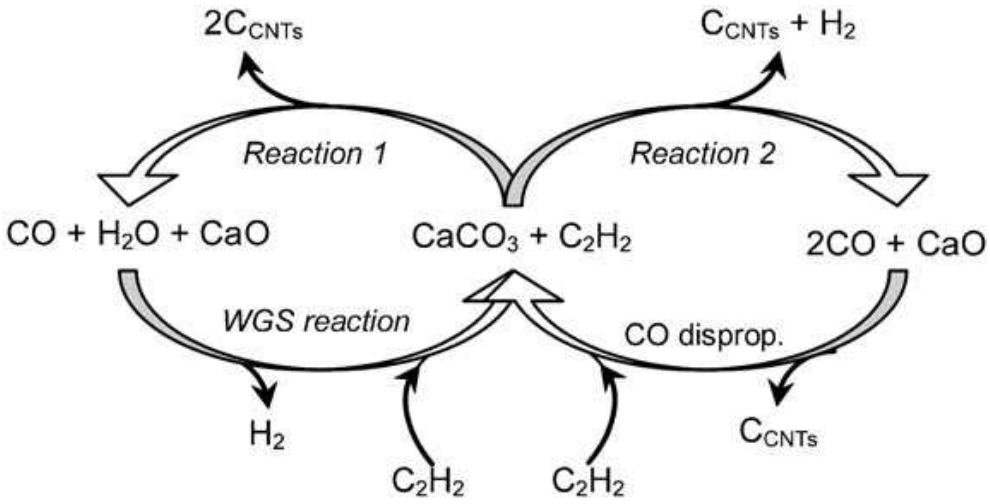

Scheme 3.1: Chemical cycles involved in the growth of carbon nanotubes from an equimolar mixture of C_2H_2 and CO_2. WGS = water gas shift, CO disprop. = CO disproportionation [28].

(vi) Analysis of the kinetics of the growth mechanism allowed for an improvement of the catalyst lifetime and initial growth rate. These properties of the catalyst are drastically enhanced when carbon is produced by the C_2H_2-CO_2 reaction compared with those of the synthesis of MWCNTs by classical acetylene decomposition [28].

3.5.4 Temperature and synthesis time

The synthesis temperature is largely determined by the nature of the support and the carbon source used. Thus, supports with low melting points would require lower synthesis temperatures. The stability of the carbon source also determines whether moderate or extremely high temperatures must be applied. Generally temperatures in the range 550 - 1100°C are suitable for CNT synthesis depending on the reagents used. Supports that undergo phase change (e.g. $CaCO_3$) at high temperatures are temperature sensitive and can be only be effective within a specific optimum temperature range for maximum CNT growth. CNT growth generally occurs over time and studies have shown that the quality of CNTs can deteriorate if the synthesis

time is too long (refer to Chapter 8 for a detailed study). Thus, while high yields can be obtained by extending the synthesis time, the quality of the CNTs can be compromised.

3.6 Purification of the CNTs

As-synthesized CNTs prepared by catalytic CVD methods generally contain carbonaceous materials, the support and the metal catalyst particles. The co-existence of the materials (hereafter to be referred to as impurities) is inevitable and remains a challenge since pure CNTs are generally required for application purposes. An excellent review by Hou *et al.* [95] gives a comprehensive survey and analysis of the purification of CNTs. The challenges existing in the purification methods, synthesis techniques and purity assessments, which have to be overcome in order to enable the wide applications of CNTs, are discussed.

Purification methods of CNTs can basically be classified into three categories, namely chemical, physical, and a combination of both [95]. In summary, purification of CNTs by chemical oxidation includes the following techniques: (i) gas phase oxidation, (ii) liquid phase oxidation and (ii) electrochemical oxidation. Physical-based purification of CNTs includes: (i) filtration, (ii) centrifugation, (iii) solubilization of CNTs with functional groups and (iv) high temperature annealing.

The nature of some supports requires combinations of both chemical and physical purifications (*multi-step purification*) in order to achieve desirable CNTs with high purity and high yield. Thus several purification processes have been explored including hydrothermally initiated dynamic extraction (HIDE) or sonication-assisted multi-step purification; microfiltration in combination with oxidation; sonication in combination with oxidation; as well as high temperature annealing in combination with extraction. A hefty challenge though is that these procedures have disadvantages including damage to the CNT structure, high cost and the long reaction times involved. Moreover, according to Hou *et al.* [95] there are still many technical barriers to be overcome when cost, reproducibility, environment compatibility, and scaling-up are taken into account. In our studies, these factors were taken into consideration.

3.7 References

1. (a) A.-C. Dupuis, Progr. Mater. Scie. **50** (2005) 929; (b) H. Liu, D. Takagi, H. Ohno, S. Chiashi, T. Chokan, Y. Homma, Appl. Phys. Express **1** (2008) 014001.
2. F. Pinna, Catal. Today **41** (1998) 129.
3. C. Perego, P. Villa, Catal. Today **34** (1997) 281.
4. C. Park, M.A. Keane, J. Catal. **221** (2004) 386.
5. (a) Z. Yu, D. Chen, B. Tøtdal, A. Holmen, Catal. Today **100** (2005) 261; (b) P.M. Ajayan, Nature **427** (2004) 402; (c) O.A. Nerushev, S. Dittmar, R.-E. Morjan, F. Rohmund, E.E.B. Campbell, J. Appl. Phys. **93** (2003) 4185; (d) M. Yudasaka, R. Kikuchi, Y. Ohki, E. Ota, S. Yoshimura, Appl. Phys. Lett. **70** (1997) 1817.
6. (a) K. Hernadi, Z. Kónya, A. Siska, J. Kiss, A. Oszkó, J.B. Nagy, I. Kiricsi, Mater. Chem. Phys. **77** (2002) 536; (b) A. Fonseca, K. Hernadi, J.B. Nagy, D Bernaerts, A.A. Lucas. J. Mol. Catal A: Chem. **107** (1996) 159.
7. R.C. Weast, M.J. Astle, W.M. Beyer, *CRC handbook of Chemistry and Physics*, CRC Press, Inc., Boca Raton, Florida, 65th Ed., (1984-1985).
8. G.L. Haller, D.E. Resasco, Adv. Catal. **132** (1991) 269.
9. G.M. Schwab, Adv. Catal. **27** (1982) 1.
10. V. Ponec, Stud. Surf. Sci. Catal. **11** (1982) 63.
11. X.-Z. Jiang, S.A. Stevenson, J.A. Dumesic, J. Catal. **91** (1985) 11.
12. (a) M.A. Ermakov, D.Y. Ermakov, A.L. Chuvilin, G.G. Kuvshinov, J. Catal. **201** (2001) 183.
13. M. Endo, T. Hayashi, Y.A. Kim, M. Terrones, M.S. Dresselhaus, Phil. Trans. Roy. Soc. Lond. A **362** (2004) 2223.
14. R.S. Wagner, W.C. Ellis. Trans AIME **233** (1965) 1053.
15. R.T.K Baker, Carbon **27** (1989) 315.
16. H. Kanzow, A. Ding, Phys. Rev. B **60** (1999) 11180.
17. Yasuda, Ayumu, Kawase, Noboru, and Mizutani, Wataru, J. Phys. Chem. B, **106** (2002) 51.
18. S.B. Sinnot, R. Andrews, D. Qian, A.M. Rao, Z. Mao, E.C. Dickey, F. Derbyshire, Chem. Phys. Lett. **315** (1999) 25.

19. K. Liu, K. Jiang, C. Feng, Z. Chen, S. Fan, Carbon **43** (2005) 2850.
20. R. Seidel, G.S. Duesberg, E. Unger, A.P. Graham, M. Liebau, F. Kreupl, J. Phys. Chem. B **108** (2004) 1888.
21. M. Pérez-Cabero, E. Romeo, C. Royo, A. Monzón, A. Guerrero-Ruíz, and I. Rodríguez-Ramos, J. Catal. **224** (2004) 197.
22. A. Reina, M. Hofmann, D. Zhu, J. Kong, J. Phys. Chem. C **111** (2007) 7292.
23. C. Jin, K. Suenaga, S. Iijima, ACS Nano **2** (2008) 1275.
24. R. Brukh, S. Mitra, Chem. Phys. Lett. **424** (2006) 126.
25. M. Grujicic, G. Cao, B. Gersten, Appl. Surf. Scie. **191** (2002) 223.
26. Y. Homma, Y. Kobayashi, T. Ogino, D. Takagi, R. Ito, Y.J. Jung, P.M. Ajayan, J. Phys. Chem. B **107** (2003) 12161.
27. Wondrous world of carbon nanotubes, Eindhoven University of Technology, http://students.chem.tue.nl/ifp03/Wondrous%20World%20of%20Carbon%20Nanotubes_Final.pdf. (accessed on 18th July 2008)
28. A. Magrez, J. W. Seo, V.L. Kuznetsov, L. Forró, Angew. Chem. Int. Ed. **46 (**2007) 441.
29. A. Zhang, C. Li, S. Bao, Q. Xu, Microp. & Mesop. Mater. **29** (1999) 383.
30. F. Rohmund L.K.L. Falk, E.E.B. Campbell, Chem. Phys. Lett. **328** (2000) 369.
31. J.W. Jang, C.E. Lee, T.J. Lee, C.J. Lee, S.J. Noh, Solid State Commun. **127** (2003) 29.
32. Z. Yang, Y. Xia, R. Mokaya, Chem. Mater. **17** (2005) 4502.
33. C.J. Lee, J. Park, J.A. Yu, Chem. Phys. Lett. **360** (2002) 250.
34. M. Pérez-Cabero, I. Rodríguez-Ramos, A.R. Overweg, I. Sobrados, J. Sanz, A. Guerrero-Ruiz, Carbon **43** (2005) 2618.
35. J-B. Park, G-S. Choi, Y-S. Cho, S-Y. Hong, D. Kim, S-Y. Choi, J-H. Lee, K-I. Cho, J. Cryst. Growth **244** (2002) 211.
36. M. Pérez-Cabero, I. Rodríguez-Ramos, and A. Guerrero-Ruíz, J. Catal. **215** (2003) 305.
37. A. Bakandritsos, A. Simopoulos, D. Petridis, Chem. Mater. **17** (2005) 3468.
38. F. Zheng, L. Liang, Y. Gao, J.H. Sukamto, C.L. Aardahl, Nano Lett., **2** (2002) 729.

39. Ch. Emmenegger, P. Mauron, A. Züttel, Ch. Nützenadel, A. Schneuwly, R. Gallay, L. Schlapbach, Appl. Surf. Scie. **162-163** (2000) 452.
40. T.Y. Lee, J-H. Han, S.H. Choi, J-B. Yoo, C-Y. Park, T. Jung, S. Yu, J. Lee, W. Yi, J. M. Kim, Surf. Coat. Technol. **169-170** (2003) 348.
41. M.A. Ermakova, D.Y. Ermakov, A.L. Chuvilin, G.G. Kuvshinov, J. Catal. **201** (2001) 183.
42. C. Müller A. Leonhardt, S. Hampel, B. Büchner, phys. stat. sol. (b) **243** (2006) 3091.
43. W. Qian, T. Liu, Z. Wang, H. Yu, Z. Li, F. Wei, G. Luo, Carbon **41** (2003) 2487.
44. Z. Yu, D. Chen, B. Tøtdal, A. Holmen, Catal. Today **100** (2005) 261.
45. K. Hernadi, A. Fonseca, J. B. Nagy, D. Bernaerts, A.A. Lucas, Carbon **34** (1996) 1249.
46. Ph. Mauron, Ch. Emmenegger, P. Sudan, P. Wenger, S. Rentsch, A. Züttel, Diam. Rel. Mater. **12** (2003) 780.
47. B. Louis, G. Gulino, R. Vieira, J. Amadou, T. Dintzer, S. Galvagno, G. Centi, M.J. Ledoux, C. Pham-Huu, Catal. Today **102-103** (2005) 23.
48. C.J. Lee, K.H. Son, J. Park, J.E. Yoo, Y. Huh, J.Y. Lee, Chem. Phys. Lett. **338** (2001) 113.
49. A. Fonseca, K. Hernadi, J.B. Nagy, D. Bernaerts, A.A. Lucas, J. Mol. Catal. A: Chemical **107** (1996) 159.
50. D. Venegonia, P. Serp, R. Feurer, Y. Kihn, C. Vahlas , P. Kalck, Carbon **40** (2002) 1799.
51. G. Che, B.B. Lakshmi, C.R. Martin, and E.R. Fisher, Chem. Mater. **10** (1998) 260.
52. C. Du, N. Pan, Mater. Lett. **59** (2005) 1678.
53. J.I. Sohn, C. Nam, S. Lee, Appl. Surf. Scie. **197-198** (2002) 568.
54. A.K.M. Fazle Kibria, Y.H. Mo, K.S. Nahm, M.J. Kim, Carbon **40** (2002) 1241.
55. C. Emmenegger, J.-M. Bonard, P. Mauron, P. Sudan, A. Lepora, B. Grobety, A. Züttel, L. Schlapbach, Carbon **41** (2003) 539.
56. Y. Hao, Z. Qunfeng, W. Fei, Q. Weizhong, L. Guohua, Carbon **41** (2003) 2855.
57. I. Willems, Z. Kónya, J.-F. Colomer , G. Van Tendeloo, N. Nagaraju, A. Fonseca, J. B. Nagy, Chem. Phys. Lett. **317** (2000) 71.
58. A. Eftekhari, P. Jafarkhani, F. Moztarzadeh, Carbon **44** (2006) 1298.

59. V. Ivanov, J.B. Nagy, Ph. Lambin, A. Lucas, X.B. Zhang, X.F. Zhang, D. Bemaerts, G. Van Tendeloo, S. Amelinckx, J. Van Landuyt, Chem. Phys. Lett. **223** (1994) 329.
60. Y. Yang, Z. Hu, Y.N. Lü, Y. Chen, Mater. Chem. Phys. **82** (2003) 440.
61. M. Escobar, M. S. Moreno, R.J. Candal, M.C. Marchi, A. Caso, P.I. Polosecki, G.H. Rubiolo, S. Goyanes, Appl. Surf. Scie. **254** (2007) 251.
62. M. Su, B. Zheng, J. Liu, Chem. Phys. Lett. **322** (2000) 321.
63. Y. Li, X. Zhang, L. Shen, J. Luo, X. Tao, F. Liu, G. Xu, Y. Wang, H.J. Geise, G. Van Tendeloo, Chem. Phys. Lett. **398** (2004) 276.
64. Y-L. Li, I.A. Kinloch, M.S.P. Shaffer, C. Singh, J. Geng, B.F.G. Johnson, A.H. Windle, Chem. Mater. **16** (2004) 5637.
65. S. Bhaviripudi, E. Mile, S.A. Steiner III, A.T. Zare, M.S. Dresselhaus, A.M. Belcher, J. Kong, J. Am. Chem. Soc. **129** (2007) 1516.
66. X. Wang, W. Yue, M. He, M. Liu, J. Zhang, Z. Liu, Chem. Mater. **16** (2004) 799.
67. Y.C. Choi, W. Choi, Carbon **43** (2005) 2737.
68. B.C. Liu, S.C. Lyu, T.J. Lee, S.K. Choi, S.J. Eum, C.W. Yang, C.Y. Park, C.J. Lee, Chem. Phys. Lett. **373** (2003) 475.
69. J.W. Ward, B.Q. Wei, P.M. Ajayan, Chem. Phys. Lett. **376** (2003) 717.
70. M. Ritschel, A. Leonhardt, D. Elefant, S. Oswald, Bernd Büchner, J. Phys. Chem. C **111** (2007) 8414.
71. Y. Murakami, Y. Miyauchi, S. Chiashi, S. Maruyama, Chem. Phys. Lett. **374** (2003) 53.
72. H. Ago, S. Imamura, T. Okazaki, T. Saito, 74 M. Yumura, M. Tsuji, J. Phys. Chem. B **109** (2005) 10035.
73. E. Flahaut, A. Govindaraj, A. Peigney, Ch. Laurent, A. Rousset, C.N.R. Rao, Chem. Phys. Lett. **300** (1999) 236.
74. H. Igarashi, H. Murakami, Y. Murakami, S. Maruyama, N. Nakashima, Chem. Phys. Lett. **392** (2004) 529..
75. S. Maruyama, E. Einarsson, Y. Murakami, T. Edamura, Chem. Phys. Lett. **403** (2005) 320.
76. J. Zhu, M. Yudasaka, S. Iijima, Chem. Phys. Lett. **380** (2003) 496.
77. B.C. Liu, B. Yu, M.X. Zhang, Chem. Phys. Lett. **40**7 (2005) 232.

78. N. Yoshihara, H. Ago, M. Tsuji, J. Phys. Chem. C **111** (2007) 11577.
79. T. Hiraoka, T. Kawakubo, J. Kimura, R. Taniguchi, A. Okamoto, T. Okazaki, T. Sugai, Y. Ozeki, M. Yoshikawa, H. Shinohara, Chem. Phys. Lett. **382** (2003) 679.
80. R.R. Bacsa, E. Flahaut, Ch. 84 Laurent, A. Peigney, S Aloni, P. Puech, W.S. Bacsa, New J. Phys. **5** (2003) 131.1.
81. W.Z. Li, J.G. Wen, M. Sennett, Z.F. Ren, Chem. Phys. Lett. **368** (2003) 299.
82. E. Couteau, K. Hernadi, J.W. Seo, L. Thiên-Nga a, Cs. Mikó, R. Gaál, L. Forró, Chem. Phys. Lett. **378** (2003) 9.
83. H. Kathyayini, N. Nagaraju, A. Fonseca, J.B. Nagy, J. Mol. Catal. A: Chemical **223** (2004) 129.
84. J. Cheng, X. Zhang, Z. Luo, F. Liu, Y. Ye, W. Yin, W. Liu, Y. Han, Mater. Chem. Phys. **95** (2006) 5.
85. T.C. Schmitt, A.S. Biris, D.W. Miller, A.R. Biris, D. Lupu, S. Trigwell, Z.U. Rahman, Carbon **44** (2006) 2032.
86. Z. Balogh, G. Halasi, B. Korbély, K. Hernadi, Appl. Catal. A: General **344** (2008) 191.
87. A. Magrez, J.W. Seo, C. Mikó, K. Hernádi,, L. Forró, J. Phys. Chem. B **109** (2005) 10087.
88. M.C. Bahome, L.L. Jewell, D. Hildebrandt, D. Glasser, N.J. Coville, Appl. Catal. A: General **287** (2005) 60.
89. C-T. Hsieh, Y-T. Lin, J-Y. Lin, J-L. Wei, Mater. Chem. Phys. **114** (2009) 702.
90. C.H. See, A.T. Harris, Particle Technology and Fluidization **54** (2008) 657.
91. R. Vajtai, B.Q. Wei, P.M. Ajayan, Phil. Trans. R. Soc. Lond. A **362** (2004) 2143.
92. X-Y. Liu, B-C. Huang, N.J. Coville, Carbon **40** (2002) 2791.
93. W.B. Kim, T. Voitl, G.J. Rodriguez-Rivera, J.A. Dumesic, Science **305** (2004) 1280.
94. H.J. Dai, A.G. Rinzler, P. Nikolaev, A. Thess, D.T. Colbert, R.E. Smalley, Chem. Phys. Lett. **260** (1996) 471.
95. P-X. Hou, C. Liu, H-M. Cheng, Carbon **46** (2008) 2003.

Chapter 4

The use of organometallic transition metal complexes in the synthesis of shaped carbon nanomaterials: a review[#]

4.1 Introduction

Whilst numerous organometallic complexes were known prior to 1950, the synthesis of ferrocene (FcH) is regarded as the pivotal event that led to the field of organometallic chemistry as practiced today [1]. The realization that transition metal–carbon bonds were indeed facile to make and had reasonable stability was coupled to the implementation of appropriate characterization techniques that were being developed and used at the time [2]. These included IR and NMR spectroscopy as well as X-ray crystallography [3]. The clear link between homogeneous catalysis and organometallic chemistry has ensured the continued interest in this area of chemistry [4].

A recent development in the field of organometallic chemistry has been the use of organometallic complexes in the high yield catalytic synthesis of carbon nanotubes (CNTs) [5]. The development of appropriate characterization techniques, for example transmission and scanning electron microscopes (TEM, SEM), has assisted in the development of this field. Again, the area is driven by the potential uses of CNTs; in this instance, their use in interconnects, nanosensors, nanobalances, field emission displays and in the manufacture of strong and lightweight composites, etc. Indeed, today CNTs are made industrially in the tons pa level [6]. CNTs can be made by a variety of procedures and these include numerous variations of the arc-discharge [7], the laser ablation [8], and the CVD (chemical vapour deposition) processes [9]. While organometallic complexes can be used to make the catalysts required for the former two synthesis methods, the catalysts are generally made from metals or metal salts.

[#]*V.O. Nyamori, S.D. Mhlanga, N.J. Coville, J. Organometal. Chem. 693 (2008) 2205.*

Both these methods do produce relatively pure CNTs but are currently not easy to scale up to industrial levels of production.

The CVD processes, by contrast, do allow for easy scale up. There are two main approaches to the CVD synthesis of CNTs: one method entails passage of a gas phase carbon source over a supported catalyst whilst in the other both the catalyst and carbon source are in the gas phase. This latter process is called the 'floating catalyst' method. The catalyst used in the first CVD method can be derived from any metal source including an organometallic complex. But it is the floating catalyst method that typically requires volatile organometallic complexes to make CNTs. Remarkably, much of the work in this area of synthesis entails the use of very simple organometallic complexes (ferrocene and $Fe(CO)_5$) and the emphasis has not been on studying ligand effects on CNT synthesis. Indeed most studies to date involve catalysts purchased from manufacturers with studies focused on variation of CNT synthesis parameters or on reactor design.

It is to be noted that another type of CNT synthesis method has also been developed in recent years that does not use a gas flow system. Rather the reaction to make CNTs takes place in a closed container (e.g. autoclave or sealed quartz tube), at elevated pressures. Typically, in this method, organometallic complexes (at times containing an external carbon source) are used as starting materials to synthesize CNTs [10]. CNTs are but one type of carbon nanomaterial that is synthesized by the procedures described above, and the control of the morphology and type of CNT produced is a non-trivial task. Using typical reaction conditions, it is highly unusual to obtain > 95% pure material in any current synthetic process. Thus, in a typical synthesis it is not uncommon to synthesize a mixture of single walled (SW), double walled (DW) and multiwalled (MW) CNTs with a range of diameters, lengths and helicities, together with amorphous carbonaceous materials and carbon fibres. Under appropriate conditions, it is also possible to synthesize carbon horns [11], spheres (filled [12], hollow [10i,13]), onions [14] and cages [15] or metal filled tubes or core shell spheres [16]. Some of these various shaped materials are shown in Fig. 4.1. Much work is still needed to unravel the chemistry that is taking place

and that leads to control of the synthesis of these various carbon nanostructures. All of these shaped carbon nanomaterials (SCNMs) are of interest in their own right but the high yield synthesis of 'pure' materials is still to be achieved. The outcome of making mixtures is that subsequent purification processes are needed to remove impurities but these methods can also modify/destroy the required materials.

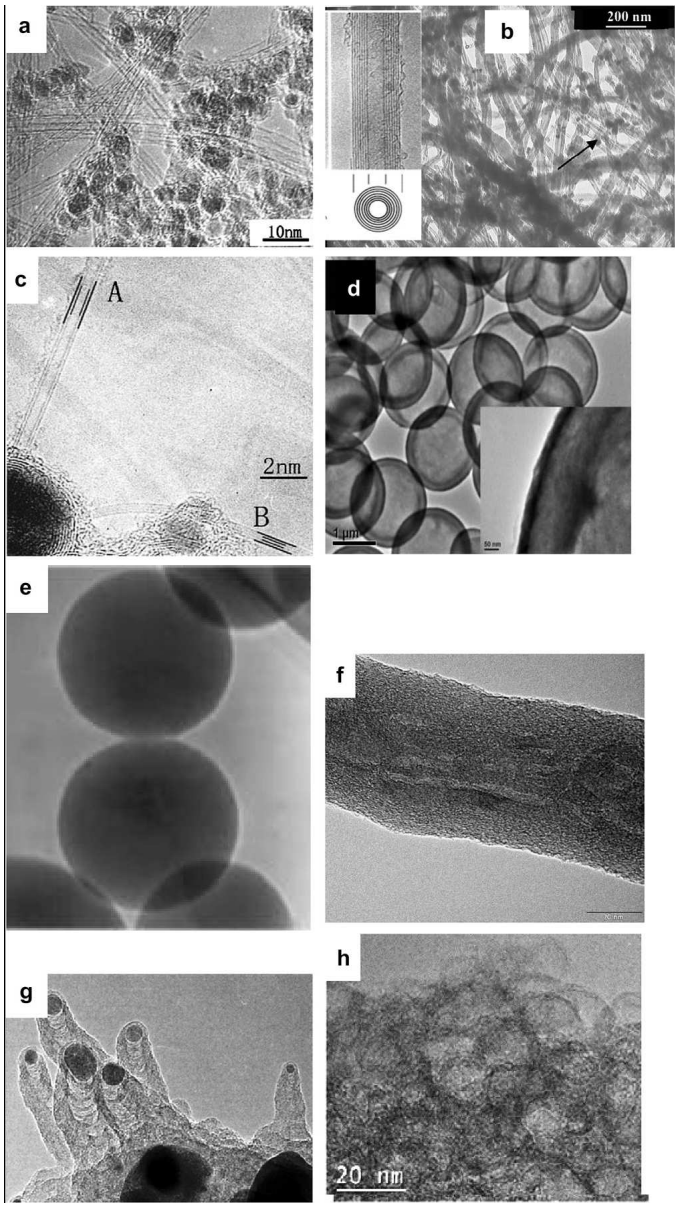

Fig. 4.1: Types of SCNMs: (a) SWCNTs [125]; (b) MWCNTs [30]; (c) DWCNTs [125]; (d) hollow carbon spheres [126]; (e) carbon spheres [127]; (f) nanofibre [128]; (g) nanohorns [11]; and (h) nanocages [129].

In this review, we have attempted to evaluate some of the factors that control the synthesis of the shaped carbon nanomaterials. In particular, we have attempted to evaluate the literature and to indicate the current status of the field from the perspective of organometallic chemistry.

We have reviewed the current literature on this topic and incorporated many of the studies into tables that permit a quick evaluation of key information. As there are many hundreds of publications that use organometallic complexes to synthesize SCNMs we have not attempted to list, in this review, all the studies that have been reported. Indeed, in many publications the organometallic complex used to make the SCNMs is purchased and the interest in the actual catalyst is marginal; this is particularly true of studies in which the electrical, mechanical or optical properties of the CNTs are the key part of the study. Thus, this review will describe the SCNM synthesis and include conclusions on the

(i) types of organometallic complexes that have been used;
(ii) effects of the carbon source;
(iii) effects of secondary elements (S, N, O, P);
(iv) effect of physical parameters (temperature, pressure, etc.);
(v) reactor design issues; and
(vi) mechanistic issues.

This literature review will not describe the properties associated with these materials as many excellent books are available that contain this information [17]. The review will also not describe the emerging chemistry associated with the purification and functionalization of these SCNMs [18]. Most of the studies on shaped carbon materials reported to date relate to the synthesis of CNTs as these are the complexes that have been most sought after. Two reviews by Rao and co-workers describe some early studies on the use of organometallic complexes on CNT synthesis, in particular from their own studies, and provide some discussion of early work in the area [5a,19]. A more recent review has focussed on the use of floating catalysts in the synthesis of CNTs [20].

4.2 The organometallic catalysts

A patent by Komatsu and Endo in 1985 appears to be the first report of the use of an organometallic complex to prepare a shaped carbon material [21]. A report by Tibbets in 1993 described the use of ferrocene (Fig. 4.2a) in carbon fibre growth [22]. In the years that followed, numerous reports appeared in which ferrocene was used to catalyze carbon shaped structures from a range of hydrocarbons [20]. Since then hundreds of articles have appeared in which ferrocene has been used to make SCNMs. This arises from the easy accessibility, price, stability in air and volatility of ferrocene.

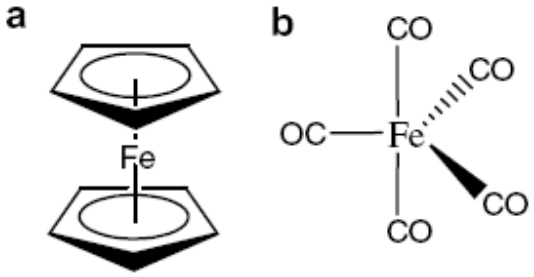

Fig. 4.2: Catalyst used for CNTs synthesis; (a) ferrocene and (b) $Fe(CO)_5$.

Another much used organometallic complex is $Fe(CO)_5$ (Fig. 4.2b) and again the advantages associated with ferrocene apply to $Fe(CO)_5$. Indeed, $Fe(CO)_5$ is used in the industrial HiPCO process to produce CNTs [23]. A listing of the conditions used, the products formed and other important information that relates to the use of ferrocene (**Table 4.1**), $Fe(CO)_5$ (**Table 4.2**) and other organometallic complexes (**Tables 4.3–4.5**) also indicates the wide range of carbon sources and physical parameters that have been used during the past 15 years. Noticeable from the tables are the limited range of organometallic complexes that have been studied. Other than ferrocene and $Fe(CO)_5$ few other organometallic complexes have been used to make SCNMs, and in particular CNTs.

Table 4.1: Ferrocene as a catalyst for the synthesis of CNTs and other SCNMs.

SNCMs	Reactor design	Carbon source and FcH concentration	Temperature	Pressure and flow rate	Secondary elements	References
SWCNTs	High-pressure CVD reactor	Ferrocene	650–900 °C (pyrolysis)	Pressure 1–5 bars 2000 sccm Ar–FcH vapour mixture flow rate	None	[52]
	Horizontal CVD reactor	Ferrocene	1100–1150 °C (pyrolysis)	Ar flow rate 1500 ml/min H_2 flow rate 150 ml/min	H_2 Sulphur (Fe:S = 10:1)	[64]
	Horizontal CVD reactor two stage furnace system	Ferrocene and acetylene	*T* (F1) 350 °C (sublimation) *T* (F2) 1100 °C (pyrolysis)	Ar flow rate 1000 sccm C_2H_2 flow rate 50 sccm H_2 flow rate 25 sccm	H_2	[37]
	Horizontal CVD reactor two stage furnace system	Ferrocene (sublimation rate $3.74–4.68 \times 10^{-5}$ mol/h); Acetylene (3–10 sccm)	*T* (F1) 60–90 °C (sublimation) *T* (F2) 900–1000 °C (pyrolysis)	Ar flow rate 1200 sccm C_2H_2 partial pressure of 5.0 Torr (best) or less	None	[51]
	Horizontal CVD reactor two stage furnace system	Ferrocene; Acetylene (1 sccm)	*T* (F1) 55 °C (sublimation) *T* (F2) 1100 °C (pyrolysis)	Ar flow rate 300–2000 sccm C_2H_2 flow rate 1 sccm Total reactor system pressure held at 1 atm.	Sulphur Ratio FcH:S = 16:1	[67]
	Vertical CVD reactor	Ferrocene (0.018 g/ml) and Thiophene (0.4 wt %) in *n*-hexane	1150 °C (pyrolysis)	FcH/hexane/thiophene soln flow rate into reactor 0.5 ml/min H_2 flow rate 250 ml/min	H_2; Thiophene	[63] [106]
	Vertical CVD reactor	Ferrocene (0.025 g/ml) and Thiophene (0.6 wt %) in *n*-hexane	1200 °C (pyrolysis)	FcH/hexane/thiophene soln flow rate into reactor 0.6 ml/min H_2 flow rate 250 ml/min	H_2 200–250 mL/min; Thiophene	[46]
	Horizontal CVD reactor two stage furnace system	Ferrocene (vaporization rate $1.5–4.5 \times 10^{-7}$); Thiophene (0.5-5 wt%) in benzene	*T* (F1) 185 °C (sublimation) *T* (F2) 1100–1200 °C (pyrolysis)	$H_2$70–90 ml/min (F2) H_2 150–225 ml/min (F1)	H_2	55 [63c]
	Vertical CVD reactor	Ferrocene; Benzene and thiophene soln	*T* (F1) 120 °C (sublimation) *T* (F2) 1150 °C (pyrolysis)	Ferrocene carrier gas flow rate 0.3–0.5 l/min Benzene carrier gas flow rate 0. 1–0.2 l/min	H_2(carrier gas) Sulphur (S/C = 1:200)	[63d]
	Horizontal CVD reactor	Ferrocene thiophene in benzene (3.0 wt%)	1150 °C (pyrolysis)	H_2 flow rate 1–10 ml/min	H_2; Thiophene	[63e]
	Horizontal CVD reactor with ultrasonic atomizer (850 kHz frequency)	Ferrocene and sulphur mixture (10:1 atomic ratio) in *m*-xylene to form 40 mg/ml.	1050 °C (pyrolysis)	Carrier gas ratio Ar:H_2 = 2:1 Total gas flow rate 300-1500 sccm	Sulfur H_2	[50]
	Horizontal CVD reactor with a sprayer system attached	Ferrocene in Ethanol 0.2–1.2 wt % FcHV (optimal 1.2 wt % FcH)	700–950 °C (optimal 950 °C) 30 min rxn time	FcH–ethanol flow rate 0.3 ml/min Ar flow rate 0.1–0.8 l/min	None	[107]
	Horizontal CVD reactor with ultrasonic atomizer (~MHz, 20-30 W)	Ferrocene in Ethanol 0.1–3 wt% FcH(optimal 1.0–1.5 wt% FcH)	650–800 °C (pyrolysis)(optimal 700 °C) 30 min rxn time	FcH–ethanol flow rate ~0.7 g/min Ar flow rate 0.5–2.5 L/min (optimal)	None	[54]
	Horizontal CVD reactor with a sprayer system attached	Ferrocene in Ethanol 1 g/100 ml to 1 g/800 ml	900–1100 °C (pyrolysis)	FcH–ethanol flow rate 50– 80 ml/hr Ar flow rate 80–120 l/h	None	[108]
	CVD vertical laminar flow reactor	Ferrocene CO	700–900 °C (pyrolysis)	Partial vapour pressure of FcH 0.8 Pa N_2/H_2 93/7 Vol%	FcH:SiO_2 = 1:4 CO_2 (Insitu)	[96]
	CVD vertical laminar flow reactor with a hot wire generator (HWG) for ferrocene aerosol	Ferrocene, CO, CO_2	575–600 °C (pyrolysis)	Partial vapour pressure of FcH 0.7 Pa CO flow rate 100 cm^3/min CO_2(600–8000 ppm)	CO_2 H_2O (150 ppm)	[61]
DWCNTs	Horizontal CVD reactor; two stage heating system	Ferrocene (vaporization rate = 6.45×10^{-6} mol/min) Tetraethoxysilane (TEOS) (vaporization rate = 1.28×10^{-4} mol/min)	*T* (F1) 120 °C (sublimation) *T* (F2) 1000–1100 °C (pyrolysis)	Ar flow rate 800 ml/min H_2flow rate 400 ml/min	H_2 $SiO_2$from TEOS decomposition	[105]
	Horizontal CVD reactor; two stage furnace system	Ferrocene Acetylene	*T* (F1) 60–90 °C (sublimation) *T* (F2) 900–1200 °C (pyrolysis) Reaction time 1.5 h	Ar flow rate 1200 sccm acetylene 8 sccm	Sulphur S:FcH = 1:8–1:64 range	[65]
	Horizontal CVD reactor; two stage furnace system	Ferrocene Acetylene	*T* (F1) 60–90 °C (sublimation) Furnace (2) 1100 °C (pyrolysis) Reaction time 1.5 h	Ar flow rate 300–2400 sccm C_2H_2 flow rate 2–20 sccm with a partial pressure of 0.25 Torr	Sulphur FcH:S = 512:1 to 6:1 range	[68a]

(*continued on next page*)

Table 4.1 (continued)

SNCMs	Reactor design	Carbon source and FcH concentration	Temperature	Pressure and flow rate	Secondary elements	References
	Horizontal CVD reactor two stage furnace system	Ferrocene Acetylene	Ferrocene/sulphur T (F1) at 60–90 °C (sublimation) T (F2); 1100 °C (pyrolysis)	Ar flow rate 1200–1600 sccm C_2H_2 flow rate 8–12 sccm Total pressure of the system was held at 1 atm	Sulphur; FcH:S = 8:1–192:1 molar ratio	[68b]
	Horizontal CVD reactor; with a three-section quatz tube with a two stage heating system	Ferrocene Acetylene	T (F1) 60–90 °C (Preheationg) T (F2) 950–1150 °C (pyrolysis) Reaction time 1.5 h	Ar flow rate 300–2400 sccm C_2H_2 flow rate 1–20 sccm with a partial pressure of 0.25 Torr system pressure at 1 atm	Sulphur FcH:S = 512:1 to 6:1 range	[66]
	Horizontal CVD reactor; two stage furnace system	Ferrocene Acetylene	T (F1) 60–90 °C (Preheating) T (F2) 900-1150 °C (pyrolysis) Reaction time 1.5 h	Ar flow rate 1600 sccm C_2H_2 flow 8 sccm	Sulphur S:FcH = 1:8–1:64	[69]
	Horizontal CVD reactor two stage furnace system	Ferrocene Methane	Ferrocene/sulphur T (F1) 100 °C (Preheating) T (F2) 1150 °C (pyrolysis) Reaction time 30 min	Ar flow rate 1500–2500 sccm	Sulfur FcH:S = 10:1	[70]
	Horizontal CVD reactor two stage furnace system with a an injector attached	Ferrocene/sulfur mixture in xylene (conc of 0.03–0.12 g/mL)	Reactor temp 900–1180 C (pyrolysis) Reaction time 10–20 min	Feeding rate 0.05–0.15 ml/min Ar flow rate 2500–3500 sccm H_2 flow rate 500 ml/min	Sulphur Fe:S = 10:1	[71]
MWCNTs	Horizontal CVD reactor with a an injector attached	Ferrocene in xylene 8.25% mole fraction of FcH (i.e. 1.00 % Fe/C ratio)	T (F1) 350 °C (sublimation) T (F2) 875 °C (pyrolysis)	Injection rate 4.0 ml/min FcH Total flow rate Ar/H_2 1500 sccm	H_2 10 % H_2 in Ar	[33b]
	Horizontal CVD reactor with two stage furnace system	Ferrocene to benzene ratio 4.2–8.6 % thiophene 0.55 wt %	T (F1) 115–125 °C (sublimation) T (F2) 1150 °C (pyrolysis)	Carrier gas (H_2) total flow rate 700 ml/min	Sulfur H_2	[43b]
	Horizontal CVD reactor two stage heating system with a an injector attached	Ferrocene in xylene 6.5 mol % of FcH in xylene i.e. ~0.75 % Fe/C ratio	T (F1) ~175 °C (sublimation) T (F2) ~675 °C (pyrolysis)	1Carrier gas (Ar:H_2 = 10:1) Ar/H_2 1688/188 sccm Feed rate FcH–xylene 2.5 ml/h Partial pressure for xylene was 4 mbar	H_2	[45c]
	Horizontal CVD reactor with a nebulizer (1.54 MHz ultrasonic)	Ferrocene 2 g in 100 ml xylene	900°C temp (pyrolysis) (30 min)	1000 sccm Ar flow rate	Ar	[45b]
	Two stage horizontal CVD reactor with a an injector attached	Ferrocene 0.02 g/ml of xylene	T (F1) 300 °C (sublimation) T (F2) 850 °C (pyrolysis)	Reagent injection flow rate 0.4 ml/min Ar/H_2flow rate 2000/400 sccm	H_2 Ar	[45a]
	Two stage horizontal CVD reactor	Ferrocene 2-9.6 wt% in toluene	T (F1) 200°C (sublimation) T (F2) 700–760°C (pyrolysis)	H_2 10% in Ar total flow rate 750 ml/min	H_2 Ar	[44b]
	Two stage horizontal CVD reactor	Ferrocene 1-9.6 wt% in toluene	T (F1) 200°C (sublimation) T (F2) 590–840°C (pyrolysis)	H_2 10% in Ar total flow rate	H_2 Ar	[44c]
Amorphous Carbon	Horizontal CVD reactor with a boat	Ferrocene	200 °C (30 min)	Pure Cl_2gas	Cl_2	[88]
nanotubes (ACNTs)	Teflon-lined autoclave (50 ml)	Ferrocene (2.97 mmol, 0.552 g) Sodium (13 mmol, 0.3 g) Benzene 3/4 of autoclave	210 °C (pyrolysis) (24 h)	Autogenic pressure	Under air	[98b]
	Vertical quartz CVD reactor	Ferrocene Benzene thiophene	1100–1200 °C	H_2 Flow rate 100 cm^3/min	H_2	[63b]
	Teflon-lined Autoclave (50 ml)	Ferrocene (1 mmol) Sulphur (2 mmol) Benzene 90% of autoclave	200 °C (pyrolysis) (70 h)	Autogenic pressure	Under air	[98a]
Hollow carbon nanosphere (HCSs)	Stainless steal autoclave (2 ml)	Ferrocene (0.186 g)	700 °C (pyrolysis) Reaction time 1 h	Reaction under N_2 atmosphere Total pressure 2.2 MPa	Reaction under N_2 atmosphere	[13b]
	Horizontal CVD reactor with two stage heating system	Ferrocene Camphor	T (F1) 50 °C (Preheating) T (F2) 1000 °C (pyrolysis)	12.5 g of solution transferred to reactor per hour with the aid of Ar gas	Ar	[101a]
Filled sphere	Horizontal CVD reactor with two stage heating system	Ferrocene Camphor	T (F1) 50 °C (Preheating) T (F2) 1000 °C (pyrolysis)	12.5 g of solution transferred to reactor per hour with the aid of Ar gas	Ar	[101a]
	Horizontal CVD reactor with two stage heating system	Ferrocene/ Anthracene (1:7)	T (F1) 160–200 °C (sublimation) T (F2) 580-700 °C (pyrolysis)	H_2 flow rate 300-400 ml/min	H_2	[47b]

Table 4.1 (continued)

SNCMs	Reactor design	Carbon source and FcH concentration	Temperature	Pressure and flow rate	Secondary elements	References
Carbon nano-onions	Horizontal CVD reactor with two stage furnace system	Ferrocene (~0.7 g) Or mixture of FcH/ $Fe_3(CO)_{12}$	*T* (F1) 300 °C at of 40 °C min^{-1}(sublimation) *T* (F2) 900 °C (pyrolysis)	Ar flow rate 260 ml min^{-1}\ 0.5% and 1.0% of O_2 in Ar	$Fe_3(CO)_{12}$	[14]
Iron-included Carbon nanocapsules and nanotubes	Horizontal CVD reactor with two stage furnace system	Ferrocene	*T* (F1) 200 °C (sublimation) *T* (F2) 625 °C (pyrolysis)	Carrier gas (H_2) Flow rate 100–300 cm^3/min	H_2	[109]
	Horizontal CVD reactor with two stage furnace system	Ferrocene	T (F1) 200 °C (sublimation) *T* (F2) 900 °C (pyrolysis)	Carrier gas (Ar:H_2 = 3:1 Flow rate 50 sccm	H_2	[5b]
	Horizontal CVD reactor with two stage furnace system	Ferrocene	T (F1) 620 °C (sublimation) *T* (F2) 1000 °C (pyrolysis)	Carrier gas (Ar) Flow rate 1000 sccm	Ar	[110]
	Stainless steal autoclave (14 mm in inner diameter, 70 mm in length)	Ferrocene (FcH) Picric acid (PA) (PA:ferrocene = 8:1–2:1)	The detonation of explosive was initiated by heating (20 °C/min) and occurred at 290 °C; Reaction temperature 1000 °C	Autogenic pressure	None	[16c]

Table 4.2: $Fe(CO)_5$ as a catalyst for the synthesis of CNTs and other SCNMs.

SNCM	Reactor design	Carbon Source	Temperature	Pressure and flow rate	Secondary elements	Reference
SWCNTs	Horizontal CVD reactor two stage furnace system	Acetylene–$Fe(CO)_5$	*T* (furnace 1) 350 °C *T* (furnace 2) 1100 °C	C_2H_2 flow rate 50 sccm $Fe(CO)_5$ vol. 1 ml Ar flow rate 1000 sccm	None	[37] [19]
	Horizontal CVD reactor	CO mixed with small amounts of $Fe(CO)_5$	800–1200 °C	CO (1–10 atm) $Fe(CO)_5$ (1–25 mTorr)	None	[23] [111]
	Horizontal CVD reactor two stage furnace system	CO	*T* (furnace 1) 700 °C *T* (furnace 2) 900 °C	CO flow rate 800 sccm H_2 flow rate 200 sccm	None	[112]
MWCNTs (aligned)	Horizontal CVD reactor with atomizer	Acetylene–$Fe(CO)_5$	900 °C	C_2H_2 flow rate 100 sccm Ar flow rate 1000 sccm	None	[45b]
MWCNTs (helically coiled)	Horizontal CVD reactor two stage furnace system with vapourization chamber and an ice cooler	1 g $Fe(CO)_5$ dissolved in (1) 99 g Pyridine (2) 99 g Toluene	1050–1150 °C	H_2 carrier gas flow rate 350–400 ml/min	None	[113]
MWCNTs	Vertical CVD reactor	Methane	1050–1150 °C	CH_4 flow rate 125–250 sccm $Fe(CO)_5$ feeding rate 0.5–2.5 ml/h N_2 flow rate 1000–2000 sccm	None	[40c]
	Horizontal CVD reactor	$Fe(CO)_5$-pentane 3.3 wt% $Fe(CO)_5$	700–800 °C	N_2/$Fe(CO)_5$ flow rate 50–100 ml/min	None	[12c]
CNFs	Vertical CVD reactor	Methane	800 °C	Methane flow rate 5300 cm^3/min He with $Fe(CO)_5$165 cm^3/min H_2S flow rate 8 cm^3/min	Sulfur	[74]
CNBs	Horizontal CVD reactor	$Fe(CO)_5$-pentane 10 wt% $Fe(CO)_5$	900–1000 °C	N_2/$Fe(CO)_5$ flow rate 50 ml/min	None	[40c]

It is quite remarkable that the use of a single catalyst, ferrocene, has led to the synthesis of such a wide range of carbon shapes (some examples are given in Fig. 4.1a-f). This reveals the rich chemistry in this field that is still being established. Other typical organometallic complexes that have shown good activity and selectivity towards SCNM synthesis, in particular CNTs include cobaltocene, nickelocene, their mixtures (**Table 4.3**) as well as metal (Fe, Co, Ni) phthalocyanines (**Table 4.4**). These latter complexes introduce nitrogen into the carbon structures and this issue is dealt with separately below.

Table 4.3: Cobaltocene, nickelocene and ruthenocene as catalysts for the synthesis of CNTs and other SCNMs.

SNCM	Reactor design	Metallocene + carbon source	Temperature	Pressure and flow rate	Secondary elements	Reference
SWCNTs	Horizontal CVD reactor two stage furnace system	1. Cobaltocene–acetylene mixture 2. Nickelocene–acetylene mixture	T (F1) = 200 °C (sublimation) T (F2) = 1100 °C (pyrolysis)	Ar flow rate 1000 sccm C_2H_2 flow rate 50 sccm	None	[5a]
	Horizontal CVD reactor two stage furnace system	Cobaltocene–ferrocene/ nickelocene–acetylene mixture	T (F1) = 200 °C (sublimation) T (F2) = 1100 °C (pyrolysis)	Ar flow rate 975 sccm H_2 flow rate 25 sccm C_2H_2 flow rate 50 sccm	None	[19] [37] [114]
	Horizontal CVD reactor with an atomizer	1. Cobaltocene–toluene mixture (20 g/l) 2. Cobaltocene–toluene mixture (20 g/l)	900 °C (pyrolysis)	Ar flow rate of 1000 sccm.	None	[45b]
MWCNTs	Horizontal CVD reactor two stage furnace system	1. Cobaltocene 2. Nickelocene	T (F1) = 200 °C (sublimation) T (F2) = 900 °C (pyrolysis)	Ar (75%)–H_2 (25%) flow rate 50 sccm	None	[5b]
	Horizontal CVD reactor two stage furnace system	1. Cobaltocene–benzene mixture 2. Cobaltocene–benzene mixture	T (F1) = 200 °C (sublimation) T (F2) = 900 °C (pyrolysis)	Ar (85%)–H_2 (15%) flow rate 1000 sccm	None	[5a] [19]
	Horizontal CVD reactor	1. Cobaltocene–benzene, toluene, xylene, cyclohexane, cyclohexanone, *n*-hexane, *n*-heptane, *n*-octane, *n*-pentane 2. Nickelocene–benzene, toluene, xylene, cyclohexane, cyclohexanone, *n*-hexane, *n*-heptane, *n*-octane, *n*-pentane	875 °C (pyrolysis)	6 g metallocene in 100 ml hydrocarbon catalyst 1 ml/min solution flow-rate Ar carrier gas flow 500 l/h	None	[38]
	Horizontal CVD reactor two stage furnace system	Cobaltocene–ferrocene mixture (1:2)	T (F1) = 120–140 °C (sublimation) T (F2) = 980 °C (pyrolysis)	Ar/H_2mixture Total flow rate 150 sccm	None	[115]
	Horizontal CVD reactor	1. Cobaltocene in supercritical toluene with hexane or ethanol as supplemental carbon source 2. Nickelocene in supercritical toluene with hexane or ethanol as supplemental carbon source	600–645 °C (pyrolysis)	Pressure 8.3 MPa Solution injection flow rate 1 ml/min	None	[116]
	Horizontal CVD reactor two stage furnace system	Xylene–ruthenocene–ferrocene mixture	T (F1) = 200 °C (sublimation) T (F2) = 700 °C (pyrolysis)	Ar/H_2 (10%) carrier gas	None	117
	Horizontal CVD reactor two stage furnace system	Nickelocene–tetrahydrofuran mixture	T (F1) = 171–173 °C (sublimation) T (F2) = 600 °C (pyrolysis)	No carrier gas used	None	[118]
DWCNTs	Horizontal CVD reactor two stage furnace system	Cobaltocene–acetylene mixture	T (F1) = 60–90 °C (sublimation) T (F2) = 950–1150 °C (pyrolysis)	Ar flow rate 300–2400 sccm C_2H_2 flow rate 2–20 sccm	Sulphur	[68a]
Y-Junction MWCNTs	Horizontal CVD reactor two stage furnace system	1. Cobaltocene–thiophene mixture 2. Nickelocene–thiophene mixture	1000 °C	Ar flow rate 100–200 sccm H_2 flow rate 50–150 sccm	None	[75]
CNFs	Horizontal CVD reactor two stage furnace system	Cobaltocene–acetylene–thiophene mixture	T (F1) = 140–180 °C (sublimation) T (F2) = 1100–1150 °C (pyrolysis)	H_2 carrier gas flow rate 20 mg min^{-1}	None	[119]
CNBs	1. Stainless steel autoclave placed in a horizontal furnace 2. Horizontal CVD reactor two stage furnace system	Ruthenocene–ethylene mixture	T (F1) = 400 °C (sublimation) T (F2) = 900–1300 °C (pyrolysis)	Ar flow rate 200 sccm H_2 flow rate 150 sccm C_2H_4 flow rate 50 sccm	None	[28]

Table 4.4: Fe, Co and Ni phthalocyanines as catalysts for the synthesis of CNTs and other SCNMs.

SNCM	Reactor design	Carbon source	Temperature	Pressure and flow rate	Secondary elements	Reference
SWCNTs	Two-zone CVD electrical furnace	Iron phthalocyanine	T (F1) = 480–520 °C (vapourization) T (F2) = 800–920 °C (pyrolysis)	Ar/H_2 flow (1:1v/v) 40 cc/min	None	[120]
MWCNTs	Horizontal CVD reactor two stage furnace system	1. Iron phthalocyanine 2. Nickel phthalocyanine 3. Cobalt phthalocyanine	T (F1) = 550 °C (vapourization) T (F2) = 700–1000 °C (pyrolysis)	Ar flow rate 30–150 sccm H_2 flow rate 5–10 sccm	None	[121]
Y-junction MWCNTs	Horizontal CVD reactor two stage furnace system	1. Iron phthalocyanine + thiophene mixture 2. Nickel phthalocyanine + thiophene mixture	T (F1) = 440–520 °C (vapourization) T (F2) = 1000 °C (pyrolysis)	Ar flow rate100–200 sccm H_2 flow rate 50–150 sccm	None	[75] [81b] [19]

Another approach has been to use substituted ferrocenes and this has permitted the exploration of ligand effects associated with the catalysts (**Table 4.5**). Here, both carbon and non-carbon elements can be introduced into the reaction using this procedure. The use of simple carbon ligand substituents impacts on ferrocene in terms of both physical (volatility) and chemical (electronic) factors and consequently SCNM synthesis. For example, a comparison of FcH with $(C_5H_4Me)(C_5H_5)Fe$ as catalyst under identical reaction conditions, revealed the formation of MWCNTs with larger diameters when the Me group is present [24]. Further, Keller and co-workers have decomposed alkyne substituted ferrocenes to give CNTs with Fe embedded in the CNT [25].

Table 4.5: Ferrocenyl derivatives as a catalyst for the synthesis of CNTs and other SCNMs.

SNCM	Reactor design	Carbon source	Temperature	Pressure and flow rate	Secondary elements	Reference
MWCNTs	Horizontal CVD furnace	Ferrocenylethynyl benzenes	500–1400 °C	Ambient pressure under argon	None	[25a]
	Horizontal CVD furnace	1,4-Diferrocenylbutadiyne	500–1400 °C	Ambient pressure under argon	None	[25c]
	Horizontal CVD furnace	Butadiynyl–ferrocene-containing compounds	500 – 1400 °C	Ambient pressure under argon	None	[25b]
	Horizontal CVD furnace	1. Dimethylferrocene in toluene 2. Diethylferrocene in toluene	800–1000 °C	1. 5 wt% H_2/Ar flow rate 100 ml/min 2. Solution injection rate 0.2 and 0.8 ml/min	None	[24]
	Horizontal CVD furnace	$CpFe(CO)_2Me$ in toluene	800–1000 °C	5 wt%H_2/Ar flow rate 100 ml/min Solution injection rate 0.2–0.8 ml/min	None	[30]
	Horizontal CVD furnace	Ferrocene and ferrocenyl disulfide mixture	800–1000 °C	5 wt%H_2/Ar flow rate 100 ml/min Solution injection rate 0.2–0.8 ml/min	None	[77]
	Two zone horizontal CVD furnace	1. Cyclopentadienyliron dicarbonyl dimer 2. Cyclooctatetraene iron tricarbonyl	T (F1) = 200 °C (sublimation) T (F2) = 685–750 °C (pyrolysis)	1. Solution injection rate 1.5–2.0 ml/h 2. 4 wt% H_2/Ar flow rate 1.5 slpm	None	[27]
	Two stage horizontal CVD furnace	Ferrocene–$Fe_3(CO)_{12}$mixture	T (F1) = 300 °C (sublimation) T (F2) = 900 °C (pyrolysis)	Ar carrier gas flow rate 260 ml/min	None	[14]
SWCNTs	Horizontal CVD furnace	Polyferrocenylsilane block copolymer	500 °C	Not applicable	None	[122] [123]
	Horizontal CVD furnace	Poly(ferrocenylsilane)-*block*-polysiloxane Diblock Copolymers	900 °C	1. H_2 flow rate 500 sccm 2. Methane flow rate 800 sccm 3. Ethylene flow rate 20 sccm	None	[124]
CNFs and CSs	Horizontal CVD furnace	1. Dimethylferrocene in toluene 2. Diethylferrocene in toluene	800–1000 °C	5 wt%H_2/Ar flow rate 100 ml/min Solution injection rate 0.2 and 0.8 ml/min	None	[24]
	Horizontal CVD furnace	Ferrocene and ferrocenyl disulfide mixture	800–1000 °C	5 wt%H_2/Ar flow rate 100 ml/min Solution injection rate 0.2–0.8 ml/min	None	[77]

Remarkably, few other studies have been reported in which other organometallic complexes have been studied. Some of these include $(CO)_5W = C(OCH_3)(C_6H_4OCH_3)$ [26], $[CpFe(arene)]^+[PF]^{6-}$ [10b], $[CpFe(CO)_2]_2$ [27], ruthenocene [28], $Ru_3(CO)_{12}$ [29], $[Co_2(CO)_6RCCR]$ and other related cobalt organometallic complexes [10d,10e,10f,10g]. Studies in our research group have the effect of iodine, where $CpFe(CO)_2I$ was used a the catalysts precursor [30a]. Most recently, Nxumalo *et al.* [30b] synthesized nitrogen doped carbon nanotubes (N-CNTs) by the CVD floating catalyst method using either 4-ferrocenylaniline or mixtures of varying concentrations of ferrocene/aniline together with toluene as added carbon source. The N-CNTs produced were less stable (thermogravimetric analysis measurements), less graphitic and more disordered (transmission electron microscope measurements) than their undoped counterparts [30b]. Other studies involving the use of $Mo(CO)_6$ have been reported [31].

Pol and co-workers have reported that apart from thermal dissociation of hydrocarbons at autogenic pressure at elevated temperature (RAPET), organometallic precursors (Co, Ni, Mo, V, Zr or W) have also been reacted and typically yielded products in the nanometric range, either as core shell structures or well-dispersed particles [32].

Organometallic complexes have been used to synthesize SCNMs in a closed environment, typically in an autoclave or sealed quartz container. In these studies, performed at elevated temperatures, the organometallic complex can provide both catalyst and carbon source. Again, very few complexes have been studied with most based on Co and Fe metal catalysts [10]. The carbon source has been varied and the influence of reducing reagents has also been explored [33]. This approach has led to the synthesis typically of CNTs, fibres and spheres [10a,34].

Organometallic complexes have also been used to provide metal complexes for typical CVD processes, but this entails decomposing the complexes on a support prior to SCNM synthesis. Any source of metal (as a salt or coordination complex) can be used to achieve this result but organometallic complexes do have the advantage of not necessarily requiring the presence of a counter-ion.

4.3 Bimetallic catalysts

The control of catalyst nanoparticle size and distribution can be achieved by the use of bimetallic catalysts. In this approach, two or more metals can be either bonded to each other in a metal cluster complex or can be added as a mixture of two separate complexes. The latter approach is easier to use and indeed nearly all studies involving organometallic complexes, reported to date, have applied this approach. Generally the CVD method uses the former approach. For example, it has been observed that catalysts made by the addition of molybdenum to iron stabilized the active Fe nanoparticles [36]. The higher yield of CNTs achieved with bimetallic catalysts has been attributed to particle melting point reduction, increase in carbon solubility and the formation of well-dispersed metal clusters upon segregation during CNT formation [35].

The method involving a mixture of two metal complexes has been used in the floating catalyst process. Rao and co-workers reported a successful synthesis of SWCNTs by the pyrolysis of mixtures of acetylene with binary metallocenes in flowing Ar or Ar + H_2 at 1100°C [37]. The diameter of the nanotubes was generally around 1 nm. They have also shown that the pyrolysis of a dilute acetylene-metallocene mixture gives rise to very fine metal particles essential for the formation of SWCNTs. Further, the use of hydrogen along with Ar, minimized the amorphous carbon coating on the nanotubes. Binary metallocene (nickelocene–cobaltocene) mixtures occasionally give bundles of nanotubes on pyrolysis with acetylene. Horváth *et al.* have studied the efficiency of bimetallic catalyst particles by investigating ferrocene-cobaltocene, ferrocene-nickelocene and cobaltocene-nickelocene mixtures against a ferrocene standard [38]. Their findings show that ferrocene-cobaltocene and ferrocene-nickelocene mixtures increased the carbon nanotube production compared to ferrocene on its own, and the highest yield was obtained using the ferrocene-nickelocene mixture. The samples contained mainly straight nanotubes and negligible amounts of amorphous carbon implying that these bimetallic catalysts also improved the quality and purity of the nanotube samples.

Mohlala *et al.* utilized bimetallic catalyst systems (ferrocene/$M(CO)_5$tBuNC, where M =W or Mo) to synthesis MWCNTs in 5% H_2 in Ar at temperature range 700-900°C [39]. TEM analysis revealed the formation of large metal particles in the MWCNTs determined to be Mo/Fe alloys rich in Fe, indicating that an alloy had been formed under the reaction conditions. Under similar reaction conditions, ferrocene yielded MWCNTs and carbon balls (CBs) while the $M(CO)_5$tBuNC complex yielded little carbonaceous material. It was observed that the diameters of the CNTs formed in the presence of ferrocene are smaller while the diameters of CBs are larger relative to the diameters of CNTs and CBs produced by the bimetallic catalyst systems.

4.4 The carbon source

The synthesis of SCNMs requires some source of carbon to create the carbon structures and this can be supplied by a catalyst and/or by an external source. When supplied by a

catalyst such as ferrocene or $Fe(CO)_5$, C is derived from the Cp or CO ligands. It is generally believed that the ligands break down into C1 (or similar small C radicals) in the gas phase and that these small species then 'condense' into the shaped materials. However, formation of larger gas phase radicals is also possible and these certainly play a role in the formation of SCNMs. This issue will be dealt with in Section 4.8.

In most studies the carbon used to make the SCNMs is derived from an external source and this can be any carbon containing material. Typically, hydrocarbons are used and include CH_4 [40], C_2H_4 [41], C_2H_2 [5c,42], C_6H_6 [5b,34,43], $C_6H_5CH_3$ [44], xylene [45], pentane [12c], hexane [21,46], anthracene [10a,47], toluene [30b] etc. Factors such as C/H or C/M (M = metal) ratios, reactant volatility, reactant stability as well as radical and ion formation play key roles in determining the eventual products obtained.

The morphology of the SCNMs should be influenced by the carbon source, as indeed has been found when CNTs are synthesized. However, a range of hydrocarbons used in the synthesis of carbon spheres did not have a significant effect on their properties (e.g. size) [48]. However, in the presence of a heteroatom (e.g. oxygen from alcohols) the size and yield of the spheres were affected [49]. The common heteroatoms used in the synthesis of SCNMs are discussed in the following sections. Several studies have indicated that the diameters and distribution of the carbon spheres [48] as well as CNTs can be controlled by varying the reaction time, feed time and reactant flow rate [50]. Variation of these parameters not only affected the sizes but also controlled the product SCNM yields and distribution [24]. In addition, it has been reported that adjusting the partial pressure of the carbon source in the CVD synthesis of CNTs in the floating catalyst method, can control the mean diameters as well as the amount of material produced [51,52].

4.5 Other elements

The addition of heteroatoms to the reactant streams used to make SCNMs plays a key role in producing either doped materials or 'cleaner' materials. Thus, the heteroatom can be introduced by incorporation into the carbon source or into the catalyst ligand and this

can lead to modified chemical and physical properties of the SCNMs formed from the reactants. Alternatively, the heteroatom can selectively react with debris or defects associated with the carbon products and lead to the generation of more perfect SCNMs.

4.5.1. Hydrogen

In general, the catalyzed synthesis of CNTs requires the presence of a reducing agent to ensure the catalyst remains in a low oxidation state. This can be achieved by the use of ligands (CO) or the presence of H atoms. Most carbon sources used to make CNTs contain hydrogen, but in numerous studies hydrogen gas (H_2) is also added to the carbon source to act as a reducing agent. Many studies have been undertaken that indicate the role of hydrogen in CNT synthesis. Wasel *et al*. have carried out studies on the CVD synthesis of MWCNTs and investigated the role of hydrogen on CNT synthesis using ferrocene as the catalyst and xylene as the carbon source [33b]. The results revealed a competition between the formation of the different carbon products (soot, carbon fibres and CNTs) altered by the addition of hydrogen.

4.5.2 Oxygen

Addition of ethanol to FcH has been shown to give SWCNTs at lower temperature than that found for hydrocarbon reagents [54]. This could be due to the lower decomposition temperature of ferrocene in ethanol [55] and/or the etching effect of OH radicals generated from the ethanol precursor [56]. Here, the presence of the OH radical formed from ethanol at high temperature is said to oxidize the amorphous C formed in the reaction and this has led to cleaner and more crystalline tubes covered with less debris [57]. In general, it appears that when the reactant C/O ratio is high, then cleaner tubes are formed. If the oxygen level becomes too high then the catalyst becomes oxidized and poor SCNM yields are obtained. Further, this effect does not hold when the oxygen is added via a sonication process. In this instance, low levels of oxygen kill all catalyst activity [58].

In recent work, it has been shown that the presence of CO_2 can be beneficial to MWCNT growth [59]. This could relate to participation of the water gas shift reaction influencing the composition of the reactants [60]. Nasibulin *et al.* showed that addition of a small amount of CO_2 and H_2O vapour to a ferrocene/CO reaction mixture resulted in an increase in the CNT length and a drop in the reaction temperature for CNT synthesis (from 890°C to below 600°C) [61]. Thus, the role of CO_2 and H_2O most likely can be explained by an etching effect during the formation of CNTs. The presence of both CO_2 and H_2O is believed to etch amorphous carbon that can poison catalyst particles needed for CO disproportionation as well as for CNT nucleation and growth. Hence, the function of these etching agents is to clean the catalyst particle surface and remove the carbon graphitic layer or amorphous carbon at the nucleation stage.

4.5.3 Sulfur

The impact of sulfur on SCNM synthesis has been known for decades [62]. The sulfur is typically added as part of a volatile complex (thiophene [63]) or even as sulfur [50,64-71] to a reactant stream required to make carbon materials. The addition of sulfur to FcH has led to the selective synthesis of SWCNTs, DWCNTs, MWCNTs, etc. and has even impacted on the quality and yield of CNTs produced [66]. Thus, addition of thiophene or pure sulfur to ferrocene has been found to be effective in promoting the growth of SWCNTs and in increasing the yield of SWCNTs under a range of different growth conditions [50,55,67]. Others have reported the growth of DWCNTs upon the addition of thiophene [72] or of pure sulfur [65,66,71,73] under similar conditions [55,66].

Tibbetts and co-workers described the role of sulfur in the production of carbon fibres in the vapour phase using $Fe(CO)_5$ as the catalyst [74]. The increase of filamentous carbon was influenced by the addition of small amounts of H_2S to the feed as this reagent enhanced the filament nucleation on the iron particles. Further addition of H_2S increased the filamentous growth but decreased the quality of the fibres as measured by length and straightness. Deepak et al. prepared Y-junction nanotubes in large quantities by carrying out the pyrolysis of a mixture of a metallocene with thiophene [75]. Pyrolysis of various

organometallic complexes (e.g. $Fe(CO)_5$, ferrocene and cobaltocene) and sulfur containing compounds (thiophene) has yielded excellent Y-junction nanotubes. Buds can also be formed as seen in the low magnification TEM image of the products from the pyrolysis of a cobaltocene/thiophene mixture (Fig. 4.3a). Many of the nanotubes shown in Fig. 4.3 show multiple Y-junctions. A TEM image of a single long Y-junction nanotube is shown in Fig. 4.3b.

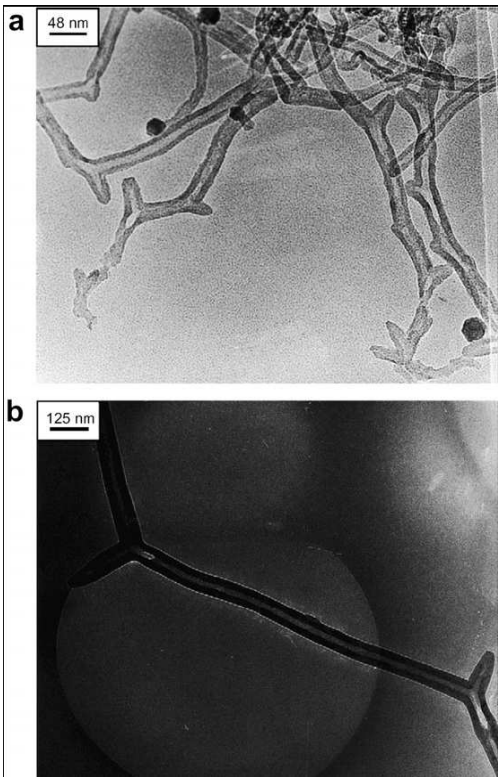

Fig. 4.3: TEM images of Y-junction nanotubes obtained by the pyrolysis of cobaltocene-thiophene mixtures: (a) image with several Y-junction nanotubes and (b) image showing a single multiple junction nanotube [75].

A comparison of the reactivity of ferrocene-benzene and ferrocene-thiophene mixtures, without hydrogen addition, has been made [76]. The diameter of the tubes decreased with increasing reactant flow rate in the high temperature range (above 850ºC). The use of thiophene instead of benzene yielded a significantly narrower diameter distribution for the straight nanotubes with a considerable yield of L and Y carbon nanotube junctions

being observed (Fig. 4.4). The inner core of these straight tubes was frequently continuously filled with the catalyst material and indicated that the presence of sulfur may facilitate the filling of tubes.

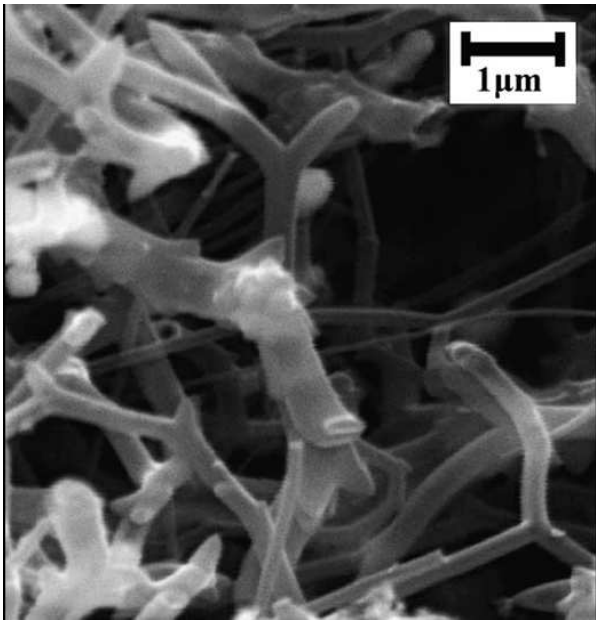

Fig. 4.4: SEM image showing a significant yield of carbon nanotube junctions, in the samples grown at 875°C, 60 ml/h active solution flow rate and 0.06 g/ml solution of ferrocene in thiophene [76].

The use of ligand modified catalysts allows for introduction of doping atoms in a CNT synthesis, e.g. addition of S as part of a ferrocene ligand (e.g. $(C_5H_4SMe_2)(C_5H_5)Fe$) has been reported and indicated that the proximity of the S to the Fe plays a role in affecting the MWCNT product formed [77].

4.5.4 Nitrogen

Doping of CNTs by heteroatoms may lead to an increase in the electrical conductivity of CNTs by formation of electron excess n-type (e.g. N-doped CNTs) or electron deficient p-type (e.g. B-doped CNTs) semi conducting nanotubes [78]. The presence of nitrogen in

SCNM formation has been well studied [79]. Addition of nitrogen as NH_3 and carbon *via* a 'carbon' source provides a simple route to adding nitrogen to the SCNM.

The presence of nitrogen leads to a major change in the morphology of the carbon structures formed, since the N atom is incorporated into the structure. For example, the presence of nitrogen in MWCNTs is detected by the presence of 'bell shaped' structures (Fig. 4.5). N can be present as a pyridinic or pyrrolic N atom, detected by XPS (X-ray photoelectron spectroscopy) studies and the N content can be as high as 10% in a MWCNT. The presence of nitrogen also leads to a modified chemical behaviour of the SCNM. The addition of N atoms derived from the pyrolysis of pyridine with ferrocene as the catalyst with either pure NH_3 or a mixture of NH_3 and argon atmosphere using an injection CVD method has been reported [80].

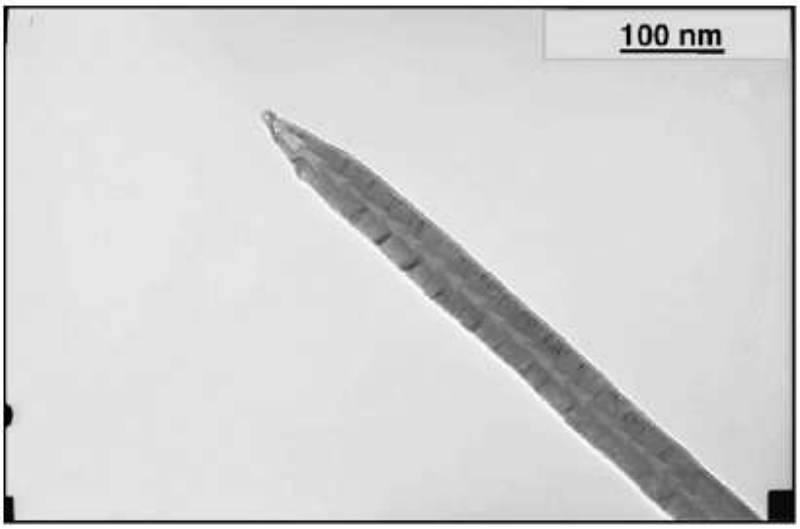

Fig. 4.5: TEM image of a MWCNT with 'bell shaped' structures synthesized using pyridine [130].

Nitrogen addition has also been achieved by adding the N atom as part of a metal ligand. Indeed, early studies by Rao and co-workers achieved success using metal phthalocyanines (metal = Fe, Co, Ni) [19,75,81]. A recent comparative study on the use of 4-ferrocenylaniline and a ferrocene/aniline mixture revealed that using a constant Fe/N

ratio, a higher N content was achieved using the substituted ferrocene compound as the catalyst [82].

4.5.5 Boron

Presently boron doped nanotubes have been produced using an arc-discharge method [83] or by a CVD method [84]. However, the use of volatile organometallic catalysts and boron containing reactants has not been exploited. The use of ferrocenyl containing boron ligands to produce boron substituted CNTs was not successful [85].

4.5.6 Phosphorous

Whereas nitrogen can be incorporated into SCNMs the role of phosphorus is to modify the catalyst. In a study using ferrocene and benzene, spheres were formed while the addition of PPh_3 led to the formation of filamentous carbon. This was suggested to be due to the formation of a eutectic Fe-P melt that increased the fluidity of the liquid particles. Phosphorus was also suggested to enhance the diffusion of carbon atoms in catalyst particles and hence the growth of carbon filaments. No phosphorus was incorporated into the CNTs [86]. More recently reaction of $W(CO)_6$ with PPh_3 in an autoclave was reported [87]. It is also possible that the presence of PF_6 ions in the synthesis of SCNMs from $[CpFe(arene)]^+[PF_6]^-$ may have impacted on the type of SCNM products formed [10b].

4.5.7 Halides

The role of halogens in SCNM formation is not clear. Halogen atoms have been added to reaction mixtures as part of a carbon reactant, as the element, or as part of a catalyst. Numerous reactions entailing the use of halogen atoms/radicals have been performed in an autoclave. For example, the reaction of Cl_2 with ferrocene gives rise to several different carbon forms, such as amorphous nanotubes, nanobags and elliptical hollow particles at $T < 300°C$, whereas hollow carbon nanospheres were observed at $T = 900°C$ [88]. Spherical carbon nanoparticles have also been produced by direct chlorination of

cobaltocene [89]. Many reactions have also been performed with chlorinated carbon reactants, e.g. C_2Cl_4 [90] and the products obtained have included hollow carbon nanospheres [91]. Lv *et al.* have reported on the effect of using chlorine-containing precursors to synthesize micrometer-long continuous FeNi nanowires inside thin-walled CNTs [92]. The degree of 'hollowness' of the CNTs increases with the increase of Cl content in carbon precursors, hence providing a convenient way to control the morphology of CNTs.

4.5.8 Other elements

The effect of numerous other elements has also been investigated in the CVD syntheses of CNTs. However, very few elements have been incorporated into the CNT (or other SCNM) products. One element that has potential is silicon as Si-C bonds are known to be stable. Indeed, templating of carbons using porous silica(s) has been extensively studied [93a-c] and volatile Si complexes have been used to make CNTs [93d,e].

4.6 Physical parameters

Variation in the type of SCNM produced using an organometallic catalyst and a carbon source is strongly influenced by the temperature and pressure conditions. In a flow system, the reaction is influenced by the decomposition temperatures of the catalyst and the carbon source. At atmospheric pressure, this typically requires temperatures above 450°C for ferrocene but the maximum temperature is limited by the physical characteristics of the quartz reactor (<1200°C).

The kind and size of SCNMs produced are temperature dependent. Chaisitsak *et al.* observed that the diameter of SWCNTs that were produced when T > 650°C increased with temperature [54]. This was confirmed by the appearance of narrow radial breathing mode (RBM) peaks in the Raman spectra (ca 200 cm^{-1}) of the SWCNTs. The report is also supported by Singh *et al.* [44d], Zhan *et al.* [94a] and Moisala *et al.* [94b]. The assumption is that under the high temperature conditions used the frequency of metal

particle collision increases resulting in an increase in the particle diameter [95]. As a consequence, the diameter of the CNTs becomes larger.

Studies to date suggest that the catalyst must be in a reduced state and this can be achieved by (i) using a reducing carbon source, e.g. CO, (ii) by adding H_2 to the reactants, (iii) by using the H generated from the carbon source, e.g. CH_4, or (iv) by using a catalyst with the metal in the zero oxidation state, e.g. $Fe(CO)_5$. Reactions with ferrocene require a reductant.

Reactions performed in a confined space permit the effect of pressure on SCNM formation to be explored. Most reactions have been carried out at autogeneous pressures but in some studies reactions at high pressures have been reported [52,96]. The addition of a solid reductant (Na, Ca, K, etc.) to ferrocene and a carbon source is possible using this approach. This has resulted in the formation of CNTs at low temperatures (< 210°C). These CNTs tend to be amorphous [97]. Luo *et al.* used an autoclave reactor which was filled with benzene to 90% of total volume and a mixture of ferrocene/ sulfur to synthesize amorphous CNTs at 200°C [98a]. They investigated the effect of sulfur on the growth of amorphous CNTs and it was found that an optimal amount of sulfur (molar ratio ferrocene: sulfur (1:2); near the stoichiometric proportion of FeS_2) is needed to obtain the amorphous CNTs.

The gas flow rates for introduction of the catalyst/carbon source in the CVD process also influence the type, quality and quantity of SCNMs produced. Barreiro and co-workers showed that a decrease in the SWCNT mean diameter distribution can be obtained by increasing the total gas flow [50]. With a high flow rate they were also able to synthesize very long SWCNTs. Tapasztó *et al.* have also made a similar observation and they suggested that the strong effect of flow rate on the average tube diameter must be related to the size of liquid droplets produced in the gas phase and hence to a larger number of catalyst particles formed in the reaction [76]. The shorter duration time of the growth cycle for larger flow rates may also make a contribution to the uncatalysed thermal decomposition of benzene at high temperatures. This process can lead to the formation of

a pyrolytic carbon overcoat on the nanotubes. An increase in gas flow rate beyond the optimum also leads to an increase in the amount of amorphous carbon formed [34]. The alignment of tubes can be improved by increasing the flow rate of the active solution.

4.7 Reactor design

Numerous procedures have been developed to ensure that a volatile organometallic catalyst can be transferred into a reactor to generate the SCNMs. In the simplest system an inert gas is bubbled through a liquid organometallic complex (e.g. $Fe(CO)_5$) and the vapour is passed through an oven held typically between 700 and 1100°C. In this temperature range, a quartz reactor tube can be used; use of a metal reactor leads to the possibility of the reactor wall playing a part in the reaction [98b].

In most instances however the organometallic reagent is a solid at room temperature (e.g. ferrocene) and a number of methods can be used to introduce the catalyst into a reactor. These include the use of a two furnace system in which the catalyst is placed in a low temperature furnace under a flow of an inert gas (and/or carbon source). The volatile catalyst is transferred to a second higher temperature furnace where product formation occurs. A horizontal reactor is generally used in the reaction (Fig. 4.6).

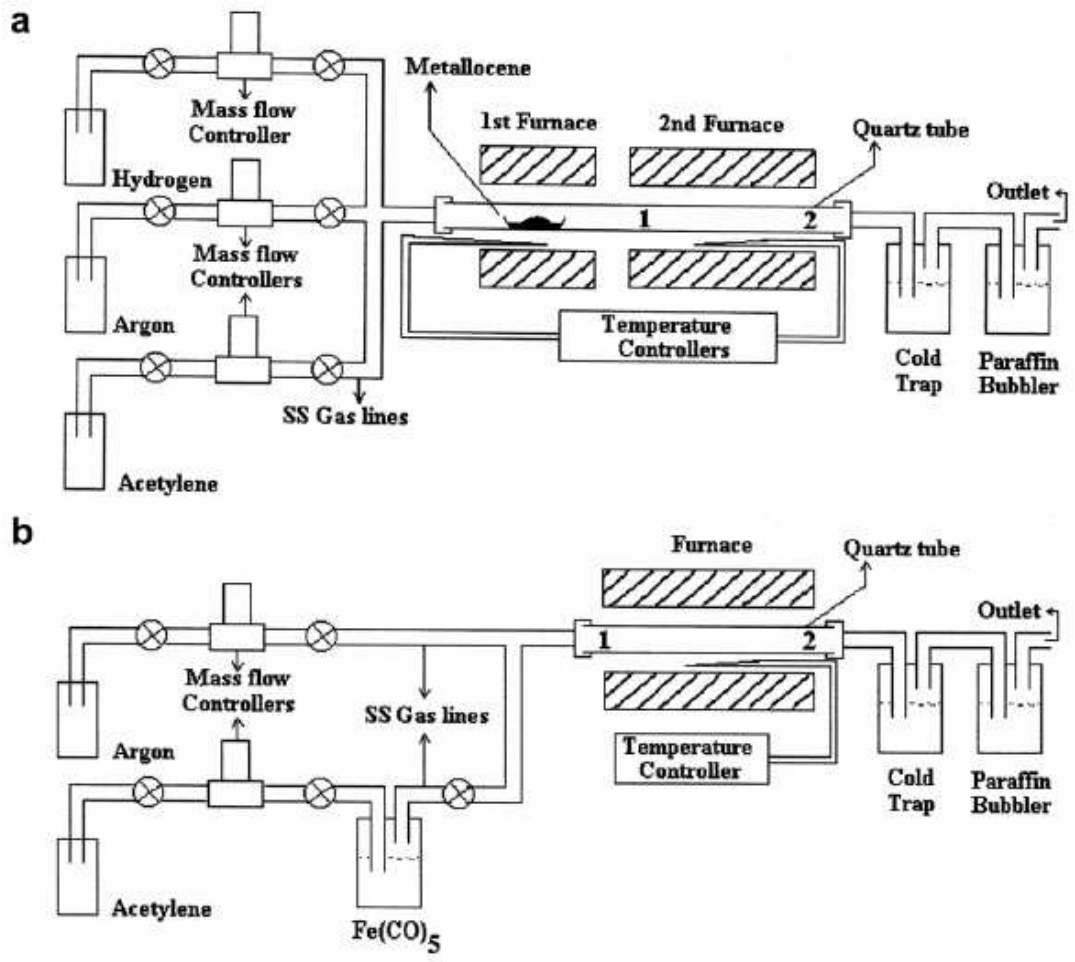

Fig. 4.6: Pyrolysis apparatus employed for the synthesis of SWCNTs by pyrolysis of (a) metallocenes and (b) $Fe(CO)_5$ along with acetylene [37].

If the organometallic complex is soluble in some carbon source then the dissolved catalyst can be added directly to the reactor hot zone. This will permit the use of both horizontal and vertical reactor designs. The dissolved material can be added by means of a syringe (Fig. 4.7) or by bubbling an inert gas through the reactant solution.

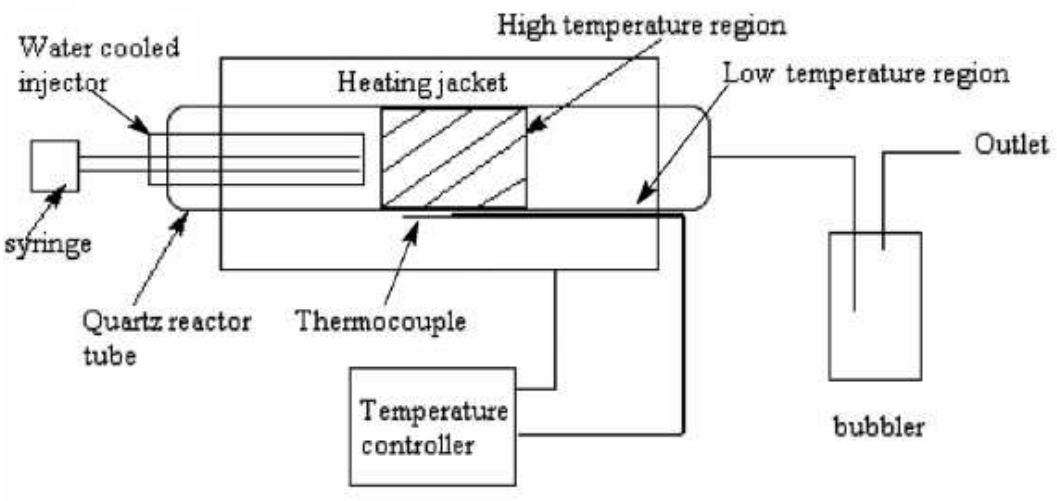

Fig. 4.7: Floating catalyst CVD reactor for the synthesis of CNTs [39].

Alternatively, a catalyst/carbon source can be sonicated and the sonicated mist (aerosol) transferred to the reactor in an inert gas (Fig. 4.8).

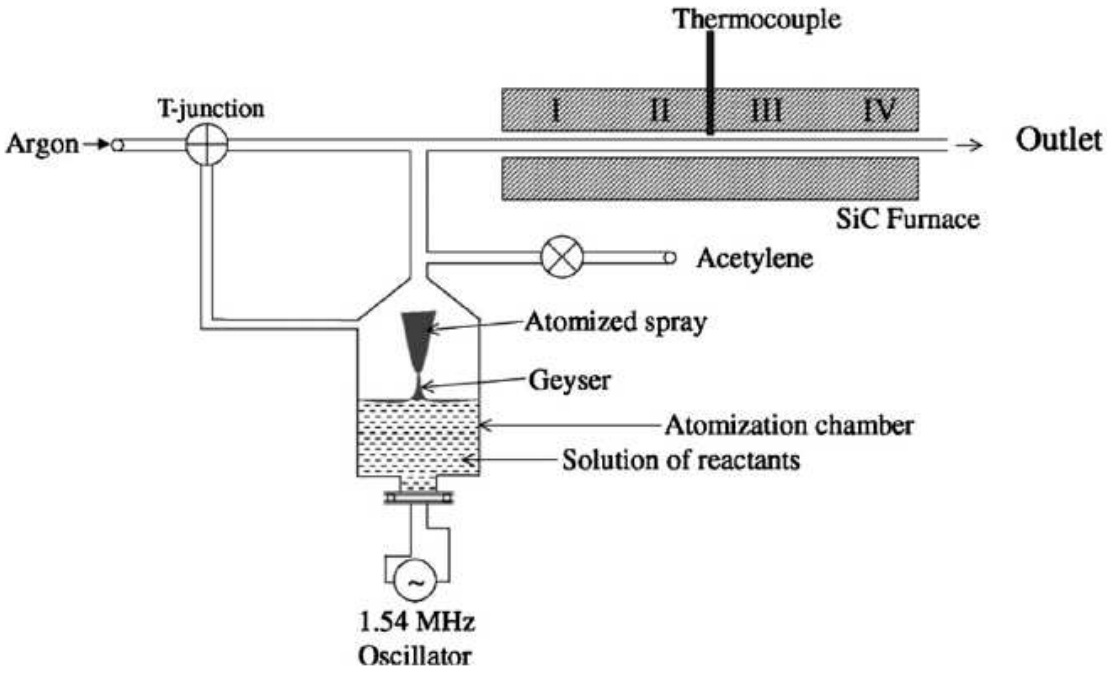

Fig. 4.8: Schematic representation of a CVD furnace with an atomizer [23].

Recently, SCNMs have been prepared under static conditions, i.e. in a confined reactor. This includes reaction in an autoclave or in a sealed glass reactor [10]. In both instances, the organometallic complex is placed in the reactor and the reaction carried out under autogeneous (or higher) pressures. This approach allows for the use of solid carbon and/or solid organometallic complex reactants.

4.8 Growth mechanism

The use of a floating catalyst methodology eliminates the need for a support [99] and although concepts of carbon deposition/crystallisation/growth are assumed to be similar the mechanism becomes simplified (tip-growth and base-growth lose their meaning). The metal catalyst particles are still believed to act as nuclei for the growth of CNTs in the gas phase and a mechanism for gas phase CNT growth is shown in Fig. 4.9. Control of the catalytic growth of SCNMs is achieved by control of the catalyst nanoparticle size and distribution during the high temperature reaction. Indeed, control of the catalyst diameter determines whether SWCNTs, DWCNTs, or MWCNTs among other SCNMs will be formed in the reaction. The control of the diameter also controls the helicity and hence the conducting properties, the mechanical properties, and the magnetic properties of the product CNTs [17c].

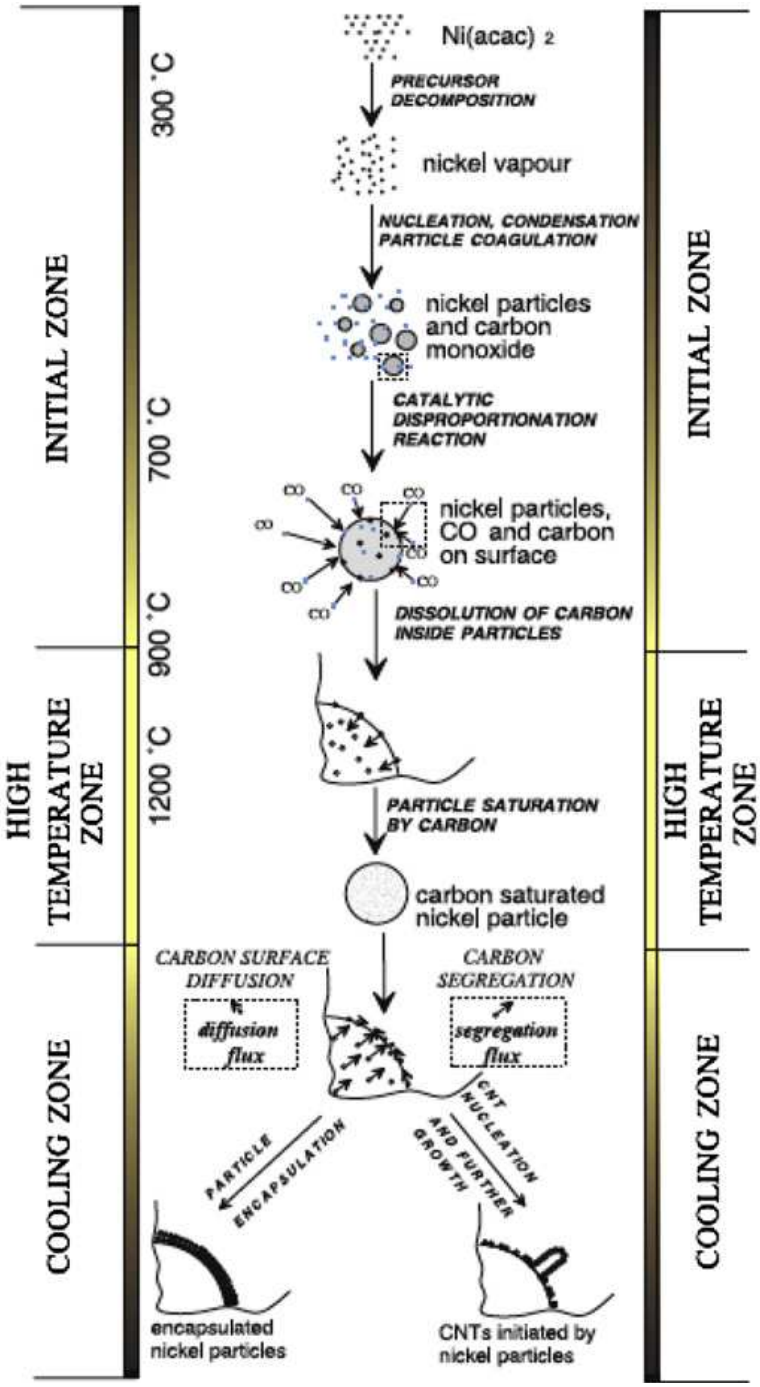

Fig. 4.9: SWCNT formation mechanism during aerosol synthesis with nickel acetylacetonate as the catalyst precursor [131].

4.8.1 The role of the metal-floating catalyst

The role of an organometallic complex is to provide a metal in the zero oxidation state that will catalyse the condensation of carbon. The general picture that has emerged can be summarized as follows.

The volatile organometallic complex decomposes at high temperature into metal ions/radicals/neutrals and these can coalesce to form larger particles in the gas phase. Depending on the reactants used, these metal clusters may contain carbon as well as heteroatoms. The clusters can then react with more carbon atoms or metal atoms either in the gas phase or after deposition on the reactor walls. It appears that the metal cluster catalyst will be in the gas or liquid phase under typical reaction conditions used. Reaction with carbon then leads to dissolution of the carbon into the metal cluster or deposition onto the metal cluster surface. This appears to be metal dependant.

Fe in particular has the ability to dissolve carbon. Beyond a certain C/Fe ratio, precipitation of carbon occurs. Depending on the cluster size and composition, SCNMs with different shapes and sizes are formed. If the particles are small SWCNTs form and if larger, MWCNTS or even fibrous materials appear. If the carbon forms without the intervention of the Fe, carbon spheres and amorphous carbon are preferably formed. Studies on Cu suggest that the carbon does not dissolve in the Cu clusters [100]. The carbon rather precipitates on the Cu surface and carbon condensation takes place on the Cu catalyst particle surface.

4.8.2 The carbon growth species

Many different types of carbon ions/radicals/neutrals are formed by decomposition of the carbon source in the gas phase. The metal will also catalyse bond making/breaking in the reaction chamber. The species formed include C1 radicals/ions, large structures such as PAHs (polyaromatic hydrocarbons) and all intermediate size radicals/ions. These species will be determined by C/H ratios, bond strengths, temperature, metal, pressure, flow

rates, etc. Clearly, the type of ligand used in the organometallic catalyst precursor will impact on the gas phase species.

It appears that small carbon species will dissolve in the metal catalyst particle and precipitate out to give CNTs in which the carbon forms graphitic layers. The layer formation is independent of the carbon source and provided there is a constant source of carbon the CNT will grow in length. However, studies have indicated that while the inner diameter may remain the same as a function of time the outer diameter can grow with time [57]. This indicates that carbon can also deposit on the outer layers of the CNTs. This growth generates carbon that appears as ‘flakes’ of aromatic fragments. A similar growth process occurs when carbon spheres, once nucleated, grow. In this instance NO catalyst is required and the surface appears as a patchwork of aromatic rings (Fig. 4.10). These spheres grow in diameter with time [101].

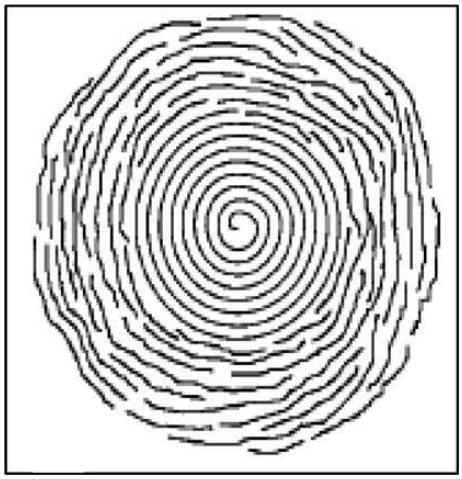

Fig. 4.10: A patchwork of aromatic rings that make up a carbon sphere synthesized in the absence of a catalyst [127].

This secondary material that grows on CNTs is sometimes referred to as debris [57] and has been observed by TEM in most (if not all) studies that have been reported on the synthesis of MWCNTs. This will impact on the functionalization reactions that occur on the ‘walls’ of CNTs. The implication from the above is that PAHs are formed in the gas phase and can provide a source of material for SCNM growth.

4.8.3 The role of the heteroatoms

The hydrogen from a hydrocarbon is expelled at some point from the hydrocarbon reactant. This could occur in the gas phase or after reaction with a metal atom/cluster. The SCNMs are hence expected to be predominantly formed of C atoms. After condensation 'dangling bonds' will be saturated with heteroatoms (typically H and O atoms).

Radicals containing H atoms will certainly influence the final carbon deposits. Reilly *et al.* [102] have recently summarised the possible role of hydrocarbon species in CNT formation and implicated the importance of 'free radical condensates' [103] in the formation of CNTs. His proposal would apply to the formation of all SCNMs. The importance of this work is that it shifts the thinking on a carbon growth mechanism back onto the carbon precursors and this will again relate to the structure of carbons and volatile organometallic catalysts used as SCNM reactants. In particular, Reilly states that 'models built on the notion of elemental carbon diffusing on or through a metal lack completeness' [102].

The role of oxygen is to remove or saturate 'dangling carbon atoms' and remove amorphous carbon that would poison the metal sites. TGA studies have revealed that amorphous carbon is more readily oxidized than is aromatic carbon (i.e. sp^2 versus sp^3 carbon). Again, the role of oxygen radicals/ions/neutrals in the gas phase are important as has been shown by sonication studies with ferrocene/oxygenate mixtures [58].

4.9 A case study - ferrocene and SCNMs

Remarkably, ferrocene has been implicated in the synthesis of SWCNTs, DWCNTs, MWCNTs, amorphous CNTs, branched CNTs, spheres, etc. An evaluation of the literature allows for an understanding of how such a wide range of shaped carbons can be synthesized from one catalyst system. An analysis of the literature reveals that the control of reaction parameters permits control (partial) of the morphology of the final polymerized carbon material.

The morphology of the SCNMs is also influenced by the choice of reactor and reactants.
SWCNTs: Produced in a flow system at high temperature (>1000°C) [63c]; very high flow rate (1500 ml/min) [64]; argon/ hydrogen carrier mixture with a ratio of Ar:H_2 of 2:1 [50]; numerous carbon sources used including acetylene [37,51,67], hexane [63] benzene [63c-e], xylene [50], carbon monoxide [61,96]; thiophene [63] or solid sulfur [64], as an additional promoter. High pressure CVD reactor at 1-5 bar at high temperature of 900°C [52]. Apart from the above conditions, the synthesis of SWCNTs is favoured by a high iron to carbon ratio, e.g. ferrocene/benzene mole ratio is above 7 [43b].

DWCNTs: Produced in a flow system at high temperature (>1000°C) [104]; lower flow rate used (800 ml/min) [104]; numerous carbon sources used including acetylene [65,66], methane [70], xylene [71] and an additional sulfur promoter in the optimal ratio range of S:FcH at 1:8-1:64 [65]. The conditions for synthesis of SWCNTs are similar to those used to produce DWCNTs but in many instances a decrease in flow rate favours the formation of DWCNTs.

MWCNTs: Produced in a flow system at moderate temperature (~875°C) [33b]; moderate carrier flow rate (~1000 ml/min) [45b]; numerous carbon sources used including benzene [43b], xylene [33b,45a-c], toluene [44b]; the use of sulfur (thiophene) as a promoter is not very common [43b]. Produced in a confined space under autogenic pressure and temperature in the range 700-800°C [10a,13b,c] carbon sources used include anthracene [10a] and tetrachloroethene [13c].

Amorphous CNTs: Produced in a confined space at autogenic pressure and at a low temperature of ~200°C [97,98]; carbon sources used include benzene [97,98]. Additives include sodium [97] or sulfur [98]. Materials are produced in a flow system at high temperature 1100-1200°C with benzene as carbon source, thiophene as additive and under a H_2 flow rate of 100 ml/min [63b].

HCSs: Produced in a confined space under nitrogen at pressure of 2.2 MPa and at moderate temperature of 700°C [13b] or at a pressure of 8 MPa at 550°C with C_2Cl_4 [90]. Materials are produced in a flow system at high temperature (1000°C) with camphor as carbon source, thiophene as additive and under an Ar flow with a feedstock input rate of 12.5 g/h [101a]. Alternatively they are produced in a flow system at high temperature 900 °C with no external carbon source but under the flow of pure Cl_2 gas for 30 min [13a].

Filled spheres: Produced in a confined space at autogenic pressure and at a temperature of 800°C when the Fe/C ratio is less than 0.033 using anthracene as carbon source [10a]. Materials are produced in a flow system in a moderate temperature range of 580-700°C with anthracene as carbon source under H_2 with a flow rate of 300-400 ml/min. The key issue is the use of a low iron content; typically the ratio of ferrocene: anthracene is 1:7.

Carbon onions: Produced in a flow system at a high temperature of 900°C with Fe_3CO_{12} as additional carbon source under an Ar gas (flow rate of 260 ml/min) containing 0.5% and 1.0% of O_2 [14].

Fe-filled CNTs: Produced in a confined space at autogenic pressure and at high temperature 1000°C with thiophene as a carbon source [14]. CNTs are produced in a flow system at a high temperature of 900°C in Ar/H_2 mixture (3:1) as the carrier gas with a total flow rate of 50 ml/min [5b].

Core shells: Produced in a confined space at autogenic pressure and at high temperature 1000°C with picric acid as carbon source with low C/Fe ratio (< 34:1) [16c].

CNTs with Y-Juctions: Produced inflow system at a high temperature of 1000°C with thiophene as an additive and an Ar/H_2 mixture as carrier gas with flow rates of 225 ml/min and 25 ml/min, respectively [75].

4.10 Conclusions

From the above discussions it can be seen that organometallic reagents have played a key role in both the synthesis of SCNMs and in providing mechanistic information on the synthesis reactions. The role of the organometallic complex is to provide a source of both metal and ligand (carbon, heteroatoms) for SCNM growth. Currently temperatures of above 700°C are required in flow systems to generate graphitic CNTs but lower temperatures can produce other shaped carbons. Clearly, the role of the organometallic complex is to provide a source of carbon and metal fragments for the reaction. These fragments are determined by the actual complexes used. As lower temperatures become possible for the synthesis of SCNMs the role of the specific organometallic catalyst used will become more important.

In the pioneering days in organometallic chemistry the ‘black’ decomposition residues formed in many synthetic reactions that did not produce the required product from a synthesis were always discarded. It is possible that many of these residues may have contained unique shaped carbon nanomaterials. The ready accessibility of electron microscopes now permits a re-evaluation of some of these materials. Systematic studies could be revealing [87,105].

4.11 References

1. (a) R.D. Adams (Ed.), *Special issue: 50th anniversary of the discovery of ferrocene*, J. Organomet. Chem. **637-639** (2001) 1; (b) A. Togni, T. Hayashi (Eds.), *Ferrocenes*, VCH, Weinheim, 1995.
2. D. Baird, *Thing knowledge, a philosophy of scientific instruments*, University of California Press Ltd., London, England, 2004.
3. (a) J.P. Collman, L.S. Hegedus, J.R. Norton, R.G. Finke, *Principles and applications of organotransition metal chemistry*, University Science books, Mill Valley, CA, 1987; (b) C. Elschenbroich, *Organometallics*, 3rd ed., Wiley–VCH, Weinheim, 2006; (c) M.A. Cato, *New developments in organometallic chemistry Research*, Nova Science Pub. Inc., New York, 2006.
4. (a) C. Masters, *Homogeneous transition-metal catalysis*, Chapman and Hall Ltd., Methuen Inc., New York, 1981; (b) G.W. Parshall, *Homogeneous catalysis*, John Wiley and Sons, New York, 1980.
5. (a) A. Govindaraj, C.N.R. Rao, Pure Appl. Chem. **74** (2002) 1571; (b) R. Sen, A. Govindaraj, C.N.R. Chem. Phys. Lett. **267** (1997) 276; (c) C.N.R. Rao, R. Sen, B.C. Satishkumar, A. Govindaraj, Chem. Commun. (1998) 1525.
6. (a) A.M. Thayer, Chemical and Engineering News (2007) 29; (b) J. Evans, Chemistry World (2007) 17.
7. (a) T.W. Ebbesen, P.M. Ajayan, Nature **358** (1992) 220; (b) H. Huang, H. Kajiura, S. Tsutsui, Y. Hirano, M. Miyakoshi, A. Yamada, M. Ata, Chem. Phys. Lett. **343** (2001) 7.
8. (a) A. Thess, R. Lee, P. Nikolaev, H. Dai, P. Petit, J. Robert, C. Xu, Y.H. Lee, S.G. Kim, A.G. Rinzler, D.T. Colbert, G.E. Scuseria, D. Tománek, J.E. Fischer, R.E. Smalley, Science **273** (1996) 483; (b) S. Bandow, S. Asaka, Y. Saito, A.M. Rao, L. Grigorian, E. Richer, P.C. Eklund, Phys. Rev. Lett. **80** (1998) 3779; (c) J. Liu, A.G. Rinzler, H. Dai, J.H. Hafner, R.K. Bradley, P.J. Boul, A. Lu, T. Iverson, K. Shelimov, C.B. Huffman, F. Rodriguez-Macias, Y. Shon, T.R. Lee, D.T. Colbert, R.E. Smalley, Science **101** (1998) 1253.

9. (a) M. Joseyacaman, M. Mikiyoshida, L. Rendon, J.G. Santiesteban, Appl. Phys. Lett. **62** (1993) 657; (b) M. Endo, K. Takeuchi, K. Kobori, K. Takahashi, H.W. Kroto, A. Sarkar, Carbon **33** (1995) 873; (c) S. Amelinckx, X.B. Zhang, D. Bernaerts, X.F. Zhang, V. Ivanov, J.B. Nagy, Science **265** (1994) 635; (d) A.-C. Dupuis, Prog. Mater. Sci. **50** (2005) 929; (e) J.B. Park, G.S. Choi, Y.S. Cho, S.Y. Hong, D. Kim, S.Y. Choi, J.H. Lee, K.I. Cho, J. Cryst. Growth **244** (2002) 211.
10. (a) V.O. Nyamori, N.J. Coville, Organometallics **26** (2007) 4083; (b) D. Jain, A. Winkelm, R. Wilhelm, Small **2** (2006) 752; (c) J. Liu, M. Shao, Q. Xie, L. Kong, W. Yu, Y. Qian, Carbon **41** (2003) 2101; (d) M. Laskoski, W. Steffen, J.G.M. Morton, M.D. Smith, U.H.F. Bunz, J. Am. Chem. Soc. **124** (2002) 13814; (e) B. El Hamaoui, L. Zhi, J. Wu, U. Kolb, K. Müllen, Adv. Mater. **17** (2005) 2957; (f) L. Zhi, T. Gorelik, R. Friedlein, J. Wu, U. Kolb, W.R. Salaneck, K. Müllen, Small **1** (2005) 798; (g) J. Wu, B. El Hamaoui, J. Li, L. Zhi, U. Kolb, K. Müllen, Small **1** (2005) 210; (h) S. Liu, X. Tang, Y. Mastai, I. Felner, A. Gedanken, J. Mater. Chem. **10** (2000) 2502; (i) C. Wu, X. Zhu, L. Ye, C. OuYang, S. Hu, L. Lei, Y. Xie, Inorg. Chem. **45** (2006) 8543; (j) P.I. Dosa, C. Erben, V.S. Iyer, K.P.C. Vollhardt, I.M. Wasse, J. Am. Chem. Soc. **121** (1999) 10430; (k) V.S. Iyer, K.P.C. Vollhardt, R. Wilhelm, Angew. Chem., Int. Ed. **42** (2003) 4379.
11. J. Geng, C. Ducati, D.S. Shephard, M. Chhowall, B.F.G. Johnson, J. Robertson, Chem. Commun. (2002) 1112.
12. (a) Y.Z. Jin, C. Gao, W.K. Hsu, Y. Zhu, A. Huczko, M. Bystrzejewski, M. Roe, C.Y. Lee, S. Acquah, H. Kroto, D.R.M. Walton, Carbon **43** (2005) 1944; (b) Ph. Serp, R. Feurer, P. Kalck, Y. Kihn, J.L. Faria, J.L. Figueiredo, Carbon **39** (2001) 621; (c) X.-Y. Liu, B.-C. Huang, N.J. Coville, Carbon **40** (2002) 2791.
13. (a) N.A. Katcho, E. Urones-Garrote, D. Ávila-Brande, A. Gómez-Herrero, S. Urbonaite, S. Csillag, E. Lomba, F. Agulló-Rueda, A.R. Landa-Cánovas, L.C. Otero-Díaz, Chem. Mater. **19** (2007) 2304; (b) G. Zou, D. Yu, J. Lu, D. Wang, C. Jiang, Y. Qian, Solid State Commun. **131** (2004) 749; (c) L. Xu, W. Zhang, Q. Yang, Y. Ding, W. Yu, Y. Qian, Carbon **43** (2005) 1090.
14. M.C. Schnitzler, M.M. Oliveira, D. Ugarte, A.J.G. Zarbin, Chem. Phys. Lett. **381** (2003) 541.

15. Z. Li, M. Jaroniec, P. Papakonstantinou, J.M. Tobin, U. Vohrer, S. Kumar, G. Attard, J.D. Holmes, Chem. Mater. **19** (2007) 3349.
16. (a) S. Liu, R.J. Wehmschulte, Carbon **43** (2005) 1550; (b) R. Sen, A. Govindaraj, C.N.R. Rao, Chem. Mater. **9** (1997) 2078; (c) Y. Lu, Z. Zhu, Z. Liu, Carbon **43** (2005) 369.
17. (a) R. Saito, G. Dresselhaus, M.S. Dresselhaus, *Physical Properties of Carbon Nanotubes*, Imperial College Press, London, 1998; (b) G. Cao, *Nanostructures and Nanomaterials: Synthesis, Properties and Applications*, Imperial College Press, London, 2004; (c) M.S. Dresselhaus, G. Dresselhaus, P.C. Eklund, *Science of Fullerenes and Carbon Nanotubes*, Academic Press, San Diego, 1996; (d) M.J. O'Connell, *Carbon Nanotubes: Properties and Applications*, Taylor and Francis Group, LLC, 2006.
18. (a) B. Fei, H. Lu, Z. Hu, J.H. Xin, Nanotechnology **17** (2006) 1589; (b) A. Hirsch, Angew. Chem., Int. Ed. **41** (2002) 1853; (c) Y.P. Sun, K. Fu, Y. Lin, W. Huang, Acc. Chem. Res. **35** (2002) 1096; (d) K.S. Coleman, S.R. Bailey, S. Fogden, M.L.H. Green, J. Am. Chem. Soc. **125** (2003) 8722; (e) Y. Li, X. Zhang, J. Luo, W. Huang, J. Cheng, Z. Luo, T. Li, F. Liu, G. Xu, X. Ke, L. Li, H.J. Geise, Nanotechnology **15** (2004) 1645; (f) R. Verdejo, S. Lamoriniere, B. Cottam, A. Bismarck, M. Shaffer, Chem. Commun. (2007) 513.
19. C.N.R. Rao, A. Govindaraj, Acc. Chem. Res. **35** (2002) 998.
20. K.C. Mondal, N.J. Coville, in: H.S. Nalwa (Ed.), Encyclopedia of Nanoscience and Nanotechnology, American Scientific Publishers, Valencia, CA, USA, 2008.
21. Y. Komatsu, M. Endo, Japanese Patent 60-32818, February 22, 1985.
22. G.G. Tibbetts, D.W. Gorkiewicz, Carbon **31** (1993) 809.
23. P. Nikolaev, M.J. Bronikowski, R.K. Bradley, F. Rohmund, D.T. Colbert, K.A. Smith, R.E. Smalley, Chem. Phys. Lett. **313** (1999) 91.
24. M.S. Mohlala, X.-Y. Liu, N.J. Coville, J. Organomet. Chem. **691** (2006) 4768.
25. (a) T.M. Keller, S.B. Qadri, Chem. Mater. **16** (2004) 1091; (b) M. Laskoski, T.M. Keller, S.B. Qadri, Carbon **45** (2007) 443; (c) T.M. Keller, M. Laskoski, S.B. Qadri, J. Phys. Chem. C **111** (2007) 2514.
26. Y. Huh, M.L.H. Green, J.Y. Lee, C.J. Lee, Diam. Rel. Mater. **15** (2006) 100.

27. J.D. Harris, R.P. Raffaelle, T. Gennett, B.J. Landi, A.F. Hepp, Mater. Sci. Eng. B **116** (2005) 369.
28. L.S. Panchakarla, A. Govindaraj, Bull. Mater. Sci. **30** (2007) 23.
29. V.O. Nyamori, N.J. Coville, Unpublished Paper.
30. (a) M.S. Mohlala, N.J. Coville, J. Organomet. Chem. **692** (2007) 2965; (b) E.N. Nxumalo, V.O. Nyamori, N.J. Coville, J. Organometal. Chem. **693** (2008) 2942.
31. M. Motiei, J. Calderon-Moreno, A. Gedanken, Chem. Phys. Lett. **357** (2002) 267.
32. V.G. Pol, S.V. Pol, J.M.C. Moreno, A. Gedanken, Carbon **44** (2006) 3285.
33. (a) N. Das, A. Dalai, J.S.S. Mohammadzadeh, J. Adjaye, Carbon **44** (2006) 2236; (b) W. Wasel, K. Kuwana, P.T.A. Reilly, K. Saito, Carbon **45** (2007) 833.
34. K.M. Samant, S.K. Haram, S. Kapoor, J. Phys. **68** (2007) 51.
35. (a) A.M. Cassell, J.A. Raymakers, J. Kong, H. Dai, J. Phys. Chem. B **103** (1999) 6484; (b) J.E. Herrera, L. Balzano, A. Borgna, W.E. Alvarez, D.E.J. Resasco, J. Catal. **204** (2001) 129.
36. (a) R.G. Lacerda, A.S. Teh, M.H. Yang, K.B.K. Teo, N.L. Rupesinghe, S.H. Dalal, K.K.K. Koziol, D. Roy, G.A.J. Amaratunga, W.I. Milne, Appl. Phys. Lett. **84** (2004) 269; (b) S.C. Lyu, B.C. Liu, C.J. Lee, H.K. Kang, C.-W. Yang, C.Y. Park, Chem. Mater. **15** (2003) 3951; (c) B.C. Liu, S.C. Lyu, T.J. Lee, S.K. Choi, S.J. Eum, C.W. Yang, C.Y. Park, C.J. Lee, Chem. Phys. Lett. **373** (2003) 475; (d) H. Cui, G. Eres, J.Y. Howe, A. Puretkzy, M. Varela, D.B. Geohegan, D.H. Lowndes, Chem. Phys. Lett. **374** (2003) 222.
37. B.C. Satishkumar, A. Govindaraj, R. Sen, C.N.R. Rao, Chem. Phys. Lett. **293** (1998) 47.
38. Z.E. Horváth, K. Kertész, L. Peth}o, A.A. Koós, L. Tapasztó, Z. Vértesy, Z. Osváth, Al. Darabont, P. Nemes-Incze, Zs. Sárk}ozi, L.P. Biró, Curr. Appl. Phys. **6** (2006) 135.
39. M.S. Mohlala, X.-Y. Liu, J.M. Robinson, N.J. Coville, Organometallics **24** (2005) 972.
40. (a) L.C. QIN, J. Mater. Sci. Lett. **16** (1997) 457; (b) J.-M. Ting, T.-P. Li, C.-C. Chang, Carbon **42** (2004) 2997; (c) C.-S. Kuo, A. Bai, C.-M. Huang, Y.-Y. Li, C.-C. Hu, C.-C. Chen, Carbon **43** (2005) 2760.

41. (a) K. Awasthi, A.K. Singh, ON. Srivastava, J. Nanosci. Nanotechnol. **3** (2003) 540; (b) J.H. Hafner, M.J. Bronikowski, B.R. Azamian, P. Nikolaev, A.G. Rinzler, D.T. Colbert, K.A. Smith, R.E. Smalley, Chem. Phys. Lett. **296** (1998) 195.
42. Y.T. Lee, N.S. Kim, J. Park, J.B. Han, Y.S. Choi, H. Ryu, H.J. Lee, Chem. Phys. Lett. **372** (2003) 853.
43. (a) Y.-Y. Fan, F. Li, H.-M. Cheng, G. Su, Y.-D. Yu, Z.-H. Shen, J. Mater. Res. **13** (1998) 2342; (b) S. Bai, F. Li, Q.H. Yang, H.-M. Cheng, J.B. Bai, Chem. Phys. Lett. **376** (2003) 83; (c) M. Mayne, N. Grobert, M. Terrones, R. Kamalakaran, M. Rühle, H.W. Kroto, D.R.M. Walton, Chem. Phys. Lett. **338** (2001) 101.
44. (a) X. Li, K. Li, H. Li, J. Wei, C. Wang, Carbon **45** (2007) 1662; (b) C. Singh, M.S.P. Shaffer, K.K.K. Koziol, I.A. Kinloch, A.H. Windle, Chem. Phys. Lett. **372** (2003) 860; (c) C. Singh, M. Shaffer, I. Kinloch, A. Windle, Physica B **323** (2002) 339; (d) C. Singh, M.S.P. Shaffer, A.H. Windle, Carbon **41** (2003) 359; (e) D.C. Lee, F.V. Mikulec, B.A. Korgel, Am. Chem. Soc. **126** (2004) 4951; (f) M. Pinault, M.M.-L. Hermite, C. Reynaud, V. Pichot, P. Launois, D. Ballutaud, Carbon **43** (2005) 2968; (g) H.-L. Ma, D.S. Su, G.-Q. Jin, X.-Y. Guo, Carbon **45** (2007) 1622.
45. (a) X. Zhang, A. Cao, B. Wei, Y. Li, J. Wei, C. Xu, D. Wu, Chem. Phys. Lett. **362** (2002) 285; (b) S.R.C. Vivekchand, L.M. Cele, F.L. Deepak, A.R. Raju, A. Govindaraj, Chem. Phys. Lett. **386** (2004) 313; (c) R. Andrews, D. Jacques, A.M. Rao, F. Derbyshire, D. Qian, X. Fan, E.C. Dickey, J. Chen, Chem. Phys. Lett. **303** (1999) 467; (d) B.Q. Wei, R. Vajtai, Y. Jung, J. Ward, R. Zhang, G. Ramanath, P.M. Ajayan, Chem. Mat. **15** (2003) 1598; (e) A. Cao, X. Zhang, J. Wei, Y. Li, C. Xu, J. Liang, D. Wu, B. Wei, J. Phys. Chem. B **105** (2001) 11937; (f) A. Cao, L. Ci, G. Wu, B. Wei, C. Xu, J. Liang, D. Wu, Carbon **39** (2001) 152; (g) N.A. Koratkar, B. Wei, P.M. Ajayan, Compos. Sci. Technol. **63** (2003) 1525; (h) H.-C. Shin, M. Liu, B. Sadanadan, A.M. Rao, J. Power Sources **112** (2002) 216; (i) H. Kim, W. Sigmund, Carbon **43** (2005) 1743; (j) Q.-M. Gong, Z. Li, Y. Wang, B. Wu, Z. Zhang, J. Liang, Mater. Res. Bull. **42** (2007) 474.
46. H. Zhu, B. Jiang, C. Xu, D. Wu, Chem. Commun. (2002) 1858.
47. (a) A.K. Schaper, H. Hou, A. Greiner, F. Phillipp, J. Catal. **222** (2004) 250; (b) H. Hou, A.K. Schaper, F. Weller, A. Greiner, Chem. Mater. **14** (2002) 3990.

48. (a) Y.Z. Jin, C. Gao, W.K. Hsu, Y. Zhu, A. Huczko, M. Bystrzejewski, M. Roe, C.Y. Lee, S. Acquah, H. Kroto, D.R.M. Walton, Carbon **43** (2005) 1944; (b) V.G. Pol, S.V. Pol, J.M.C. Moreno, A. Gedanken, Carbon **44** (2006) 3285.
49. S.D. Mhlanga, A. Shaikjee, I. Mosiane, N.J. Coville, to be published results.
50. A. Barreiro, C. Kramberger, M.H. Rümmeli, A. Grüneis, D. Grimm, S. Hampel, T. Gemming, B. Büchner, A. Bachtold, T. Pichler, Carbon **45** (2007) 55.
51. L. Ci, S. Xie, D. Tang, X. Yan, Y. Li, Z. Liu, X. Zou, W. Zhou, G. Wang, Chem. Phys. Lett. **349** (2001) 191.
52. A. Barreiro, S. Hampel, M.H. Rümmeli, C. Kramberger, A. Grüneis, K. Biedermann, A. Leonhardt, T. Gemming, B. Büchner, A. Bachtold, T. Pichler, J. Phys. Chem. B **110** (2006) 20973.
53. P.T.A. Reilly, W.B. Whitten, Carbon **44** (2006) 1653.
54. S. Chaisitsak, J. Nukeaw, A. Tuantranont, Diam. Relat. Mater. **16** (2007) 1958.
55. H.M. Cheng, F. Li, G. Su, H.Y. Pan, L.L. He, X. Sun, M.S. Dresselhaus, Appl. Phys. Lett. **72** (1998) 3282.
56. R. Kojima, Y. Miyauchi, S. Chiashi, M. Cono, Chem. Phys. Lett. **360** (2002) 229.
57. M. Monthioux, H. Allouche, R.L. Jacobsen, Carbon **44** (2006) 3183.
58. L.M. Cele, CNTs and nanospheres: Synthesis by nebulized spray pyrolysis and use in catalysis, Ph.D. Thesis, University of Johannesburg, submitted 2008.
59. A. Magrez, J.W. Seo, V. Kuznetsov, L. Forró, Angew. Chem., Int. Ed. **46** (2007) 441.
60. I. Chorkendorf, J.W. Niemantsverdriet, Concepts of Modern Catalysis and Kinetics, Wiley–VCH Verlag GmbH and Co. KGaA, Weinheim, 2003. p. 325.
61. A.G. Nasibulin, D.P. Brown, P. Queipo, D. Gonzalez, H. Jiang, E.I. Kauppinen, Chem. Phys. Lett. **417** (2005) 179.
62. N. Demoncy, O. Stéphan, N. Bran, C. Colliex, A. Loiseau, H. Pascard, Synth. Met. **3** (1999) 2380.
63. (a) B. Wei, R. Vajtai, Y.Y. Choi, P.M. Ajayan, NanoLetters **2** (2002) 1105; (b) L. Ci, B. Wei, C. Xu, J. Liang, D. Wu, S. Xie, W. Zhou, Y. Li, Z. Liu, D. Tang, J. Cryst. Growth **233** (2001) 823; (c) H.M. Cheng, F. Li, X. Sun, S.D.M. Brown, M.A. Pimenta, A. Marucci, G. Dresselhaus, M.S. Dresselhaus, Chem. Phys. Lett. **289** (1998) 602; (d) Q.H. Yang, S. Bai, T. Fournier, F. Li, G. Wang, H.M. Cheng, J.B.

Bai, Chem. Phys. Lett. **370** (2003) 274; (e) Y.-Y. Fan, A. Kaufmann, A. Mukasyan, A. Varma, Carbon **44** (2006) 2160.

64. H. Zhu, B. Wei, Chem. Commun. (2007) 3042.
65. L. Ci, Z. Rao, Z. Zhou, D. Tang, X. Yan, Y. Liang, D. Liu, H. Yuan, W. Zhou, G. Wang, Wei Liu, Sishen Xie, Chem. Phys. Lett. **359** (2002) 63.
66. Z. Zhou, L. Ci, L. Song, X. Yan, D. Liu, H. Yuan, Y. Gao, J. Wang, L. Liu, W. Zhou, G. Wang, S. Xie, Carbon **41** (2003) 2607.
67. Z. Zhou, L. Ci, L. Song, X. Yan, D. Liu, H. Yuan, Y. Gao, J. Wang, L. Liu, W. Zhou, G. Wang, S. Xie, Phys. Chem. B **108** (2004) 10751.
68. (a) Z. Zhou, L. Ci, X. Chen, D. Tang, X. Yan, D. Liu, Y. Liang, H. Yuan, W. Zhou, G. Wang, S. Xiea, Carbon **41** (2003) 337; (b) L. Ci, Z. Zhou, D. Tang, X. Yan, Y. Liang, D. Liu, H. Yuan, W. Zhou, G. Wang, S. Xie, Chem. Vap. Depos. **9** (2003) 11.
69. L. Ci, Z. Zhou, X. Yan, D. Liu, H. Yuan, L. Song, J. Wang, Y. Gao, J. Zhou, W. Zhou, G. Wang, S. Xie, J. Phys. Chem. B **107** (2003) 8760.
70. J. Wei, L. Ci, B. Jiang, Y. Li, X. Zhang, H. Zhu, C. Xua, D. Wu, J. Mater. Chem. **13** (2003) 1340.
71. J. Wei, B. Jiang, D. Wu, B. Wei, J. Phys. Chem. B **108** (2004) 8844.
72. H. Zhu, C. Xu, B. Wei, D. Wu, Carbon **40** (2002) 2023.
73. Y. Li, K. Wang, J. Wei, Z. Gu, Z. Wang, J. Luo, D. Wu, Carbon **43** (2005) 31.
74. G.C. Tibbetts, C.A. Bernardo, D.W. Gorkiewicz, R.L. Align, Carbon **32** (1994) 569.
75. F.L. Deepak, A. Govindaraj, C.N.R. Rao, Chem. Phys. Lett. **345** (2001) 5.
76. L. Tapasztó, K. Kertész, Z. Vértesy, Z.E. Horváth, A.A. Koós, Z. Osváth, Zs. Sárközi, Al. Darabont, L.P. Biró, Carbon **43** (2005) 970.
77. M.S. Mohlala, X.-Y. Liu, M.J. Witcomb, N.J. Coville, Appl. Organomet. Chem. **21** (2007) 275.
78. Q.-H. Yang, P.-X. Hou, M. Unno, S. Yamauchi, R. Saito, T. Kyotani, NanoLetters **5** (2005) 2465.
79. C.P. Ewels, M. Glerup, J. Nanosci. Technol. **5** (2005) 1345.
80. J. Liu, S. Webster, D.L. Carroll, J. Phys. Chem. B **109** (2005) 15769.

81. (a) M. Nath, B.C. Satishkumar, A. Govindaraj, C.P. Vinod, C.N.R. Rao, Chem. Phys. Lett. **322** (2000) 333; (b) C.N.R. Rao, A. Govindaraj, G. Gundiah, S.R.C. Vivekchand, Chem. Eng. Sci. **59** (2004) 4665.
82. E. Nxumalo, V.O. Nyamori, N.J Coville, J. Organometal. Chem. **693** (2008) 2942.
83. (a) Ph. Redlich, M.J. Loeffler, P.M. Ajayan, J. Bill, F. Aldinger, M. Ruhle, Chem. Phys. Lett. **260** (1996) 465; (b) M. Terrones, W.K. Hsu, S. Ramos, R. Castillo, H. Terrones, Fullerene Sci. Technol. **6** (1998) 787; (c) W.K. Hsu, S. Firth, P. Redlich, M. Terrones, H. Terrones, Y.Q. Zhu, G. Grobert, A. Schilder, R.J.H. Clark, H.W. Kroto, D.R.M. Walton, J. Mater. Chem. **10** (2000) 1425.
84. K. Mondal, N.J. Coville, M.J. Witcomb, J. Havel, G. Tejral, Chem. Phys. Lett. **437** (2007) 87.
85. M.S. Mohlala, Organometallic iron complexes as catalysts for carbon nanotube synthesis, Ph.D. Thesis, University of the Witwatersrand, Johannesburg, June 2007.
86. L. Ci, H. Zhu, B. Wei, J. Liang, C. Xu, D. Wu, Carbon **37** (1999) 1652.
87. P.P. George, V.G. Pol, A. Gedanken, J. Nanopart. Res. **9** (2007) 1187.
88. E. Urones-Garrote, D. Ávila-Brande, N. Ayape-Katcho, A. Gómez-Herrero, A.R. Landa-Cánovas, L.C. Otero-Díaz, Carbon **43** (2005) 978.
89. E. Urones-Garrote, D. Ávila-Brande, N.A. Katcho, A. Gómez-Herrero, A.R. Landa-Cánovas, E. Lomba, L.C. Otero-Díaz, Carbon **45** (2007) 1696.
90. Z. Li-yun, Z. Li-xin, W. Yi-zao, W. Yu-lin, X. Wei-hao, Carbon **43** (2005) 1084.
91. C. Wu, X. Zhu, L. Ye, C. OuYang, S. Hu, L. Lei, Y. Xie, Inorg. Chem. **45** (2006) 8543.
92. R. Lv, F. Kang, W. Wang, J. Wei, J. Gu, K. Wang, D. Wu, Carbon **45** (2007) 1433
93. (a) J. Lee, S.H. Joo, R. Ryoo, J. Am. Chem. Soc. **124** (2002) 1156; (b) R. Ryoo, S.H. Joo, S. Jun, J. Phys. Chem. B **103** (1999) 7743; (c) T.-W. Kim, I.-S. Park, R. Ryoo, Angew. Chem., Int. Ed. **42** (2003) 4375; (d) Y.-F. Shi, H.-J. Quan, G.-B Zheng, H. Sano, Y. Uchiyama, Carbon **411** (2002) 1645; (e) P. Carreira, M. Martınez-Escandell, R. Santamarıa, F. Rodrıguez-Reinoso, Carbon **39** (2001) 1001.
94. (a) H. Zhang, E. Liang, P. Ding, M. Chao, Phys. B: Condens. Mat. **337** (2003) 10; (b) A. Moisala, A.G. Nasibulin, D.P. Brown, H. Jiang, L. Khriachtchev, E.I. Kauppinen, Chem. Eng. Sci. **61** (2006) 4393.

95. K. Kuwana, K. Saito, Carbon **43** (2005) 2088.
96. H. Yang, P. Mercier, S.C. Wang, D.L. Akins, Chem. Phys. Lett. **416** (2005) 18.
97. Y. Xiong, Y. Xie, X. Li, Z. Li, Carbon **42** (2004) 1447.
98. (a) T. Luo, L. Chen, K. Bao, W. Yu, Y. Qian, Carbon **44** (2006) 2844; (b) Y. Li, J. Chen, Y. Ma, J. Zhao, Y. Qin, L. Chang, Chem. Commun (1999) 1141.
99. M. Endo, T. Hayashi, Y.A. Kim, M. Terrones, M.S. Dresselhaus, Phil. Trans. Roy. Soc. Lond. A **362** (2004) 2223.
100. C.P. Deck, K. Vecchio, Carbon **44** (2006) 267.
101. (a) M. Sharon, K. Mukhopadhyay, K. Yase, S. Iijima, Y. Ando, X. Zhao, Carbon **36** (1998) 507; (b) S. Mhlanga, K. Mondal, N. Kunjuzwa, N. Naidoo, N.J. Coville, S. Afr. J. Sci., to be resubmitted (2009).
102. P.T.A. Reilly, W.B. Whitten, Carbon **44** (2006) 653.
103. P.T.A. Reilly, R.A. Whitten, J.M. Ramsey, Combust. Flame **122** (2000) 90.
104. Y.-F. Shi, H.-J. Quan, G.-B. Zheng, H. Sano, Y. Uchiyama, Carbon **41** (2003) 1674.
105. E.C. Walter, T. Beetz, M.Y. Sfeir, L.E. Brus, M.L. Steigerwald, J. Am. Chem. Soc. **128** (2006) 15590.
106. H.W. Zhu, C.L. Xu, D.H. Wu, B.Q. Wei, R. Vajtai, P.M. Ajayan, Science **296** (2002) 884.
107. F. Lupo, J.A. Rodríguez-Manzo, A. Zamudio, A.L. Elías, Y.A. Kim, T. Hayashi, M. Muramatsu, R. Kamalakaran, H. Terrones, M. Endo, M. Rühle, M. Terrones, Chem. Phys. Lett. **410** (2005) 384.
108. L.F. Su, J.N. Wang, F. Yu, Z.M. Sheng, H. Chang, C. Pak, Chem. Phys. Lett. **420** (2006) 421.
109. N. Sano, H. Akazawa, T. Kikuchi, T. Kanki, Carbon **41** (2003) 2159.
110. P.C.P. Watts, W.K. Hsu, D.P. Randall, V. Kotzeva, G.Z. Chen, Chem. Mater. **14** (2002) 4505.
111. M.J. Bronikowski, P.A. Willis, D.T. Colbert, K.A. Smith, R.E. Smalley, J. Vac. Sci. Technol. A **19** (2001) 1800.
112. S. Huang, X. Cai, C. Du, J. Liu, J. Phys. Chem. **107** (2003) 13251.
113. H. Hou, Z. Jun, F. Weller, A. Greiner, Chem. Mater. **15** (2003) 3170.

114. C.N.R. Rao, A. Govindaraj, R. Sen, B.C. Satishkumar, Mat. Res. Innovat. **2** (1998) 128.
115. I. Mönch, A. Meye, A. Leonhardt, K. Krämer, R. Kozhuharova, T. Gemming, M.P. Wirth, B. Büchner, J. Magnetism Mag. Mater. **290-291** (2005) 250.
116. D.K. Smith, D.C. Lee, B.A. Korgel, Chem. Mater. **18** (2006) 3356.
117. E.C. Dickey, C.A. Grimes, M.K. Jain, K.G. Ong, D. Qian, P.D. Kichambare, R. Andrews, D. Jacques, Appl. Phys. Lett. **79** (2001) 4022.
118. P. Mahanandia, P. N Vishwakarma, K.K. Nanda, V. Prasad, S.V. Subramanyam, S.K. Dev, P.V. Satyam, Mater. Res. Bull. **41** (2006) 2311.
119. C. Singh, T. Quested, C.B. Boothroyd, P. Thomas, I.A. Kinloch, A.I. Abou-Kandil, A.H. Windle, J. Phys. Chem. B **106** (2002) 10915.
120. A.R. Harutyunyan, G. Chen, P.C. Eklund, Appl. Phys. Lett. **82** (2003) 4794.
121. N.S. Kim, Y.T. Lee, J. Park, J.B. Han, Y.S. Choi, S.Y. Choi, J. Choo, G.H. Lee, J. Phys. Chem. B **107** (2003) 9249.
122. S. Lastella, Y.J. Jung, H. Yang, R. Vajtai, P.M. Ajayan, C.Y. Ryu, D.A. Rider, I. Manners, J. Mater. Chem. **14** (2004) 1791.
123. J.Q. Lu, T.E. Kopley, N. Moll, D. Roitman, D. Chamberlin, Q. Fu, J. Liu, T.P. Russell, D.A. Rider, I. Manners, M.A. Winnik, Chem. Mater. **17** (2005) 2227.
124. J.Q. Lu, D.A. Rider, E. Onyegam, H. Wang, M.A. Winnik, I. Manners, Q. Cheng, Q. Fu, J. Liu, Langmuir **22** (2006) 5174.
125. S. Xiea, L. Song, L. Ci, Z. Zhou, X. Dou, W. Zhou, G. Wang, L. Sun, Sci. Technol. Adv. Mat. **6** (2005) 725.
126. F. Su, X.S. Zhao, Y. Wang, L. Wang, J.Y. Lee, J. Mater. Chem. **16** (2006) 4413.
127. Z.C. Kang, Z.L. Wang, J. Phys. Chem. **100** (1996) 5163.
128. I. Martin-Gullon, J. Vera, J.A. Conesa, J.L. Gonza'lez, C. Merino, Carbon **44** (2006) 1572.
129. Y. Ma, Z. Hu, K. Huo, Y. Lu, Y. Hu, Y. Liu, J. Hu, Y. Chen, Carbon **43** (2005) 1667.
130. M. Mamo, W.A. van Otterlo, N.J. Coville, submitted for publication.
131. A. Moisala, A.G. Nasibulin, E.I. Kauppinen, J. Phys.: Condens. Mat. **15** (2003) S3011.

Chapter 5

The effect of synthesis parameters on the catalytic synthesis of multiwalled carbon nanotubes using Fe-Co/$CaCO_3$ catalysts[#]

5.1 Introduction

Since the synthesis of carbon nanotubes (CNTs) by Iijima in 1991 [1], methods to produce these materials have been extensively investigated [2]. The synthesis of CNTs has sparked a worldwide escalation in research interest within the scientific community focussing on synthesis, modification or functionalization and application of these nanomaterials. The potential applications of CNTs are due to their outstanding mechanical and unique electrical properties [3]. Such applications include their use as chemical sensors, as nano-conveyors, nanoelectronic devices, field emission sources, scanning probes and as supports in catalysis [3-5].

Several methods including arc discharge [6,7] laser ablation [8], pyrolysis [9] and chemical vapour deposition (plasma enhanced, thermal and catalytic) have been developed for the production of CNTs [10,11]. While all these methods seek to produce high-quality CNTs, the production of CNTs by the catalytic chemical vapour deposition (CCVD) method remains the prominent route for their large scale production. This bottom-up approach of producing CNTs is favoured by the fact that it is a low cost process that is versatile and results in relatively pure materials. Controlled growth of CNTs can be obtained through manipulation of the size of the nanoparticles that are used as catalysts in the CNT synthesis. The most widely used metals are Fe, Co and Ni as well as the alloys of these nanoparticles. The metals are usually supported on materials that are stable at high temperatures such as SiO_2, Al_2O_3, TiO_2 and zeolites [12-16].

[#]*Sabelo D. Mhlanga, Kartick C. Mondal, Robin Carter, Michael J. Witcomb, Neil J. Coville, South Afr. J. Chem.* ***62*** *(2009) 67.*

However, purification of CNTs produced on these supports remains a challenge and requires several steps that result in damage to the CNT structures. Also, the solvents used during the purification process have to be disposed of to minimize environmental issues. To circumvent these problems, the use of readily removable supports (e.g. calcium carbonate) has been studied both by ourselves and others [17-22].

Calcium carbonate ($CaCO_3$), albeit a low surface area material, has been shown to be a good support for the CCVD production of multiwalled carbon nanotubes (MWCNTs). At 700°C, $CaCO_3$ changes to CaO (lime), which is an environmentally friendly material that can readily be dissolved in dilute acids such as HNO_3 and HCl. As a result, this support can be removed from the produced CNTs with ease, resulting in clean materials that are relatively free of contaminants [17-22]. It is also a cheap material that is readily available. The CNTs produced on $CaCO_3$ have been used as supports for catalysts in the Fischer-Tropsch reaction [19] and for the thermal decomposition of hydrocarbons [23].

The investigation of CNT synthesis over metals supported on silica and alumina has been actively studied and factors that affect the catalytic activity and ultimately the structure of the CNTs produced have been determined [24-28]. In contrast, the behavior of metals supported on $CaCO_3$ for CNT production has been inadequately studied [17-22,29,30].

Kathyayini *et al.* [18] studied the activity of Fe, Co, and Fe-Co supported on Ca and Mg oxides, hydroxides and carbonates for the synthesis of CNTs. Their catalyst-support mixtures were prepared by the wet impregnation method and the study revealed that Fe-Co supported catalysts gave the best activity. The excellent activity was achieved by favorable metal-support interactions, which greatly influenced the CNT selectively. Cheng *et al.* [20] recently reported on the use of $CaCO_3$ nanocrystals as a catalyst support for the CVD synthesis of CNTs. The catalyst-support mixtures were also prepared by the wet impregnation method and the authors observed that the nanocrystalline $CaCO_3$ produced high yields of CNTs.

Magrez *et al.* [21] reported on a systematic study of the effect of catalyst composition, catalyst carrier, and synthesis time on the yield and quality of CNTs grown by CCVD. The study revealed that the carbon yield is influenced by the Fe-Co catalyst composition mixtures and that maximum yield is obtained at about a Fe to Co ratio of 2/1. They also reported on the carbon yield obtained from the catalysts after different synthesis times (2 - 100 min.) showing that maximum CNT growth occurred between 2 to 30 min.; no clear variation in the length or in the outer diameter of CNTs was observed within this growth time. The presence of CO_2 in the system was also proposed to assist in the formation of CNTs [22].

Schmitt *et al.* [30] observed that $CaCO_3$ decomposed into CaO and CO_2 at high temperature and in doing so gave catalyst particles with outer diameters belonging to two main groups with sizes of 8 - 35 nm and 40 - 60 nm respectively. Dervishi *et al*.[29] also reported on the synthesis of MWCNTs on a $CaCO_3$ supported Fe-Co catalyst. They observed that the outer diameter of the MWCNT products obtained fell into two groups; one associated with growth on Fe-Co/CaO and the other with growth on Fe-Co/$CaCO_3$. Finally See *et al.* [31] have reported on the high yield synthesis of MWCNTs on Fe-Co catalysts supported on a $CaCO_3$ substrate using a fluidized bed reactor.

In all the reported studies, catalyst-support mixtures were prepared by the impregnation methods using different sources of carbon (e.g acetylene and ethylene) and different carrier gases (e.g. argon and nitrogen). Similar MWCNT products were obtained from all studies but the products had a varied diameter distribution.

In this study we have investigated factors that affect the morphology of the CNTs in particular using an Fe-Co/$CaCO_3$ catalyst prepared by the wet impregnation method. This study revealed the key role of reaction time on both CNT quantity and quality. We show, by means of TEM, that as the synthesis time is increased, carbon continues to deposit on the already formed CNTs resulting in the thickening and the destruction of the CNTs [33]. To further explore the Fe-Co/$CaCO_3$ catalysts an investigation of the effect of the catalyst preparation route and the catalyst counter-ion on the synthesis of CNTs was

undertaken. To this end, the synthesis strategy was to produce CNTs with similar diameters from different routes. In this work this was achieved by preparing catalysts using wet impregnation, deposition-precipitation and water-in-oil microemulsion (reverse micelles) methods [32].

5.2 Preparation of catalysts

5.2.1 Wet impregnation

$Fe(NO_3)_3 \cdot 9H_2O$, $Co(NO_3)_2 \cdot 6H_2O$, $Fe(CH_3CO_2)_2$ and $Co(CH_3CO_2)_2$ (Sigma Aldrich) were used to prepare the different catalysts. A calculated amount of the Fe and Co nitrates were mixed, ground to a fine powder and dissolved in distilled water to make a 0.3 M Fe-Co (50:50 w/w) precursor solution. A similar Fe-Co acetate precursor solution was made from the metal acetates. This solution (28 ml) was added to the $CaCO_3$ support (10 g) and the mixture was left to stir for 30 minutes. The metal-support mixture was then filtered and the insoluble product was dried in an air oven at 120°C for 12 h, cooled to room temperature, ground and finally screened through a 150 μm sieve. The catalyst powder was then calcined at 400°C for 16 h in a static air oven. The 5% metal loaded catalysts were named IMPN (prepared from nitrate solution) and IMPA (prepared from acetate solution).

5.2.2 Deposition-precipitation

The $CaCO_3$ support was stirred in distilled water (100 ml) for 5 min. An aqueous 0.3 M solution (28 ml) of the catalyst precursor was added dropwise to the stirred $CaCO_3$ slurry and the mixture left to stir for another 5 min. Ammonium hydroxide (12.5%) was then added dropwise to the slurry and when the pH reached 7.2 the mixture was left to stir for another 10 min. The resulting metal-support mixture was then filtered and dried in an oven at 120°C for 12 h, cooled to room temperature and then ground and screened through a 150 μm sieve. The total loading of the Fe-Co catalysts on the $CaCO_3$ was 5 wt%. The material was then calcined at 400°C for 16 h in static air. The catalysts

prepared from the nitrate and acetate Fe/Co precursor solution were labelled DPN and DPA respectively.

5.2.3 Reverse micelles

Isooctane, n-butanol, sodium borohydride ($NaBH_4$) and cetyl-trimethyl-ammonium-bromide (CTAB) were purchased from Sigma Aldrich and were used as received. CTAB and n-butanol were used as the surfactant and co-surfactant molecules respectively. Isooctane was used as the oil phase while distilled water was used as the aqueous phase. $NaBH_4$ was added to the aqueous solution to reduce the metals under a flow of N_2 [32]. $Fe(NO_3)_3 \cdot 9H_2O$ and $Co(NO_3)_2 \cdot 6H_2O$ were used as the Fe and Co sources.

Two microemulsions were prepared (Fig. 5.1). Microemulsion A consisted of an aqueous solution containing Fe^{3+} (0.3 M) and Co^{2+} (0.3 M) ions obtained by dissolving $Fe(NO_3)_3 \cdot 9H_2O$ and $Co(NO_3)_2 \cdot 6H_2O$ in 14 ml distilled water. This was added to a mixture containing 20 ml of isooctane, 5 ml of n-butanol and 0.46 g of CTAB. The microemulsion was stirred vigorously for ten minutes. Microemulsion B consisted of a solution of $NaBH_4$ (14 ml, 0.5 M) and CTAB (0.46 g), n-butanol (5 ml) and isooctane (20 ml). The microemulsion was stirred vigorously for ten minutes.

Microemulsion B was then slowly added to microemulsion A using ultrasonic agitation for 90 min under a continuous N_2 flow to minimize oxidation. The solution immediately turned black after the two microemulsions were mixed, due to the formation of metallic Fe and Co in the micelles. The micelle solution was then disrupted with an excess of ethanol (150 ml) and centrifuged. The precipitate was repeatedly washed with methanol to remove the surfactant. The resulting powder, which was dark brown in colour, was dried at 100^oC for 12 h in an air oven. It was then calcined at 600°C to obtain the crystalline nanoparticles, which were then deposited on the $CaCO_3$ support using ethanol to give a 5 wt% Fe-Co/$CaCO_3$ catalyst. The catalyst prepared was labelled as RM.

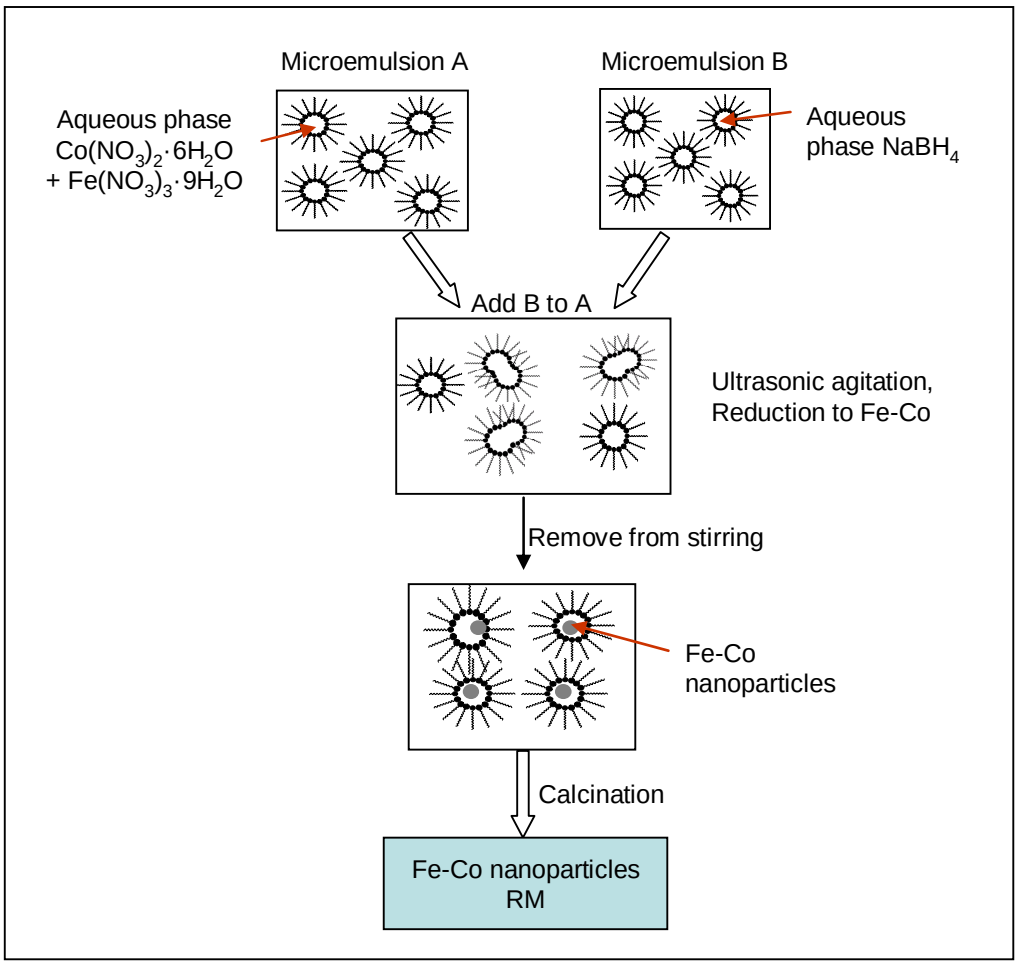

Fig. 5.1: The synthetic pathway for the preparation of Fe-Co nanoparticles using reverse micelles.

The metal loading concentrations on the $CaCO_3$ support were confirmed by Inductively Coupled Plasma - Atomic Emission Spectroscopy (ICP-AES) measurements using semiconductor detectors (CCD) and by quantitative thermogravimetric analysis (TGA) using a Perkin Elmer Pyris 1 TGA. For thermal analysis, the CNTs were decomposed under a continuous flow of air or nitrogen (40 ml/min) and the heating rate was 10°C/min.

5.3 Carbon nanotube synthesis

CNTs were synthesized by the decomposition of acetylene (C_2H_2) (Afrox) in a tubular quartz reactor (51 cm × 1.9 cm i.d.) that was placed horizontally in a furnace (Fig. 5.2). The furnace was electronically controlled such that the heating rate, reaction temperature and gas flow rates could be accurately maintained as desired. The catalyst (0.2 g) was spread to form a thin layer in a quartz boat (120 mm × 15 mm) and the boat was then placed in the centre of the quartz tube. The furnace was then heated at 10°C/min under flowing N_2 (40 ml/min). Once the temperature had reached 700°C, the N_2 flow rate was set to 240 ml/min and C_2H_2 was introduced at a constant flow rate of 90 ml/min. After 60 min of reaction time, the C_2H_2 flow was stopped and the furnace was left to cool down to room temperature under a continuous flow of N_2 (40 ml/min). The boat was then removed from the reactor and the carbon deposit that formed along with the catalyst was weighed.

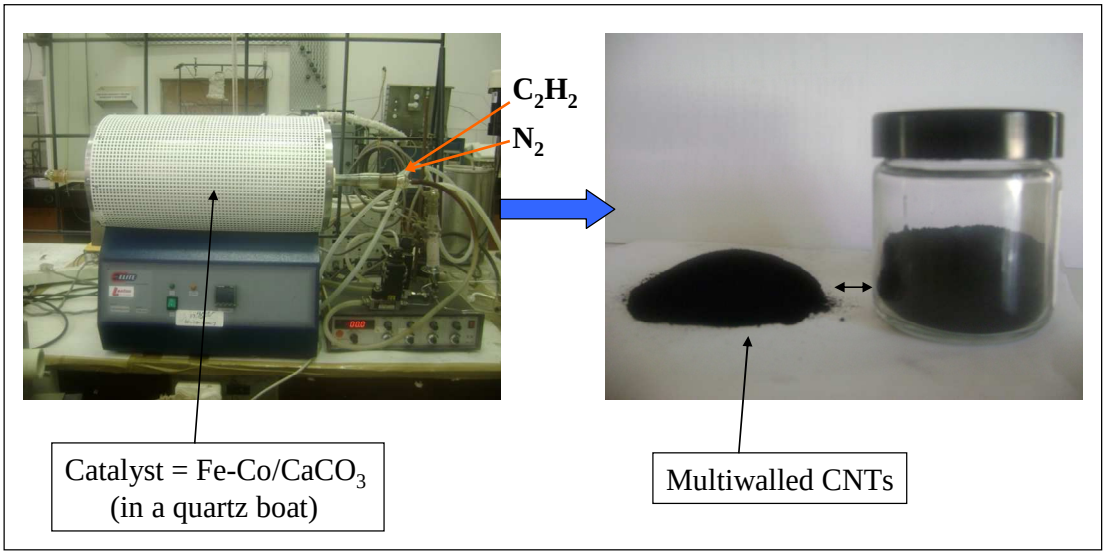

Fig. 5.2: The horizontal CVD setup used for the synthesis of CNTs.

5.4 Characterization of catalysts and CNTs

The Fe-Co catalysts supported on $CaCO_3$ were characterized by a range of techniques. The morphology of the support was characterized by transmission electron microscopy (TEM) (JEOL 100S Electron Microscope), while the size and distribution of the Fe-Co

nanoparticles was determined at higher magnification using a Philips CM200 equipped with a Gatan Imaging Filter. For TEM observation, the samples were sonicated in ethanol for 10 min and thereafter deposited on a TEM Cu grid. Energy dispersive X-ray spectroscopy (EDX) and powder X-ray spectroscopy (PXRD) were used to confirm the elemental composition of the Fe-Co bimetallic nanoparticles. The metal loading (wt %) on the support was confirmed by Inductively Coupled Plasma–Atomic Emission Spectrometry (ICP-AES) measurements using semiconductor detectors (CCD) and by quantitative TGA using a Perkin Elmer Pyris 1 TGA. The total surface area and porosity of the catalysts was ascertained using a Micromeritics TriStar Surface Area and Porosity Analyzer. A slight variation (within error bar) on the diameter distribution of the MWCNTs was observed within each sample as well as with the different catalysts used. Carbon nanotube structures and size distributions were ascertained from TEM studies.

The percentage carbon deposit (%C) was determined as described elsewhere [18]. In the calculation it was assumed that all $CaCO_3$ was converted to CaO [29,30]. The selectivity of the catalysts was determined based on the different forms of carbon materials produced *before purification* of the product. TEM was used to distinguish the CNTs from other carbonaceous products (e.g. carbon spheres and carbon nanofibers) that were formed along with the CNTs under non-ideal reaction conditions. Under the optimal reaction conditions the selectivity towards CNTs was close to 100%. The % selectivity was determined using counting procedures i.e. by literally counting images in not less than 25 TEM images. Under non-optimal conditions spheres also formed. Long reaction times at T = 700°C resulted in tube thickening and tube shortening. Thus, product selectivity to CNT formation at t > 2 hours was determined by measuring and counting the tube fragments.

The properties of the CNTs observed under TEM were also confirmed by Raman Spectroscopy (Jobin-Yvon T64000 micro-Raman spectrometer) equipped with a liquid nitrogen cooled charge coupled device detector**.** All samples were measured after excitation with a laser wavelength of 514.5 nm. The CaO and residual Fe-Co particles in the product were removed by stirring the products in 30% HNO_3 for at least 30 minutes at

room temperature. The acid treated CNTs were then washed with distilled water until the washings were neutral. The purification of CNTs was monitored by TEM, TGA and PXRD (Bruker axs D8 Advance PXRD).

5.5 Results and Discussion

5.5.1 Analysis of the catalyst

The surface area of commercial $CaCO_3$ was found to be about 10 m^2/g. The Fe-Co/$CaCO_3$ materials also possess similar surface areas (**Table 5.1**). The freshly prepared supported catalysts were heated under normal carbon nanotube synthesis conditions (t = 60 min, T= 700°C) in N_2 (240 ml/min) but in the absence of the carbon source (C_2H_2). It was observed that the surface areas of the support and catalysts almost doubled within an hour when subjected to the reaction conditions in the absence of C_2H_2. This result is due to the decomposition reaction $CaCO_3 \rightarrow CaO + CO_2$ that occurs at 700°C [22]. When the supported catalysts, were further heated at 700°C for up to 2 h, the surface area of the supported catalyst did not increase any further.

Table 5.1: Surface areas of $CaCO_3$ and supported catalysts before and after heating at 700°C under N_2 (300 ml/min).

Sample identification	BET Surface area before heating (m^2/g)[a]	BET Surface area after heating for 60 min (m^2/g)[a]
$CaCO_3$ support	9.6	22.3
IMPN	10.8	18.2
IMPA	11.5	22.6
DPN	13.6	22.5
DPA	10.6	19.4
RM	10.3	21.4

a ± 5%

In this study, the dispersion of the metal particles on the support prior to heating to 700°C could not be effectively studied by electron microscopy as the $CaCO_3$ decomposed under the electron beam. TEM analysis of the Fe-Co/$CaCO_3$ prepared by the three synthesis procedures (wet impregnation, deposition-precipitation and reverse micelles) *after*

heating to 700℃ for 1 h in N_2, but prior to CNT synthesis, revealed that the metal particles were all ~ 20 - 30 nm in diameter (Fig. 5.3). Some variation in particle sizes within the 20 - 30 nm range was observed for the different methods used. In particular the RM samples gave on average smaller particles in the 20 - 30 nm range. This effect did not however impact on the parametric studies that were performed. The source of the catalyst (i.e. whether nitrate or acetate) also did not influence the Fe-Co particle size when either the IMP or PPN methods were used. HRTEM revealed the presence of lattice-fringe patterns (~ 0.2 nm apart), displaying the highly crystalline nature of the nanoparticles.

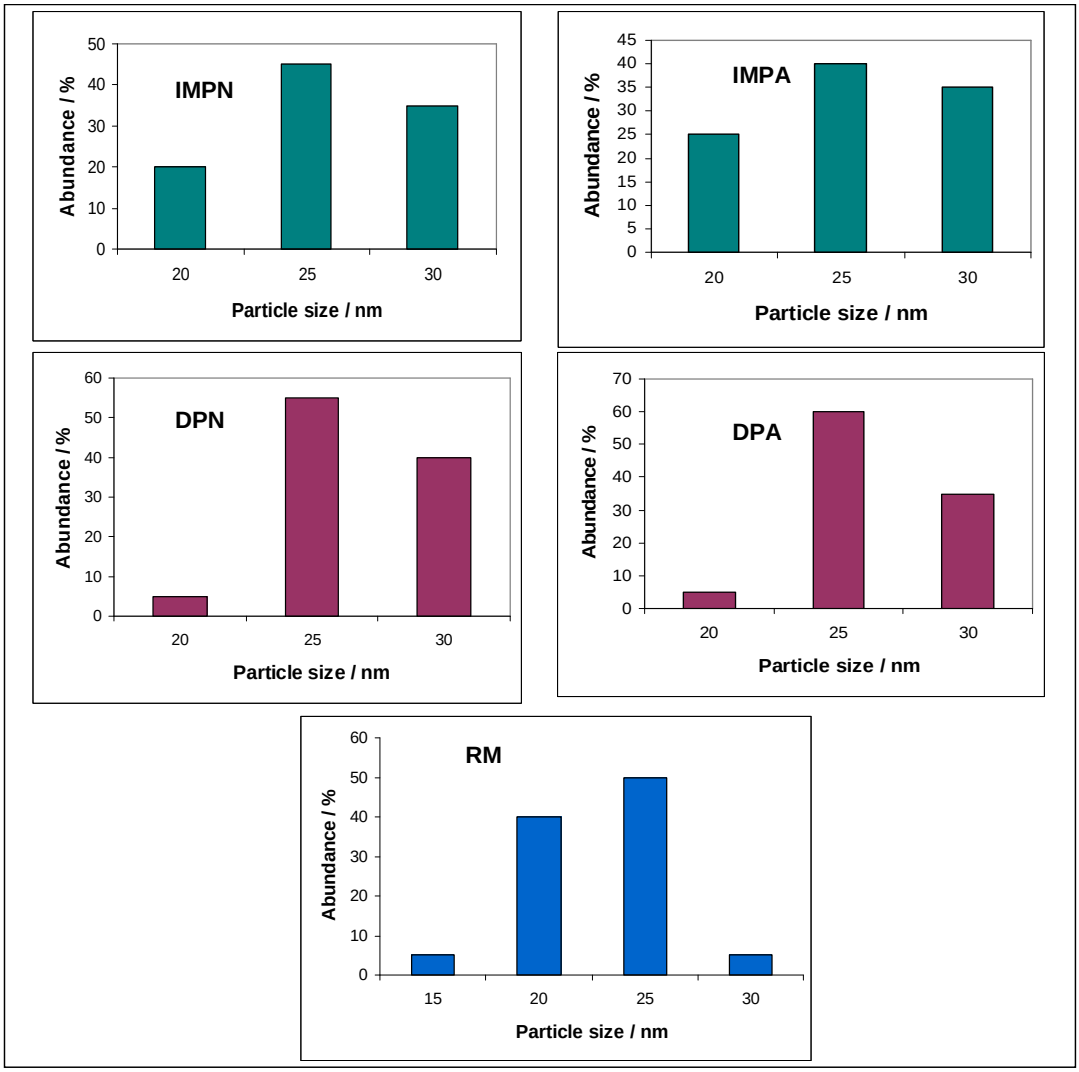

Fig. 5.3: Diameter distribution of the Fe-Co particles prepared by the IMP, DP and RM methods.

A qualitative and quantitative elemental analysis of the particles using energy dispersive X-ray spectroscopy (EDX) revealed that all particles contained both Fe and Co in a close to 1:1 wt% ratio in all the individual particles that were analyzed. An example of a TEM image of the Fe-Co on $CaCO_3$ catalyst prepared by the impregnation process is shown in Fig. 5.4 (see Fig. 5.4b for EDX data).

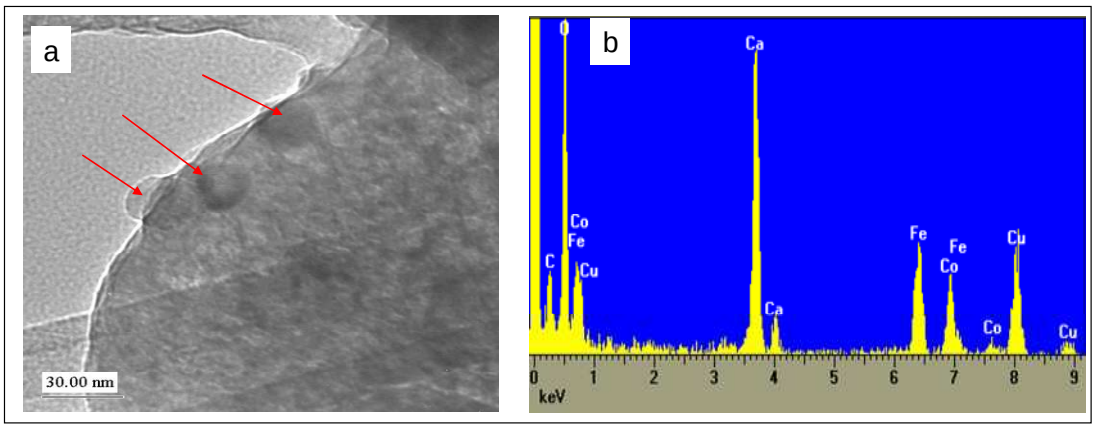

Fig. 5.4: (a) TEM image of IMPN. Arrows show some Fe-Co nanoparticles (~ 30 nm) supported on $CaCO_3$ after calcination and (b) An EDX spectrum of the IMPN indicating the presence of Fe-Co nanoparticles.

5.5.2 Catalytic reactions

Experiments were carried out under conditions found to be optimum to produce CNTs (i.e. ratio = 1:3 or 90 ml/min C_2H_2: 240 ml/min N_2) which involved passage of the gas mixture over the $CaCO_3$ (no metal) at 700°C. TEM analysis of samples taken at different times (0.5 h, 1 h, 3 h and 6 h) revealed that no carbon nanotubes were formed. The TEM images revealed that after one hour, the support was still well dispersed. Further, the surface area of the support initially increased and the remained unchanged from 30 - 120 min (22.3 m^2/g). However, after six hours of reaction time, the support appeared to have sintered and now had a low surface area (4.0 m^2/g) (Fig. 5.5). These observations reveal that $CaCO_3$/CaO at 700°C is stable under the reaction conditions for $t < 2$ h and is suitable for the synthesis of CNTs [18].

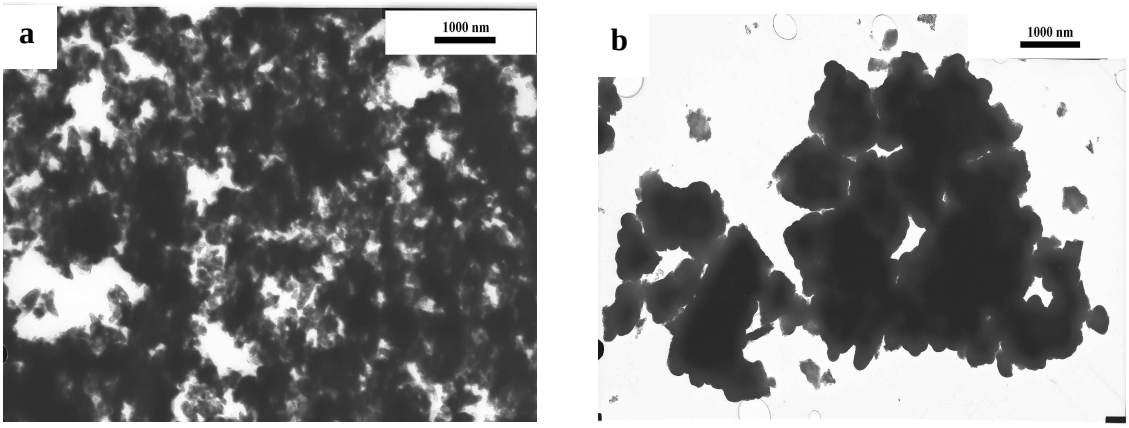

Fig. 5.5: TEM images of $CaCO_3$ heated at 700°C under C_2H_2 for (a) 1 h and (b) 6 h.

The effect of catalyst particle size on CNT production is now well established [26,34]. This also applies to catalysed reactions performed over $CaCO_3$ [22,35]. Further, studies have also shown that Fe-Co bimetallic catalysts are more effective than either Fe or Co catalysts when supported on $CaCO_3$ [18,20-22,29,30]. We have chosen to prepare a 50/50 Fe-Co catalyst as our studies indicated good activity for this mixture (Fig. 5.6), although some authours have suggested that a 2/1 Fe-Co (i.e. Fe_2Co) catalyst may be even more active [21,29].

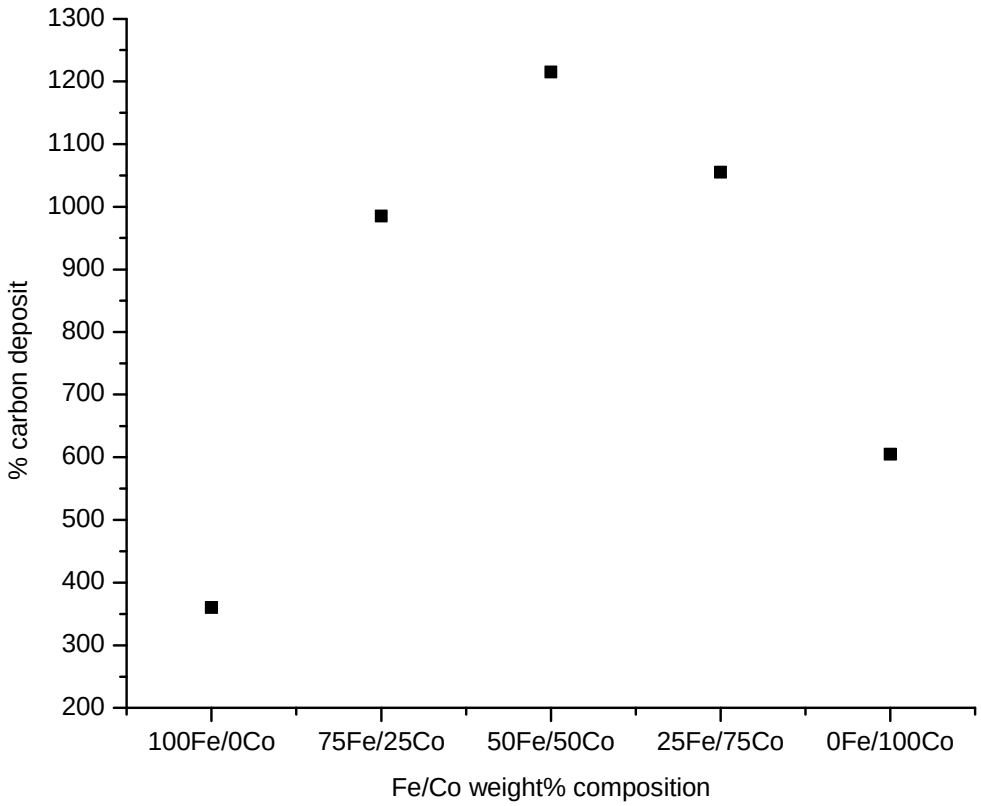

Fig. 5.6: Amount of carbon deposit produced using 5 wt% Fe-Co/$CaCO_3$ with different amounts of Fe and Co in the alloy.

While some work has previously been reported on the effect of reaction conditions on the synthesis of CNTs using $CaCO_3$ as a substrate, in this work we have investigated (i) the effect of the catalyst synthesis process on the CNT yield and quality (using *ca*. same size metal particles) and (ii) three reaction parameters, namely C_2H_2/N_2 ratio, temperature and time on stream (synthesis time), on the formation of CNTs.

(i) Effect of catalyst preparation method

We chose to synthesize CNTs from Fe-Co catalysts prepared by three routes and with different sources of Fe and Co. Conditions were chosen to keep the particle sizes *ca*. the same (20 - 30 nm). Fig. 5.7 shows TEM images of the CNTs produced from the IMPN, DPN and RM methods. The image reveals that all the CNTs are multiwalled in nature with a random (spaghetti-like) orientation. Analysis of the CNTs using TEM (Fig 5.7d)

revealed that all the CNTs have defects in the graphite tubes and the degree of disorder was similar for all the CNTs. TEM analysis indicated that the CNTs produced using the three different preparation methods contained no catalyst particles in their tips and little residual metal inside their tube cavities. Thus the synthesized CNTs form *via* a base-growth mode involving a strong interaction between Co-Fe metal particles and the CaO [25].

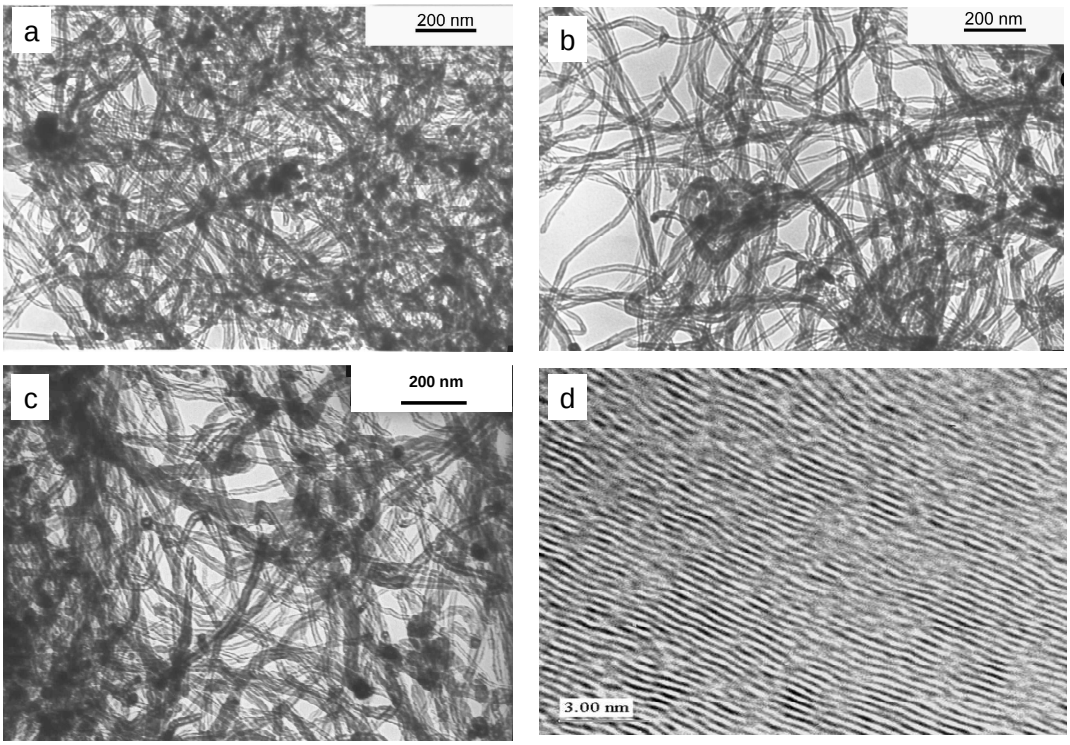

Fig. 5.7: TEM images of MWCNTs prepared by the IMPN (a), DPN (b) and RM (c) and a general higher magnification TEM image (d) showing a much closer look at the 'wavey-like' structures of the CNTs.

Fig. 5.8 shows a graphical representation of the percentage carbon deposit obtained from the different catalysts and the amount of MWCNTs produced at different temperatures. Calculation of the percentage yield of the actual CNTs formed is not straightforward especially when the carbon deposit contains a mixture of the nanomaterials as well as amorphous carbon. This problem can be eliminated by improving the selectivity of the catalyst such that the carbon deposit percentage (*C%*) consists mainly of the desired

material, hence the *C%* will be equal to the yield of CNTs. The *C%* was calculated using equation (1) [18].

$$C\% = \frac{w_3 - (w_1 - w_2)}{w_1 - w_2} \times 100 \qquad (5.1)$$

Where w_1 is the initial weight of the catalyst, w_2 the weight loss of the catalyst at the reaction temperature, and w_3 is the weight of the carbon deposit and the catalyst. Since the weight of the catalyst at the reaction temperature (w_1-w_2) is less than the initial weight (w_1), it is important to know this difference in order to be able to calculate the *C%*. To find this loss in weight of the catalyst, an equivalent amount of the catalyst was weighed and heated under the same conditions as in the reaction but in the absence of the carbon source, C_2H_2.

Gas flow rates were kept fixed (C_2H_2 = 90 ml/min, N_2 = 240 ml/min) for each experiment. The reaction time was 60 min and 0.2 g of catalyst was used in each experiment. The data indicates that the best temperature to produce MWCNTs using a 5wt% Fe-Co/$CaCO_3$ catalyst is 700°C. At this temperature, all the catalysts show excellent selectivity (~ 100%) towards MWCNTs. The tendency of the catalyst to possess maximum activity at ~ 700°C (Fig. 5.8) was explained by Magrez *et al.* [22]. They suggested that the production of CNTs is enhanced by the presence of oxygen which comes from CO_2, which is liberated when $CaCO_3$ decomposes. In their study, they showed that at higher temperatures (e.g. at 820°C) the carbonate is fully decomposed, the reactor is CO_2-free, and MWCNTs are entirely produced by acetylene decomposition ($C_2H_2 \rightarrow 2C + H_2$). At 820°C a MWCNTs growth rate of 0.7 mg min^{-1} was measured whereas at 660°C, a growth rate of 14.6(8) mg/min was obtained due to the presence of C_2H_2-CO_2 mixtures.

The yields of MWCNTs obtained were relatively high for the IMPN and DPN catalyst. Lower yields of MWCNTs were obtained with the RM catalysts. The cause of the

difference in the amount of carbon deposit produced is unknown and was not explored further.

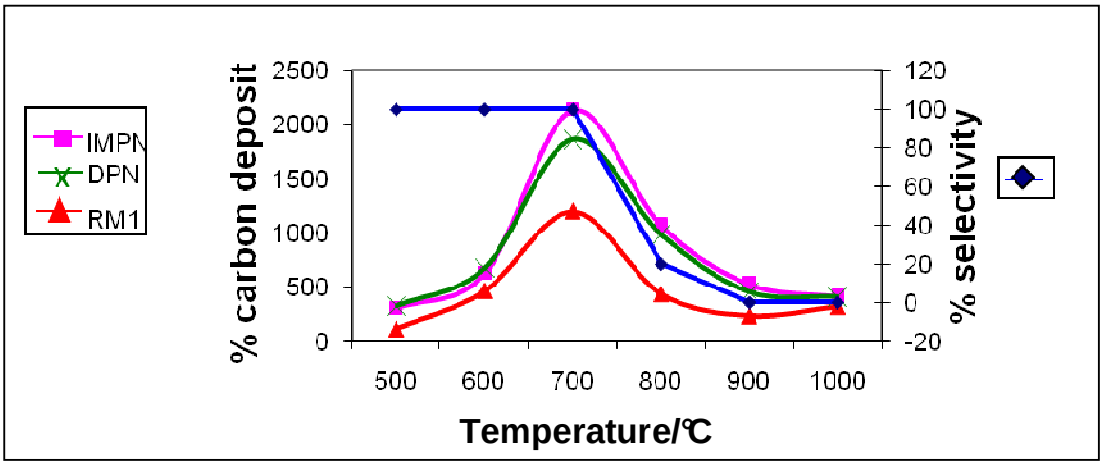

Fig. 5.8: Graph showing the amount of CNTs produced and the percentage selectivity at different reaction temperatures in the CVD of C_2H_2 diluted with N_2 (C_2H_2:N_2 = 1:3, t = 1 h). The selectivity profile is similar for all the supported catalysts.

Raman spectroscopy analysis was also used to characterize the CNTs. Two peaks at 1344 cm^{-1} and 1574 cm^{-1} corresponding to the disorder induced band (D band) and the Raman-allowed tangential mode (G band) were observed (Fig. 5.9). The D mode indicates the disorder features of the carbon while the G mode is associated with the ordered graphite in the CNTs [36]. A small shoulder on the G band corresponding to the D′ band was observed at 1615 cm^{-1}, which is typical of CVD synthesized MWCNTs. The intensity ratio of the D band to G band (I_D/I_G) was found to be ~ 0.7 for all the CNTs suggesting similar structures for the CNT samples.

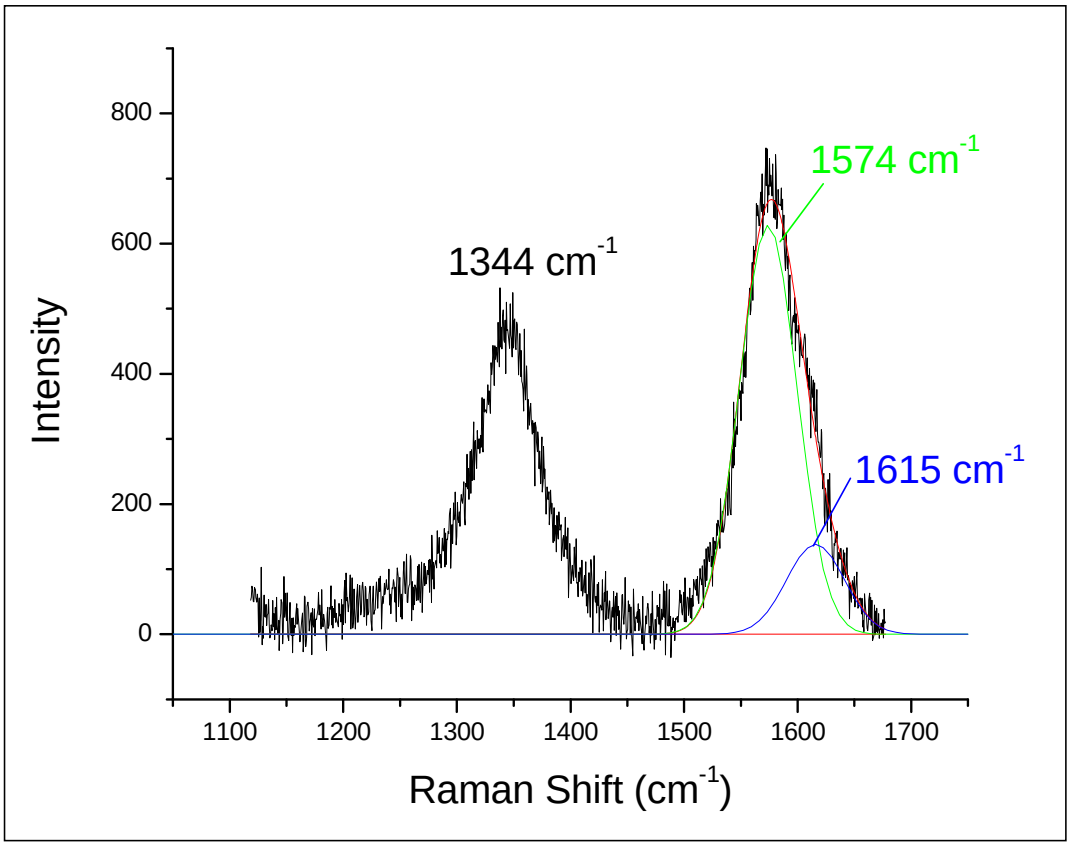

Fig. 5.9: Raman spectrum of MWCNTs synthesized on Fe-Co/$CaCO_3$ catalyst.

(ii) Effect of carbon source dilution

The effect of dilution of the carbon source by N_2 on the activity and selectivity of 5wt% Fe, 5wt% Co and 5wt% Fe-Co/$CaCO_3$ supported catalysts is shown in Fig. 5.10. This study was performed on catalysts that were prepared by the wet impregnation method. The study was carried out at 700°C for 1 h. A total gas flow rate of 330 ml/min was used in all experiments. The ratio of C_2H_2 to N_2 was changed from 1:10 (i.e. 30 ml/min C_2H_2 and 300 N_2) to 1:0 (330 ml/min C_2H_2 and no N_2).

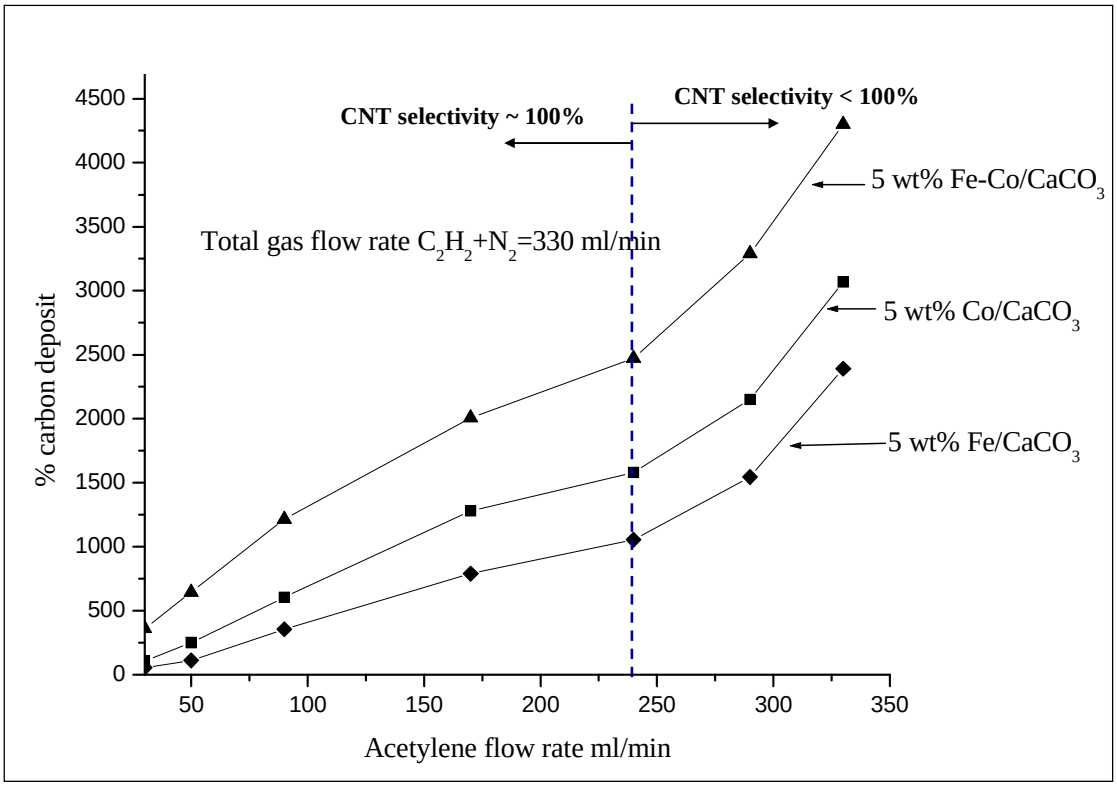

Fig. 5.10: A graph showing %C obtained by varying the gas flow ratio of C_2H_2 to N_2. The synthesis time was 1 h for all reactions and the reaction temperature was 700^oC.

Figure 5.10 reveals:

- The order of activity is Fe-Co > Co > Fe.
- When the flow rate ratio of C_2H_2 to N_2 was changed from 1:10 to ~1:3 the CNT yield also increased for all the catalysts. In every case the selectivity to CNTs was ~ 100% (Fig. 5.11a).
- The maximum %C obtained with ~100% selectivity to CNTs was 1215% using a Co-Fe catalyst. This was obtained when the flow rate ratio of C_2H_2 to N_2 was 90 ml/min C_2H_2 and 240 ml/min N_2 (~1:3).
- When the ratio of C_2H_2 and N_2 was greater than 1:2.67, the product contained a mixture of CNTs, carbon spheres (CSs) and carbon fibers (CFs) (Fig. 5.11b).
- When the carbon source was not diluted (i.e. 100% C_2H_2), the product contained only CSs and a few CFs (Fig. 5.11c).

- The inner diameters of the CNTs as well as the lengths were not affected by the C_2H_2/N_2 ratio. About 90% of the tubes have inner diameters within 5-10 nm and outer diameters (o.d.) within 15 - 30 nm for the C_2H_2/N_2 ratios that were used. However a small variation in the CNT outer diameter was observed. The o.d. increases slightly with increase in the C_2H_2 concentration.

Significant yields of accreted (agglomerated) CSs were observed, when the reaction conditions did not favour CNT formation (i.e. when C_2H_2: N_2 > 1: 2.67). TEM analysis revealed that the carbon microspheres are round, smooth, clean, solid and did not show large porosity [37,38]. We attribute the formation of these CSs to the direct pyrolysis of the C_2H_2 that occurs without intervention of a catalyst via a mechanism similar to the acetylene black process [39]. This proposal is supported by the observation that CS formation was observed when $CaCO_3$ contained no catalyst was used. In conclusion the dilution of the carbon source (C_2H_2) with N_2 significantly affects the product yield and the selectivity of the catalysts towards CNT formation [17,18,20-22,29,30].

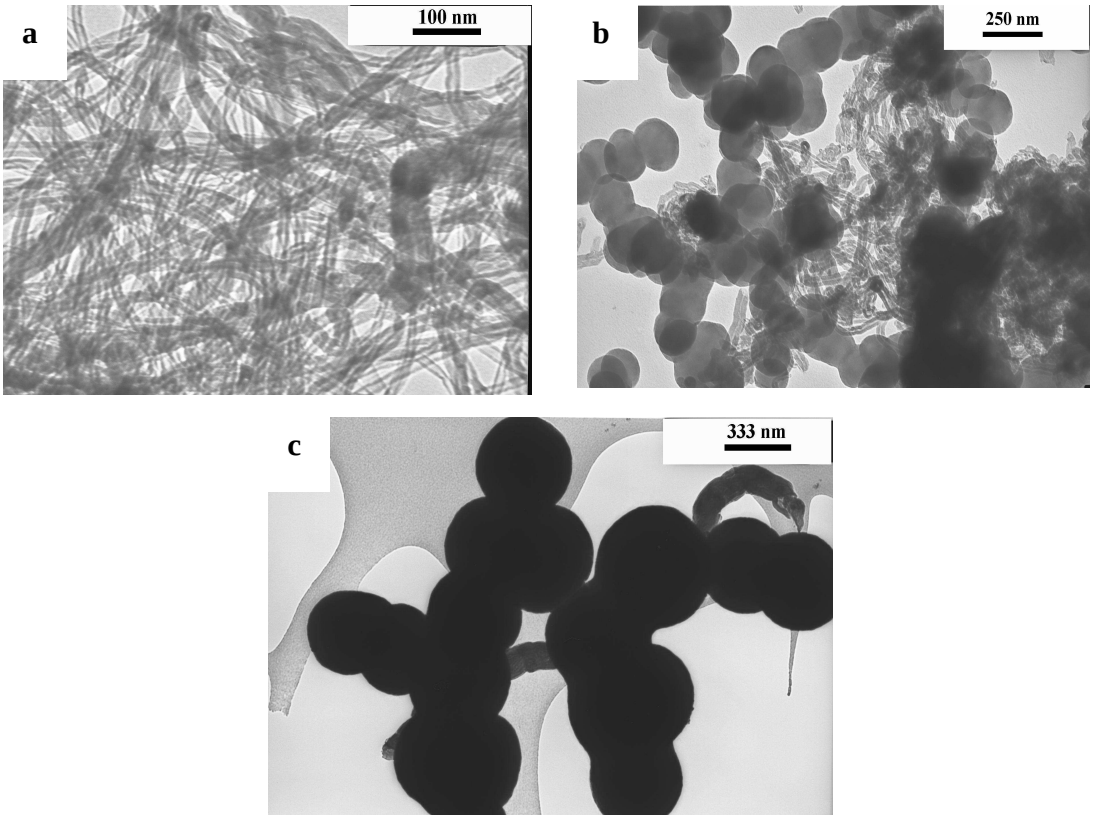

Fig. 5.11: Low magnification TEM images of the carbon deposit produced with different dilution ratios of feed stock gases: a) C_2H_2: N_2 = 1:2.7 (100% CNTs), b) C_2H_2: N_2 = 1:1 (CNTs and CSs), c) C_2H_2: N_2 = 1:0 (CSs and CFs); T = 700°C, t = 1 h.

5.5.3 Effect of time on stream (TOS)

Experiments were performed to investigate the effect of reaction time on catalyst activity and the types of products formed. The study was undertaken on the catalysts synthesized by the wet impregnated method. The reaction temperature was fixed at 700°C and the flow rates used were: C_2H_2 = 90 ml/min, N_2 = 240 ml/min in all experiments. The product yield, as expected, was found to increase as the reaction time was increased from 15 to 360 min (Fig. 5.12). The reaction was also monitored by TEM. The TEM studies revealed that both the diameters and the lengths of the products varied with reaction time. TEM images for the CNTs produced from the IMPN catalyst after different times are shown in Fig. 5.13.

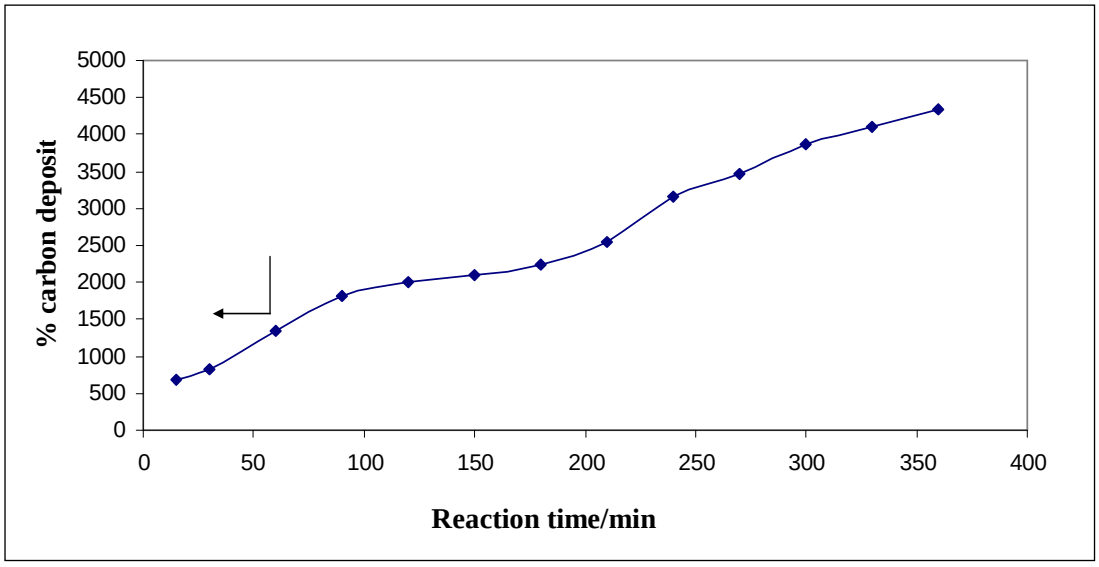

Fig. 5.12: Graph showing the amount of CNTs produced after different reaction times using IMPN catalysts (T = 700°C).

After 1 h the product was comprised of long multiwalled CNTs with outer diameters of 20 - 30 nm (Fig. 5.13b). These CNTs were spongy in texture and very light. CNTs measured after 2.5 h were short with a rough surface and their outer walls had thickened (Fig. 5.13c). After 3 and 6 h the tubes were even shorter and thicker and had a fiber-like morphology (Fig. 5.13d,e). These materials were coarser with a sand-like texture. It can thus be seen that the quality of the CNTs deteriorated with time. This change in quality of the CNTs relates to the deposition of carbon on the already formed CNTs [33] and also fragmentation of the tubes. It appears that the presence of the catalyst on the $CaCO_3$/CaO at the high reaction temperature results in tube cleavage. To our knowledge there are no reports in the literature in which carbon nanotubes have been reported to be broken by the procedures described, although there is precedent for carbon deposition on fibres and tubes [40].

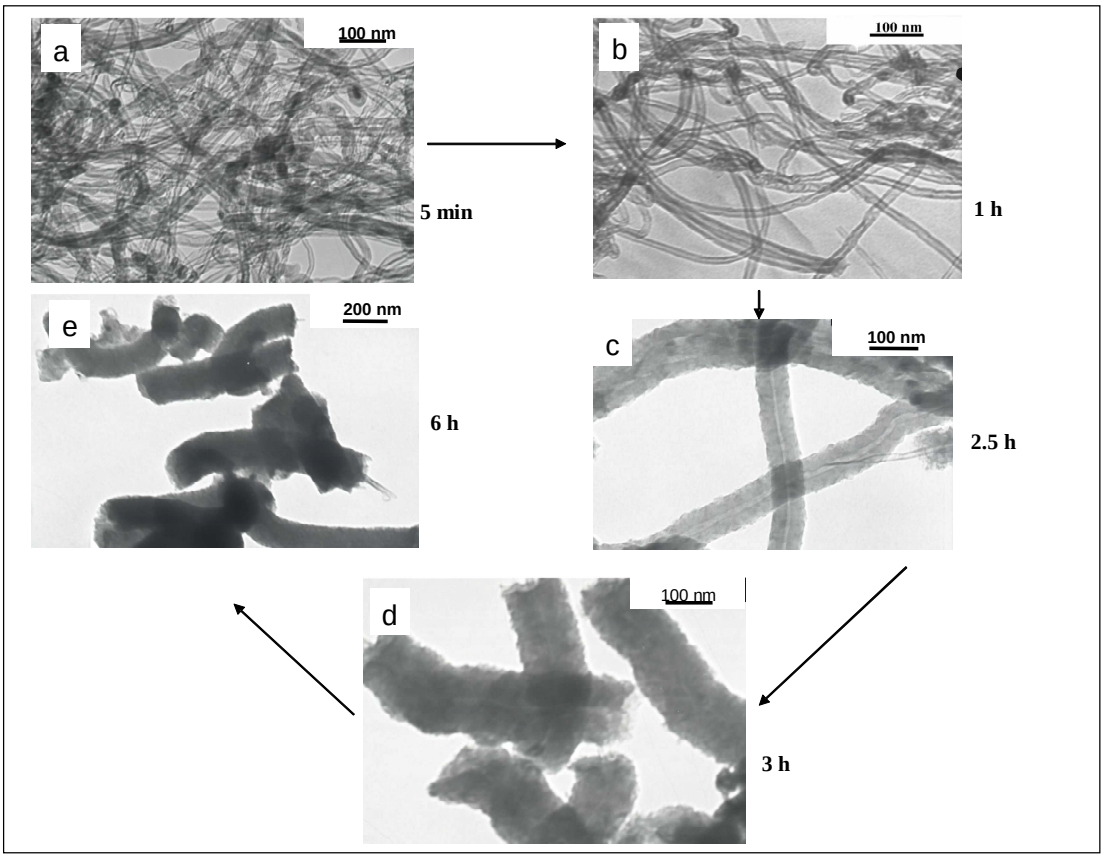

Fig. 5.13: Low magnification TEM images of impure CNTs produced after a) 5min, b) 1 h, c) 2.5 h, d) 3 h, and e) 6 h reaction time at 700°C using IMPN catalysts.

Also of note is the observation that the outer diameters of the CNTs increased with increase in synthesis time while the inner diameters (~ 10 nm) were not affected (Fig. 5.14). Clearly shorter synthesis times (t < 60 min.) result in higher quality CNTs with higher aspect ratios compared to longer times (e.g. t > 60 min.).

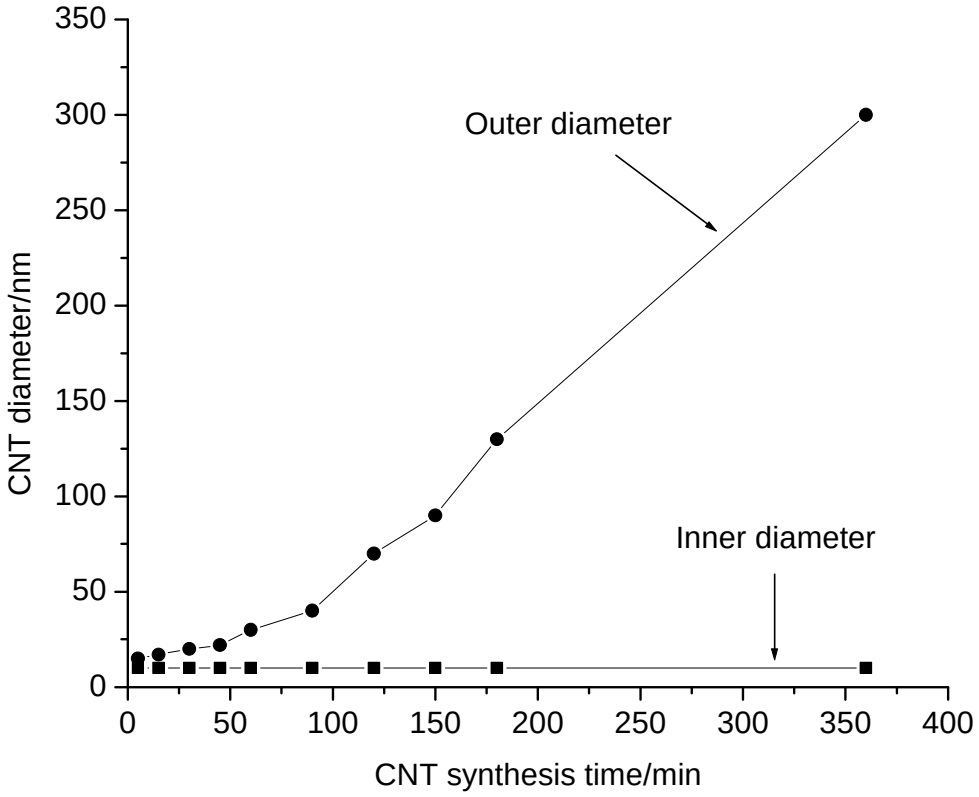

Fig. 5.14: A plot of variation of the CNT diameter with time for CNTs synthesized over (a) IMP Fe-Co/$CaCO_3$ catalysts.

To verify the observation that the CNTs broke into smaller pieces due to the deposition of carbon, CNTs (100 mg) synthesized for 5 min and 1 h were purified by washing in 30% HNO_3 for 3 h to remove the Fe-Co catalyst and the support. The CNTs were then placed in a quartz boat in a reactor that was heated to 700°C under N_2 (40 ml/min). A 1/3 C_2H_2 and N_2 gas mixture was then passed over the CNTs for a period of 3 h and 6 h respectively. TEM images revealed that these CNTs were similar to those shown in Fig.

5.13d and Fig. 5.13e. Thus the tubes were thickened and broken by the deposition of carbon on the pre-prepared CNTs.

5.6 Purification of CNTs

A TGA study revealed that the as-synthesized carbon material contained residue (Fe-Co and CaO). To purify the CNTs, 30% nitric acid (HNO_3) solution was used. The product was stirred in an excess amount of the acid for 30 h and for 3 days at room temperature and then washed with distilled water until neutral. In another procedure the samples were stirred in an excess HNO_3 solution for 5 h and rinsed with distilled water every 30 minutes. Small samples were removed after the 30 min washings, dried and analyzed by TGA.

The CNTs prepared by the IMP and DP contained less residual substrate (CaO) and metal particles in the final product (~12 and 15% respectively) than the CNTs prepared by the RM method. This related to the lower yield of CNTs formed in this reaction. The TGA profiles of the CNTs show that all the unpurified catalysts are thermally stable up to 550ºC where oxidation of carbon begins to occur (Fig. 5.15). At temperatures > 550ºC only the CaO and possibly some Fe-Co catalyst remains. After acid treatment, the amount of residue remaining was reduced to between 3 and 6% (Fig. 5.15a). The data shows that washing the CNTs in acid for 30 min is sufficient to remove most of the support and metal particles. Clearly some CaO and Fe-Co is not removed despite the different acid treatment conditions. The derivative weight curves also show the presence of shoulder peaks at around 650°C (Fig. 5.15b). These peaks are attributed to the decomposition of other materials such as graphitic soot [31].

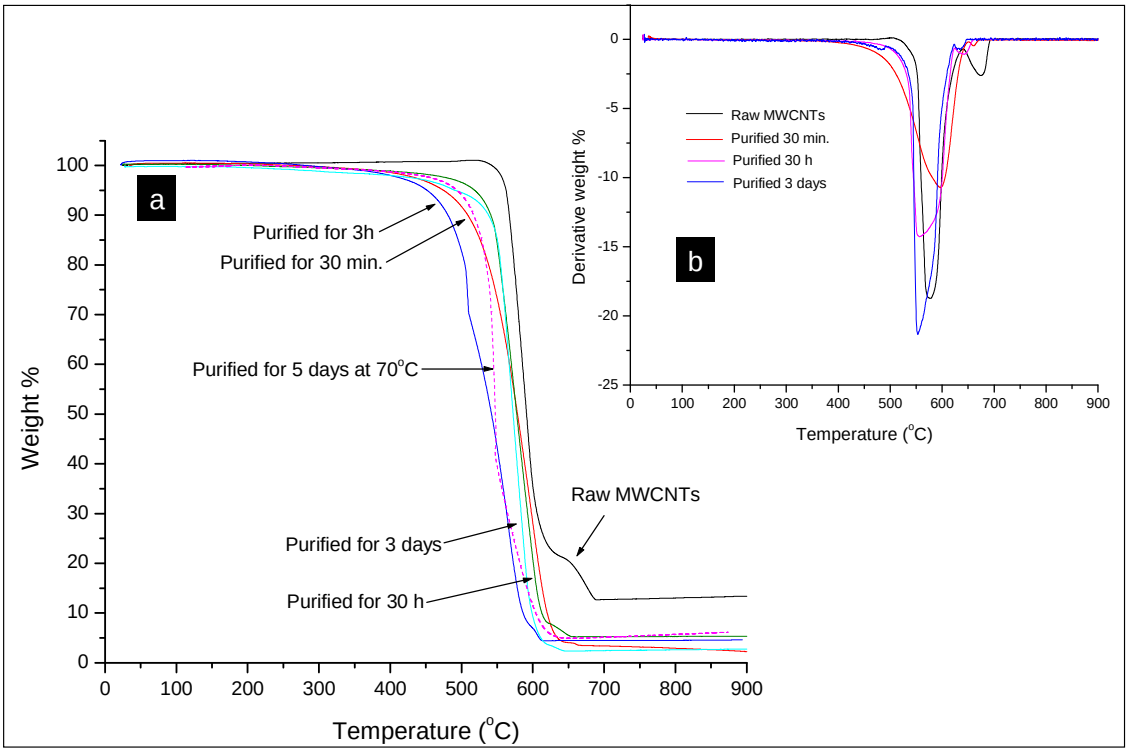

Fig. 5.15: TGA profiles of (a) crude and purified CNTs synthesized from IMPN catalysts and (b) corresponding derivative profiles.

TEM analysis revealed that there was no significant impact of the acid treatment on the CNT structure. The CNTs possessed similar widths and lengths even after purification. The efficacy of the purification process was also verified by PXRD analysis which revealed removal of the CaO (< 1% detected) (Fig. 5.16). The dominant peak ($2\theta = 26°$) and the one at 45° on the XRD pattern of the purified sample are characteristic of the graphitic walls of the CNTs. No peaks corresponding to lime were identified on the purified sample. The other broad peak close to the one 45°C is attributed to the presence of small amounts of carbides in the carbon deposit.

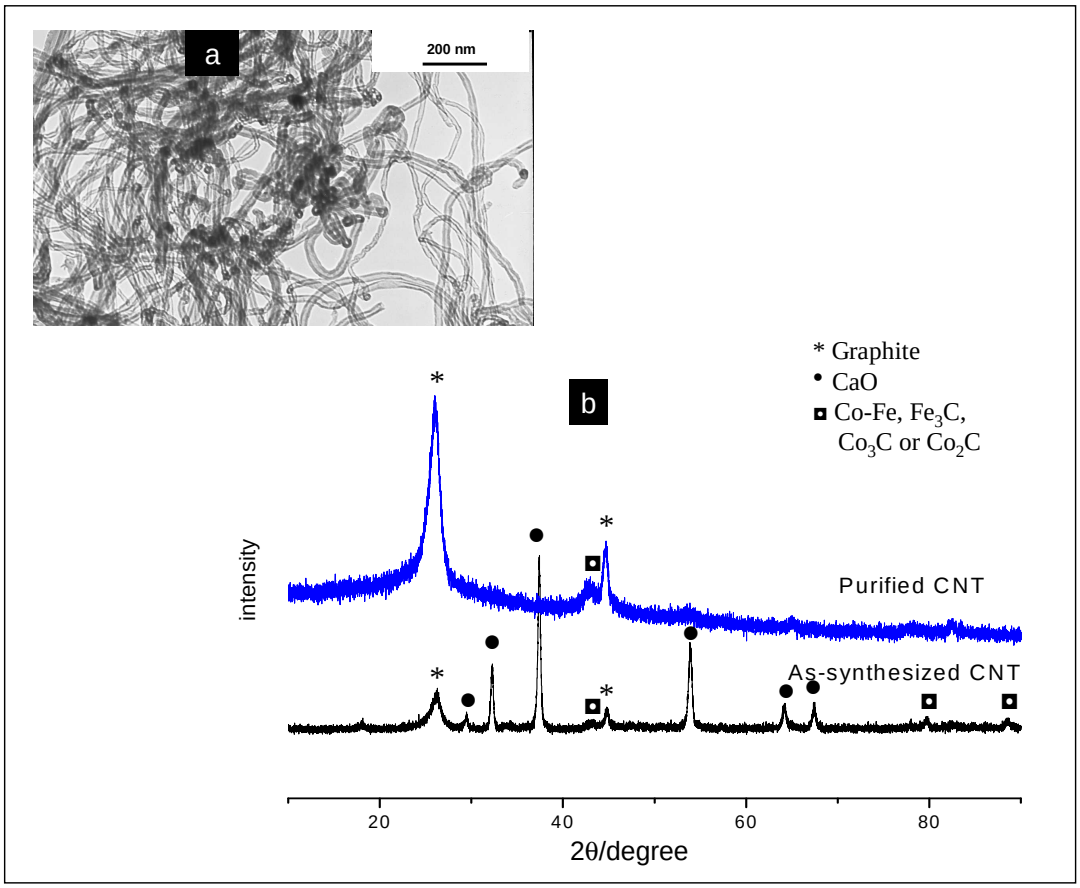

Fig. 5.16: (a) A TEM image of purified CNTs and (b) PXRD pattern of the purified and as-synthesized (raw) CNTs.

5.7 Conclusions

High quality MWCNTs were synthesized in excellent yields using three different catalyst preparation methods. Parametric studies using Fe, Co and Fe-Co bimetallic catalysts supported on $CaCO_3$ and prepared by a wet impregnation method reveal that the production of CNTs from C_2H_2 is affected by the temperature, gas flow rates as well as synthesis time. The different synthesis methods generated CNTs with similar sizes and physical properties when the catalyst particles were of the same size. The Fe-Co bimetallic catalysts showed the best activity and near 100% selectivity to CNTs can be observed under optimum reaction conditions. In particular, short CNT synthesis times (t < 1 h) resulted in good quality CNTs with smaller diameters and higher aspect ratios

whereas long reaction times resulted in fragmentation of the CNTs that had thick rod/fiber-like structures. By varying the synthesis time, the outer diameters of the CNTs could be varied between 10 - 300 nm. Similar results were obtained for Fe-Co catalysts prepared by the deposition-precipitation method.

The CNTs were purified using 30% HNO_3. The $CaCO_3$ support as well as catalyst particles were removed without affecting their CNT wall structures. Some residual material (~ 3%) appears to be left behind after the washing. Studies to investigate the use of less dilute acids are presented in Chapter 7.

5.8 References

1. S. Iijima, Nature **354** (1991) 56.
2. S. Iijima, Physica B **323** (2002) 1.
3. B.M. Endo, T. Hayashi, Y.A. Kim, M. Terrones, M.S. Dresselhaus, Phil. Trans. R. Soc. Lond. A **362** (2004) 2223.
4. P. Ball, Made to measure: *New materials for the 21st Century*, USA: Princeton University Press, 1997.
5. M. Terrones, A. Jorio, M. Endo, Y.A. Kim, T. Hayashi, H. Terrones, J-C. Charlier, G. Dresselhaus and M.S. Dresselhaus, Mater. Today **7** (2004) 30.
6. H. Zeng, L. Zhu, G. Hao, R. Sheng, Carbon **36** (1998) 259.
7. Z.J. Shi, Y.F. Lian, X.H. Zhou, Z.N. Gu, Y. Zhang, S. Iijima, L. Zhou, K.T. Yue, Carbon **37** (1999) 1449.
8. A. Thess, R. Lee, P. Nikolaev, H. Dai, P. Petit, J. Robert, C. Xu, Y.H. Lee, S.G. Kim, A.G. Rinzler, D.T. Colbert, G.E. Scuseria, D. Tombnek, J.E. Fischer, Science **273** (1996) 483.
9. D.C. Li, L. Dai, S. Huang, A.W.H. Mau, Z.L. Wang, Chem. Phys. Lett. **316** (2000) 349.
10. V. Ivanov, J.B. Nagy, P. Lambin, A. Lucas, X.B. Zhang, X.F. Zhang, D. Bernaerts, G. Van Tendeloo, S. Amelinckx, J. Van Landuyt, Chem. Phys. Lett. **223** (1994) 329.
11. R. Brukh, S.C. Mitra, Chem. Phys. Lett. **424** (2006) 126.

12. K. Hernadi, A. Fonseca, J.B. Nagy, D. Bernaerts, J. Riga, A. Lucas, Synthetic Metals **77** (1996) 31.
13. K. Hernadi, Z. Kónya, A. Siska, J. Kiss, A. Oszkó, J.B. Nagy, I. Kiricsi, Mat. Chem. & Phys **77** (2002) 536.
14. A.L. Balch, M.M. Olmstead**,** Chem. Rev. **98** (1998) 2123.
15. K. Hernadi, A. Fonseca, J.B. Nagy, A. Fudala, D. Baenaerts, A. Lucas, Zeolites, **17** (1996) 416.
16. P. Francesco, Catal. Today **41** (1998) 129.
17. E. Couteau, K. Hernadi, J.W. Seo, L. Thiên-Nga, Cs. Mikó, R. Gaá1, L. Forró, Chem. Phys. Lett. **378** (2002) 9.
18. H. Kathyayini, N. Nagaraju, A. Fonseca, J.B. Nagy, J. Mol. Catal. **223** (2004) 129.
19. M.C. Bahome, L.L. Jewell, D. Hildebrandt, D. Glasser, N.J. Coville, Appl. Catal. A: General **287** (2005) 60.
20. J. Cheng, X. Zhang, Z. Luo, F. Liu, Y. Ye, W. Yin, W. Liu, Y. Han, Mat. Chem. Phys. **95** (2006) 5.
21. A. Magrez, J.W. Seo, C. Mikó, K. Hernádi, L. Forro, J. Phys. Chem. B **109** (2005) 10087.
22. A. Magrez, J.W. Seo, V.L. Kuznetsov, and L. Forró, Angew. Chem. Int. Ed. **46** (2007) 441.
23. P. Serp, M. Cossias, P. Kalck, Appl. Catal. A: General **253** (2003) 337.
24. Z. Yu, D. Chen, B. Tøtdal, A. Holmen, Catal. Today **100** (2005) 261.
25. A-C. Dupuis, Prog. Mat. Sci., **50** (2005) 17.
26. W. Qian, T. Liu, Z. Wang, H. Yu, Z. Li, F. Wei, G. Luo, Carbon **41** (2003) 2487.
27. B. Louis, G. Gulino, R. Vieira, J. Amadou, T. Dintzer, S. Galvagno, G. Centi, M.J. Ledoux, C. Pham-Huu, Catal. Today **102-103** (2005) 23.
28. G. Che, B.B. Lakshmi, C.R. Martin, and E.R. Fisher, Chem. Mater. **10** (1998) 260.
29. E. Dervishi, Z. Li, A.R. Biris, D. Lupu, S. Trigwell, A.S. Biris, Chem. Mater. **19** (2007) 179.
30. T.C. Schmitt, A.S. Biris, D.W. Miller, A.R. Biris, D. Lupu, S. Trigwell, Z.U. Rahman, Carbon **44** (2006) 2032.
31. C.H. See, A.T. Harris, Particle Tech. Fluidization **54** (2008) 657.

32. (a) M. Boutonnet, J. Kizling, P. Stenius, Colloids and Surfaces **5** (1982) 209; (b) E.E. Carpenter, J. Magnetism & Magnetic Mater. **225** (2001) 17; (c) C.T. Seip, C.J. O'Connor, Nanostr. Mater. **12** (1999) 183; (d) I. Ban, M. Drofenik, D. Makovec, J. Magnetism & Magnetic Mater. **307** (2006) 250; (e) Y. Lee, J. Lee, C.J. Bae, J-G. Park, H-J. Noh, J-H. Park, T. Hyeon, Adv. Funct. Mater. **15** (2005) 503; (f) V. Pillai, P. Kumar, M.S. Multani, D.O. Shah, Colloids and Surfaces A: Physicochem. Eng. Aspects **80** (1993) 69.
33. M. Escober, M.S. Moreno, R.J. Candal, M.C. Marchi, A. Caso, P.I. Polosecki. G.H. Rubiolo, S. Goyanes, Appl. Surf. Sci. **254** (2007) 251.
34. (a) A. Zhang, C. Li, S. Bao, Q. Xu, Microp. & Mesop. Mater. **29** (1999) 383; (b) J-B. Park, G-S. Choi, Y-S. Cho, S-Y. Hong, D. Kim, S-Y. Choi, J-H. Lee, K-I. Cho, J. Cryst. Growth **244** (2002) 211; (c) Ch. Emmenegger, P. Mauron, A. Züttel, Ch. Nützenadel, A. Schneuwly, R. Gallay, L. Schlapbach, Appl. Surf. Sci. **162–163** (2000) 452.
35. S.D. Mhlanga, N.J. Coville, Diam. Rel. Mater. **17** (2008) 1489.
36. A. Jorio, M.A. Pimenta, A.G.S. Filho, R. Saito, G. Dresselhaus, M.S. Dresselhaus, New J. Phys. **5** (2003) 139.1.
37. Z.L. Wang, Z.C. Kang, J. Phys. Chem. **100** (1996) 5163.
38. V.G. Pol, M. Motiei, A. Gedanken, J. Calderon-Moreno, M. Yoshimura, Carbon, **42** (2004) 111.
39. http://www.carbonblack.jp/en/cb/youto.html#top (accessed on 6th February 2008).
40. M. Monthioux, H. Allouche, R.L. Jacobsen, Carbon **44** (2006) 3183.

Chapter 6

Iron–cobalt catalysts synthesized by a reverse micelle impregnation method for controlled growth of carbon nanotubes[#]

6.1 Introduction

Carbon is known to exist as various structures (e.g. diamond, graphite, amorphous carbon, fullerenes, fibers, onions, spheres or balls, and nanotubes) that emanate from its unique ability to combine and use various forms of sp, sp^2 and sp^3 electronic configurations. While great attention has been paid to these carbon structures, carbon nanotubes (CNTs) have in recent times received the greatest attention due to their vast potential applications [1-5].

The use of mesoporous materials such as SiO_2 [6,7], Al_2O_3 [8], TiO_2 [9] and zeolites [10,11] has revealed that these materials provide excellent supports for catalytic CNT production in catalytic chemical vapour deposition (CVD). However, due to the chemical nature of the support materials, purification of CNTs produced on these supports remains a challenge and often requires several steps that result in damage to the CNT graphitic structures.

Also, the solvents used during the purification process have to be disposed of to minimize environmental issues. To circumvent these chemical and environmental problems, the use of readily removable supports such as $CaCO_3$ has recently been investigated [12-14].

In this study we sought to control the sizes of CNTs synthesized using a CVD process by manipulating the size of Fe-Co bimetallic nanoparticles supported on $CaCO_3$. The order of catalyst activity in the CVD synthesis of CNTs was found to be Fe-Co>>Co >Fe by ourselves and others [12-14]; hence the use of the Fe-Co bimetallic system in this study.

[#]*Sabelo D. Mhlanga, Neil J. Coville, Diamond & Related Materials 17 (2008) 1489.*

The metal-support mixtures (catalysts) were prepared by the wet impregnation, deposition-precipitation and reverse micelle impregnation methods. While the wet impregnation and deposition-precipitation methods have been used extensively in the past for making catalysts for CNT synthesis, the reverse micelle approach has been little exploited for this purpose [15].

6.2 Experimental

6.2.1 Preparation of catalysts

The wet impregnation and deposition-precipitation methods were applied as described in Chapter 5 [14,16]. The 5 wt.% Fe-Co loaded catalysts obtained from these methods were named IMP and DP and the CNTs produced from these catalysts were labelled IMPCNTs and DPCNTs respectively.

A reverse micelle process reported by Lee *et al.* [17] was used for the preparation of the nanoparticles. Uniform Fe-Co nanoparticles were synthesized from the reaction of iron and cobalt salts in reverse micelles. The process was selected because it is economically and environmentally friendly, since it involves inexpensive and less toxic iron salts and a minimal amount of organic solvents. Also, it does not involve the use of halide salts (e.g. chlorides) that can act as a poison during further use of the nanoparticles. The nanoparticles were produced without going through any size-selection process or post-synthetic heat treatment and could be produced in gram quantities in a single reaction [18]. All chemicals were purchased from Sigma-Aldrich and were used as received without further purification.

The following chemicals were used: Iron (III) nitrate ($Fe(NO_3)_3 \cdot 9H_2O$, 99%), Cobalt (II) nitrate ($Co(NO_3)_2 \cdot 6H_2O$, 99%), sodium dodecylbenzenesulfonate (NaDBS, ~80%), xylene (99.9%), hydrazine hydrate (N_2H_5OH, 98%) and ethanol (99.9%).

A turbid emulsion was prepared by adding 10 mmol of NaDBS surfactant to 30 ml of xylene, followed by sonication for 10 min. A metal salt solution prepared by dissolving 1 mmol $Co(NO_3)_2 \cdot 6H_2O$ and 1 mmol of $Fe(NO_3)_3 \cdot 9H_2O$ in 1.5 ml of ethanol was added to the emulsion under vigorous stirring. The murky solution was left to stir for 12 h at room temperature and pressure, resulting in the stabilization of the reverse micelle solution. After stirring, the homogeneous micelle solution was slowly heated to 90°C under a continuous flow of argon, and 5 mmol of hydrazine solution was injected into the solution. The colour of the solution immediately turned to black upon addition of the hydrazine solution due to the reduction of the metal oxides. The resulting mixture was refluxed for 5 h to produce Fe-Co nanoparticles.

The nanoparticles were separated by washing with excess ethanol and subsequent centrifugation. They were then loaded onto a $CaCO_3$ support using the wet impregnation procedure. The total nanoparticle loading on the support was 5 wt.%. This loading was calculated based on the dominant phase of Fe-Co after calcination and confirmed by thermogavimetric analysis (TGA) (Fig. 6.1). The catalysts were named RM and the CNTs produced from these catalysts were labelled RMCNTs.

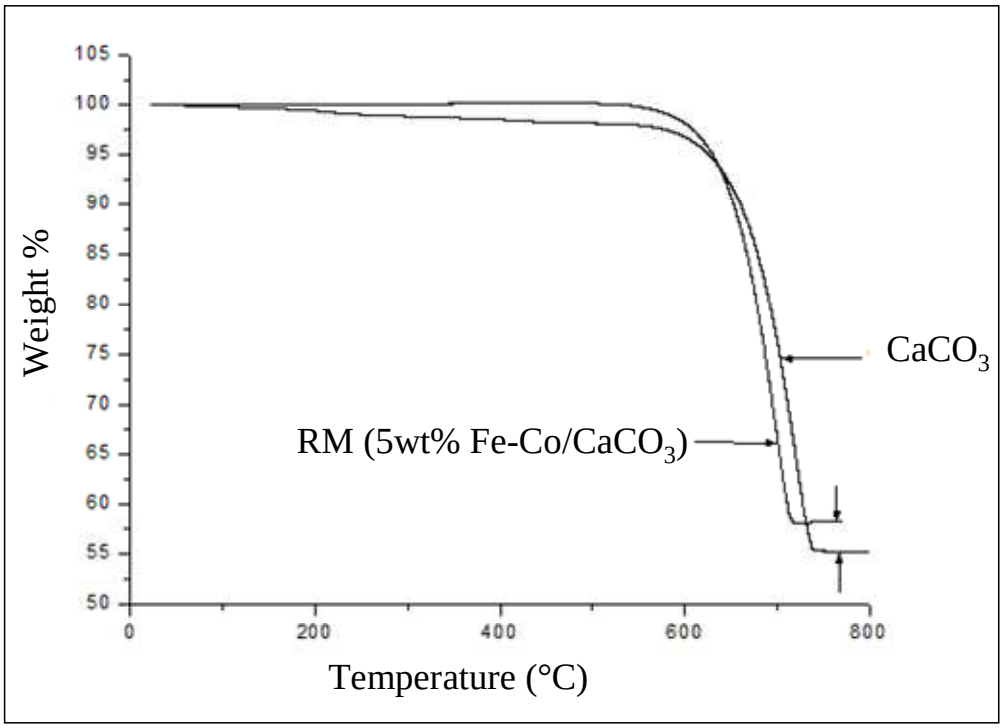

Fig. 6.1: TGA profiles of $CaCO_3$ and the RM catalyst heated under N_2 (40 ml/min). The ~ 5 wt% difference after complete weight loss indicates the amount of Fe-Co on the support.

6.2.2 Carbon nanotube synthesis

CNTs were synthesized by the decomposition of acetylene (C_2H_2) (Afrox) in a tubular fixed-bed quartz reactor (51 cm×1.9 cm i.d.) that was placed horizontally in a furnace. The furnace was electronically controlled such that the heating rate, reaction temperature and gas flow rates could be accurately maintained as desired. The catalyst (0.1 g) was loaded into a quartz boat (120 mm×15 mm) at room temperature and the boat was placed in the centre of the quartz tube. The furnace was then heated at 10 °C/min while N_2 was flowing over the catalyst at 40 ml/min. Once the temperature had reached 700 °C, the N_2 flow rate was changed to 240 ml/min and C_2H_2 was introduced at a constant flow rate of 90 ml/min. After 60 min of reaction time, the C_2H_2 flow was stopped and the furnace was left to cool down to room temperature under a continuous flow of N_2 (40 ml/min). The

boat was then removed from the reactor and the product (carbon deposit) formed along with the catalyst and support was weighed.

6.2.3 Characterization techniques

Bimetallic Fe-Co catalysts supported on $CaCO_3$ were characterized by a range of techniques. The morphology of the support was characterized by transmission electron microscopy (TEM) (JEOL 100S Electron Microscope), while the size and distribution of the Fe-Co nanoparticles was determined at higher magnifications using a Philips CM200 equipped with a Gatan Imaging Filter. For TEM observation, the samples were sonicated in ethanol for 10 min and thereafter deposited on a TEM Cu grid. Energy dispersive x-ray spectroscopy (EDX) and powder X-ray diffraction (PXRD) spectroscopy was used to confirm the elemental and chemical composition of the Fe-Co bimetallic nanoparticles. The metal loading on the support was confirmed by ICP-AES and TGA (Perkin Elmer Pyris 1 TGA). The total surface area and porosity of the catalysts was ascertained using a Micromeritics TriStar Surface Area and Porosity Analyzer. CNT structures and size distributions were ascertained from TEM studies using counting procedures. TEM was also used to distinguish the CNTs from other carbonaceous products (e.g. carbon particles and nanofibers), if present. The properties of the CNTs observed under TEM were also confirmed by Raman Spectroscopy (Jobin-Yvon T64000 micro-Raman spectrometer). The purification of CNTs was monitored by PXRD (Bruker axs D8 Advance PXRD), TEM and TGA.

6.3 Results and discussion

6.3.1 Catalyst characterization

The Fe-Co particle sizes could not be effectively controlled using the IMP and DP methods. The particles obtained were ~ 30 nm and yielded CNTs with ~10 nm inner diameter (i.d.) and 25 - 30 nm outer diameters (o.d.). In order to better control the size of the Fe-Co nanoparticles, we made use of the reverse micelle method. The reaction

mixtures and the average diameters of the nanoparticles are listed in **Table 6.1.** The different sizes of Fe-Co nanoparticles were obtained by changing the concentrations of Fe^{3+} and Co^{2+} in each reaction that was performed. It was observed from TEM analysis that the size of the nanoparticles was reduced significantly by reducing the concentration of Fe and Co in the micelle. All the obtained nanoparticles were not aggregated and they were relatively uniform in size.

Table 6.1: Average particle diameters and reaction mixture composition of the Fe-Co nanoparticles.

Catalyst name	**Av. Fe-Co diam. (nm)**	**Reaction mixture composition**				
		Fe^{3+} (mmol)	Co^{2+} (mmol)	Ethanol (ml)	NaDBS (g)	Xylene (ml)
A	3	1	1	1.5	3.5	30
B	6	2	2	1.5	3.5	30
C	13	3	3	1.5	3.5	30
D*	25	-	-	-	-	-
E*	70	-	-	-	-	-

* These nanoparticles were synthesized using the RM method described in Chapter 5.

Fig. 6.2 shows a HRTEM image of the 6 nm nanoparticles (sample B) and the corresponding energy dispersive X-ray (EDX) spectrum. The EDX spectrum confirmed the presence of Fe and Co in an approximately 50:50 ratio after a quantitative analysis. The nanoparticles could be readily dispersed in water and many organic solvents.

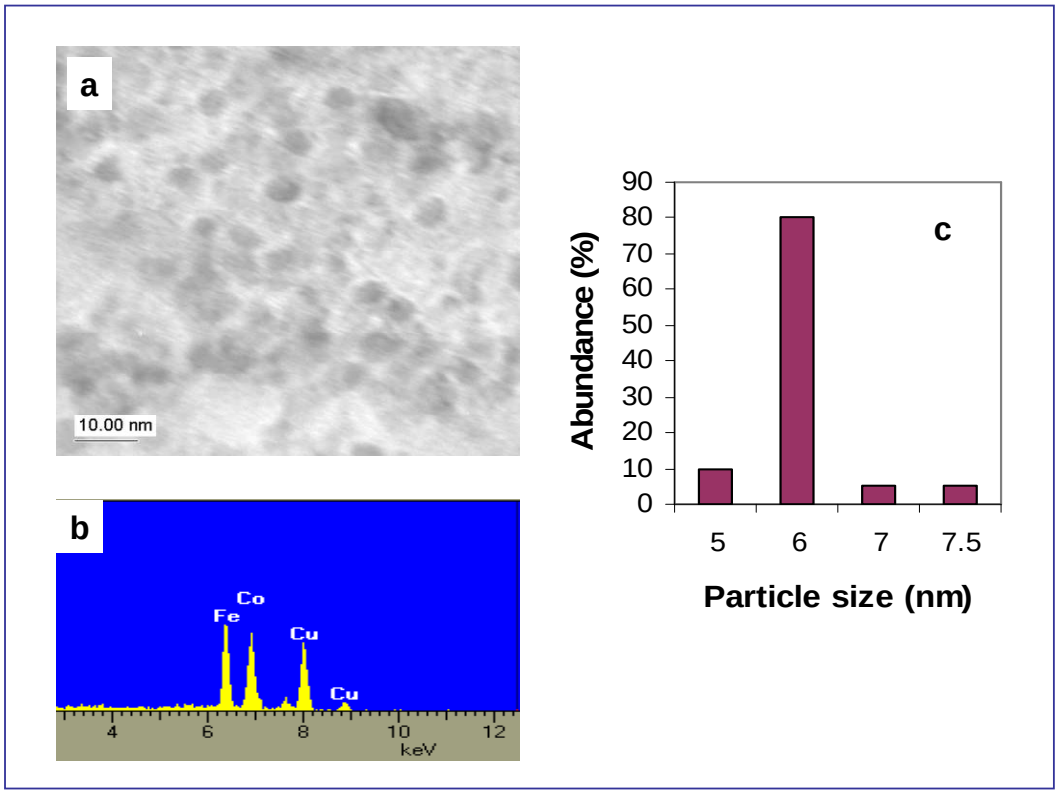

Fig. 6.2: A HRTEM image (dark spots are Fe-Co nanoparticles) (a), EDX spectrum (b) and particle size distribution graph (c) of nanoparticles synthesized using the RM method.

A closer investigation at the nanoparticles (sample C) using HRTEM revealed the presence of lattice-fringe patterns (~ 0.2 nm apart), displaying the highly crystalline nature of the nanoparticles [17]. The TEM image reveals that not all the particles prepared by the RM technique are spherical in shape as shown in Fig. 6.3b. Some of the particles were rectangular in shape.

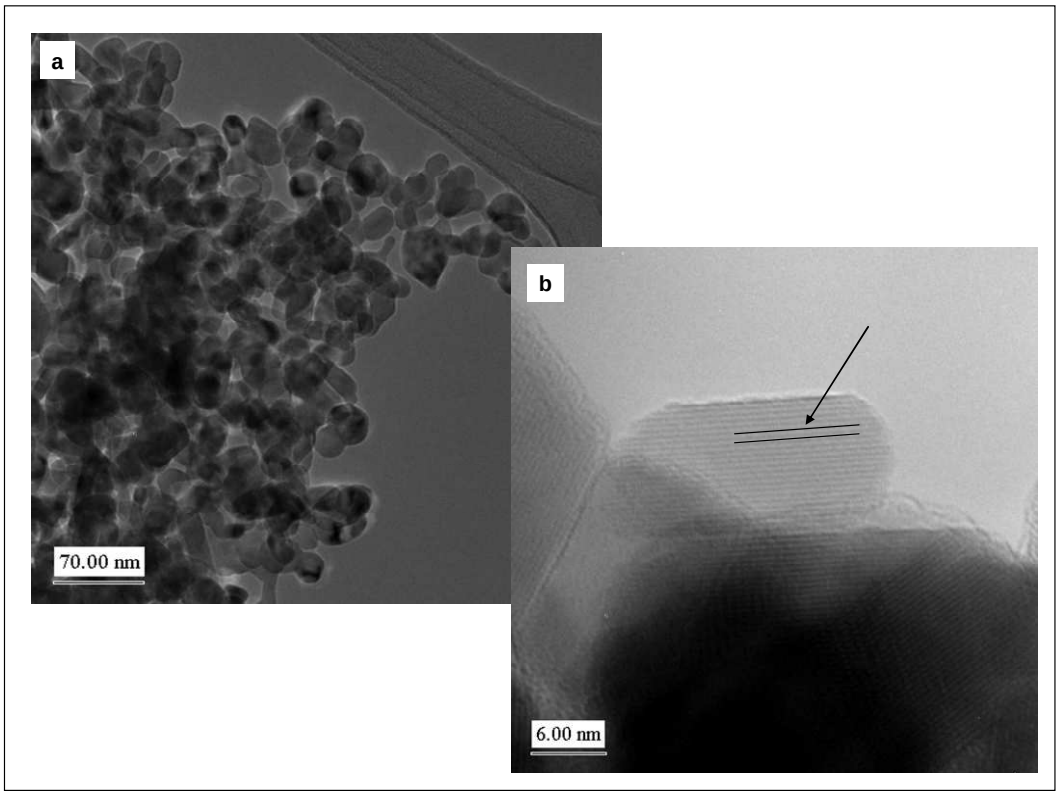

Fig. 6.3: (a) A TEM image of RM nanoparticles (sample C) and (b) a closer look of the nanoparticles at higher magnification (indicated by arrow) showing their high crystallinity.

PXRD patterns of the RM synthesized Co-Fe nanoparticles revealed that the calcined nanoparticles are a mixed oxide phase, cobalt ferrite ($CoFe_2O_4$) (Fig. 6.4). The pattern revealed that the materials are free of impurities. Temperature programmed reduction (TPR) analyses of the nanoparticles were performed in a TPR reactor under a continuous flow of a 5wt% H_2/Ar gas mixture (30 ml/min). The samples were reduced over a temperature range (25°C to 800°C) with a heating rate of 10°C/min. The profiles obtained were quite similar to TPR profiles of Co-Fe oxide nanoparticles reported elsewhere [19].

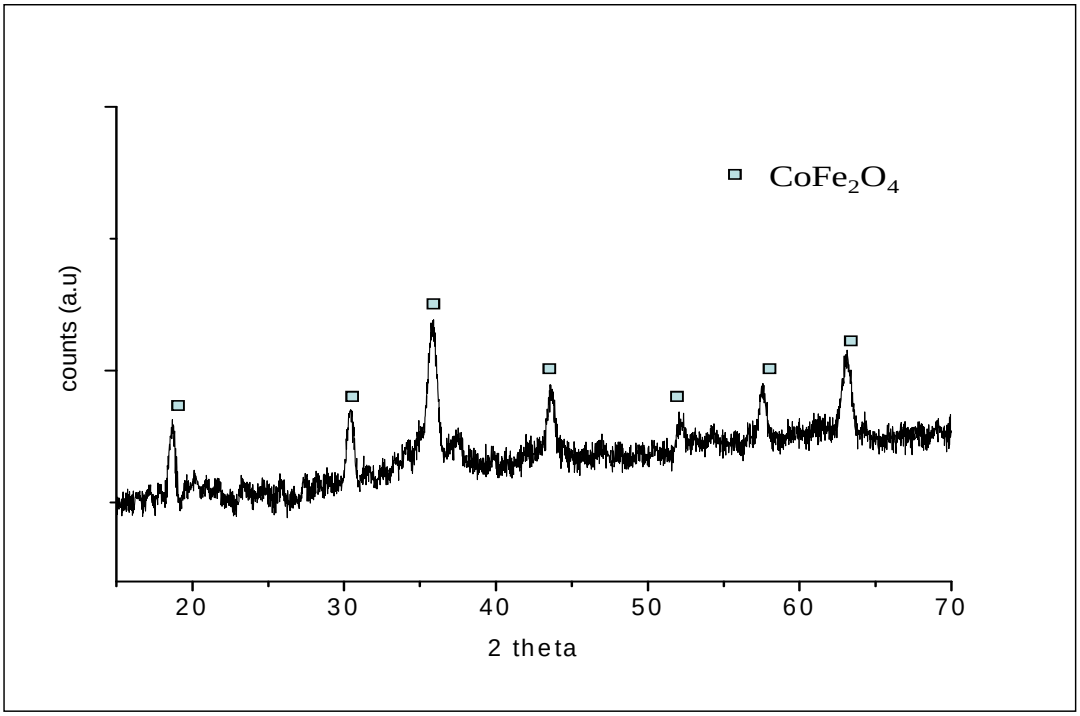

Fig. 6.4: A PRXD pattern of calcined Fe-Co nanoparticles of sample C showing their presence as a mixed oxide phase.

6.3.2 CNT analyses

Reactions were performed under a set of standard conditions using acetylene as a carbon source, so that quantitative and qualitative information of the produced CNTs could be compared. The RM synthesized nanoparticles were deposited onto the $CaCO_3$ support and were used to synthesize CNTs with diameters ranging in between 3 - 30 nm i.d. and 5 - 90 nm o.d. depending on the size of the nanoparticles used (Fig. 6.5).

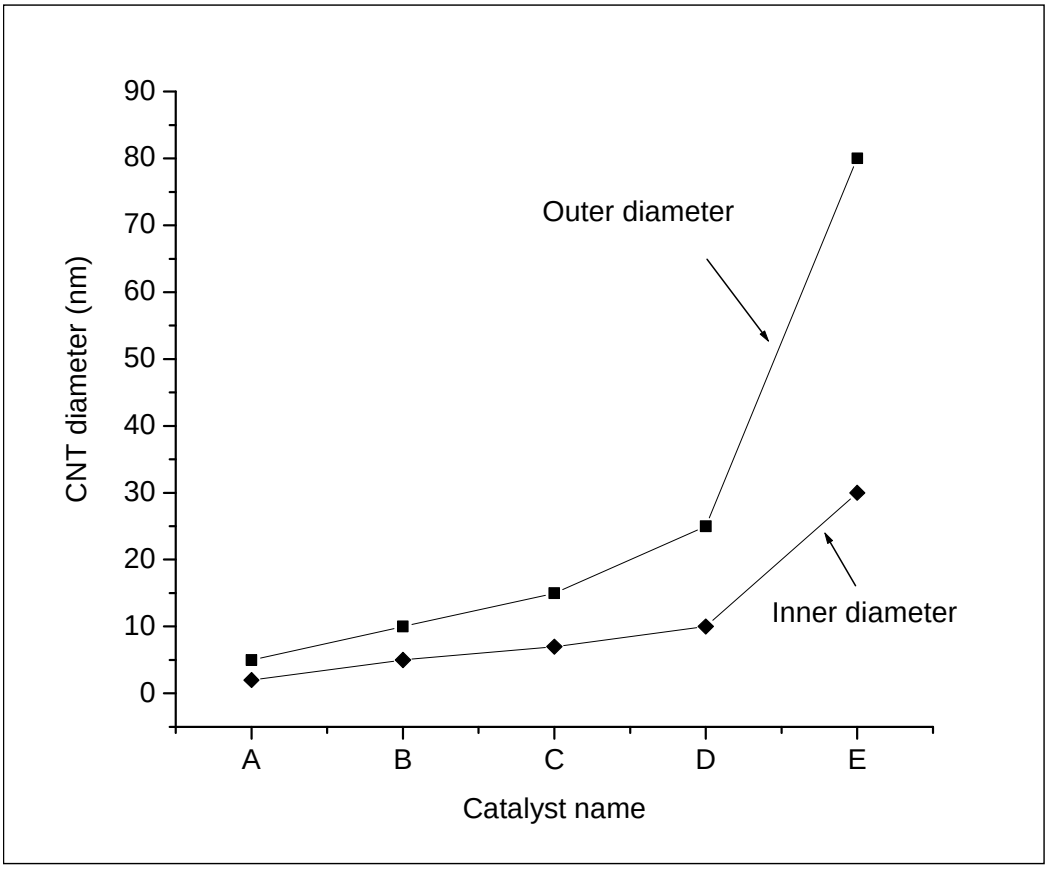

Fig. 6.5: A plot of variation of CNT diameter for CNTs synthesized over RM Fe-Co/$CaCO_3$ catalysts with different Fe-Co particle sizes as given in Table 1.

TEM analysis of the CNTs revealed that the diameters of the CNTs were slightly wider than the diameters of nanoparticles used. The yields obtained were very low but no optimization was attempted since our aim was to establish a correlation between the catalyst particle size and the size of the CNTs obtained from them. No CNTs were formed when the 3 nm particles were used. The reason why no CNTs were formed cannot be explained at this point and is subject for further investigation. The assumption was that single walled CNTs would be obtained from the smaller particles. Clearly by using the RM method, smaller CNTs in diameter could be obtained compared with the IMP and DP methods which could only produce nanoparticles in the range 25 - 30 nm despite the source of Fe and Co used (presented in Chapter 5).

While the size of the metal particles could control the diameters of the CNTs synthesized from them, an additional effect of the positioning of the particles on the support (metal-support interaction) as well as the existence of Fe-Co/$CaCO_3$ and Fe-Co/CaO systems during the CNT synthesis also affects the diameters of the tubes and hence a variation of size is observed within the same batch of CNTs [20,21]. However, it can be seen here that the best way to control the diameters of the CNTs obtained using the Fe-Co/$CaCO_3$ catalyst system is to control the particle size and the synthesis times. Clearly shorter synthesis times ($t < 60$ min.) result in higher quality CNTs with higher aspect ratios compared to longer times (e.g. $t > 60$ min.). The inner diameters remain unchanged (~ 10 nm) with variation in time. The inner diameters are much smaller than the metal-particles used, suggesting that carbon nucleation occurs preferably at the tip of the metal particle. With the RM technique both the inner and outer diameters of the CNTs could be controlled. Thus, CNTs of desired size can be obtained via this technique by controlling the particle size and varying the synthesis time.

TEM analysis revealed that the CNTs prepared by the three different methods of catalyst preparation were all multiwalled. The impregnation and deposition-precipitation methods gave CNTs with an average outer diameter of 20 - 30 nm (*ca* 80%) and an internal diameter of ~ 10 nm. Studies on the effect of temperature (500 - 1000°C) and reaction time (5 - 360 min) indicated that temperature affects mainly the selectivity of the catalysts while the synthesis time affects the diameters as well as lengths of the CNTs. Fig. 6.6 shows TEM images of the CNTs produced after 60 min (T = 700°C, C_2H_2 flow rate = 90 ml/min) prepared over selected RM catalysts. Similar size distribution graphs were found for samples made after different reaction times, temperatures and dilution of the carbon feed stock gas.

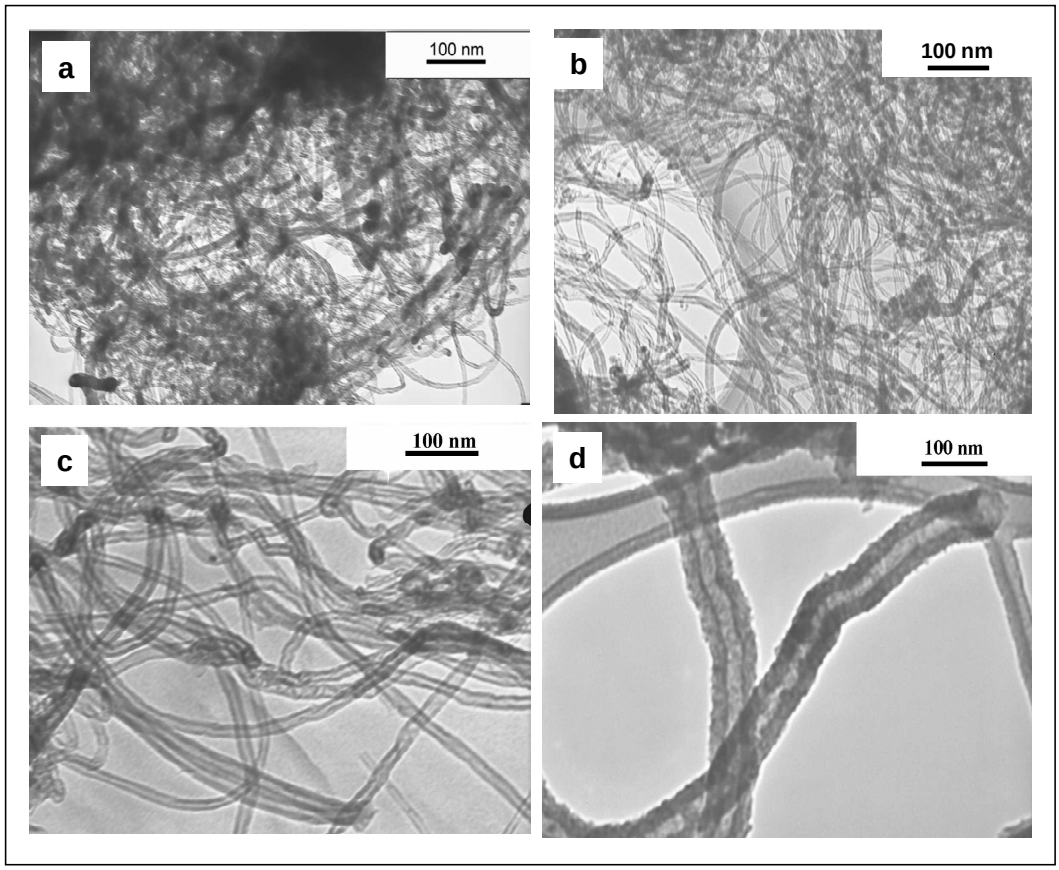

Fig. 6.6: TEM images of MWCNTs synthesized over RM catalyst (a) sample B (6 nm), b) sample C (13 nm), (c) sample D (25 nm) and sample E (70 nm).

Attempts were also made to synthesize CNTs using methane at high temperature. Various reaction temperatures (i.e. 900, 1000, 1100°C), methane flow rates and dilution ratios with N_2 and 5 wt% H_2/Ar were used. Catalysts prepared using the IMP and DP methods were also tested but these catalysts were inactive for the decomposition of methane. No CNTs were produced in any of the reactions.

Fig. 6.7 shows the TGA profiles of unpurified CNTs. The IMP and DPCNTs contained less residual substrate (CaO) and metal particles in the final product (~ 12 and 15% respectively) than the RMCNTs. The RMCNTs contained ca. 22% residual CaO and Fe-Co nanoparticles due the lower activity of this catalyst. The TGA of the CNTs shows that all the catalysts are thermally stable up to 550°C where oxidation of carbon begins to

occur. At temperatures (> 550°C) only the support and catalyst remain. The CNTs were purified by stirring vigorously in excess 30% HNO_3 for 48 h at room temperature. The TGA data shows that the graphite nature of the CNTs was not affected by this process.

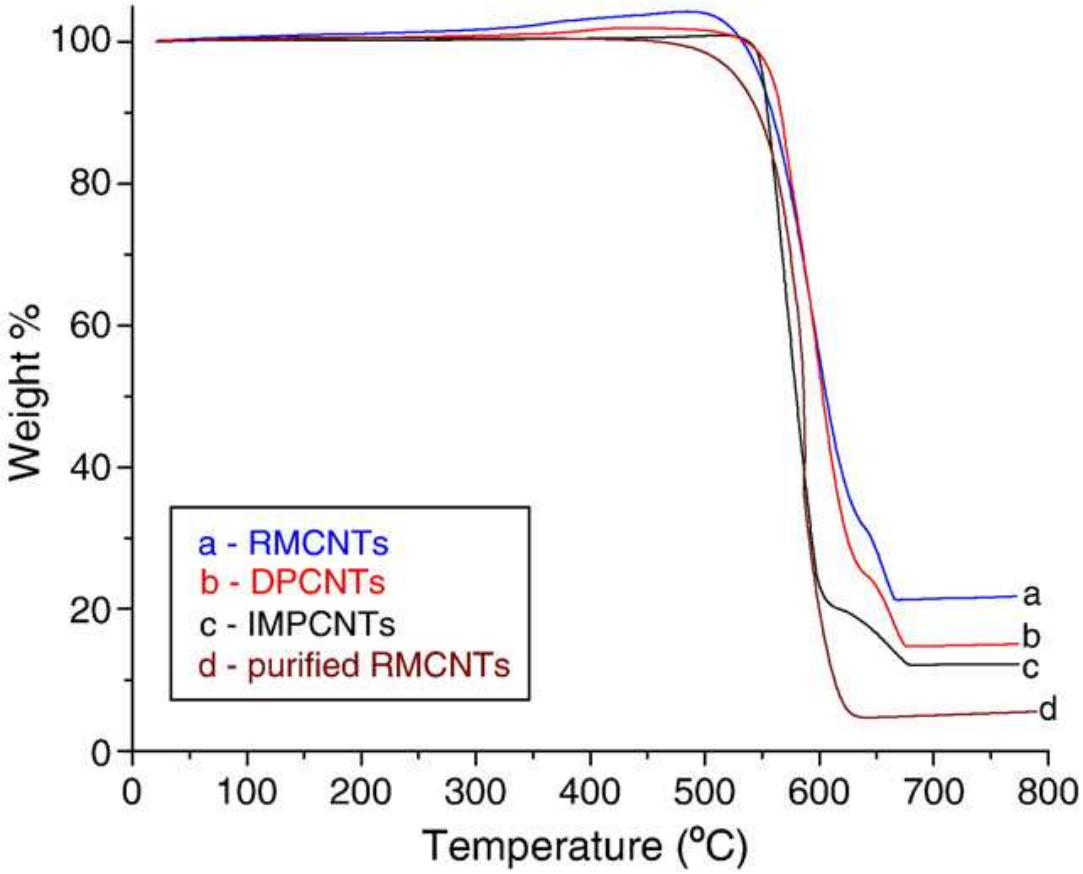

Fig. 6.7: TGA profiles of raw MWCNTs synthesized from IMP, DP and RM catalysts (sample C).

The BET surface areas of the raw IMPCNTs, DPCNTs and RMCNTs were 73, 63 and 40 m^2/g respectively. The results show that the IMPCNTs have the highest surface area followed by the DPCNTs. The RMCNTs also possessed lower pore sizes (IMPCNTs=198 Å, DPCNTs=166 Å, RMCNTs=167 Å). The lower surface area may be explained by the fact that the material contained a higher percentage of CaO which is likely to have covered or filled up some of the CNTs. Several studies focussing on the adsorption of MWCNTs [22] and SWCNTs [23] have highlighted the porous nature of the materials. The pores in MWCNTs are mainly made up of the inner hollow cavities

which are of smaller diameter and aggregated pores that are formed by the interaction of MWCNTs [24].

The IMP and DP methods of catalyst preparation gave MWCNTs from both catalysts with inner diameters of comparable sizes (~ 10 - 15 nm) and outer diameters of ~ 20 -30 nm. The RM method gave MWCNTs with smaller inner and diameters that were influenced by the particle size. An investigation of the wall structures using HRTEM revealed the existence of some defects in the wall structures. The degree of graphitization of the CNT graphene layers was confirmed by Raman spectroscopy. Small fullerene-like structures were observed on some of the wall structures (Fig 6.8) inset). These are not typical for substrate CVD synthesized CNTs and may be due to interactions taking place between the CNT walls and the CaO.

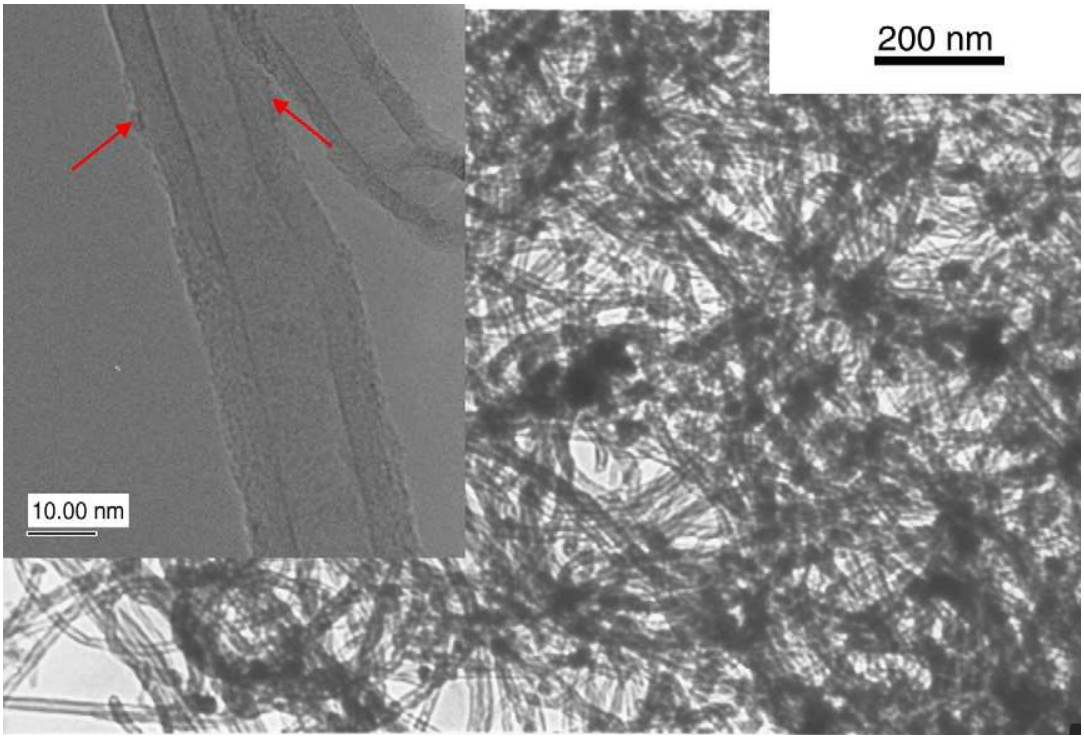

Fig. 6.8: TEM image of IMPCNTs and a corresponding HRTEM image (inset). Arrows show fullerene-like structures on the walls of the CNT.

The micro-Raman spectra of the IMPCNTs, DPCNTs and RMCNTs are shown in Fig. 6.9. Two bands occurring at 1350 cm^{-1} and 1585 cm^{-1} corresponding to the G and D modes of the graphene layers were observed [22,23,25]. The I_D/I_G ratios of the purified and unpurified CNTs are in the range 0.5 and 0.75 suggesting a defective structure, to an extent that is common in CVD synthesized CNTs. The purified IMPCNTs showed less disorder of the graphene sheets. The purification process generally had no significant impact on the structure of the CNTs as determined by the Raman data.

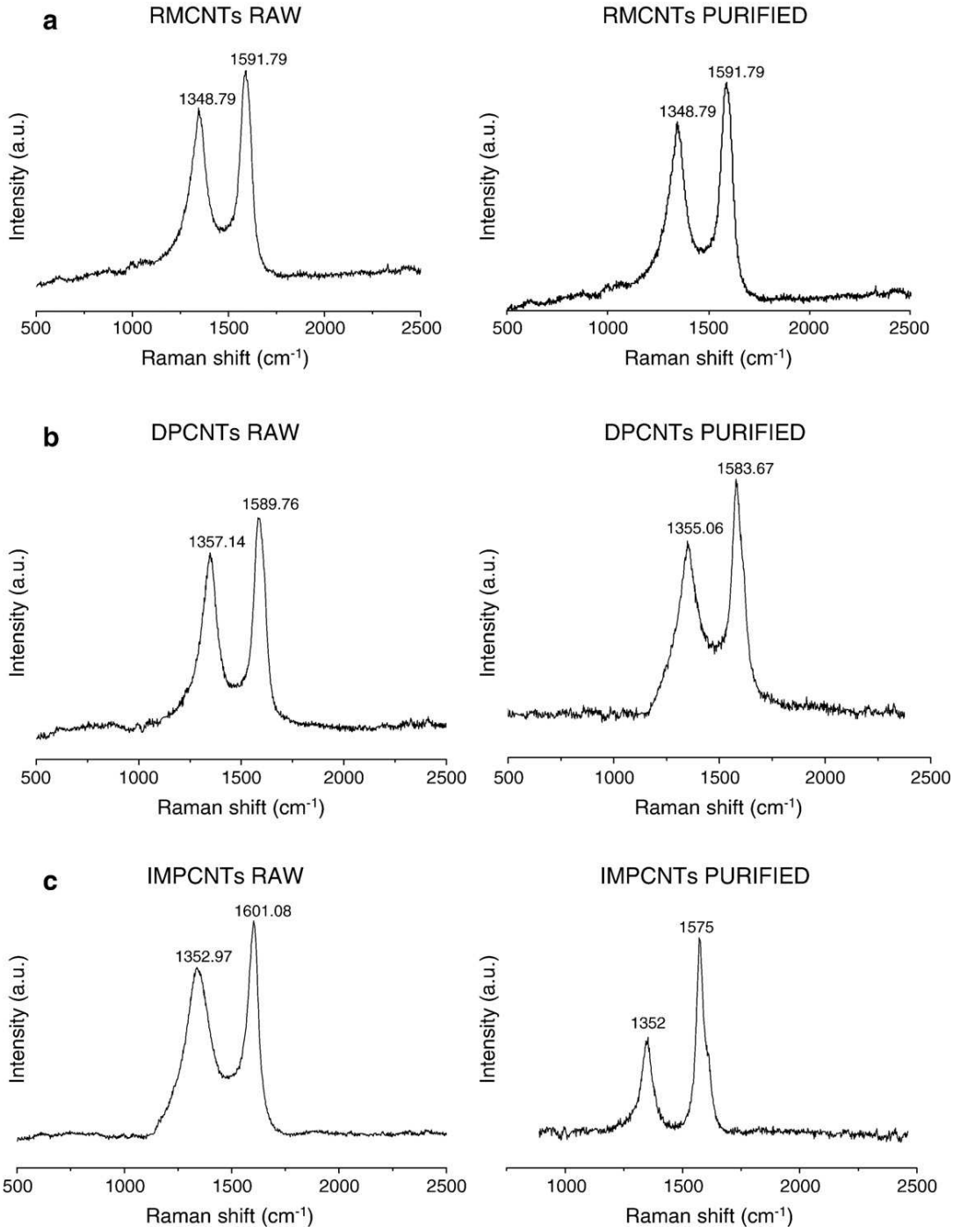

Fig. 6.9: Raman spectra of unpurified and purified CNTs: (a) RMCNTs, (b) DPCNTs, and (c) IMPCNTs.

Scanning electron microscope (SEM) characterization of the CNTs confirmed the high density of the raw CNTs randomly entangled in a noodle-like fashion. It can clearly be

seen that the products were highly selective towards CNTs; no other by-products were obtained. The CNTs were uniformly distributed in size. This distribution was influenced by the diameter distribution of the particles used, while their lengths varied extensively to several micrometers long. Similar images were obtained for the IMPCNTs, DPCNTs and RMCNTs. Fig. 6.10 shows the SEM image of an unpurified sample of RMCNTs.

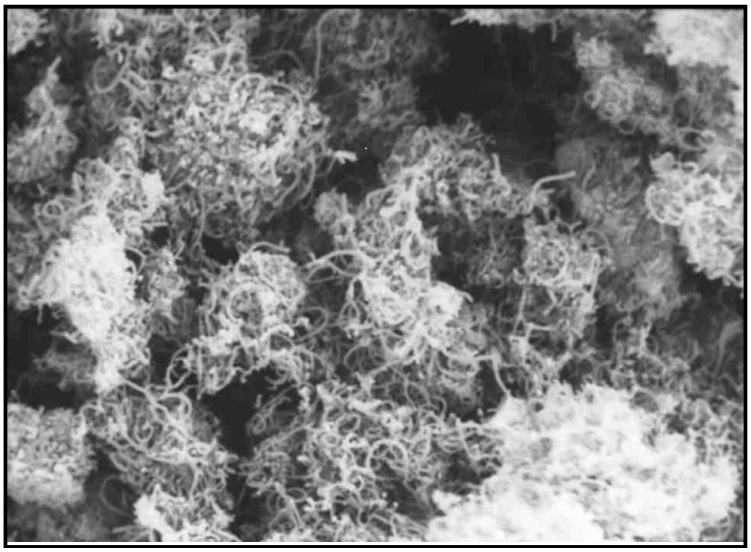

Fig. 6.10: SEM image of unpurified RMCNTs.

6.4 Conclusions

'Clean' multiwalled CNTs have been synthesized in large amounts. The wet impregnation and deposition–precipitation methods gave the highest yields of MWCNTs with diameters in the range 10 - 15 nm i.d and 20 - 30 nm o.d. These methods were less effective in controlling the size of the metal particles and sizes were affected by the concentration of the metal particles on the support and the concentration of the metal precursor solution. The nanoparticle sizes obtained from these methods were in the order of 20 - 30 nm. Particle sizes < 15 nm could not be obtained. Therefore these methods have a limitation if tubes with smaller diameters are sought.

A reverse micelle process was used to synthesize Fe-Co nanoparticles that were highly crystalline and uniform in size. The reverse micelle technique displayed the ability to

prepare nanoparticles of controlled size (3, 6 and 13 nm) obtained by varying the concentrations of Fe and Co in the micelle. The nanoparticles were deposited on a $CaCO_3$ support and were used to synthesize CNTs with diameters in ranging between 3 - 5 nm i.d and 5 - 15 nm o.d. Using the RM method, smaller diameter CNTs could be obtained compared with the IMP and DP methods because smaller particles were obtained with the RM method. The CNT diameter was found to correlate with the size of the catalyst particle used. HRTEM and Raman spectroscopy analysis showed that CNTs could be purified using a single step process that involved their dissolution in 30% HNO_3 for 48 h without any obvious effect on the wall structure of these materials. The methods of catalyst preparation and CNT synthesis used in this study can readily be scaled up for industrial applications.

6.5 References

1. S. Iijima, Nature **354** (1991) 56.
2. L. Dai, *Carbon nanotechnology*, University of Dayton, Dayton, Ohio 45469-0240, USA, Elsevier, 2006.
3. J. Robertson, Mater. Today **10** (2007) 37.
4. M. Trojanowicz, Trend. Anal. Chem. **25** (2006) 480.
5. M. Paradise, T. Goswami, Mater. Design **28** (2007) 1477.
6. C.J. Lee, J. Park, Carbon **39** (2001) 1891.
7. J.E. Herrera, D.E. Resasco, J. Catal. **221** (2004) 354.
8. W. Qian, F.Wei, T. Liu, Z.W.Wang, Solid State Commun. **126** (2003) 365.
9. R.L. Vander Wala, T.M. Ticichb, V.E. Curtisb, Carbon **39** (2001) 2277.
10. S. Inoue, Y. Kikuchi, Chem. Phys. Lett. **410** (2005) 209.
11. S. Inoue, T. Nakajima, Y. Kikuchi, Chem. Phys. Lett. **406** (2005) 184.
12. E. Couteau, K. Hernadi, J.W. Seo, L. Thiên-Nga, Cs. Mikó, R. Gaá1, L. Forró, Chem. Phys. Lett. **378** (2002) 9.
13. H. Kathyayini, N. Nagaraju, A. Fonseca, J.B. Nagy, J. Mol. Catal. **223** (2004) 129.
14. M.C. Bahome, L.L. Jewell, D. Hildebrandt, D. Glasser, N.J. Coville, Appl. Catal. A: General **287** (2005) 60.

15. M. Su, Y. Li, B. Maynor, A. Buldum, J.P. Lu, J. Liu, J. Phys. Chem. B **104** (2000) 6505.
16. F. Pinna, Catal. Today **41** (1998) 129.
17. Y. Lee, J. Lee, C.J. Bae, J-G. Park, H-J. Noh, J-G. Park, T. Hyeon, Adv. Funct. Mater. **15** (2005) 503.
18. M. Perez-Cabero, A. Monzón, I. Rodríguez-Ramos, A. Guerrero-Ruíz, Catal. Today **93-95** (2004) 681.
19. E. Manova, T. Tsoncheva, D. Paneva, I. Mitov, K. Tenchev, L. Petrov, Appl. Catal. A: General **277 (**2004) 119.
20. E. Dervishi, Z. Li, A.R. Biris, D. Lupu, S. Trigwell, A.S. Biris, Chem. Mater. **19 (**2007) 179.
21. T.C. Schmitt, A.S. Biris, D.W. Miller, A.R. Biris, D. Lupu, S. Trigwell, Z.U. Rahman, Carbon **44 (**2006) 2032.
22. S. Inoue, N. Ichikuni, T. Suzuki, T. Uematsu, K. Kaneko, J. Phys. Chem. **102** (1998) 4689.
23. A. Chambers, C. Park, R.T.K. Baker, N.L. Rodriguez, J. Phys. Chem. **102** (1998) 4253.
24. P. Serp, M. Corrias, P. Kalck, Appl. Catal. A: General **253** (2003) 337.
25. J. Cheng, X. Zhang, Z. Luo, F. Liu, Y. Ye, W. Yin, W. Liu, Y. Han, Mater. Chem. Phys. **95** (2006) 5.

Chapter 7

A novel $Ca_3(PO_4)_2$-$CaCO_3$ support mixture for the CVD synthesis of roughened multiwalled carbon nanotubes[#]

7.1 Introduction

Carbon nanotubes (CNTs) are classified as an allotrope of carbon. Other allotropes include diamond, graphite, fullerene and amorphous carbon. The CNTs are one of the strongest and stiffest materials known, in terms of their tensile strength and elastic modulus respectively, which is the consequence of the covalent sp^2 bonds formed between the individual carbon atoms [1-5]. The extraordinary properties of CNTs (e.g. electrical conductivity, thermal stability and mechanical properties) have made these materials potentially useful in many applications in nanotechnology such as electronics, optics, catalysis, biomedicine, fuel cells etc [2,3,6-13]. Since the report of the identification of CNTs by Iijima [14], these materials have attracted much attention from researchers within the scientific community and methods to make CNTs have been extensively investigated.

The synthesis of carbon nanotubes (CNTs) can be done using arc discharge [15,16], by laser ablation [17], by thermolysis in a closed environment at high pressure [18] or by chemical vapour deposition (CVD) [19] procedures. The latter method is generally classified into two categories namely, the floating catalyst process, a gas phase process, and the substrate CVD process. This latter process involves the use of a thermally stable material to *support* metal particles that are responsible for the molecular decomposition of carbon to form the CNTs [13]. The CVD process is generally the most widely used method because it is a low cost process that is industrially scaleable, versatile, and allows for the controlled growth of high purity CNTs.

[#]*Sabelo D. Mhlanga, Michael J. Witcomb, Rudolf M. Erasmus, Neil J. Coville, Mater. Chem. Phys., submitted, 2009.*

The support in the substrate CVD process plays an important role in influencing the activity of the catalyst used to make the CNTs. Several factors need to be taken into consideration when choosing a support. These include

(iv) the decomposition temperature of the support and hence its useful reaction range,
(v) the surface area of the support and
(vi) the metal catalyst-support interaction that controls the size of the catalyst particle and the sintering potential of the catalyst.

High surface area materials such as SiO_2, Al_2O_3, TiO_2 and zeolites provide excellent supports for catalytic CNT production. However, the nature of these materials does not allow for their easy removal and thus purification of CNTs produced on these supports remains a challenge and often requires several acidic/oxidation steps that result in damage to the CNT graphitic structures. Environmental aspects should also be taken into consideration because the solvents used during the purification process must be disposed of. To circumvent these environmental problems, the use of readily removable supports has been studied both by us and others [20-31].

Calcium carbonate ($CaCO_3$) has proven to be a support of choice for mono- and bimetallic transition metal particles (typically Fe, Ni and Co) because it satisfies both the catalyst activity and environmental aspects in the synthesis of CNTs. Previous studies have revealed the advantages of using this material as a support for CNT synthesis [20-28]. The disadvantage, however, is that the $CaCO_3$ loses CO_2 to give low surface area CaO at T > 800°C. The presence of small amounts of CO_2 has however been proposed to favour CNT growth [24].

In this paper, we report on the use of a novel material; calcium pyrophosphate, $Ca_3(PO_4)_2$, as an alternative support. $Ca_3(PO_4)_2$ has a high melting point (1670°C), a higher surface area of 42.4 m^2/g (compared to $CaCO_3$, 10 m^2/g), is insoluble in water and

alcohols, soluble in mild acids and is not expensive [32]. These properties would render the material highly suitable for the CVD synthesis of CNTs.

7.2 Experimental

The $Ca_3(PO_4)_2$, $Ca_3(PO_4)_2$-$CaCO_3$ (prepared by physically mixing the two materials in a beaker) and $CaCO_3$ supported Fe-Co catalysts (2.5% Fe, 2.5% Co by wt.) were prepared using a wet impregnation process [25]. $Fe(NO_3)_3 \cdot 9H_2O$ and $Co(NO_3)_2 \cdot 6H_2O$ were purchased from Sigma Aldrich and were used as sources of Fe and Co respectively. The metal loading concentrations were confirmed by Inductively Coupled Plasma – Atomic Emission Spectroscopy (ICP-AES) measurements using semiconductor detectors (CCD) and by quantitative thermogravimetric analysis (TGA) using a Perkin Elmer Pyris 1 TGA. For thermal analysis, the CNTs were decomposed under a continuous flow of air or nitrogen (40 ml/min) and the heating rate was 10°C/min.

The CNTs were characterized by transmission electron microscopy (TEM) (JEOL 100S Electron Microscope and a Philips CM200 equipped with a Gatan Imaging Filter for higher magnifications), energy dispersive X-ray spectroscopy (EDX), BET surface area analysis (Micromeritics TriStar Surface Area and Porosity Analyzer), thermogravimetric analysis (TGA) (Perkin Elmer Pyris 1 TGA), Raman spectroscopy (Jobin-Yvin T64000 micro-Raman spectrometer), X-ray photoelectron spectroscopy (XPS) (Physical Electronics Quantum 2000) and powder X-ray diffraction (PXRD) (Bruker axs D8 Advance PXRD) techniques.

MWCNTs were grown using a horizontal fixed bed reactor consisting of an electronically controlled furnace and a quartz tube reactor [22]. The calcined catalyst (typically 200 mg) was uniformly spread on a quartz boat (120 mm × 15 mm) at room temperature and the boat was placed in the middle of the reactor. The furnace was then heated at 10°C/min with N_2 flowing over the catalyst at 40 ml/min. Once the temperature had reached 700°C, the N_2 flow rate was increased to 240 ml/min and C_2H_2 was introduced at a constant flow rate of 90 ml/min. After 60 min of reaction time, the C_2H_2 flow was stopped and the

furnace was left to cool down to room temperature under a continuous flow of N_2 (40 ml/min). The boat was then removed from the reactor and the carbon deposit along with the catalyst was weighed and analyzed using transmission electron microscopy.

From our previous studies [25], we observed that the activity of Fe-Co catalysts was largely influenced by the reaction temperature and the ratios of nitrogen/acetylene gas mixtures. In this study the synthesis of CNTs was performed varying only the temperature (600 - 1000°C) at a C_2H_2:N_2 flow rate of 1:3. Experiments were also carried out using C_2H_2 without a carrier gas (N_2) in order to determine the activity of the catalyst under this condition. The effect of synthesis time on the CNT structure and yield was investigated.

Purification of the CNTs was carried out using a single step process that involved the use of mild acid (5, 10, 30% HNO_3) to dissolve the support and metal particles from the final product. This was achieved by stirring continuously at room temperature a mixture of the CNTs and acid (e.g. 3 g in 100 ml) for 30 min - 24 h. The product was washed with distilled water until the washings were neutral.

7.3 Results and discussion

Fe-Co catalysts supported on $Ca_3(PO_4)_2$-$CaCO_3$ mixtures were evaluated for CNT production.

7.3.1 BET surface area analysis

Table 7.1 shows the details of the catalysts used, the amount of raw product obtained and the average diameters of the CNTs produced. The surface areas of the catalyst materials showed that the total surface area of the catalysts decreased as the amount of $CaCO_3$ added to $Ca_3(PO_4)_2$ was increased from 5 – 95% by weight. The decrease in the surface area was expected since $CaCO_3$ has a much lower surface area (10.5 m^2/g) than $Ca_3(PO_4)_2$ (41.6 m^2/g).

Table 7.1: Chemical composition of the catalysts used (200 mg) for the synthesis of carbon nanotubes (synthesis time = 1 h) at 700°C.

Reaction	**Catalyst composition**					**Product analysis**	
	$Ca_3(PO_4)_2$ wt%	$CaCO_3$ wt%	Fe^{3+} wt%	Co^{2+} wt%	BET SA (m^2/g)	Yield (g)	Out. diam. (nm)[c]
1	100	0	2.5	2.5	41.6	0.29	-
2	95	5	2.5	2.5	39.6	0.40	50
3[a]	50	50	2.5	2.5	29.2	0.86	50
4	5	95	2.5	2.5	13.8	1.03	50
5[b]	0	100	2.5	2.5	10.5	1.15	25

[a]See Fig. 7.2b for TEM image
[b]See Fig. 7.2a for TEM image
[c] ± 5 nm

The $Ca_3(PO_4)_2$ catalysts were tested for the synthesis of CNTs under the conditions described in the experimental section. As can be observed (Table 1) reactions over pure $Ca_3(PO_4)_2$ gave very little carbon deposit; it consisted of CNTs (< 1%) and amorphous carbon. Reactions over $CaCO_3$ as expected gave a high yield of CNTs with near 100% selectivity (Table 1). The decomposition of C_2H_2 was then performed using $CaCO_3$ physically mixed with varying amounts of $Ca_3(PO_4)_2$ (5, 50 and 95 wt%) prepared using the same impregnation procedure. With the $Ca_3(PO_4)_2$-$CaCO_3$ supports, the CNT yield decreased with increase of $Ca_3(PO_4)_2$ in the mixture.

7.3.2 TEM analysis

TEM analysis was performed on the product obtained from the Fe-Co on $Ca_3(PO_4)_2$-$CaCO_3$ support mixtures. The TEM analysis revealed that CNTs were produced and that all the CNTs were multiwalled in nature with average outer diameters of about 50 nm (synthesis time = 1 h) (Fig. 7.1). The inner diameters of the CNTs were in the 5 – 10 nm range. The Fe-Co on the $Ca_3(PO_4)_2$-$CaCO_3$ produced CNTs with outer diameters twice the size of the CNTs obtained using 100% $CaCO_3$. The TEM images showed that the CNTs synthesized in the presence of $Ca_3(PO_4)_2$ posses extremely rough (pitted) surfaces when compared to CNTs produced from $CaCO_3$ (Fig. 7.2) under the same synthesis

conditions. Further, the purified CNTs synthesized from $Ca_3(PO_4)_2$-$CaCO_3$ have high surface areas ~ 132 m^2/g compared to the CNTs synthesized over $CaCO_3$ (SA = 94 m^2/g).

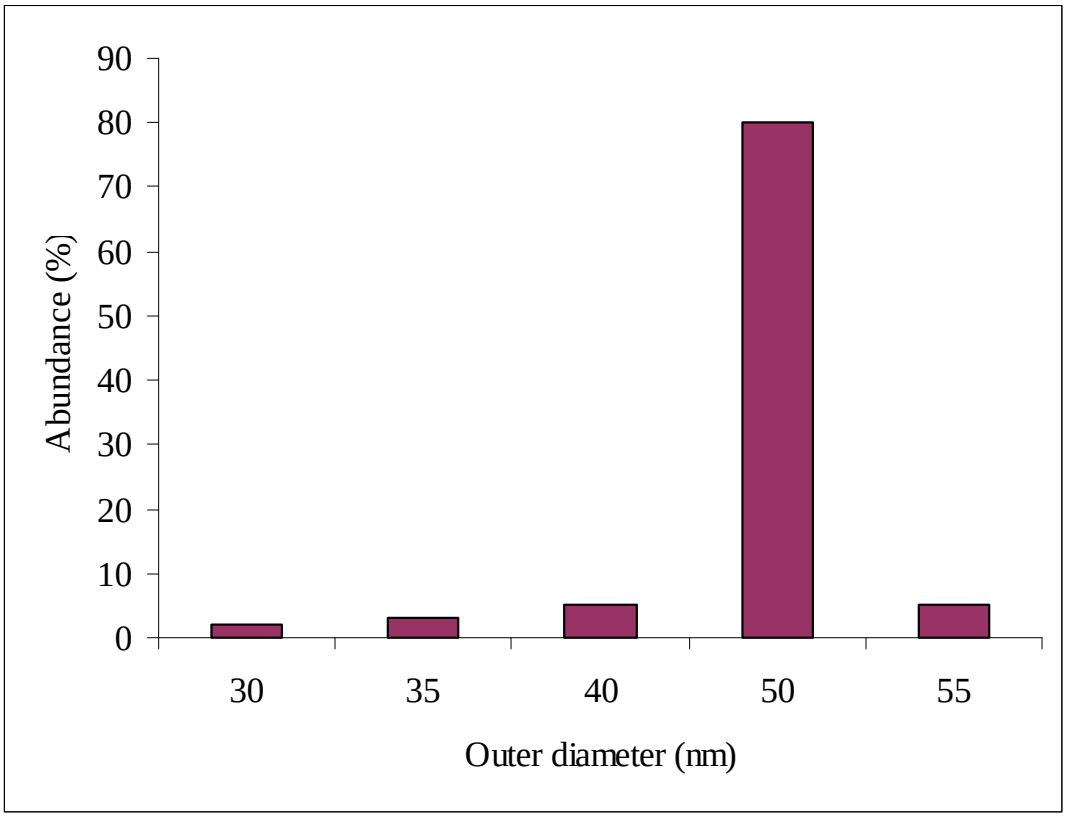

Fig. 7.1: A size distribution graph of the CNTs synthesized using a 50/50 w/w $Ca_3(PO_4)_2$-$CaCO_3$ support mixture after 1 h synthesis time.

CNTs with a rough outer wall structure have been observed by Escobar *et al* when CNTs were synthesized using Fe on a SiO_2 susbtrate [33]. The amorphous non-crystalline surface of the CNTs was attributed to the concentration of acetylene in the feed stock. At high acetylene concentrations carbon nanoparticles grew, covering the surface of CNTs, giving a compact coating [33].

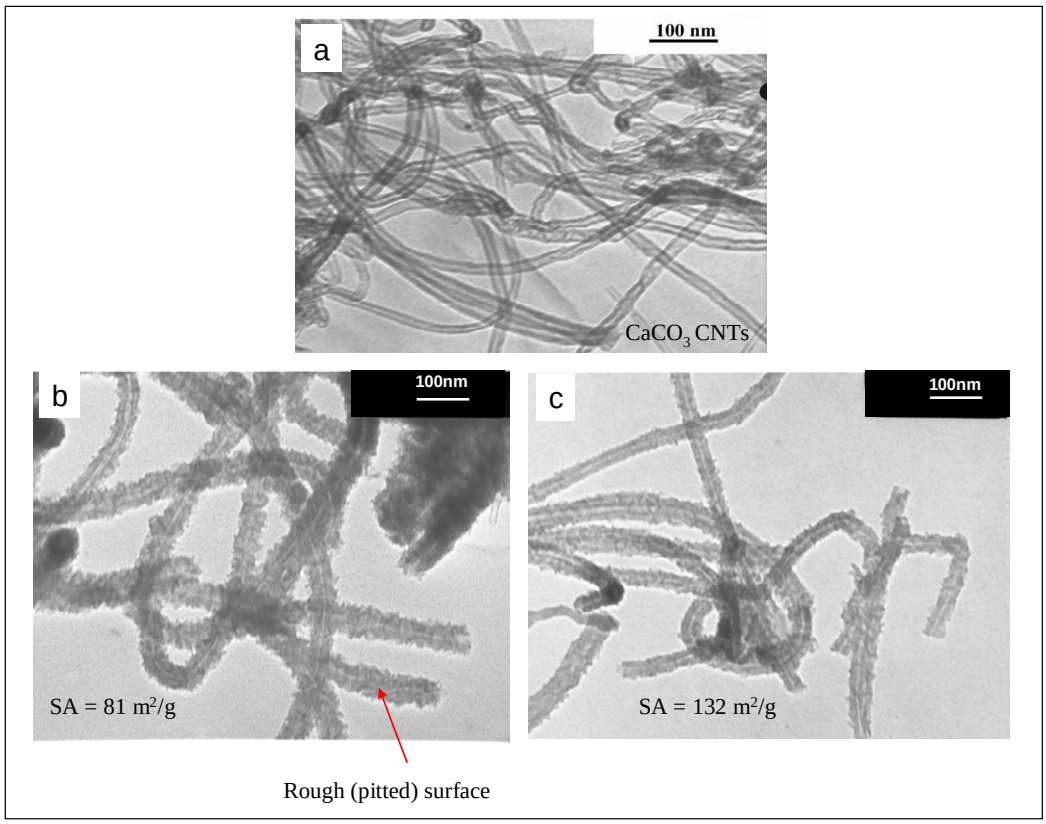

Fig. 7.2: A TEM image of MWCNTs synthesized over $CaCO_3$ (a) and TEM images of MWCNTs synthesized over 50wt%$CaCO_3$/50wt%$Ca_3(PO_4)_2$ before (b) and after purification (c) with 30% HNO_3.

A TEM image of the CNTs synthesized over $Ca_3(PO_4)_2/CaCO_3$ (50:50 w/w) with a rough surface is shown in Fig. 7.3a and Fig 7.4. A closer look at the outer surface (Fig. 7.3b) revealed that the surface is covered with an amorphous layer of carbon. The amorphous nature of the CNTs has been observed in several other studies [34]. Luo *et al* [34a] synthesized long amorphous carbon nanotubes by a solvothermal treatment, in which ferrocene and sulfur powder were the reactants and benzene served as a carbon source. The CNTs were entirely amorphous. This was also reported in a similar study by Xiong *et al* [34b]. Nishino and co-workers [34c] have also grown amorphous CNTs using poly(tetrafluoroethylene) and ferrous chloride. Amorphous CNTs have also been produced in large scale by temperature-controlled arc discharge in a hydrogen atmosphere with Co/Ni alloy powders [34d].

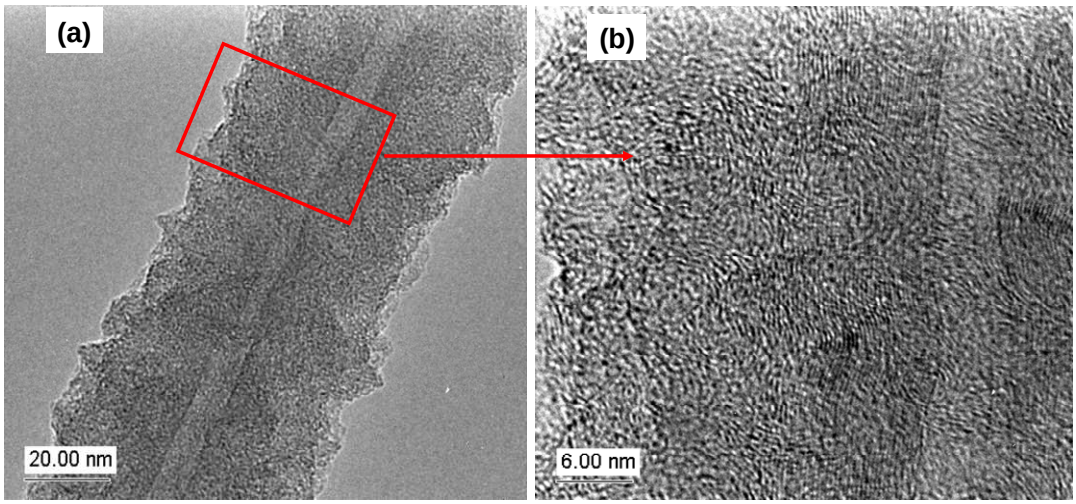

Fig. 7.3: A TEM image of a CNT synthesized over 50wt%$CaCO_3$/50wt%$Ca_3(PO_4)_2$: (a) shows a large CNT with a rough surface and (b) shows the same picture at higher magnification.

The CNTs produced in this study are not entirely amorphous. The random orientation of carbon is limited to the outer part of the CNT walls as shown by the TEM image in Fig. 7.4 (region 2). Clearly the inner wall is graphitized and the amount of defects in this region is low, as shown Fig. 7.4, region (1). The graphite sheets are arranged in a perfect orientation contrary to the outer layer shown in region (2). An X-ray diffraction pattern of region 1 revealed the crystalline nature of the nanotubes.

Escobar *et al* [33] proposed that during the synthesis of CNTs, amorphous carbon nanoparticles nucleate on the external wall of the CNTs. The mechanism of this observation has not been explained. However we believe that the deposition of carbon occurs by a mechanism similar to the nucleation of carbon black soot that takes place during the direct pyrolysis of hydrocarbons (e.g. CH_4, C_2H_2, C_2H_4) in the absence of a catalyst at high temperatures [35].

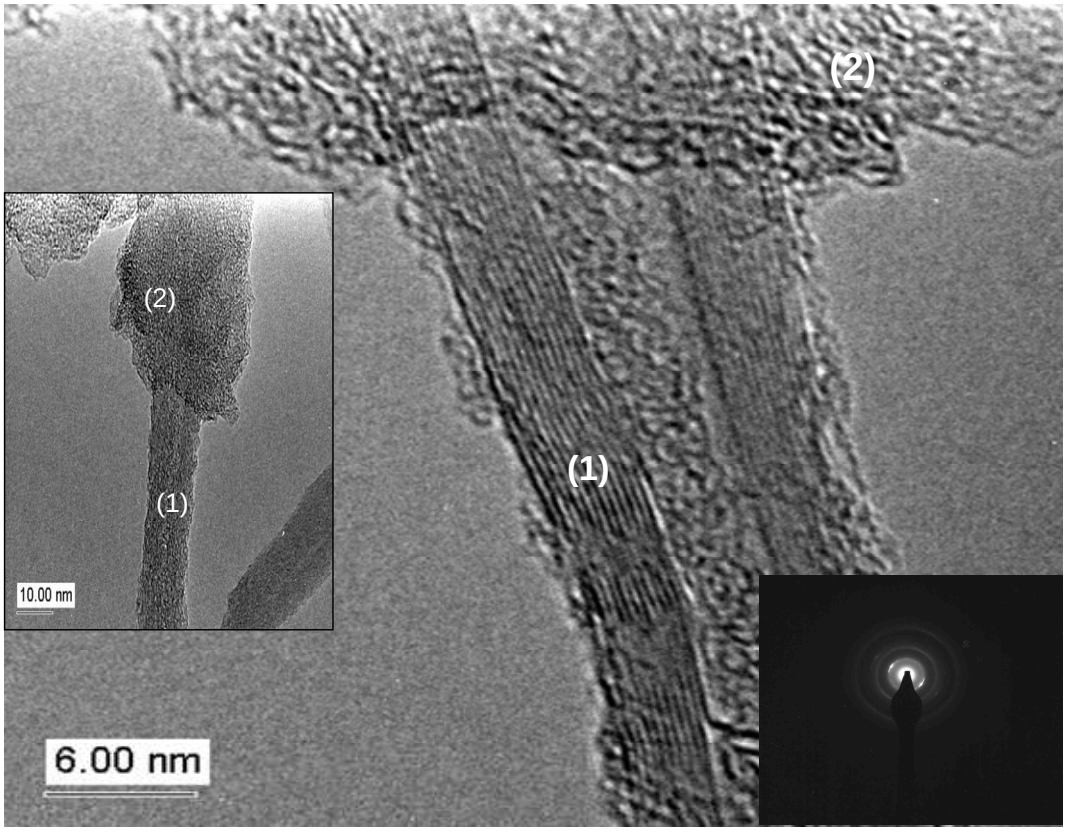

Fig. 7.4: A TEM image of CNTs synthesized over 50wt%$CaCO_3$/50wt%$Ca_3(PO_4)_2$ after 1 h showing the perfect orientation of graphite sheets of the inner tubes (region 1) and the amorphous part of the CNTs (region 2). An X-ray diffraction pattern of region 1 is shown (inset).

The synthesis of CNTs for different time periods revealed that the roughness of the CNTs is time dependant. The CNTs were synthesized under the same reaction conditions after 5 min, 30 min, 60 min, 3 h and 6 h respectively. TEM images of the CNTs synthesized after 5 min show that they do not contain rough surfaces as found for CNTs synthesized for 60 min (Fig. 7.5). Therefore while it is speculated that the $Ca_3(PO_4)_2$ substrate promotes roughness of the CNTs, these reactions occur with time.

In addition, it can be seen that the outer diameters of the CNTs increase with time and break into shorter tubes (Fig 7.5c,d). It can thus be said that the CNT synthesis time using the mixture of supports, not only results in good yield and roughening of the CNTs, but

also *causes fragmentation of the CNTs*. Such fragmentation of tubes is novel. The fragmentation of the CNTs could be associated with the deposition of carbon on the already formed CNTs which results in their fragmentation. Indeed many of the fragments revealed an amorphous carbon layer deposited on an inner crystalline tube as seen in Fig 7.5c,d (see circled regions).

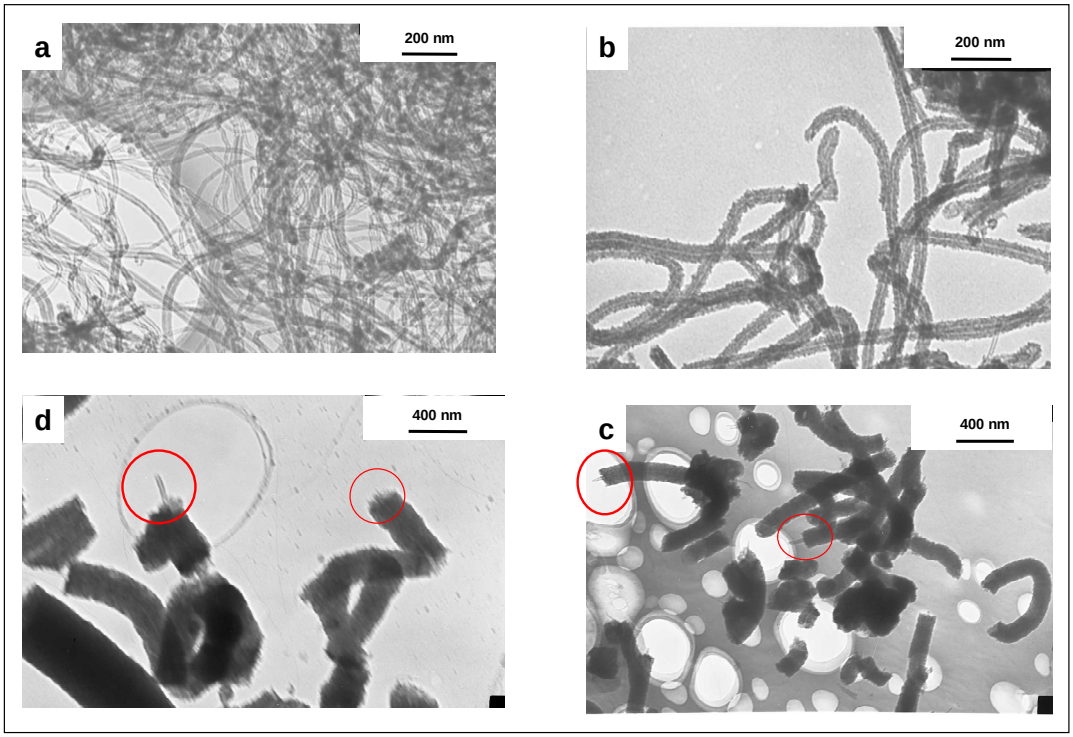

Fig. 7.5: TEM images CNTs synthesized over 50wt%$CaCO_3$/50wt%$Ca_3(PO_4)_2$ for (a) 5 min (b) 60 min (c) 3 h and (d) 6 h synthesis time.

The rough surface of the CNTs was also confirmed by Raman analysis (Fig. 7.6). The two peaks occurring at 1348 and 1597 cm^{-1}, corresponding to the D and G-vibration modes of the graphite sheets can be used to indicate the degree of defects/disorder of the graphite sheets. The degree of disorder is given by the ratios of the intensities of the D and G-bands (I_D/I_G). The I_D/I_G ratios of the MWCNTs synthesized for 5 and 60 min were ~0.8 and 1.0 respectively suggesting that the disorder of the graphite sheets was very high for the CNTs synthesized for 60 min.

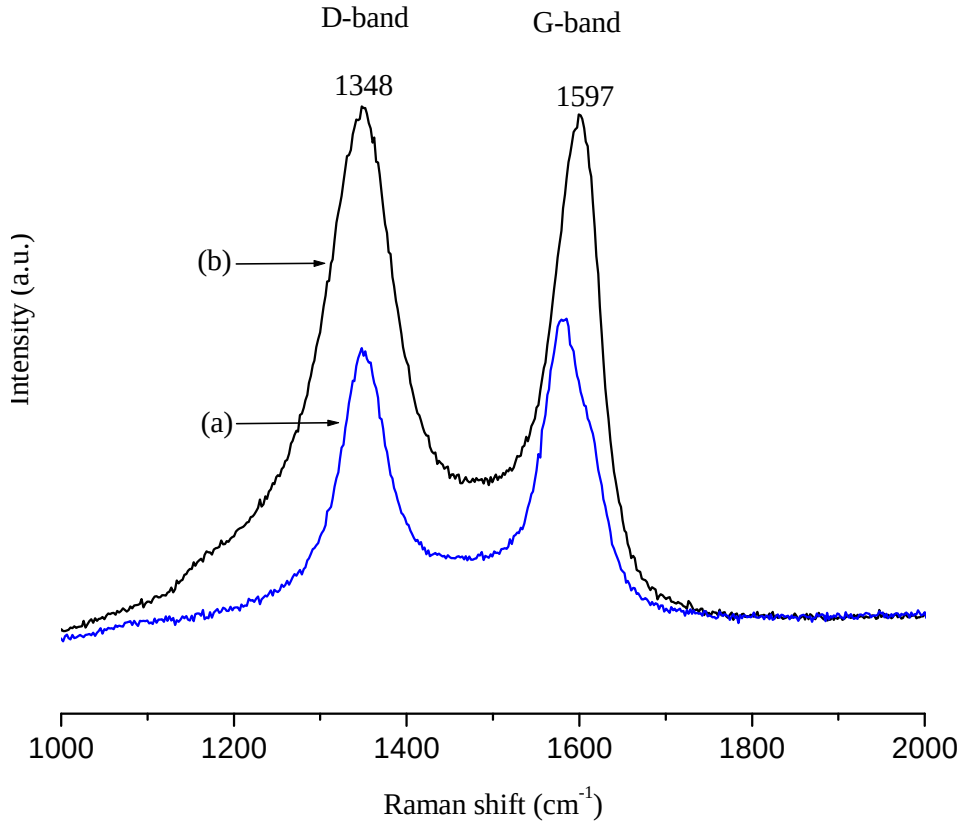

Fig. 7.6: Raman spectra of MWCNTs synthesized over 50wt%$CaCO_3$/50wt%$Ca_3(PO_4)_2$ for (a) 5 min and (b) 60 min.

7.3.3 Thermogravimetric analysis

Differential thermogravimetric (DTG) profiles of purified CNTs synthesized over $CaCO_3$ and $CaCO_3$-$Ca_3(PO_4)_2$ are shown in Fig 7.7. The profiles indicate that the decomposition of carbon occurs at the same temperature (550°C) for the different types of CNTs. Thus the type of support used or the CNT roughness has little effect on the thermal stability of the CNTs. However, the CNTs synthesized over the support mixture has a broader DTG profile. This suggests that the carbon decomposes over a wider temperature range, which could be due to the presence of small amounts of phosphorus. Phosphorus is known to be a fire retardant [36] and this property could be responsible for the modified decomposition of these CNTs. The presence of P in the $CaCO_3$-$Ca_3(PO_4)_2$ support is also

believed to “kill” the CNT growth as reflected by the lower yields of CNTs formed as a function of phosphate concentration.

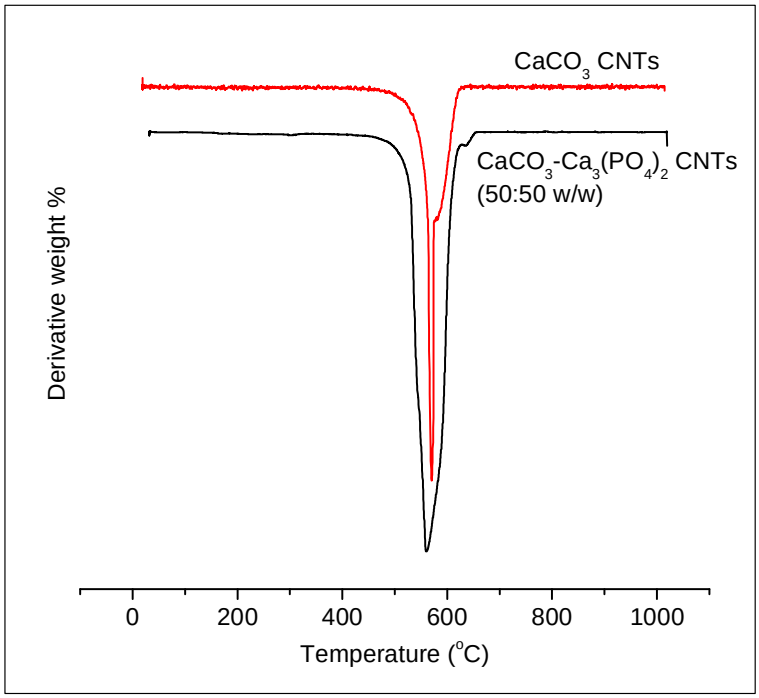

Fig. 7.7: DTG graphs of CNTs synthesized over $CaCO_3$ and 50wt%$CaCO_3$/50wt%$Ca_3(PO_4)_2$ (under air).

7.3.4 Elemental composition and purification

The elemental composition of the as-synthesized CNTs was carried out using XPS analysis. The CNT wall structure was shown to contain only C (96.3%) and O (3.3%) (Fig. 7.8). The spectrum of the raw and purified CNTs revealed that the materials are composed mainly of carbon. The elemental composition of the materials was also confirmed by EDS. The elemental analysis revealed that the CNTs are relatively pure and contain undetectable amounts (< 0.5%) of Ca or P implying that large particles of CaO or $Ca_3(PO_4)_2$ are not embedded in the CNT walls. It is, however, possible that small particles < 3 nm were deposited in the nanotubes walls [37]. No large crystalline particles of Ca, P or CaO were observed by TEM.

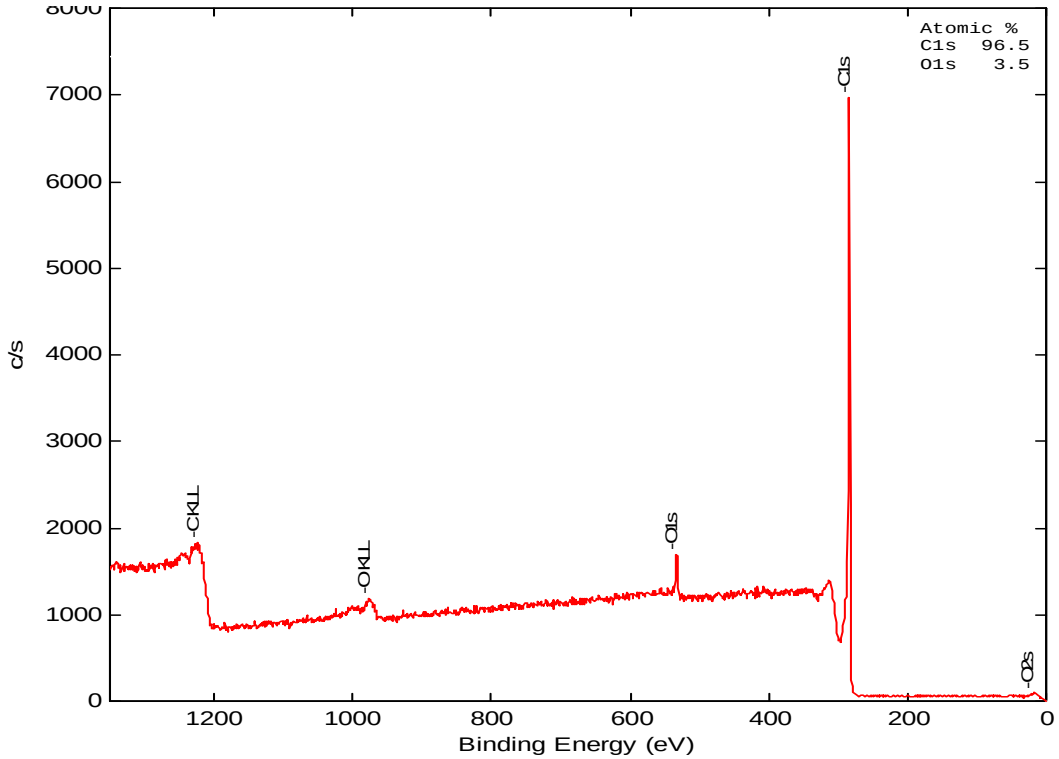

Fig. 7.8: An XPS spectrum of as-synthesized CNTs obtained using 50wt%$CaCO_3$/50wt%$Ca_3(PO_4)_2$.

Raman analysis was carried out on the as-synthesized and purified (24 h, r.t., 30% HNO_3) CNT samples (Fig. 7.8). It can been seen from the intensities of the two peaks occurring at 1350 and 1600 cm^{-1} corresponding to the D and G-vibration modes of the graphitic sheets, that the structures are highly disordered. The I_D/I_G ratios for the as-synthesized and purified MWCNTs (synthesized in 1h) were ~1.0. Thus the acid treatment process did not affect the graphitic nature of the wall structure of the CNTs.

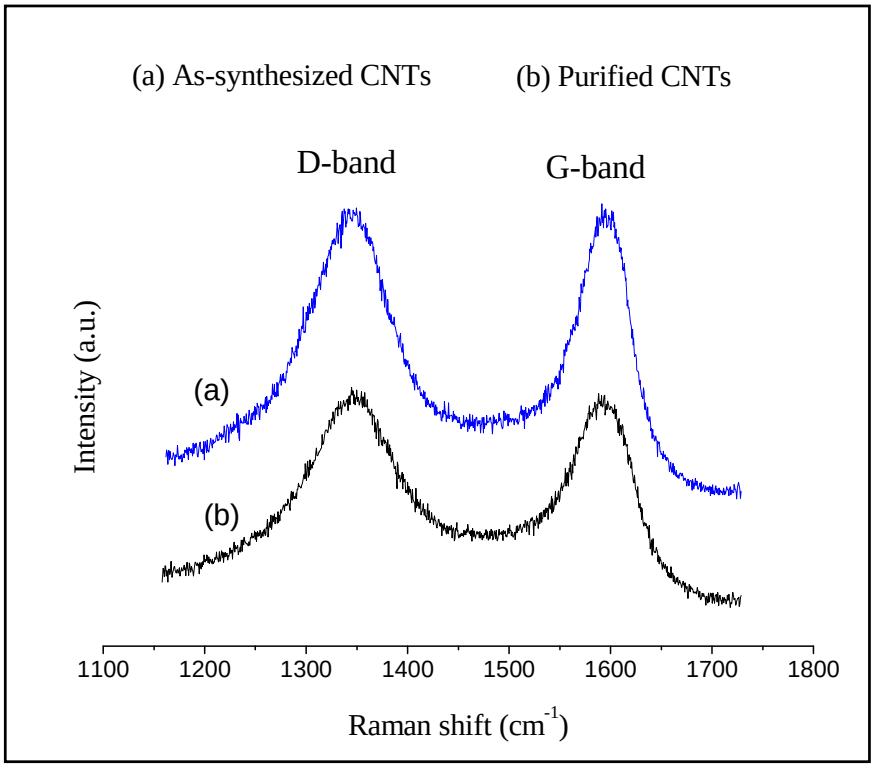

Fig. 7.9: Raman spectra of MWCNTs synthesized over 50wt%$CaCO_3$/50wt%$Ca_3(PO_4)_2$ before (a) and after purification (b) with 30% HNO_3.

The effectiveness of the purification process was also studied using PXRD and TGA. The acid was able to remove the impurities as shown in Fig. 7.10b. Very dilute solutions of HNO_3 (5, 10%) were also found to be effective in removing the support and metal particles (Fig 7.11), thus the use of concentrated acids and multi-step purification can be avoided. However, it can be seen that a minimum amount of impurities cannot be removed by the acid washing as shown depicted by the 3% and 4.6% residues corresponding to washing with 5 and 15% respectively, as observed similarly in Chapter 5.

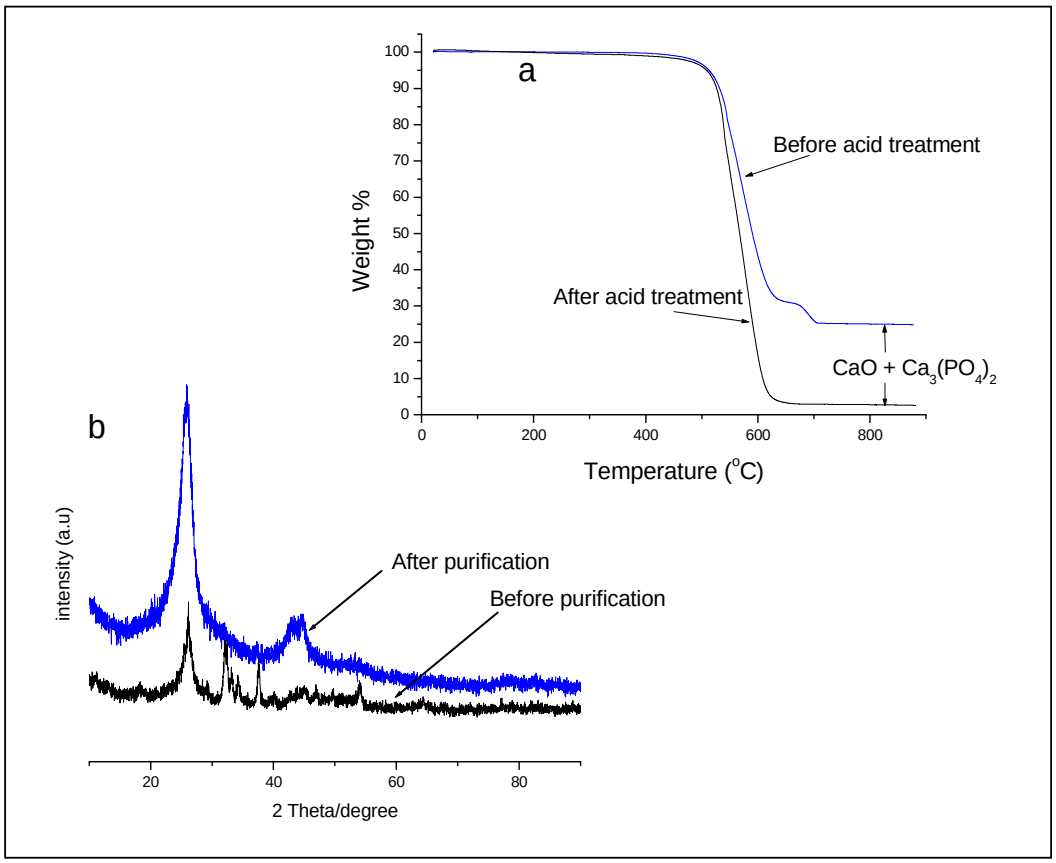

Fig. 7.10: (a) TGA profiles and (b) PXRD pattern of CNTs synthesized over 50wt%$CaCO_3$/50wt%$Ca_3(PO_4)_2$ before and after purification with 30% HNO_3 for 24 h.

The XRD pattern of the unpurified and purified CNTs showed two peaks at 26° and 45° corresponding to carbon peaks. The carbon peaks are broad; an observation attributed to the low crystallinity of the outer walls of the CNTs [38]. The as-synthesized and purified MWCNTs were also characterized by TGA in air (Fig. 7.10a). The weight loss due to the combustion of carbon with oxygen, which corresponds to the carbon content in the sample, occurred in the temperature range of 550 - 600°C. The TGA of the as-synthesized and purified CNTs enabled the mass of impurities and CNTs in the carbon deposit to be determined. No amorphous carbon or any other form of shaped carbon nanomaterials were formed in the production process. The TGA profiles are similar to those of MWCNTs obtained using typical CVD processes [22,29].

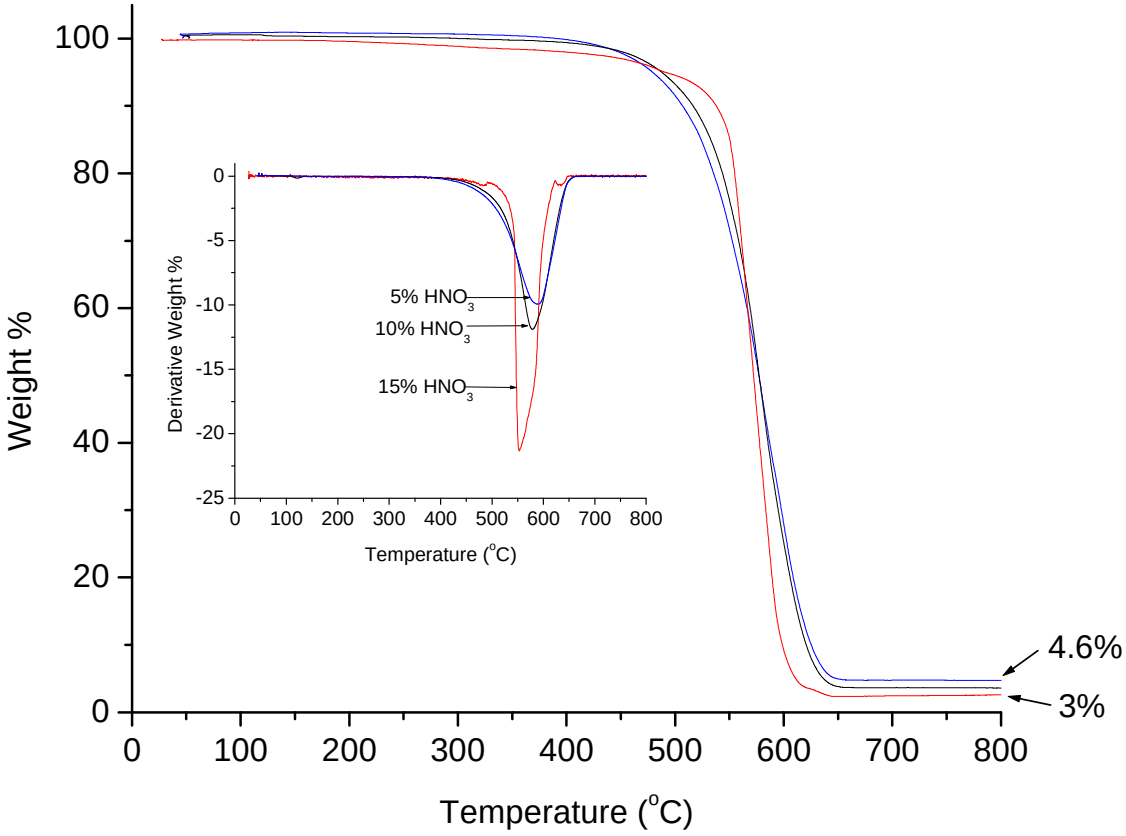

Fig. 7.11: TGA and DTG (inset) profiles of purified MWCNTs synthesized over 50wt%$CaCO_3$/50wt%$Ca_3(PO_4)_2$ supported Fe-Co catalyst with different amounts of acid (5, 10, 30% HNO_3; t = 12 h).

7.4 Conclusion

The work presented herein reports a novel approach for the synthesis of 'rough' MWCNTs in high yields. While these CNTs possess a rough surface, TEM analysis revealed that the CNT inner walls possess a regular array of crystalline graphite sheets (typically 3 - 5 nm in length). Raman analysis revealed that the rough CNTs synthesized in 1 h contained a high degree of defects on the graphite sheets. The study showed that the growth of CNTs over longer synthesis times (t > 2 h) results in thickening and fragmentation of the CNTs due to the deposition of carbon on the formed CNTs. The $Ca_3(PO_4)_2$-$CaCO_3$ (50:50 w/w) mixtures can readily be removed from the CNTs by dissolving them in very dilute acid (5% HNO_3). The purification process does not affect

the graphitic structure of the CNTs. The support mixture is thus ideal for the large scale production of CNTs. The rough surfaces 'pits' of the CNTs can serve as 'docking stations' [36] for metal particles in catalytic reactions such as the Fischer-Tropsch synthesis, thus reducing deactivation of catalyst through sintering of the metal particles.

7.5 References

1. M.S. Dresselhaus, G. Dresselhaus, P.C. Eklund. *Science of fullerenes and carbon nanotubes*, San Diego, Calif: Academic press, 1996.
2. M.S. Dresselhaus, G. Dresselhaus, P. Avouris. *Carbon nanotubes: synthesis, structure, properties, and applications*, Berlin: Springer, 2001.
3. P.J.F. Harris. *Carbon nanotubes and related structures: new materials for the twenty-first century*, Cambridge, U.K.; New York: Cambridge University Press, 2001.
4. R. Saito, G. Dresselhaus, M.S. Dresselhaus, *Physical properties of carbon nanotubes*, London: Imperial College Press, 1998.
5. S. Reich, C. Thomsen, J. Maultzsch, Weinheim; Cambridge: Wiley-VCH, 2004.
6. B.M. Endo, T. Hayashi, Y.A. Kim, M. Terrones, M.S. Dresselhaus, Phil. Trans. R. Soc. Lond. A **362 (**2004) 2223.
7. P. Ball, *Made to measure: new materials for the 21st century*, USA: Princeton University Press, 1997.
8. M. Terrones, A. Jorio, M. Endo, Y.A. Kim, T. Hayashi, H. Terrones, J-C. Charlier, G. Dresselhaus and M.S. Dresselhaus, Mater. Today **7** (2004) 30.
9. Melissa Paradise, Tarun Goswami, Carbon nanotubes - Production and industrial applications, Materials and Design **28** (2007) 1477.
10. J.K. Ong, N.R. Franklin, C. Zhou, M.G. Chapline, S. Peng, K. Cho, H. Dai, Science **287** (2000) 622.
11. S.J. Tans, R.M. Verschueren, C. Dekker, Nature **393** (1998) 49.
12. J.M. Planeix, N. Coustel, B. Coq, V. Brotons, P.S. Kumbhar, R. Dutartre, P. Geneste, P. Bernier, P.M Ajayan, J. Am. Chem. Soc. **116** (1994) 7935.
13. C.N.R. Rao, A.K. Cheetham, J. Mater. Chem. **11** (2001) 2887.
14. S. Iijima, Nature **354** (1991) 56.

15. H. Zeng, L. Zhu, G. Hao, R. Sheng, Carbon **36 (**1998) 259.
16. Z.J. Shi, Y.F. Lian, X.H. Zhou, Z.N. Gu, Y. Zhang, S. Iijima, L. Zhou, K.T. Yue**,** Carbon **37 (**1999) 1449.
17. A. Thess, R. Lee, P. Nikolaev, H. Dai, P. Petit, J. Robert, C. Xu, Y.H. Lee, S.G. Kim, A.G. Rinzler, D.T. Colbert, G.E. Scuseria, D. Tombnek, J.E. Fischer, Science **273** (1996) 483.
18. (a) V.O. Nyamori, N.J. Coville, Organometallics **26** (2007) 4083; (b) D. Jain, A. Winkelm, R. Wilhelm, Small **2** (2006) 752; (c) J. Liu, M. Shao, Q. Xie, L. Kong, W. Yu, Y. Qian, Carbon **41** (2003) 2101; (d) M. Laskoski, W. Steffen, J.G.M. Morton, M.D. Smith, U.H.F. Bunz, J.Am. Chem. Soc. **124** (2002) 13814; (e) B.El Hamaoui, L. Zhi, J. Wu, U. Kolb, K. Müllen, Adv. Mater. **17** (2005) 2957; (f) L. Zhi, T. Gorelik, R. Friedlein, J. Wu, U. Kolb, W.R. Salaneck, K. Müllen, Small **1** (2005) 798; (g) J. Wu, B. El Hamaoui, J. Li, L. Zhi, U. Kolb, K. Müllen, Small **1** (2005) 210; (h) S. Liu, X. Tang, Y. Mastai, I. Felner A. Gedanken, J. Mater. Chem. **10** (2000) 2502; (i) C. Wu, X. Zhu, L. Ye, C. OuYang, S. Hu, L. Lei, Y. Xie, Inorg.Chem. **45** (2006) 8543; (j) P.I. Dosa, C. Erben, V.S. Iyer, K.P.C. Vollhardt, I.M. Wasse, J. Am. Chem. Soc. **12**1 (1999) 10430.
19. D.C. Li, L. Dai, S. Huang, A.W.H. Mau, Z.L. Wang, Chem. Phys. Lett. **316** (2000) 349.
20. E. Couteau, K. Hernadi, J.W. Seo, L. Thiên-Nga, Cs. Mikó, R. Gaá1, L. Forró, Chem. Phys. Lett. **378 (**2002) 9.
21. H. Kathyayini, N. Nagaraju, A. Fonseca, J.B. Nagy, J. Mol. Catal. **223 (**2004) 129.
22. M.C. Bahome, L.L. Jewell, D. Hildebrandt, D. Glasser, N.J. Coville, Appl. Catal. A: General **287 (**2005) 60.
23. J. Cheng, X. Zhang, Z. Luo, F. Liu, Y. Ye, W. Yin, W. Liu, Y. Han, Mater. Chem. Phys. **95 (**2006) 5.
24. A. Magrez, J.W. Seo, V.L. Kuznetsov, L. Forró, Angew. Chem. Int. Ed. **46** (2007) 441.
25. S.D. Mhlanga, K.C. Mondal, R. Carter, M.J. Witcomb, N.J. Coville, S. Afr. J. Chem. 62 (2009) 67.

26. E. Dervishi, Z. Li, A.R. Biris, D. Lupu, S. Trigwell, A.S. Biris, Chem. Mater. **19** (2007) 179.
27. T.C. Schmitt, A.S. Biris, D.W. Miller, A.R. Biris, D. Lupu, S. Trigwell, Z.U. Rahman, Carbon **44 (**2006) 2032.
28. C.H. See, A.T. Harris, Particle Tech. Fluidization **54 (**2008) 657.
29. A. Eftekhari, P. Jafarkhani, F. Moztarzadeh, Carbon **44** (2006) 1298.
30. B.H. Liu, J. Ding, Z.Y. Zhong, Z.L. Dong, T. White, J.Y. Lin, Chem. Phys. Lett. **358** (2002) 96.
31. A. Sazbo, A. Mehn, Z. Konya, A. Fonseca, J.B. Nagy, Phys. Chem. Commun. **6** (2003) 40.
32. Aldrich Chemical Company, Handbook of Fine Chemicals, South Africa, 2007/2008.
33. M. Escobar, M.S. Moreno, R.J. Candal, M.C. Marchi, A. Caso, P.I. Polosecki, G.H. Rubiolo, S. Goyanes, Appl. Surf. Scie. **254** (2007) 251.
34. (a) T. Luo, L. Chen, K. Bao, W. Yu, Y. Qian, Carbon **44** (2006) 2844; (b) Y. Xiong, Y. Xie, X. Li, Z. Li, Carbon **42** (2004) 1447; (c) H. Nishino, R. Nishida, T. Matsui, N. Kawase, I. Mochida, Carbon **41** (2003) 2819; (d) T. Zhao, Y. Liu, J. Zhu, Carbon **43** (2005) 2907.
35. Z.C. Kang, Z.L. Wang, J. Phys. Chem. **100** (1996) 5163.
36. http://en.wikipedia.org/wiki/Flame_retardants (accessed on 10th June 2008).
37. U.M. Graham, R.A. Khatri, A. Dozier, N.J. Coville, M.C. Bahome, L.L. Jewell, B.H. Davis, Prepr. Pap. - Am. Chem. Soc., Div. Fuel Chem. **52** (2007) 364.
38. X.Z. Jin, C. Gao, W.K. Hsu, A. Huczko, M. Bustrzejewski, M. Rue, C.Y. Lee, S. Acquah, H. Kroto, D.R..M. Walton, Carbon **43** (2005) 1944.

Chapter 8

The effect of reagent residues on the stability and structure of CVD carbon nanotubes[#]

8.1 Introduction

Pure carbon is known to exist in various forms including diamond, graphite, fullerenes and carbon nanotubes (CNTs). CNTs, which exist as single, double and multiwalled are known to be the strongest materials, in terms of their tensile strength and elastic modulus. Due to their outstanding mechanical and unique electronic properties, CNTs are now being tested and applied in catalysis as catalyst supports, as fillers in nanocomposite materials, in nanoelectronic devices, in energy devices, in chemical and biochemical sensors, as transport devices, in fuel cells and in many more applications [1-10].

CNTs can be synthesized using arc discharge [11,12], laser ablation [13], high pressure autoclave procedures [14a] and catalytic chemical vapour deposition (CCVD) methods [14b]. The latter method is the most widely used due to its ability to produce CNTs cheaply and in large scale. The synthesis involves the use of a support; thus removal of the support after CNT synthesis is required. The materials produced via the CCVD process contain less amorphous material than those obtained from other methods. Further, the CVD method can produce CNTs that are covered by reagent residues that can degrade the quality of the CNTs. Support materials have to be removed from the CNTs produced by the CCVD method. To overcome the issue of support material removal, we have chosen to use $CaCO_3$ over other materials such as silica, alumina, titania etc because it can readily be removed in dilute acids [15-19].

[#]*Sabelo D. Mhlanga, Neil J. Coville, Journal of Nanoscience and Nanotechnology, submitted, 2009.*

Since 2003 [20], the number of studies reporting the synthesis of CNTs using $CaCO_3$ as a support has been increasing at a fast rate [21-29] and most of the factors affecting the CNT growth have been considered in these studies. Such factors include:

(i) The catalyst properties such as the type of catalyst (monometallic and bimetallic), the catalyst precursor, the support and the concentration of catalyst on the support.
(ii) The CVD synthesis conditions such as carbon source, carrier gas, temperature, pressure, carbon to metal ratio, gas flow rates, amount of substrate, and reaction/synthesis time.

No reports have focussed on the effect of synthesis time on the CNT morphology [29]. In this study the issue of carbon build up on the CNTs as a function of time was investigated. The long CNTs were observed to become short fragments after increase in synthesis time. Herein we report on the possible causes that generate these CNT fragments.

8.2 Experimental

8.2.1 Carbon nanotubes synthesis

CNTs were synthesized by the decomposition of acetylene (C_2H_2) (Afrox, 99% purity) in a tubular quartz reactor that was placed horizontally in a furnace [20,30]. The furnace was electronically controlled such that the heating rate, reaction temperature and gas flow rates could be accurately maintained as desired. The catalyst was loaded into a quartz boat (120 mm × 15 mm) at room temperature and the boat was placed in the centre of the quartz tube. The furnace was then heated at 10°C/min while N_2 was flowing over the catalyst at 300 ml/min. Once the temperature had reached 700°C, the N_2 flow rate was reduced to 240 ml/min and C_2H_2 was introduced at a constant flow rate of 90 ml/min. After some time, the C_2H_2 flow was stopped and the furnace was left to cool down to room temperature under a continuous flow of N_2 (40 ml/min). The boat was then removed from the reactor and weighed to quantify the amount of CNTs that had been synthesized.

All reactions were carried out at atmospheric pressure in the absence of oxygen. The CNTs were purified by stirring them in dilute HNO_3 for 12 h at room temperature, washed repeatedly with distilled water until the pH was about 7. The treated CNT samples were then dried in an oven at 120°C for 2 h.

The procedure used above was also used to synthesize CNTs using silica gel [30], Al_2O_3 [30], and a $CaCO_3$-$Ca_3(PO_4)_2$ support [31]. The floating catalyst method was used to synthesize undoped [32] and nitrogen doped CNTs [33]. Hydrofluoric acid was used to remove support material from CNTs synthesized over the silica support and nitric acid for all other support materials.

8.2.2 Heat treatment studies

The effect of deposited reactant material on CNT synthesis was examined by performing 'heat treatment experiments' on several carbon materials under the CNT synthesis conditions described in the experimental section but over extended reaction times (1 to 12 h). Since Ca, CaO, O_2 and Co-Fe oxides were identified in the final product of the CNTs by various elemental analysis techniques, their effect on CNT morphology was investigated. These materials shall henceforth be referred to as *impurities* in this study.

In order to monitor weight loss and thermal stability, all the experiments were performed in a thermal analysis instrument (Pyris 1 TGA analyzer). The experiments were carried out under a continuous flow of nitrogen (40 ml/min). A summary of the carbon materials used and the procedure followed in performing the heat treatment experiments is shown in **Scheme 8.1**. A typical method used for the heat treatment studies in the TGA was as follows: (i) hold for 1 min at ambient temperature (*ca.* 25°C), (ii) heat from 25°C to 700°C @ 10°C/min, (iii) hold for t minutes @ 700°C (t = 60, 360, 720 min.), (iv) cool to room temperature for electron microscopy and other analysis.

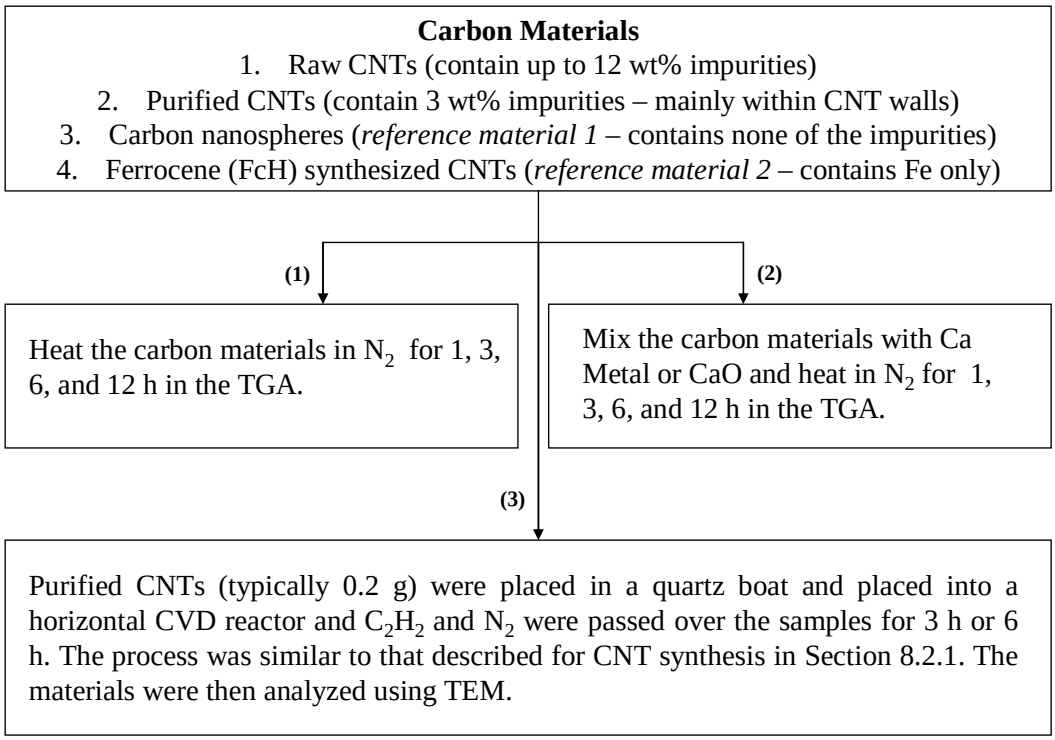

Scheme 8.1: A summary of the procedure used in performing heat treatment experiments on various carbon materials.

8.2.3 Use of excess carbon

The effect of depositing excess carbon on a range of differently prepared CNTs was studied. The CNTs synthesized by different methods were purified by acid treatment until no more impurities could be removed. The following CNTs were used in the study:

(i) CNTs synthesized over Fe-Co/$CaCO_3$ (substrate CVD method).

(ii) CNTs synthesized over Fe-Co/Silica (substrate CVD method).

(iii) CNT coils synthesized over Fe-Co-In/Al_2O_3 (substrate CVD method).

(iv) CNTs synthesized using FcH/toluene (floating catalyst method).

(v) CNTs synthesized using FcH/triethylamine/toluene (N-doped CNTs) (floating catalyst method).

(vi) CNTs synthesized using Fe-Co/$CaCO_3$-$Ca_3(PO_4)_2$ (substrate CVD method).

The CNTs were synthesized for not longer than 30 min; thus they possessed small outer diameters in the range 20 - 80 nm and lengths within the millimetre range. The CNTs (typically 100 mg) were then placed in a quartz boat and acetylene (90 ml/min) and nitrogen (240 ml/min) were simultaneously introduced over the materials at 700°C for 3 h. The experimental conditions were kept similar to the usual CNT synthesis procedure described in the experimental section.

8.2.4 Characterization of CNTs

The raw and purified CNTs had the appearance of black soot and were characterized by transmission electron microscopy (TEM) (JEOL 100S Electron Microscope and a Philips CM200 equipped with a Gatan Imaging Filter for higher magnifications), energy dispersive X-ray spectroscopy (EDX), BET surface area analysis (Micromeritics TriStar Surface Area and Porosity Analyzer), thermogravimetric analysis (TGA) (Perkin Elmer Pyris 1 TGA), Raman spectroscopy (Jobin-Yvon T64000 micro-Raman spectrometer), X-ray photoelectron spectroscopy (XPS) (Physical Electronics Quantum 2000) and powder X-ray diffraction (PXRD) (Bruker axs D8 Advance PXRD) techniques. Further details can be found in reference [30].

8.3 Results and Discussion

8.3.1 Effect of synthesis time

The effect of synthesis time on CNT yield and diameters has been briefly mentioned in earlier studies [29,30]. The CNT yield increases with increase in synthesis time. TEM analysis revealed that while the yield increased with time, so did the outer diameter of the CNTs. The outer diameter of the CNTs increased from 15 nm (5 min synthesis time) to about 300 nm (6 h synthesis time). Thus the outer diameters could be controlled by varying the synthesis time. The inner diameter remained the same (~10 nm) throughout the synthesis period [30].

The tubes do not only become bigger in size with time, but they broke into smaller pieces ('fragments'). Such *fragmentation* of CNTs synthesized over the $CaCO_3$ substrate has not been reported previously. No chemical reaction is likely to occur during the synthesis because of the inert conditions used.

It is generally believed that CNTs are one of the strongest and stiffest materials known, in terms of their tensile strength and elastic modulus respectively [34]. This strength results from the covalent sp^2 bonds formed between the individual carbon atoms as similarly observed in graphite. For example, a MWCNT was tested to have a tensile strength of 63 GPa by Yu and co-workers (2000) [34]. In comparison, high-carbon steel has a tensile strength of approximately 1.2 GPa. In addition CNTs have a very high elastic moduli of 1 TPa magnitude [35].

High resolution scanning tunnelling electron microscopy (HRSTEM) studies of the CNTs synthesized over $CaCO_3$ using similar procedures to those discussed here have shown that the CNTs contain small amounts of calcium, oxygen and catalyst (Fe/Co) nanoparticles in the CNT wall structure [36]. The carbon signal revealed the presence of nanosized channels or "docking stations" that were oriented on the CNT structure (Fig. 8.1). These docking stations were associated with interactions between carbon and calcium [36].

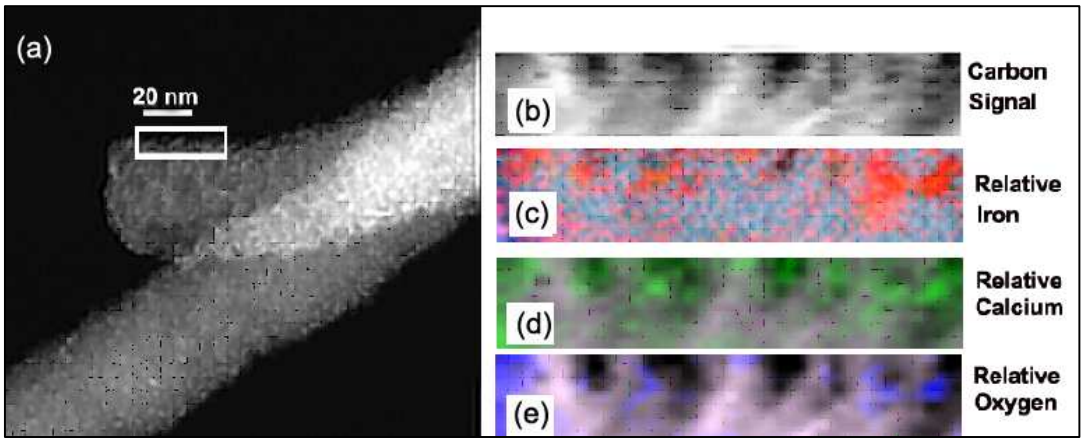

Fig. 8.1: (a) HRSTEM of two CNTs with catalyst in docking stations; (b) carbon signal shows presence of docking stations; (c) Fe-nanoparticles inside docking stations; (d) Ca-nanoparticles lining docking stations; (e) relative oxygen signal on CNT surface [36].

Elemental analyses of the CNTs using XPS (detection limit = 0,1 at%) revealed that the wall structure of the raw CNTs contain C (96.3%) and O (3.3%). PXRD analysis of the TGA residue (done in air) of the raw CNTs revealed the presence of CaO and $CoFe_2O_4$ particles. The HRSTEM and TGA analyses indicated that the raw CNTs were mixed with CaO and Fe-Co oxides that not all the residues could be removed using a dilute acid wash. A TGA profile of purified CNTs revealed the presence of small quantities and Co-Fe that could not be removed after a wide range of acid treatments. These materials are believed to be embedded within the graphite walls of the CNTs or in the inner tubes.

8.3.2 Effect of impurities on the fragmentation of the CNTs

The effects of the impurities on the CNT quality was achieved by performing heat treatment experiments on various carbon materials under similar CNT synthesis conditions, and over extended reaction times (see section 8.2.2). Fig. 8.2 gives the TGA profiles of a range of carbon materials heated in air (40 ml/min). The profiles enabled the quantification of the impurities in both the purified and raw samples. The raw and purified $CaCO_3$ synthesized CNTs decomposed at ~ 600°C. As expected the raw CNTs contained a higher amount of impurities (~ 12%).

The purified CNTs contained 4 - 6% impurities in the range that could not be removed even after extended acid treatment. The FcH synthesized CNTs before and after purification, decomposed at 500 and 550°C respectively and contained about 12% and 5% impurity (mainly Fe). Carbon nanospheres decomposed completely (0% residue) over a temperature range of 600 - 700°C. This suggested that the carbon nanospheres contained pure carbon. The slow decomposition was ascribed to the thickness of the carbon layers that make up the sphere, which includes some oxidation debris on the surface of the sphere.

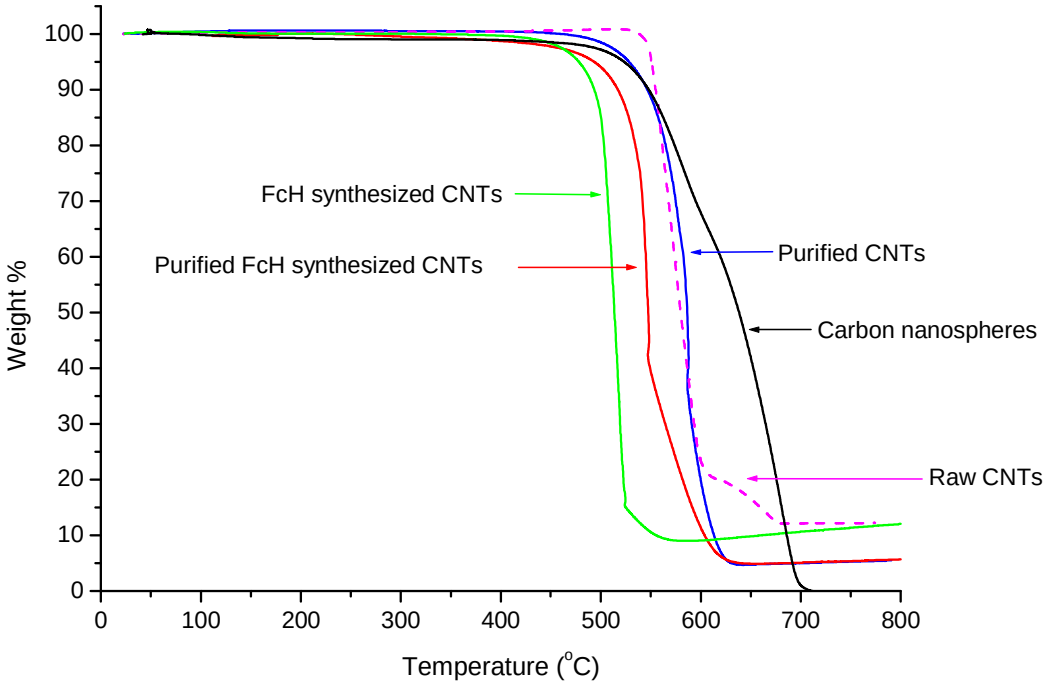

Fig. 8.2: TGA profiles of carbon materials performed in air.

The thermal stability graphs of four of the carbon materials (given in Scheme 8.1) heated up to 12 h at 700°C in N_2 are given in Fig. 8.3. The materials show some decomposition with time (Fig. 8.2a). The small % weight loss observed was attributed to the removal of some oxidation debris as well as removal of small amounts of oxygen that was detected on the carbon materials. The 16% weight loss for the purified CNTs was ascribed to loss of surface functional groups on the surface of the CNTs resulting from the acid treatment. After the heat treatment, the materials were however quite stable and no fragmentation of the structure was observed under TEM (Fig. 8.3b-e). The TEM analysis also showed no pitting or disintegration of the CNTs. The presence of Fe nanoparticles (from the FcH synthesized CNTs) suggested that the metal particles do not play a role in the fragmentation of the CNTs.

Small amounts (5 mg) of the carbon materials (given in Scheme 1) were homogeneously mixed with Ca or CaO (5 mg) using a pestle and mortar and transferred to the TGA sample pan. Heat treatment experiments were then performed on these mixtures (as above). Again, no effect on the CNT structure was observed except for a small weight

loss from the materials. TGA was performed on the Ca metal and CaO under N_2 in separate experiments so that any weight loss resulting from them could be accounted for. The results obtained also suggest that the impurities present did not affect the CNT structure; no fragmentation and further pitting of the CNTs was observed. A reaction between carbon and CaO (or Ca) is known to occur at very high temperatures, much higher than the temperature used in this study [37].

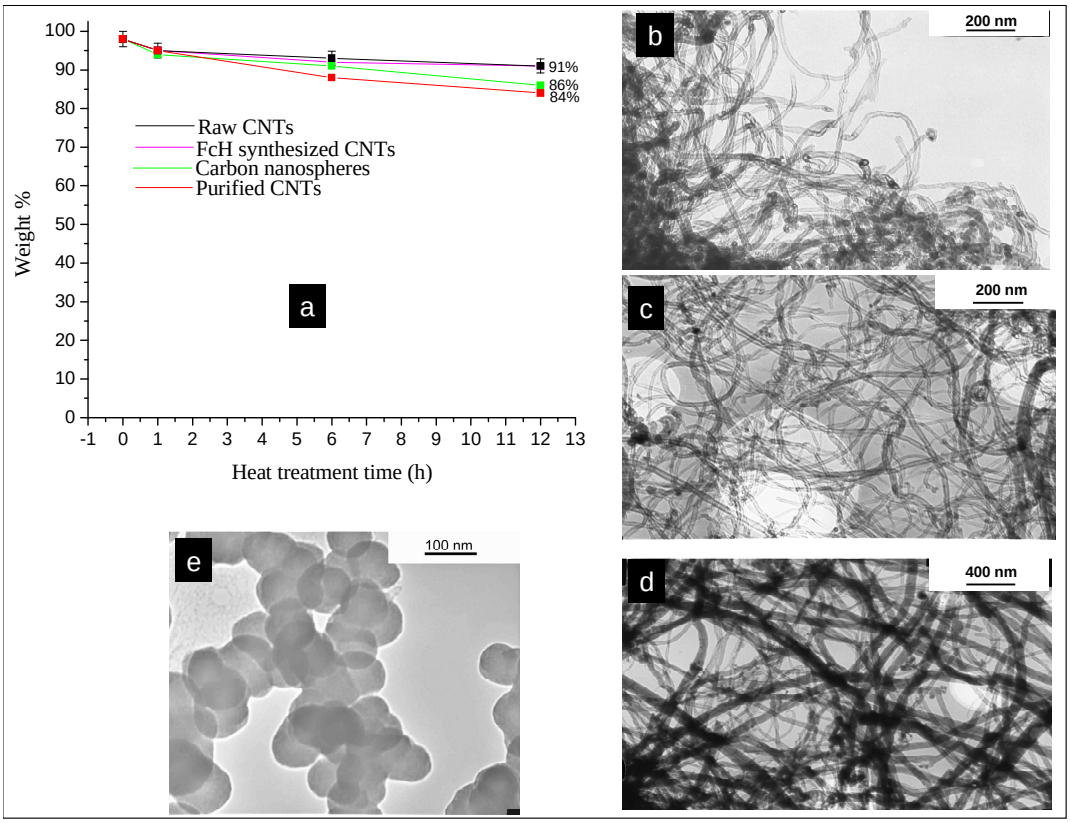

Fig. 8.3: (a) Thermal stability graphs of various carbon materials in N_2 after heat treatment for different times and TEM images of the materials after heat treatment (b) raw CNTs, (c) purified CNTs, (d) FcH CNTs, and (d) carbon nanospheres.

8.3.3 Effect of excess carbon deposition

To our knowledge there are no reports in the literature in which CNTs have been reported to be broken by the procedures described here, although there is precedent for carbon deposition on fibres and tubes [38,39]. Yu and co-workers observed the breaking of

MWCNTs under tensile load using a SEM. The study revealed that MWCNTs broke in the outermost layer ("sword-in-sheath" failure), and the tensile strength of this layer ranged from 11 to 63 gigapascals for the set of 19 MWCNTs that were loaded. Analysis of the stress-strain curves for individual MWCNTs indicated that the Young's modulus *E* of the outermost layer varied from 270 to 950 GPa [40].

It is evident that the breaking of the CNTs requires the application of enormous tensile strength. However, in this study, breaking of CNTs occurred under normal CVD conditions after extended synthesis times. Observations from the heat treatment experiments and TEM analysis suggest that the CNTs break into smaller pieces when they become bigger. The increase in size of the CNTs is due to the deposition of excess carbon. It has been shown from GC/FID and GC/MS analysis that with time the decomposition of hydrocarbons in CNT formation decreases as a result of the exhaustion of the catalyst particles [27].

TEM analysis revealed that as C_2H_2 was passed over the CNTs for 3 h, carbon was continuously deposited on the CNTs. In all the samples studied, the CNTs broke into smaller pieces as shown by the TEM images taken after 3 h (Fig. 8.3 and 8.5). The outer diameters of the CNTs also increased dramatically. The time for the study was chosen to be 3 h as all the tubes break when $t > 2$ h. Indeed this suggests that the breaking of the tubes is not caused by any reagent residues, but rather it is due to the deposition of excess carbon. The orientation of the CNTs i.e. whether randomly oriented in a spaghetti-like fashion (Fig. 8.4a,b), coiled (Fig. 8.4c), or arranged in straight bundles (Fig. 8.5b) did not have a significant effect on the breaking of the tubes. All the tubes were broken.

It can be seen from the TEM that the CNT fragments were not of specific length; a variation in the lengths was observed. Some of the fragments were as short as 100 nm while others were up to 800 nm. This observation is subject for further and could require more advanced techniques to explain.

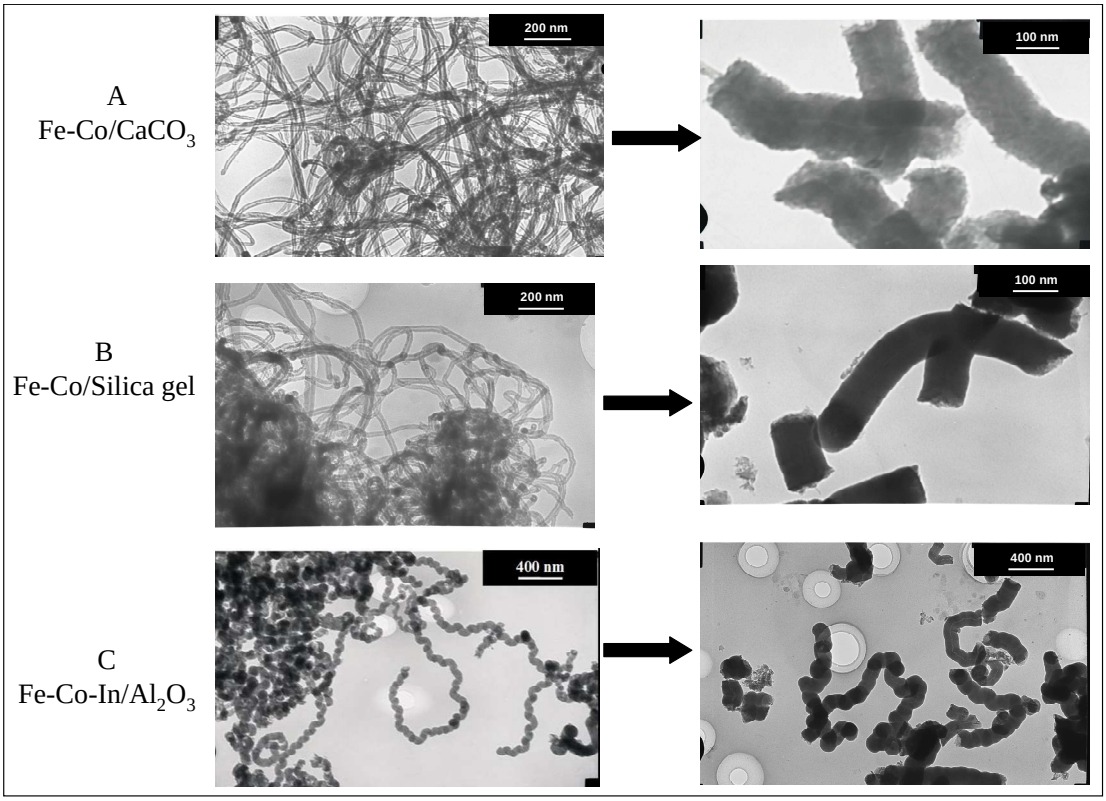

Fig. 8.4: TEM images of substrate CVD synthesized CNTs before (left) and after (right) a C_2H_2/N_2 mixture was passed over them for 3 h and 700°C.

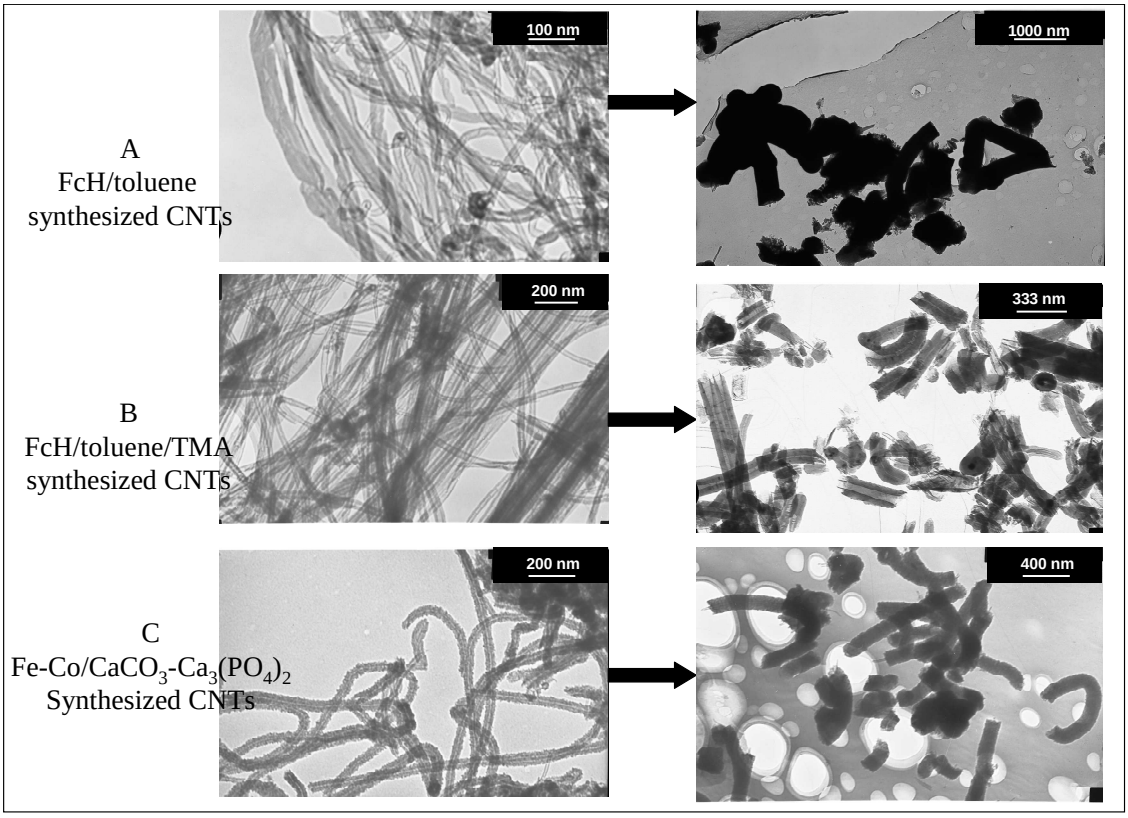

Fig. 8.5: TEM images of floating catalyst synthesized CNTs before (left) and after (right) a C_2H_2/N_2 mixture was passed over them for 3 h and 700°C.

The addition of carbon onto a tube is by deposition from the gas phase. This is identified by HRTEM as the appearance of flake-like structures. There is a distinctive change in the tube morphology that occurs when the carbon is deposited (Fig. 8.6a). The addition of the carbon will cause strain on the underlying tube. If the tube has defects, the defects will provide a point of tube rupture (points 1 and 2 in Fig. 8.6b). This rupture then leads to tube fragmentation. The results have important consequence for CNT studies and especially for the intrinsic properties of MWCNTs containing carbon residues. Further studies to explore this interesting phenomenon are in progress. The mechanism for the breaking of the CNTs is still subject to further research.

It was observed that the inner tubes are more crystalline with a more ordered arrangement of the graphite sheets (see circled regions). The entire width of the inner tubes is ~ 15 -

20 nm and it is a typical size observed when CNTs are synthesized for a shorter period of time (e.g. 5 - 30 min.) Indeed this suggest that CNTs synthesized for shorter times will have less defects that those synthesized over a longer period of time. With time carbon is deposited on the underlying tubes as described above forming an amorphous compact layer which results in the tube fragmentation as explained above.

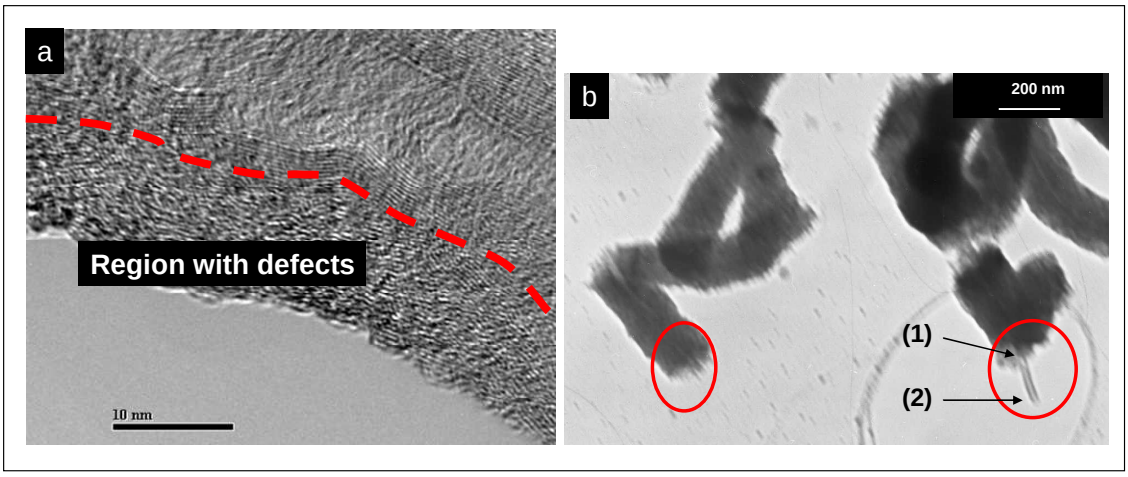

Fig. 8.6: (a) A HRTEM image of CNTs synthesized over Fe-Co/$CaCO_3$ showing the defects on the outer walls of the CNT, (b) low resolution TEM image of the CNTs showing CNT fragments and their points of rupture and (c) a HRTEM of the circled region in (b).

8.4 Conclusion

It has been shown in this study that MWCNTs can be broken into small fragments by the deposition of carbon on the tubes. Reagent residues from the CNT synthesis procedure did not cause the breaking and disintegration of the CNTs. Different CNTs (straight, coiled and randomly oriented) that were synthesized via different methods were all broken deposition of excess carbon. A common mechanism for CNT fragmentation is thus apparent.

8.5 References

1. M.S. Dresselhaus, G. Dresselhaus, P. Avouris, *Carbon nanotubes: synthesis, structure, properties, and applications*, Springer: Berlin, 2001.
2. P.J.F. Harris, *Carbon nanotubes and related structures: new materials for the twenty-first century*, Cambridge University Press: Cambridge, U.K.; New York, 2001.
3. B.M. Endo, T. Hayashi, Y.A. Kim, M. Terrones, M.S. Dresselhaus, Phil. Trans. R. Soc. Lond. A **362** (2004) 2223.
4. P. Ball, *Made to measure: New materials for the 21st Century*, Princeton University Press: USA, 1997.
5. M. Terrones, A. Jorio, M. Endo, Y.A. Kim, T. Hayashi, H. Terrones, J-C. Charlier, G. Dresselhaus, M.S. Dresselhaus, Mater. Today **7** (2004) 30.
6. M. Paradise, T. Goswami, Materials and Design **28** (2007) 1477.
7. J.K. Ong, N.R. Franklin, C. Zhou, M.G. Chapline, S. Peng, K. Cho, H. Dai, Science **287** (2000) 622.
8. S.J. Tans, R.M. Verschueren, C. Dekker, Nature **393** (1998) 49.
9. J.M. Planeix, N. Coustel, B. Coq, V. Brotons, P.S. Kumbhar, R. Dutartre, P. Geneste, P. Bernier, P.M. Ajayan, J. Am. Chem. Soc. **116** (1994) 7935.
10. C.N.R. Rao, A.K. Cheetham, J. Mater. Chem. **11** (2001) 2887.
11. H. Zeng, L. Zhu, G. Hao, R. Sheng, Carbon **36 (**1998) 259.
12. Z.J. Shi, Y.F. Lian, X.H. Zhou, Z.N. Gu, Y. Zhang, S. Iijima, L. Zhou, K.T. Yue, Carbon **37** (1999) 1449.
13. A. Thess, R. Lee, P. Nikolaev, H. Dai, P. Petit, J. Robert, C. Xu, Y.H. Lee, S.G. Kim, A.G. Rinzler, D.T. Colbert, G.E. Scuseria, D. Tombnek, J.E. Fischer, Science **273** (1996) 483.
14. (a) V.O. Nyamori, N.J. Coville, Organometallics **26** (2007) 4083; (b) D.C. Li, L. Dai, S. Huang, A.W.H. Mau, Z.L. Wang, Chem. Phys. Lett. **316** (2000) 349.
15. K. Hernadi, A. Fonseca, J.B. Nagy, D. Bernaerts, J. Riga, A. Lucas, Synthetic Metals **77** (1996) 31.
16. K. Hernadi, Z. Kónya, A. Siska, J. Kiss, A. Oszkó, J.B. Nagy, I. Kiricsi, Mat. Chem. & Phys. **77** (2002) 536.

17. A.L. Balch, M.M. Olmstead, Chem. Rev. **98** (1998) 2123.
18. K. Hernadi, A. Fonseca, J.B. Nagy, A. Fudala, D. Baenaerts, A. Lucas, Zeolites, **17** (1996) 416.
19. P. Francesco, Catal. Today **41** (1998) 129.
20. E. Couteau, K. Hernadi, J.W. Seo, L. Thiên-Nga, Mikó Cs., R. Gaá1, L. Forró, Chem. Phys. Lett. **378** (2002) 9.
21. H. Kathyayini, N. Nagaraju, A. Fonseca, J.B. Nagy, J. Mol. Catal. **223** (2004) 129.
22. M.C. Bahome, L.L. Jewell, D. Hildebrandt, D. Glasser, N.J. Coville, Appl. Catal. A: General **287 (**2005) 60.
23. J. Cheng, X. Zhang, Z. Luo, F. Liu, Y. Ye, W. Yin, W. Liu, Y. Han, Mater. Chem. Phys. **95 (**2006) 5.
24. A. Magrez, J.W. Seo, C. Mikó, K. Hernádi, L. Forro, J. Phys. Chem. B **109** (2005) 10087.
25. A. Magrez, J.W. Seo, V.L. Kuznetsov, L. Forró, Angew. Chem. Int. Ed. **46** (2007) 441.
26. E. Dervishi, Z. Li, A.R. Biris, D. Lupu, S. Trigwell, A.S. Biris, Chem. Mater. **19** (2007) 179.
27. T.C. Schmitt, A.S. Biris, D.W. Miller, A.R. Biris, D. Lupu, S. Trigwell, Z.U. Rahman, Carbon **44 (**2006) 2032.
28. S.D. Mhlanga, N.J. Coville, Diam. Rel. Mater. **17** (2008) 1489.
29. K.N. Patil, C.S. Solanki, Advances in Energy Research (2006) 480.
30. S.D. Mhlanga, K.C. Mondal, R. Carter, M.J. Witcomb, N.J. Coville, S. Afr. J. Chem. Accepted for publication, 2009.
31. S.D. Mhlanga, M.J. Witcomb, R.M. Erasmus, N.J. Coville, Mater. Chem. Phys. 2009. Submitted.
32. M.S. Mohlala, X-Y. Liu, J.M. Robinson, N.J. Coville, Organometallics **24** (2005) 972.
33. E.N. Nxumalo, V.O. Nyamori, N.J. Coville, J. Organometal. Chem. **693** (2008) 2942.
34. M-F. Yu, T. Kowalewski, R.S. Ruoff, Phys. Rev. Lett. **85** (2000) 1456.
35. http://en.wikipedia.org/wiki/Carbon_nanotube#_ref-24 (accessed 24-11-2008).

36. (a) U.M. Graham, R.A. Khatri, A. Dozier, N.J. Coville, M.C. Bahome, L.L. Jewell, B.H. Davis, Prepr. Pap. - Am. Chem. Soc., Div. Fuel Chem. **52** (2007) 364; (b) U.M. Graham, A. Dozier, R.A. Khatri, M.C. Bahome, L.L. Jewel, S.D. Mhlanga, N.J. Coville, B.H. Davis, Catal. Lett, DOI 10.1007/s10562-009-9866-5 (2009).
37. J.D. Lee, *Concise inorganic chemistry*, Blackwell Science Ltd: New York, 1996.
38. M. Escobar, M.S. Moreno, R.J. Candal, M.C. Marchi, A. Caso, P.I. Polosecki, G.H. Rubiolo, S. Goyanes, Appl. Surf. Scie. **254** (2007) 251.
39. M. Monthioux, H. Allouche, R.L. Jacobsen, Carbon **44** (2006) 3183.
40. M-F. Yu, O. Lourie, M.J. Dyer, K. Moloni, T.F. Kelly, R.S. Ruoff, Science, **287** (2000) 636.

Chapter 9

Carbon spheres: a literature review[#]

9.1 Introduction

The discovery of fullerenes in the mid 1980's [1] has led to an upsurge in interest in the structures and shapes of carbon containing materials, in particular when the carbons are in the 'nano' regime [2]. In the past two decades many different shaped carbon materials (SCMs) have since been synthesized and studies of their properties under different environments have also been conducted. These shaped materials include tubes and fibers, onions, spheres, horns, calabashes, flasks etc. and were reviewed in Chapter 4. In particular, carbon nanotubes (CNTs) have been extensively studied and this area has provided a strong focus for much work in the study of SCMs [3].

The other type of structure that has a long history of study and has again become a recent focus of attention is the spherically shaped carbon material. A spherical shape is the shape adopted by materials during synthesis (growth, nucleation) and is determined by considerations of energy minimization [4]. Spherically shaped carbon materials have been known for decades and their properties have been exploited in many areas (tyres, batteries, printer inks, rubbers, paints etc. [5-17] and they are produced and sold commercially by many suppliers (e.g. Cabot, Printex, Degussa, Tokai Carbon Co. Ltd. etc). Much of the early work has related to the synthesis of spheres in an oxidizing environment (e.g. in the formation of carbon blacks) and industries have been built on this approach to carbon sphere formation [18,19]. Spherically shaped carbon materials have been given many names. These include carbon balls, carbon nanospheres, carbon microbeads or nanobeads [20], carbon blacks [5-18] as well as carbon pearls [21].

[#]*A. Deshmukh, S.D. Mhlanga, N.J. Coville, this chapter is part of a full review submitted to Materials Science and Engineering Research Reviews.*

There appears to be no consistent nomenclature for naming these shaped materials; consequently we have chosen to use the generic term carbon sphere (CS) to cover all carbons that have a spherical or near spherical shape. This will not include the fullerene family of carbons.

The spherical shape is not peculiar to carbon; indeed numerous studies of spherical silica have indicated the wide range of synthetic strategies and approaches that can be used to make spherical materials [22]. A key target in making spherical materials is to ensure that they are monodisperse and that the size (diameter) and the chemical properties of the external rim can be controlled. The carbon sphere has been shown to comprise of layers of carbon that form broken concentric layers emanating from the core. CSs will be attracted to each other by van der Walls forces and lead to agglomerated collections of CSs. When CSs have diameters of less than 1000 nm they also tend to accrete i.e. bond together to form necklace or bead like structures. Thus, although CSs are normally discussed as though they are discrete, they generally form connected solid extended chains (Fig. 9.1).

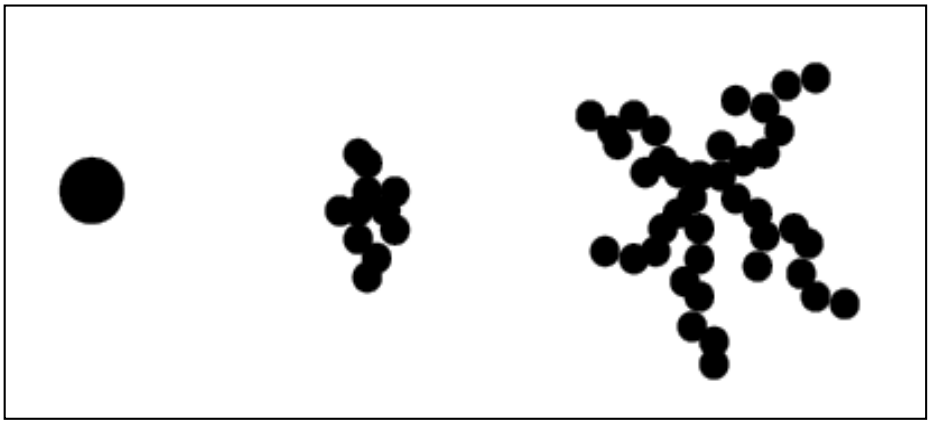

Fig. 9.1: TEM images of a discrete and a chain of connected (‘accreted’) carbon spheres.

These chains are formed early in the synthesis process and are not necessarily due to post synthesis treatments. Mechanisms that have been proposed to explain their formation are described in the review. Larger spheres can be built up from layers that are horizontal with respect to the sphere rim [23,24]. The study of carbon spheres can be categorized in

numerous different ways. Thus, spheres can be described as solid, core-shell type or hollow (Fig. 9.2) [4].

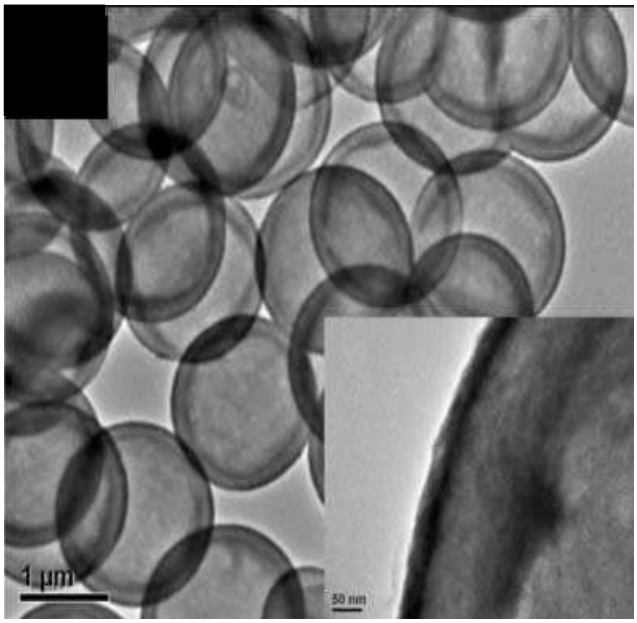

Fig. 9.2: Hollow carbon spheres [4].

Alternatively CSs can be classified according to their 'nanometric texture' i.e. in terms of whether the atoms are made of concentric, radial or random layers (Fig. 9.3) [23]. It has also been proposed that spheres can be categorized in terms of their size, in particular their diameter [25]. In this method three categories are recognized: (i) well graphitised spheres (2-20 nm), (ii) less graphitized spheres (50-1000 nm) and carbon beads (> 1000 nm). Finally it is possible to classify spheres in terms of synthetic strategies used in their synthesis. It appears that the procedures used to make spherical carbon materials (chemical vapour deposition (CVD), arc discharge, laser ablation, autoclave processes etc.) can produce quite different materials.

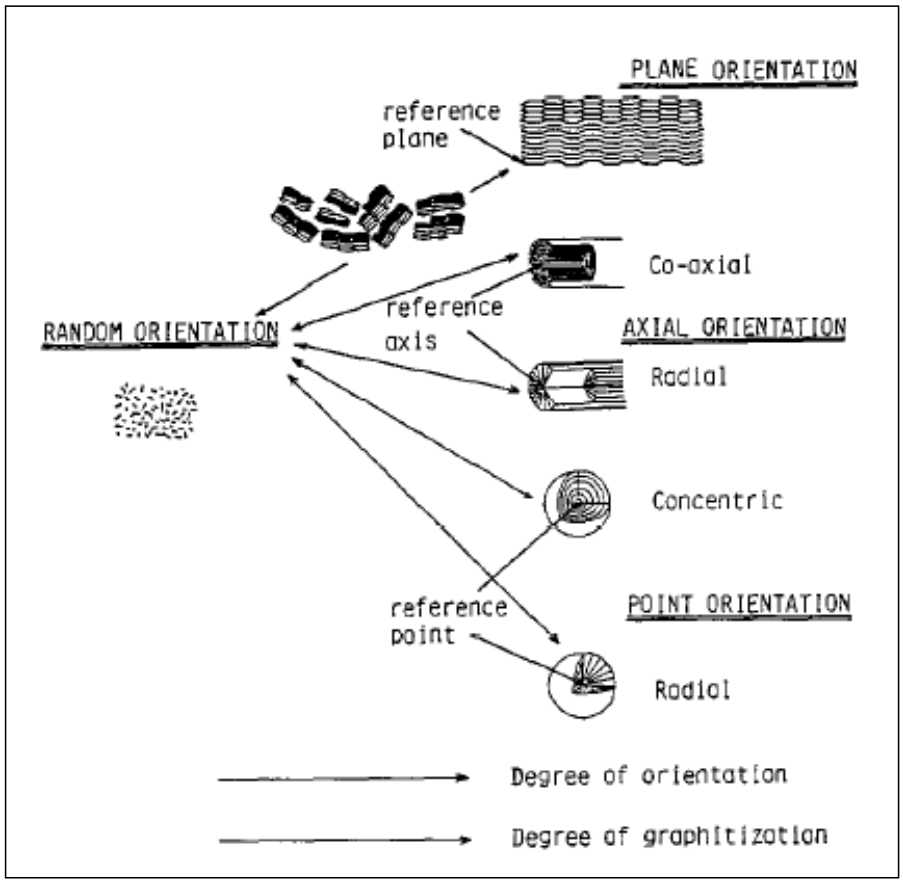

Fig. 9.3: Classification of nanometric texture in carbon materials based on the preferred orientation of the carbon layers in BSUs [23].

During the past three decades, the availability and ready access to characterization techniques at the nanometric scale (in particular scanning probe microscopy and electron microscopy techniques) have allowed a more detailed investigation of well known and novel materials. This is also true of carbon materials including CSs. A review of the area of CSs, with particular emphasis on data collected in the last three decades, is thus timely.

In this review of CSs, we have opted to categorize spheres in terms of the synthesis strategies used in their synthesis. However, the discussion and the tables accompanying the review permit an analysis of the information in terms of all the other categories mentioned above.

The literature in this area is vast as carbon materials have been made for thousands of years. It appears that carbon spheres were even formed billions of years ago as reflected by recent discoveries of their presence in meteorites [26] Early documentation reveals that carbons (as soot) were first used by humans for wall paintings [27]. The study of candle flames and the soot produced by the burning of candles has been actively studied since some early reports in the mid 1850s by Faraday [28,29]. Knowledge of the production and composition of soot is important in preserving historical and cultural artifacts that are contained in churches and chapels [28,29]. These soot particles are mainly in the form of spheres. In more recent times the products from candle soot have been collected, acid treated, separated and the components (< 2 nm spheres) have shown to possess fluorescent properties determined by their rim chemistry [30].

Most of the early work published before the 1980s focused on the synthesis and characterization of the carbon blacks (CBs) and especially their applications in industry. The production processes used to make the carbon blacks are found to be in the patent literature [31]. Thus, literature dating back to 1928 reveals that early studies were largely focused on the theories and predictions of the reinforcing properties of CBs in rubbers as well as the physical properties of CBs (adsorption, surface area and pore size measurements) [32-36].

In this review, the main focus will be on describing the synthesis of CSs. There has been an explosion of publications in this field; consequently this literature review cannot be exhaustive. It is hoped that the significant publications have been covered. The focus will also not be on studies reported prior to 1990 nor on the uses of the CSs. The CSs discussed will cover the major types: solid spheres, hollow spheres, core-shell spheres. Their diameters have been found to range from the nano to the mesoscale. The review will not cover fullerenes and their chemistry. This work can be found in numerous textbooks and reviews [37].

9.2 Synthesis of carbon spheres

The last few decades have witnessed an exponential growth in the field of carbon nanotubes worldwide and this has led (often accidentally) to the synthesis of many other shaped carbon materials (SCMs) including carbon spheres (CSs). The synthesis of these SCMs and in particular CSs can broadly be divided into two types, associated with the reaction temperature. The first procedure is based on the high temperature decomposition of carbon containing materials in an inert atmosphere (chemical vapour deposition, arc-discharge and laser ablation processes). The second procedure consists of the low-temperature pyrolysis and catalytic decomposition of organic compounds by the heat treatment of polymers or other materials, usually in an autoclave. The influence of the carbon source, oxygen, catalysts, additives, flow rates, pressure, reactor design, all play a role in influencing the properties of the synthesised CSs (surface area, chemistry, size, density etc.) formed in all the procedures.

CSs have also been synthesised in matrices by procedures that do not presently lead to their extraction and use. For example, the synthesis of spherical carbons deposited in metals such as iron, have been detected. However, their role outside of this environment has as yet not been explored. In a nutshell, CSs have been synthesized by the following processes: (i) arc discharge, (ii) plasma, (ii) chemical vapour deposition (CVD), (iv) autoclave, (v) supercritical fluids, and (vi) carbonization. In this literature review emphasis will be directed to the CVD methods, which are classified into the catalytic and non-catalytic CVD methods because they are relevant to our studies.

9.3 Chemical vapour deposition

The chemical vapour deposition (CVD) process is the one in which a volatile carbon source is converted into a solid non-volatile carbon product. The catalytic vapor phase deposition of carbon was first reported in 1959 [38]. When the process entails the use of a catalyst the process is known as catalytic chemical vapor deposition (CCVD).

The CVD process is a versatile process and many variants of the process have been used to make CSs. These processes differ in the means by which the chemical reactions are initiated (the activation process), the type of reactor used and the process conditions. Some examples are listed below:

1. Variation of operating pressure:
    a) *Atmospheric pressure CVD* (APCVD) - CVD processes at atmospheric pressure.
    b) Low-pressure CVD (LPCVD) - CVD processes at sub-atmospheric pressures. Reduced pressures tend to reduce unwanted gas-phase reactions.
    c) *Ultrahigh vacuum CVD* (UHVCVD) - CVD processes at a very low pressure, typically below 10^{-6} Pa (~ 10^{-8} torr).
2. Variation of the physical characteristics of the vapour:
    a) *Gas phase CVD*. In this process a gas is added directly to a reactor
    b) *Sublimation CVD.* A solid is converted directly into a gas for use in the CVD process.
    c) *Direct liquid injection CVD* - A CVD process in which the precursors are in liquid form (liquid or a solid dissolved in a convenient solvent). Liquid solutions are injected in a vaporization chamber. Then the precursor vapors are transported to the substrate as in a classical CVD process. This technique is suitable for use on liquid or solid precursors. High growth rates can be reached using this technique.
    d) *Aerosol assisted CVD* - A CVD process in which the precursors are transported to the substrate by means of a liquid/gas aerosol. This technique is suitable for use with involatile precursors.

In all the above procedures, the direct pyrolysis of a carbon source (either in the gas or liquid phase) is generally carried out in a quartz tube placed in an electronically controlled furnace at atmospheric pressure which may or may not contain a catalyst. Liquid carbon sources can be introduced in three ways: (i) the liquid can be injected into the hot furnace using a syringe pump, (ii) sonication or (iii) the liquid carbon source is first heated prior to the synthesis furnace and vapours are carried to the carbonization furnace with the help of an inert gas, generally nitrogen or argon. This mode of synthesis

has often been used for CVD processes used to make CNTs [39a,b]. Ensuring efficient contact between the gas phase and the growing surface in CVD processes is rarely a problem for deposition on flat substrates. Two types of reactor configurations, based on the position of the furnace, are possible; the horizontal and vertical configurations [39c].

9.3.1 Noncatalytic chemical vapour deposition

In this approach a carbon source is decomposed at high temperature in a furnace to yield CSs. This is the approach used to make industrially important CSs such as carbon black. The procedure to make CSs entails the use of oxygen to generate high surface area spheres. More recent reports on CS synthesis have focused on the generation of low surface area CSs that are produced in the absence of oxygen. A variety of parameters control the size, shape and yield of CSs. These include temperature, flow rate of carbon source and deposition time. Also of importance is the time the CSs spend in the reactor. In a vertical reactor the reaction times will be short (< 1 min) and consequently secondary reactions involving annealing of the spheres and sphere growth do not occur. In contrast, use of a horizontal reactor results in the spheres being kept at high temperatures for longer time periods (typically 15 - 60 min). The effect is that the outer shell becomes more crystalline, leading to carbon-carbon core-shell structures (Fig 9.4). Furthermore, the CS diameter increases with time on line.

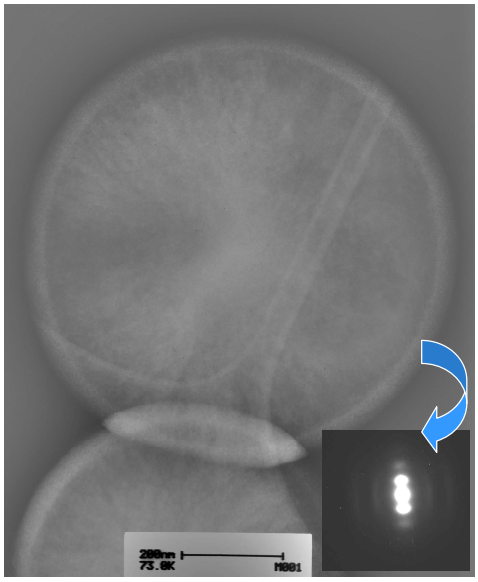

Fig. 9.4: A HRTEM image of a non catalytic CVD synthesized CS with a crystalline outer shell, leading to carbon-carbon core-shell structure [39c].

Qian *et al.* [40] reported that CSs can be produced from toluene at 1100°C using an experimental setup consisting of two furnaces. The temperature of the first furnace was kept at 200°C and was meant to vapourize the toluene injected into the furnace by means of a syringe pump. The vapours were carried to the second reactor by nitrogen and/or argon and/or hydrogen gas. The average diameter of CSs produced ranged between 60 nm and 1 µm. The effect of carrier gas, carrier gas mixtures and flow rate was studied in detail. Similarly, Aili and co-workers reported the synthesis of CSs from acetylene and toluene as carbon source at 1000°C [41]. The results showed that carbon microspheres were well graphitized while their features were undestroyed. Based on their adsorption isotherms with nitrogen, pore structures of carbon spheres were found to be changed greatly after graphitized treatments. [41]

Large scale production of CSs, with diameters ranging from 50 nm - 1 µm was achieved with different substrates such as styrene, toluene, benzene, hexane, cyclohexane and ethane (Fig. 9.5) [42]. A double furnace apparatus was used for the pyrolysis of the liquid hydrocarbons; the liquid hydrocarbon was introduced into the first furnace at 250°C. The feedstock vapor was then carried through the system by argon to the higher temperature

(900 - 1200°C) pyrolysis furnace. In this study, the effect of feed rate and reaction time on the diameters of the CSs was established.

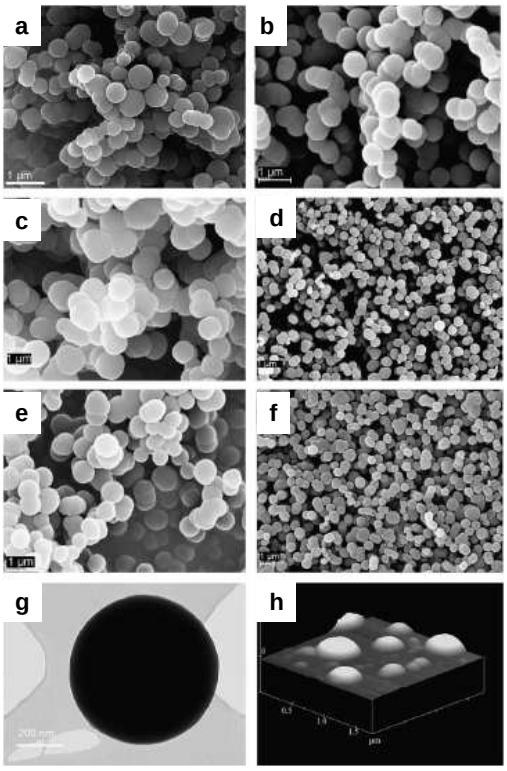

Fig. 9.5: SEM images recorded for the pyrolysis of: (a) styrene, (b) toluene, (c) benzene, (d) hexane, (e) cyclohexane; (f) ethylene; (g) typical TEM and (h) typical AFM images [42].

In recent findings from our CS synthesis studies using various sources of carbon (e.g. gases: ethylene, acetylene and liquids: pentane, isooctane, hexane, cyclohexane, benzene, toluene, heptane), it was revealed that synthesized carbon deposits were all spherical in shape with varying diameters for each hydrocarbon source. It was shown that structural properties of the hydrocarbons are regulating factors in the sphere size distribution. Hydrocarbon concentration had a less significant effect. Structural properties such as C:H ratios tend to cause an increase in sphere size with decreasing C:H ratio. Sphere size tends to increase with increasing carbon content, but decreasing linearity and branched structural isomers tended to cause a decrease in sphere size. A narrowing in size distribution was noted as the carbon hybridization changed from sp^3 to sp.

It was also revealed that the use of vertical CVD and horizontal CVD furnaces gave two divergent synthetic routes to CSs. The vertical CVD produced spheres of smaller size, decreased thermal stability and graphitization, as well as increased amorphous material content as compared to spheres prepared in the horizontal CVD process. Whether spheres prepared by vertical CVD are of greater industrial importance than spheres produced by horizontal CVD techniques remains to be probed. The vertical CVD method produces two distinct peak ranges, resulting in very small and very large spheres in the same batch.

The presence of oxygenates (alcohols) was shown to readily remove amorphous material from the surface of the carbon spheres resulting in the formation of smooth surface. The yields of the carbon spheres increased as the chain length increased from ethanol (C_1) to decanol (C_{10}) under the same experimental condition. This was largely due to the ratio of carbon and oxygen in the solvent structure. A slow injection flow rate resulted in increase in the yield, while a faster rate resulted in low yields. There exists an inverse relationship between the flow rate and the yield.

ZnSe nanoparticles were used as a template to exploit the synthesis of hollow carbon nanospheres (Fig. 9.6). Synthesis was performed under the constant flow of argon at 5 x 10^{-2} Torr. Toluene (carbon source) was injected into a horizontal furnace, containing ZnSe, at a temperature of 1100°C for 3 h. The obtained encapsulated ZnSe was removed by heating the sample at 1200°C for 60 min. Removal of the ZnSe template gave hollow CSs with a diameter range of 40 - 120 nm [43].

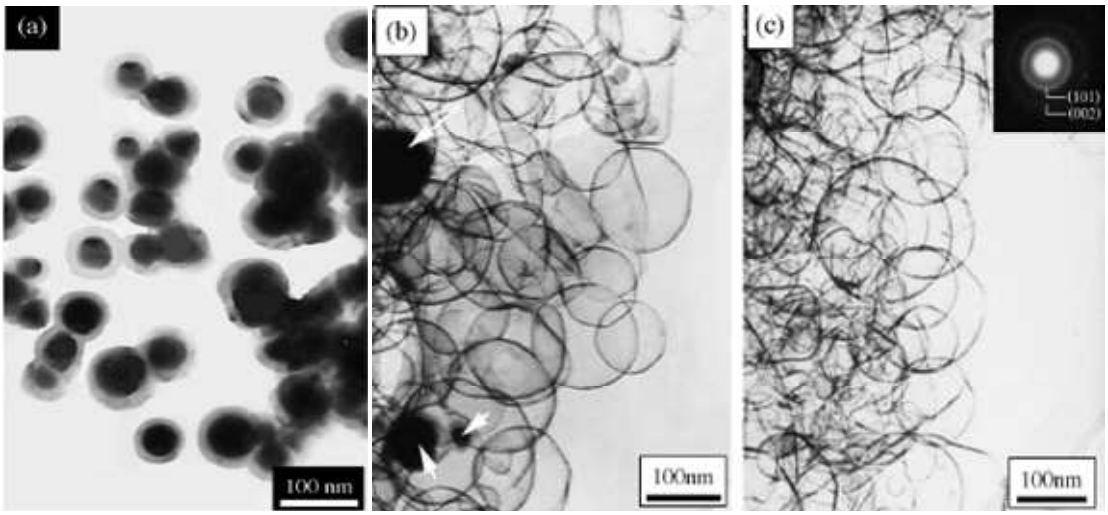

Fig. 9.6: (a) A typical TEM image of the carbon-encapsulated ZnSe nanoparticles. (b) The TEM image of the hollow carbon nanospheres obtained at 1200 ◦C for 30 min (some unconverted carbon-encapsulated ZnSe nanoparticles are shown with arrows). (c) The TEM image of the hollow carbon nanospheres obtained at 1200 ◦C for 60 min (inset is the corresponding SAED pattern of the products) [43].

A CVD method was used to make smooth single shell, deformed single shell, double shell and nitrogen doped shell carbons using silica spheres as templates and benzene as a carbon source. Before actual pyrolysis, the silica spheres were heated to 900 or 1000°C under a nitrogen atmosphere. Benzene vapors were passed over the silica spheres (4 h) placed in the centre of a quartz tube placed in the furnace, with the help of a nitrogen carrier gas. After reaction the silica spheres were dissolved away using a HF solution to generate hollow carbon spheres. The carbon coated silica spheres were dispersed in ethanol and silica was placed on the surface of the carbon-coated silica according to the procedure reported in the literature [44]. A carbon coating on the silica-carbon-silica sphere was produced by passing benzene over the spheres. The silica was removed by HF to give double shelled hollow carbon spheres **(Scheme 9.1)**. The microscopic features and shell thickness depend on the silica sphere diameter, temperature and recation time [45].

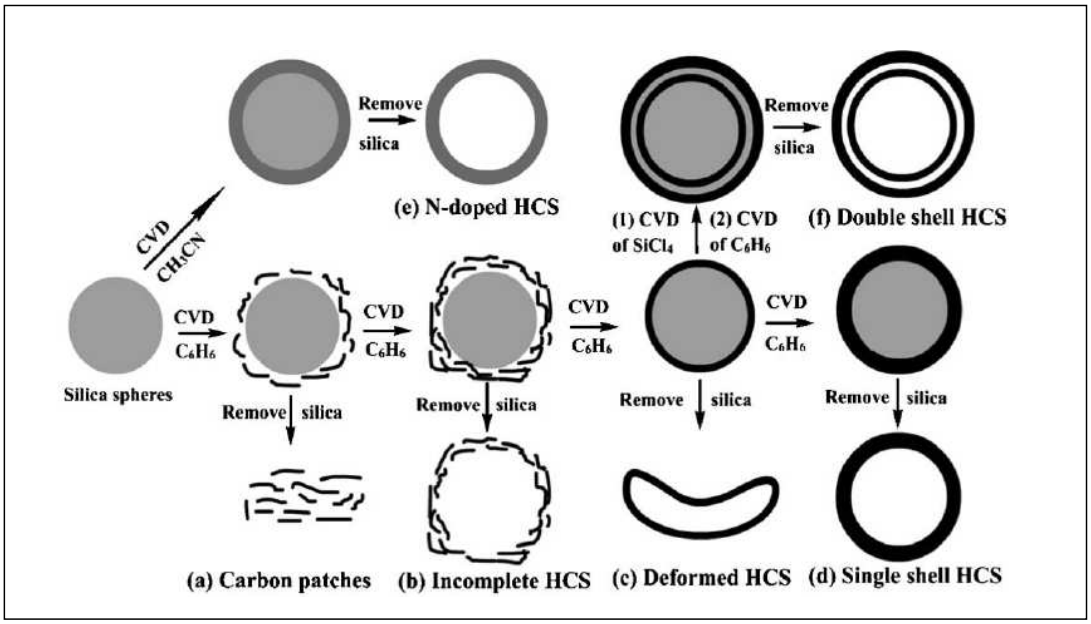

Scheme 9.1 Schematic illustration of the fabrication steps for various carbon spheres (HCSs): (a) discrete carbon patches acting as the building blocks of HCSs, (b) incomplete HCSs because of insufficient CVD time, (c) deformed HCSs prepared using large silica spheres as templates with a short CVD time, (d) intact single shell HCSs prepared with a long CVD time or a high CVD temperature, (e) N-doped HCSs prepared using acetonitrile as a carbon source, (f) double shelled HCSs prepared using a three-step CVD method: first, CVD of carbon on the surface of silica spheres; second, CVD of silicon tetrachloride on the surface of the carbon-silica spheres; third, CVD of carbon on the surface of the silica-carbon-silica spheres [45].

9.3.2 Catalytic chemical vapor deposition

This procedure represents a variation of the above non-catalytic CVD CS synthesis strategy. Many experiments have been performed to make CNTs but in the process CSs have been synthesized. Indeed it appears that the metal catalyst *plays little role* in CS synthesis in which CNTs are formed. This suggests that the metal does not play a *primary role* in CS synthesis; rather it may play the role of modifying the type of carbon radicals that are formed in the gas phase and that leads to carbon deposition to form the CSs. Clarification is, however, still needed to resolve this issue.

The various reports that have appeared in the literature on the use of catalysts in CS synthesis are described below.

Miao *et al.* [46] reported the synthesis of a large quantity of carbon spheres using Kaolin supported transition metal salts (Fe, Co, Ni, etc.) as catalysts. Aqueous solutions of transition metal salts (Co, Ni, Fe) were coated on a Kaolin catalyst surface or ceramic support in the form of a thin plate and dried at 60°C. The obtained thin layer of catalyst was placed in the ceramic boat *facing down* in the center of a quartz tube. The reactor was flushed with nitrogen until achievement of the reaction temperature. The carbon source used in this study was acetylene and the reaction temperature was 650°C. The spheres were observed to have an average diameters of 600 - 800 nm with a typical inter-layer distance of 0.33 - 0.35 nm.

A CVD synthesis method in which acetylene (as carbon source) and nitrogen were passed over nickel metal clusters (700°C) gave monodispersed CSs. The spheres were linked in a long continuous string to form a foam-like macroscopic structure. The diameter of the solid carbon spheres was 150 nm [47]. Zhong and co-workers [48] reported the preparation of carbon nanomaterials (nanotubes and spheres) by the decomposition of methane in the presence of a cobalt encapsulated catalyst. The supports used for the catalyst synthesis were aluminium, lanthanum, cerium and magnesium oxides. A detailed study using the cobalt metal supported on magnesium oxide was presented. The catalysts were prepared by a reported procedure [49]. The reaction was carried out at 600°C for one hour. After reaction the mixture was subjected to treatment with concentrated sulfuric acid to dissolve away the metallic catalyst. The diameters of the nanotubes and balls were observed to be between 10 - 40 and 50 - 200 nm respectively. The product distribution (nanotubes and balls) solely depended on the reaction conditions. The product was subjected to magnetic studies and was found to be a magnetic material.

Pradhan *et al.* [50] synthesized CNTs and beads from kerosene as carbon source in the presence of nickel and iron catalysts at 1000 and 1100°C respectively. In a typical procedure two furnaces were connected in series. The carbon source was placed in the

first furnace (held at 200°C) and a quartz boat containing the catalyst was placed in the second furnace. The temperature in the second furnace was 1000 - 1100°C. The kerosene vapour was carried to the second furnace in nitrogen gas. It was observed that Ni and Fe facilitate the growth of straight and coiled nanotubes, respectively at a temperature of 1000°C. However, with an increase of pyrolysis temperature to 1100°C, carbon nanobeads resulted in the presence of both of the catalysts [50].

Various organometallic complexes have been tested as catalysts for the synthesis of CSs. Iron complexes have been suggested to be promising candidates for the synthesis of various CSMs, including CSs, under mild experimental conditions. Sharon *et al.* [51] reported the synthesis of carbon nanobeads from the pyrolysis of camphor using ferrocene as catalyst. The synthesis was carried out in the reactor shown in Fig. 9.7; this is a variation of the two furnace system. A mixture of camphor and ferrocene, placed in the flask, was heated to 50°C and the vapour transferred to the second furnace held at 1000°C. The pyrolysis was carried out for 4 h. Spongy hollow carbon nanobeads of about 250 - 280 nm in size, covered with 80 - 100 nm thick fibrous amorphous carbon from camphor, was obtained.

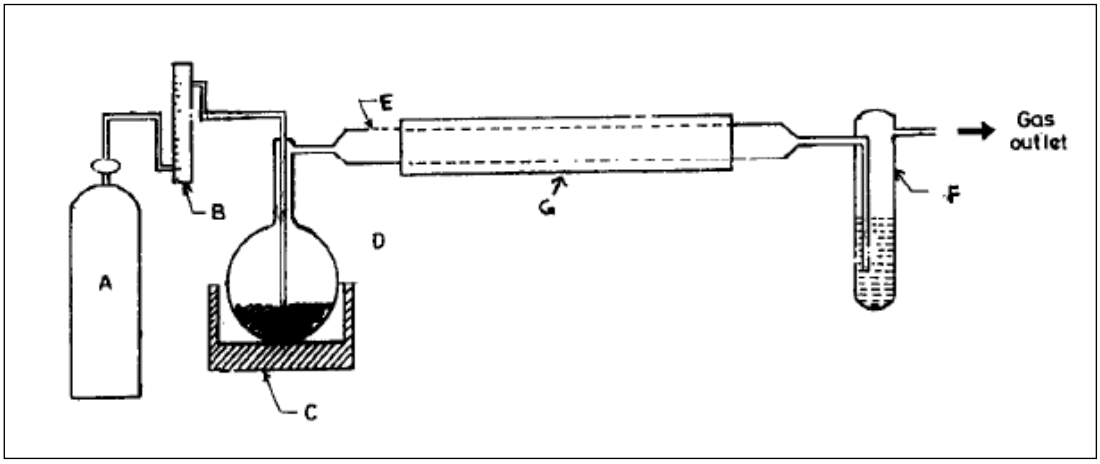

Fig. 9.7: Pyrolyzing unit to produce carbon nanobeads. A is the gas cylinder, B the flow meter, C the heating mantle, D the flask containing camphor and ferrocene mixture, E the quartz tube inside the furnace, F the water bubbler and G is the furnace [51].

Recently CSs were synthesized from varying mixtures of ferrocene and anthracene, sealed in evacuated quartz tubes placed in a furnace [52]. The pressures used were low. The temperature of the tube was raised to 500°C to achieve decomposition of the reactants after which the temperature was then raised to the 800 - 1000°C. The CS/CNT ratio increased as the temperature increased. The CS/CNT ratio was also influenced by the Fe/C ratio. The data indicated that the pyrolysis temperature and Fe/C ratio played a vital role in determining both the yields and the shape of carbons formed.

The use of mixed valence oxide catalysts (MVOCC) have also been reported for use in the synthesis of CSs in the hope that such a system would lead to easier separation of the encapsulated catalyst after carbonization [53]. The low cost process was used for the synthesis of CSs and CNTs with high purity [54]. Wang and Kang synthesized various carbon microspheres using MVOCC (transition and/or rare earth metal oxides) method using CH_4 as carbon source at 1100°C [55].

9.4 Mesoporous carbon microbeads

Another spherical form of carbon/graphite called mesoporous carbon microbeads (MCMBs) has been synthesized since the 1960's [56]. MCMBs are different from carbon blacks because they are synthesized mainly from 'pitches' which include coal-tar and petroleum derived pitches typically heat-treated at temperatures between 350 and 450°C [56-58]. The MCMBs generally have low surface areas of about 4 m^2/g and are sold commercially in particle sizes ranging from 5 to 8 µm (e.g. Osaka Gas Co. and Shanshan Co. Ltd) [59-62]. However it has been shown that MCMBs can be activated to obtain materials with very high surface areas > 2600 m^2/g [63,64].

MCMBs have recently been synthesized using other forms of pitches such as isotropic naphthalene pitches [65] as well as by the pyrolysis of polymer organic compounds [66]. Naphthalene-derived isotropic pitch was studied for the synthesis of CSs. Firstly, isotropic pitch was dissolved in quinoline, and then this solution was added into an aqueous solution of nitric acid under stirring to generate droplets. The quinoline was

extracted to avoid adhesion of the pitch particles. The dried pitch particles were oxidatively stabilized in air at 280°C for 30 min before carbonization between 600 and 900°C [67].

A water-in-oil emulsion using amphiphilic carbonaceous material (ACM) and urea were used for the synthesis of carbon nanobeads by Esumi *et al.* [68]. In a typical synthesis procedure a mixture of ACM in ammonia solution was added into heated oil to form a water-in-oil emulsion at 80°C for 1 h. The carbon nanobeads were studied using TEM and were found to have diameters in the range of 2 and 15 µm with wall thickness of 1 µm. The effect of heat treatment and urea concentration was investigated. The density of the hollow carbon microbeads decreased with increasing concentration of urea and with decrease in the heat-treatment temperature.

MCMBs have been used in various applications such as electrodes for lithium-ion batteries, conducting polymers for sensors, as filler in paints, elastomers and plastics, as adsorbants for natural gas and hydrogen, as column materials for separation science, as well as catalysts supports [56,62,63,58,69-71]. Recently CNT/MCMB composites were synthesized by in situ condensation from coal-tar pitch. The study showed that the size of samples is diminished and the microtexture of samples tends to be disordered when more CNTs are added [72].

9.5 Substituted carbon spheres

Very few studies have been reported on the doping of CSs with heteroatoms. Mondal *et al.* [74] reported the synthesis of nitrogen and boron doped CSs using acetylene and B and N sources. The experiment was carried out at atmospheric pressure in a flow reactor made of quartz tube in horizontal furnace. The temperature of the furnace was raised to the desired temperature of 800°C under the flow of inert gas. After attaining the pyrolysis temperature, acetylene was passed through the tube for 2 h. To synthesize boron or nitrogen doped spheres, acetylene gas was bubbled through methanolic solution of BF_3 or ammonia solutions. B-doping increased the disordering of the graphitic lattice and also

increased the G-band width on increasing the boron concentration, indicating the decrease of graphitization with increasing boron concentration [74].These materials were used as supports for anchoring of different transition metal, which was further utilized for the catalytic hydrogenation of ethylene.

Recent studies in our group have also focused on the synthesis of N-doped CSs using a vertical CVD reactor that enabled continuous production of the materials [74]. The N-doped CSs were characterized by CHN and XPS in order to determine the amount of nitrogen. The materials were added to polymers in order to enhance their conductivity and strength.

9.6 Chemistry of carbon spheres

The rim of a carbon sphere comprises of carbon flakes. These carbon flakes comprise of predominantly aromatic structures, made up of condensed benzene ring structures. The sp^2 carbon atoms at the edge of the flakes must contain atoms to satisfy valence requirements. These will typically be O atoms (as OH, COOH and other groups) or H atoms. This is reflected by elemental analyses and XPS data which always yield O contents of between 1 - 5% for the low surface area CSs. Further, to achieve curvature the carbon flakes must also contain C5 and C7 ring structures. Thus the chemistry of CSs will be different from that of graphite and SWCNTs, which are dominated by reactions at the graphite edges of the extended ring chains. CSs were studied for their reactivity towards different organic solvents such as HF, $KMnO_4$, CS_2, 1-methyl-napthalene, 1,2-dichlorobenzene. The spheriodal structure of CSs only changes when spheres were treated with 0.5 M $KMnO_4$ solution at 80°C [75].

Various functional groups are found in the surface of carbon black (e.g. the hydroxyl or carboxyl group). The chemistry of carbon blacks has been extensively studied. These materials are characterized by "particle size", "structure", and "surface chemistry" (Fig. 9.8). The acidic surface oxides have been the subject of many studies that have been summarized in several reviews [76-79]. The three main properties have a large effect on

practical properties such as blackness and dispersibility when they are mixed with inks, paints, or resins [76].

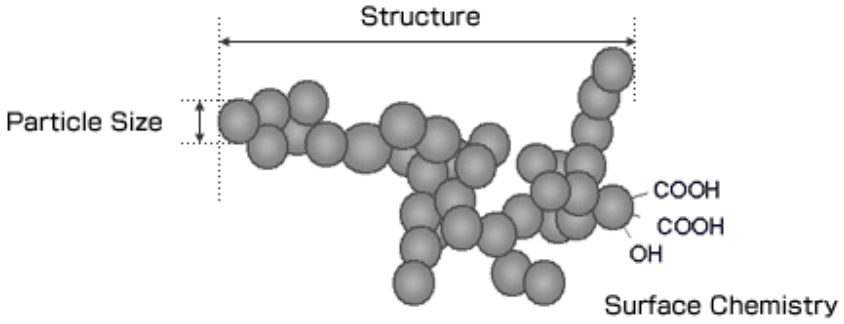

Fig. 9.8: The structure of carbon black showing some functional groups on the surface of the sphere [76].

Chemical modifications on the surface of carbon blacks has been shown to affect their performance as elastomer fillers depending on the type and amount of functional groups present and their surface areas [76,80-84]. Papirer and co-workers [81] studied carbon black reactivity by submitting the carbon blacks to a series of chemical treatments such as moderate oxidation with potassium persulfate, severe air oxidation, halogenation with chlorine or bromine, and grafting of short (ethyl, butyl, pentyl) or long (lauroic) alkyl chains in order to modify their surface properties and to compare their reactivity in relation to their atomic structure. It was observed that under similar reaction conditions, carbon blacks have different behaviours depending on their mode of preparation but they generally perform comparatively, but not to the same extent, towards a given modification procedure. Larger particles are chemically more reactive (per unit surface area) leading to higher surface coverage by oxygen, halogen and aliphatic grafts than the very fine particles of small dimensions.

The fluorination of carbon blacks was also studied by Nansé *et al.* [85]. Analysis of the XPS spectra of fluorinated carbon blacks indicated that F is fixed at the surface and in a subsuperficial layer of limited thickness and covalently bonded to C. In the furnace blacks, a minor amount of F, is trapped in micropores. When the blacks are activated (air oxidation at 450°C), the amount of fluorine fixed by the furnace and thermal blacks

increases due to a slight increase of the density of reactive sites consecutively to the development of porosity. The halogenation of carbon blacks has been reported in other studies [81b,86-88].

Surface modification of carbon blacks by oxidation and its influence on the activity of immobilized catalase and iron-phthalocyanines was studied by Sosa *et al.* [89]. The carbon black was oxidized using different reagents such as H_2O_2 3M, HNO_3, 0.3 M at 95°C and O_2 at 400 and 600°C). The usefulness of diffuse reflectance spectroscopy (DRIFTS) studies on the formation of surface groups on carbon black by oxidation was reported by Fanning *et al.* [90]. Several other studies including the use of IR spectroscopy have been used to study the functional groups of carbons [91].

9.7 Mechanism of carbon sphere formation

Many mechanisms have been proposed for the synthesis of spherically shaped carbon materials; mechanisms that appear to depend on the reaction conditions such as the carbon source, catalyst etc. In this review the proposed mechanisms for CS synthesis will be discussed according to the synthetic technique used to prepare the CSs.

Qiu *et al.* [92] synthesized CSs using the arc-discharge method (nickel catalyst/coal electrode) and speculated that at high temperature, graphitic crystallites or nano-crystals formed from the carbon source. The nickel acted as a catalyst. In the arc-discharge process large numbers of electrons are produced, which adhere to the surface of active nano-crystallites and this improved the fluidity of the crystallites or nano-cystals. In this process nickel particles play an important role in binding the smaller crystallite particles to form bigger crystallites in the gas phase.

A general mechanism for the synthesis of CNSs using organometallic compounds has been proposed [93]. In this process ferrocene was decomposed at 400°C to form iron and carbon. The iron atoms assembled together to form large particles at 2 MPa pressure and 400°C temperature. These large iron particles reacted with ammonium chloride, which

exists in the vapor phase at that temperature, to form micro sized spherical droplets of iron amine complexes. These complexes have a high sticking coefficient which enhances the adsorption of the carbon feedstock. In this way the iron amine complex acts as a plating agent. The carbon obtained after decomposition of ferrocene forms a coating on the spherical droplets of the iron amine complex. Finally the droplets seep out from the defects and pores of the carbon shell leaving behind the carbon spheres (Fig. 9.9).

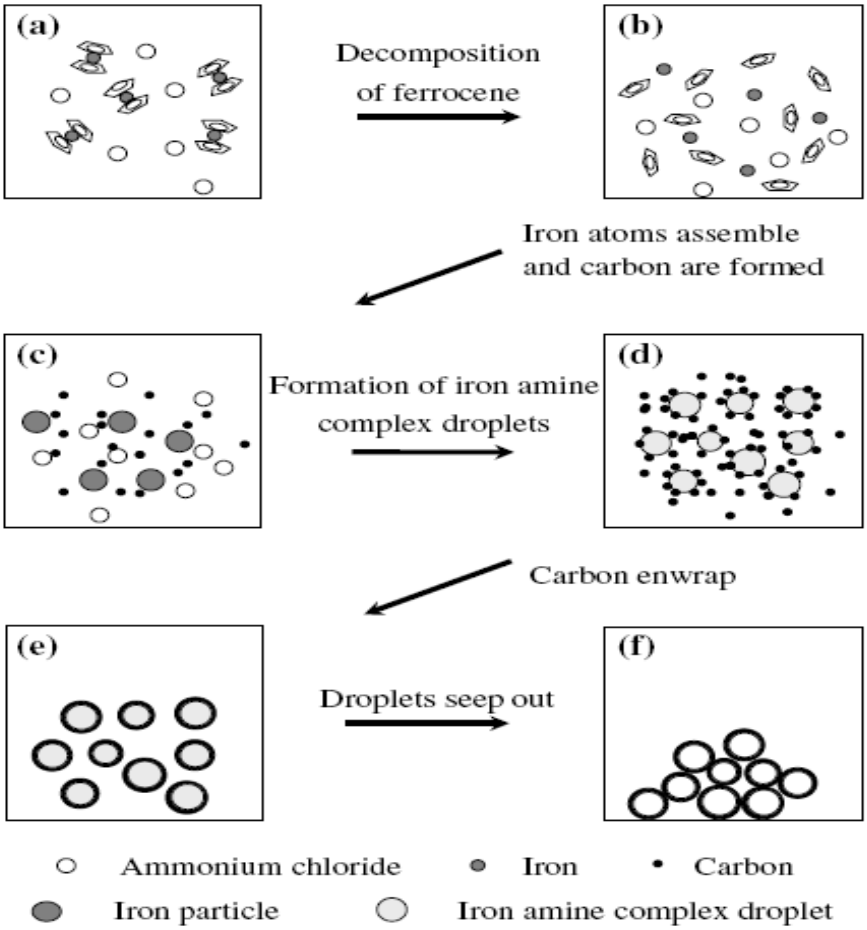

Fig. 9.9: Schematic illustration of the formation mechanism of HCSs [93].

Levesque *et al.* [94] reported the mechanism for a CCVD method for CS synthesis. In this method acetylene gas was decomposed into atomic carbon and hydrogen by a nickel nanocatalyst. The wavy 2D structure of these flakes was obtained by the combination of pentagonal and heptagonal structures with the planar hexagonal structure of graphene in

order to accommodate the curvature of the carbon sphere. Concentric aggregation gave the solid carbon nanospheres. As the flakes have this 2D dimension in the range of 4 nm, the superposition of these flakes, concentric layer by concentric layer, will statistically create 3D nanocrystallites in the range of 2 nm, on amorphous areas. Two possibilities exist; one is the formation of aggregates of the graphitic flakes *before* their inclusion into the concentric layers to form the carbon nanopearls and the second is the *direct aggregation* of individual flakes on the surface of the carbon nanopearls to form the concentric layers, then the nanocrystallites (Fig 9.10) [94].

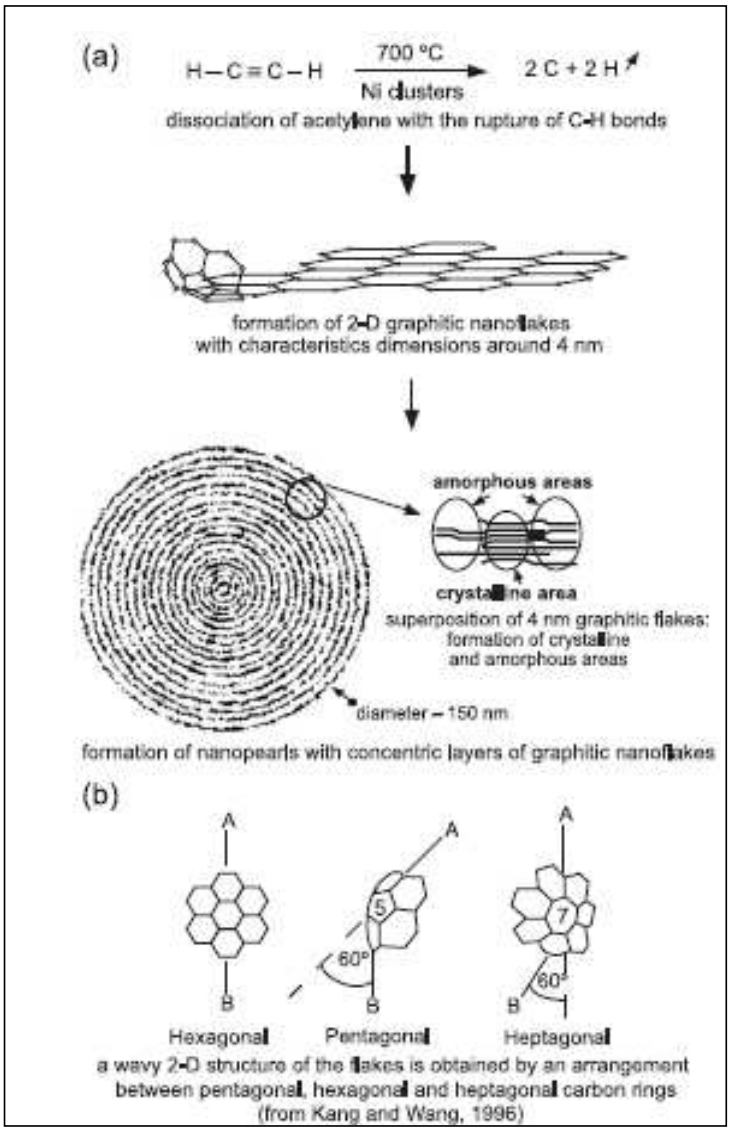

Fig. 9.10: (a) A schematic representation of the proposed mechanism for the formation of the carbon nanopearls in three steps. For the first step, there is no data regarding the end products formed between the various species present in the reactor, particularly the hydrogen and nitrogen. (b) Wavy flakes can be obtained by an insertion of pentagonal and heptagonal carbon rings within the planar hexagonal carbon rings [94].

Various mechanisms have been proposed for the pyrolysis of polymeric compounds. Jang and co-workers [95] proposed a mechanism for the synthesis of magnetic carbon nanoparticles using dodecyltrimethylammonium bromide used for the formation of

micelles and decyl alcohol as co-surfactant (Fig. 9.11). After formation of micelles the polymeric carbon source was added to form the iron based species, which was oxidized to form iron doped nanoparticles. These nano-particles on carbonization form magnetic carbon nanoparticles (MCNPs).

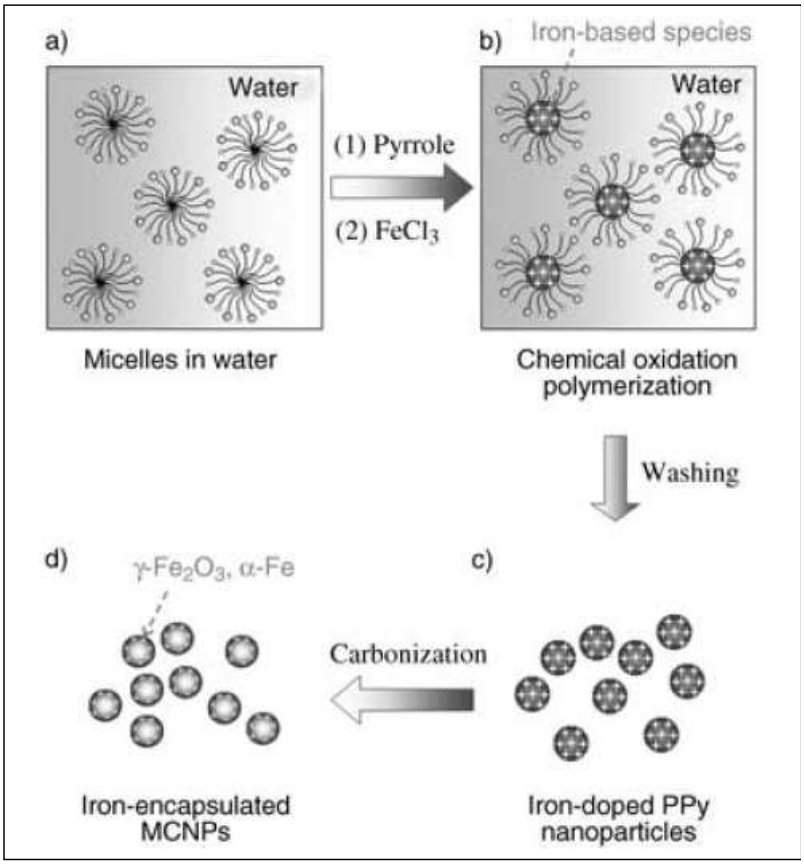

Fig. 9.11: Fabrication of PPy nanoparticles (a-c) and MCNPs (c-d) with uniform diameters [95].

Wang *et al.* [55a,b] studied the accretion (binding together) of monodispersed carbon nanospheres synthesized using a mixed-valence oxides catalytic carbonization (MVOCC) process. The MVOCC process is similar to the classical gas decomposition process under heating, but the key difference is the oxide catalyst used [55c]. The synthesized spheres were composed of graphitic flakes which were believed to exhibit many dangling bonds at the surfaces. Further, the accretion mechanism was discussed using a surface

adsorption model. The accretion of the spheres was achieved by ultrasonically treating the as-synthesized spheres in acetone.

The spheres are composed of graphitic flakes that are unclosed, with the atomic structure of each flake corresponding to one of the known graphite rings [55a,b]. The nucleation mechanism was first proposed by Kroto and McKay [96] for the formation of large fullerenes. Ideally, to form a graphitic carbon sphere, the atomic structure of each flake and the graphitic lattice must be modulated to accommodate the curvature of the sphere. The carbon atoms can form three different types of graphitic carbon rings. Thus three different ring structures, the flat hexagonal layer, the pentagonal ring structure with positive curvature and the heptagonal ring structure with negative curvature are formed (Fig. 9.12). The pentagonal, hexagonal and heptagonal rings are required so that the curvature of the carbon sphere can be achieved [55a,b].

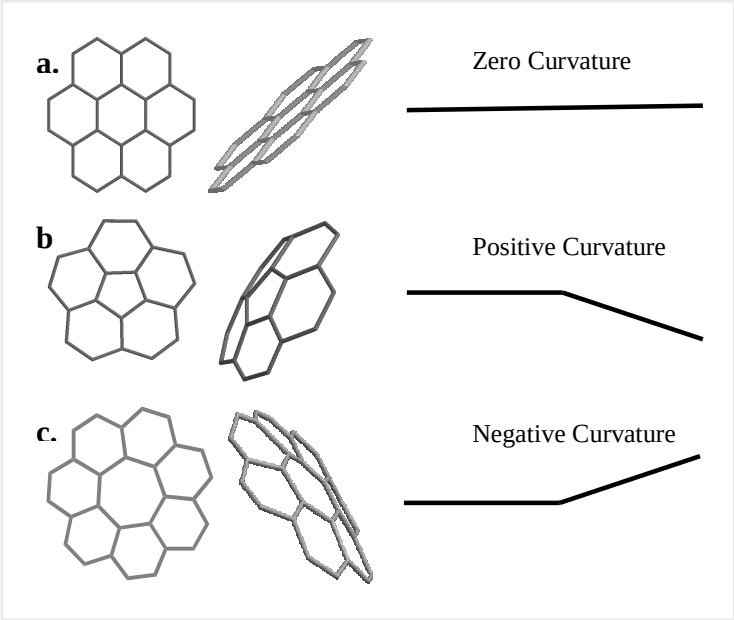

Fig. 9.12: Schematic representation of graphitic flakes. (a) hexagonal, (b) pentagonal, (c) heptagonal. Pentagonal and heptagonal carbon rings introduce changes in the curvature of the graphitic flakes [55a,b].

The sphere is believed to be nucleated from a pentagonal ring followed by a spiral shell growth (Fig. 9.13). The geometrical configurations of the graphitic flakes can be

qualitatively constructed using the combination of pentagonal, heptagonal and hexagonal rings and the variation in size of these graphitic flakes can create any curvature required to meet the geometry of the inner layers [55a,b,97]. Thus it can be said that the spheres are composed of curling graphitic flakes with random twisting, and these flakes are not closed shells.

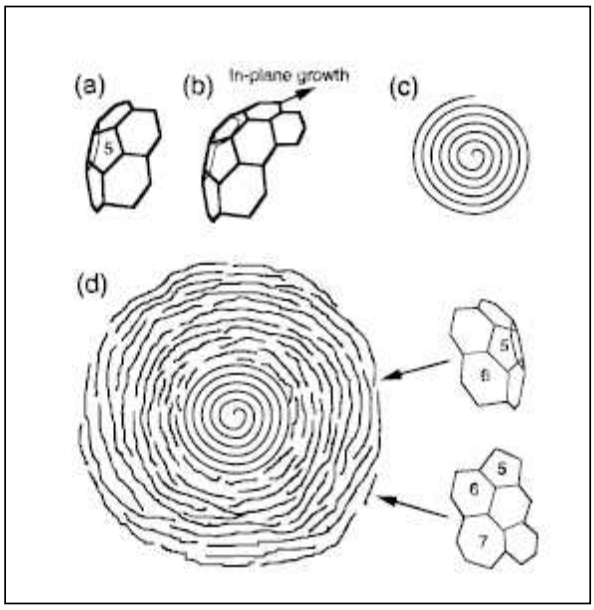

Fig. 9.13: (a) Nucleation of a pentagon, (b) growth of a quasi-icosahedral shell, (c) formation of a spiral shell carbon particle proposed by Kroto and McKay [96], and (d) growth of a large size carbon sphere.

The growth mechanism of carbon produced by gas phase non catalytic routes was studied by Lahaye *et al*. [98]. In describing the mechanism for the formation and post oxidation of particulate carbons (carbon black and soot formed in the gas phase), five factors were considered to be crucial:

(i) carbon black precursors and their formation,
(ii) carbon black particle inception,
(iii) the agglomeration of nuclei into particles and of particles into aggregates,

(iv) surface growth, and

(v) post oxidation of the carbon black.

It was confirmed that in all pyrolytic systems as well as in flames, three possible routes to carbon particles were advocated, namely (a) via polyacetylenes, (b) via polyaromatic hydrocarbons (PAHs) and (c) *via* the formation of a carbon vapour resulting from the dehydrogenation of initial hydrocarbon molecules: PAHs are the precursors of carbon nuclei. While attempts were made to study carbon particle inception, it can only be said that the PAH grows during dehydrogenation and progressively develops the properties that characterize carbon black. It was believed that in a flame, there is no true nucleation [98a].

Summary of factors impacting on CS formation

The factors impacting on the CS formation can thus be summarized as follows:
(i) carbon source; (ii) flow rate, (iii) temperature and (iv) reactor design. Chapter 10 and 11 of this thesis will provide some results that show the effect of these parameters on the synthesis of CSs.

9.8 Characterization of carbon spheres

Many techniques are available by which the morphology and structural properties of carbon materials can be studied. Transmission electron microscopy, scanning electron microscopy, X-ray diffraction, infra-red spectroscopy, Raman spectroscopy and X-ray photoelectron spectroscopy are the classic techniques that are widely used for characterization of carbon nanomaterials.

(i) Transmission electron microscopy

Transmission electron microscopy (TEM) is *the prime technique* for the evaluation of nanomaterials, and in particular CSs. TEM gives information on the structure, quality, size, diameter, shell thickness and the presence of amorphous material of CSs. The major

advantage of this technique is the high magnification images obtained and the ability to provide morphological and compositional information on a sample.

(ii) Scanning electron microscopy

This technique is widely used for the morphological studies and it also gives chemical composition of CS materials.

(iii) X-ray diffraction (XRD)

XRD is widely utilized to determine the crystallinity, inter-layer spacing, structural strain, and impurities in a CS. This is a non-distractive technique which requires little sample preparation. XRD pattern of CSs show the appearance in particular of a graphitic peak at 26.2° in 2θ.

(iv) Raman spectroscopy

Raman spectroscopy is an old technique that has been used for the characterization of carbon [99,100] Laser Raman spectra has been used to study carbonaceous materials including pyrolytic graphite, carbon black, glassy carbon, coal, “white” carbon and sputtered carbon. The Raman technique gives information on the size, strength and arrangement of chemical bonds but is less sensitive with respect to chemical composition evaluation. The most significant peaks for CSs are (a) a large peak around 1350 cm^{-1} assigned to residual disorganized graphite (called the D band); (b) high frequency peak in the range of 1500 to 1600 cm^{-1} is attributed to a graphite peak (called as G band). The I_D/I_G ratio (intensity of the D band divided by the intensity of the G band) is often calculated to evaluate the graphitic nature of spheres [100].

(v) Fourier transform infra-red spectroscopy

This technique is used to study the chemical composition of materials. CSs show two major sets of bands; one at 1630 cm^{-1} and one in the range of 2850 -2920 cm^{-1} which represents the C=C, C-H and C=O groups present on the carbon surface, respectively.

(vi) Thermoporometry

Ehrburger-Dolle *et al.* [101] measured the intra-aggregate void size distribution (VSD) and the fractal dimension of rubber grade carbon blacks in water or undecane using thermoporometry. Thermoporometry is a calorimetric method for characterizing pore structure from the melting or freezing point depression of a liquid confined in a pore, by reason of the added contribution of surface curvature to the phase-transition free energy [101c,d].

(vii) Particle induced X-ray emission (PIXE)

Since the early 90's the properties of CBs have been studied using particle induced X-ray emission (PIXE) technique for elemental analysis [102].

(viii) Mass spectroscopy

Mass spectroscopic techniques (e.g. GC-MS and SIMS) were used in many studies to determine the surface properties of carbon blacks for several decades ago. In particular, the mass spectroscopic techniques were used to study organic hydrocarbons generated from the structure of carbon particulates. Palmer *et al*. [103] observed that benzene exctracts of carbon blacks were dominated by fused-ring hydrocarbons and this was in agreement with previous studies using other methods.

(ix) Thermogravimetric analysis

TGA is another technique that has been used for the characterization of carbon spheres. A study by Tu *et al*. [104] presented data on the rate of combustion of spheres of carbon blacks in various N_2-O_2 mixtures under conditions in which both the rate of chemical reaction at the surface and the role of diffusion of oxygen to the surface were factors. A quantitative formulation of combustion rate was presented, predicting effects of temperature, gas velocity, and gas composition in agreement with the experimental measurements. The combustion of single carbon particles in an oxidizing atmosphere was investigated [105]. It was found that during extended periods of a particle lifetime thermal inertia enters significantly in the thermal balance.

9.9 Applications of carbon spheres

Due to their high surface area, thermal stability, unique electronic properties, low density and most importantly their tailored structure CSs have been used in lithium batteries, as support for catalysts, in drug delivery, encapsulation of active transition metals, as lubricants, as injectable scaffolds for tissue regeneration, in heterogeneous catalysis, in dye encapsulation, in removal of contaminants from water, enzyme and protein protection, and for magnetic data storage [106].

There are numerous catalytic reactions that have been performed in the presence of metal nanoparticles supported on CSs [106]. CSs can be used as a support to load metals in the nano scale. Even though there are a large number of advantages on the use of CSs as catalyst supports, there are very few reports available in this area. Below we have summarized the development of CSs in the field of catalysis as it has relevance to this thesis.

The development of fuel cells is one of the rapidly emerging areas of study in science. Carbon is an important material used in the fuel cell because of its high electric conductivity, corrosion resistance and low cost. Metals, particularly platinum and

ruthenium, loaded on CSs have shown very promising results in the direct methanol fuel cell [107]. Liu *et al.* [108] have shown that Pd supported on carbon balls can be used for the removal of trace amount of ethylene in the agribusiness. Ethylene hastens the ripening and aging process of fruits, vegetables and floral product in a storage environment.

High temperature annealing of CSs at 2800°C has a dramatic effect on the morphology of CSs, converting them into bead-like chains with well defined shapes. The charge-discharge capacity measurements on these annealed carbons indicates that this material has a better performance than normal spheres in terms of larger reversible capacity and longer plateaus in voltage profiles [109].

Cold electron generation via field emission is a key technology for the development of applications in vacuum microelectronics, ranging from space thrusters to miniaturized XRD, radio-frequency generators as well as flat panel displays. Generally microfabricated metallic emitters have been used. However replacement by carbon and in particular CSs reduces costs, emission instabilities and non-uniformity resulting from aging-induced surface modification of metallic tips. Indeed carbon is one of the best field emitters, so research had been done to synthesis lower cost cold emitters. Nickel clustered catalysed synthesis of carbon nanopearls showed good uniform field emission properties [47,110].

Li *et al.* [111] have successfully demonstrated that nitrogen enriched mesoporous carbon spheres can be used for electrochemical capacitors. Nitrogen doped magnetic carbon nanoparticles containing palladium metal showed good catalytic activity for Heck, Suzuki and Sonogashira coupling reactions with very good recyclability of the catalyst [112]. Similarly, Pathak *et al.* [113] developed a catalytic system for Suzuki, Heck and Stille-type C-C bond formation reactions using palladium coated CSs.

Mondal *et al.* [39c] performed catalytic hydrogenation of ethylene over Pd supported on CSs at 60°C. During this study it was discovered that acid treated CSs showed higher catalytic activity than that of non-acid treated CSs. In more recent studies the utilization

of CSs as supports for ruthenium oxidation, hydrogenation and C-C bond formation reactions has been achieved. Ruthenium loaded on nitrogen doped CNSs was found to catalyse oxidation reactions (mono, di-carbonyl compounds) as well as the hydrogenation of alkene containing compounds [114]. Beside their use as fillers in rubber and other polymeric materials, carbon blacks have also been tested for various other applications including the extraction of organic pollutants from water as well as in the modification of electronic properties of insulating materials [115].

9.10 Summary

The review has given an insight understanding of the factors that influence the synthesis of CSs. In particular the catalytic and non catalytic CVD processes were discussed in depth as well as the various mechanisms proposed for the synthesis of CSs. Thus, this chapter of the thesis indicates the necessity to undertake studies on the synthesis of these materials.

9.11 References

1. H.W. Kroto, J.R. Heath, S.C. O'Brien, R.F. Curl, R.E. Smalley, Nature **318** (1985) 162.
2. http://www.nanoword.net/library/def/bldefnano.htm (accessed on 5th January 2009).
3. V.O. Nyamori, S.D. Mhlanga, N.J. Coville, J. Organometal. Chem. **693** (2008) 2205.
4. Y. Xia, B. Gates, Y. Yin, Y. Lu, Adv. Mater. **12** (2000) 693.
5. J-S. Chang, L.L. Lauderback, J.L. Falconer, J. Catal. **122** (1990) 10.
6. P.L. Walker, Jr., Carbon **10** (1972) 369.
7. P.L. Walker, Jr., Carbon **28** (1990) 261.
8. F. Ehrburger-Dolle, S. Misono, Carbon **30** (1992) 31.
9. F. Ehrburger-Dolle, S. Misono, J. Lahaye, J. Colloid lnterf. Scie. **135** (1990) 468.
10. M. Marscini, A. Liberti, C. Morgia, Analytica Chimica Acta, **173** (1985) 157.
11. F. Mangani, G. Crescentini, P. Palma and F. Bruner, J. Chromatography **452** (1988) 527.

12. A.I. Medalia, L.W. Richards, J. Colloid Interf. Scie. **40** (1972) 233.
13. F. Bruner, P. Ciccioli and F. Di Nardo, J. Chromatography **99** (1974) 661.
14. J.M. Martin-Martinez, M.A. Vannice, Industr. Eng. Chem. Res. **30** (1991) 2263.
15. K.J. Notz, J. Phys. Chem., **71** (1967) 1965.
16. W.B. Wiegand, C.R. Bog, D.W. Kitchina, Industr. Eng. Chem. **23** (1931) 273.
17. W.B. Wiegand, J.W. Snyde, Industr. Eng. Chem. **26** (1934) 413.
18. http://www.epa.gov/ttn/chief/ap42/ch06/final/c06s01.pdf. (accessed on 12th November 2008).
19. http://www.timcal.com/SCOPI/Group/timcal/tim01cor.nsf/Attachment/4DBBCF7990B445F5C1257154004DD6C9/$file/Carbon_Black_Introduction.pdf. (accessed on 12th November 2008).
20. M. Sharon, K. Mukhopadhyay, K. Yase, S. Iijima, Y. Ando, X. Zhao, Carbon **36** (1998) 507.
21. L.P. Biró, G.I. Márk, Z.E. Horváth, K. Kertész, J. Gyulai, J.B. Nagy, Ph. Lambin Carbon **42** (2004) 2561.
22. H-H. Yang, S-Q. Zhang, X-L. Chen, Z-X. Zhuang, J-G. Xu, X-R. Wang, Anal. Chem. **76** (2004) 1316.
23. M. Inagaki, Carbon **35** (1997) 711.
24. D. Brooks, G.H. Taylor, *Chemistry and Physics of Carbon*, Vo1.4, ed. P.L. Walker, Jr., Dekker, New York, 1968.
25. Ph. Serp, R. Feurer, Ph. Kalck, Y. Kihn, J.L. Faria, J.L. Figueired, Carbon **39** (2001) 615.
26. L.A.J. Garvie, P.R. Buseck, Earth and Planetary Science Letters **224** (2004) 431.
27. D.C. Smith, A. Barbet, J. Raman Spectrosc. **30** (1999) 319.
28. M. Faraday, *The chemical history of a candle*, Courier Dover Publications, 2002; accessed online at http://books.google.co.za/books?id=x8gLCQnLTZ0C&printsec=frontcover#PPP1,M1 (accessed on 23rd October 2008).
29. C.R. Shaddix, A.B. Palotás, C.M. Megaridis, M.Y. Choi, N.Y.C. Yang, Int. J. Heat Mass Transf. **48** (2005) 3604.
30. H. Liu, T. Ye, C.D. Mao, Angew. Chem. Int. Ed. **46** (2007) 6473.

31. New patents, Carbon **15** (1989) 1.
32. J.T. Blake, Industr. Eng. Chem. **20** (1928) 1084.
33. W.B. Plummer, Industr. Eng. Chem. **22** (1930) 630.
34. C.M. Carson, L.B. Sebrel, Industr. Eng. Chem. **21** (1929) 911.
35. (a) W.B. Wiegand, J.W. Snyder, Industr. Eng. Chem. **23** (1931) 646; (b) W.B. Wiegand, J.W. Snyde, Industr. Eng. Chem. **26** (1934) 413.
36. C.R. Johnson, Industr. Eng. Chem. **21** (1929) 1288.
37. (a) R. Taylor, *The chemistry of fullerenes,* Singapore: World Scientific, 1995; (b) H.O. Pierson, *Handbook of carbon, graphite, diamond and fullerenes: properties, processing and applications*, Park Ridge, N.J., USA: Noyes Publications, 1993; (c) A. Hirsch, M. Brettreich, *Fullerenes: chemistry and reactions*, Great Britain, Wiley-VCH, 2005.
38. P.L. Walker Jr., J. Phys. Chem. **63** (1959) 133.
39. (a) M. Monthioux, P. Serp, E. Flahaut, C. Laurent, A. Peigney, M. Razafinimanana, W. Bacsa, J-M. Broto, B. Bhushan (Ed.), *Nanotechnology Handbook*, Springer-Verlag, Heidelberg, (2004) pp. 39; (b) P. Serp, P. Kalck, R. Feurer, Chem. Rev. **102** (2002) 3085; (c) K.C. Mondal, L.M. Cele, M.J. Witcomb, N.J. Coville, Catal. Commun. **9** (2008) 494.
40. H-S. Qian, F-M. Han, B. Zhang, T-C. Guo, J. Yue, Bi-X. Peng, Carbon **42** (2004) 761.
41. M. Aili, W. Xiaomin, L. Tianbao, L. Xuguang, X. Bingshe, Mater. Scie. Eng. A, **443** (2007) 54.
42. Y.Z. Jin, C. Gao. W.K. Hsu, Y. Zhu, A. Huczko, M. Bystrzejewski, M. Roe, C.Y. Lee, S. Acquah, H. Kroto, D.R.M. Walton, Carbon **43** (2005) 1944.
43. B.Y. Geng, J.Z. Ma, Q.B. Du, X.W. Liu, L.D. Zhang, Mater. Scie. Eng. A **466** (2007) 96.
44. H. Miguez, N. Tetreault, B. Hatton, S.M. Yang, D. Perovic, G.A. Ozin, Chem. Commun. (2002) 2736.
45. F. Su, X.S. Zhao, Y. Wang, L. Wang, J.Y. Lee, J. Mater. Chem. **16** (2006) 4413.

46. (a) J-Y. Miao, D.W. Hwang, K.V. Narasimhulu, P-I. Lin, Y-T. Chen, S-H. Lin, L-P. Hwang, Carbon **42** (2004) 813. (b) J-Y. Miao, D.W. Hwang, C. Change, S. Lin, K.V. Narasimhulu, L. Hwang, Diam. Rel. Mater. **12** (2003) 1368.
47. A. Levesque, V.T. Binh, V. Semet, D. Guillot, R.Y. Fillit, M.D. Brookes, T.P. Nguyen, Thin Solid Films **464-465** (2004) 308.
48. Z. Zhong, H. Chen, S. Tang, J. Ding, J. Lin, K.L. Tan, Carbon **330** (2000) 41.
49. P. Chen, H.B. Zhang, G.D. Lin, Q. Hong, K.R. Tsai, Carbon **35** (1997) 1495.
50. D. Pradhan, M. Sharon, Mater. Sci. Eng. B **96** (2002) 24.
51. M. Sharon, K. Mukhopadhyay, K. Yase, S. Iijima, Carbon **36** (1998) 507.
52. (a) X-Y. Liu, B-C. Huang, N.J. Coville, Carbon **40** (2002) 2791; (b) V.O. Nyamori, N.J. Coville, Organometallics 26 (2006) 4083.
53. S. Amelinckx, X.B. Zhang, D. Bernaerts, X.F. Zhang, V. Ivanov, J.B. Nagy, Science **265** (1994) 635.
54. W.M. Hess, C.R. Herd, Carbon Black Science and Technology, 2nd Ed., Marcel Dekker Inc., New York, (1993) pp. 106-108.
55. (a) Z.L. Wang, Z.C. Kang, J. Phy. Chem. **100** (1996) 17725; (b) Z.C. Kang, Z.L. Wang, J. Phy. Chem. **100** (1996) 5163. (c) Z.L. Wang, Z.C. Kang, Carbon **35** (1997) 419.
56. J.D. Brooke, G.H. Taylor, Carbon **3** (1965) 185.
57. M. Kodama, T. Fujira, K. Esumi, K. Meguro, M. Honda, Carbon **26** (1988) 595.
58. S-H. Yoon, Y-D. Park, I. Mochida, Carbon **30** (1992) 781.
59. M. Nishizawa, I. Uchida, Electrochimica Acta **44** (1999) 3629.
60. M. Nishizawa, H. Koshika, R. Hashitani, T. Itoh, T. Abe, I. Uchida, J. Phys. Chem. B. **103** (1999) 4933.
61. X. Wu, Z. Wang, L. Chen, X. Huang, Surf. Coat. Technol. **186** (2004) 412.
62. J.C. Arrebola, A. Caballero, L. Hernán, J. Morales, J. Power Sources **183** (2008) 310.
63. X. Shao, W. Wang, R. Xue, Z. Shen, J. Phys. Chem. B **108** (2004) 2970.
64. C. Ishiia, K. Kanekob, Progr. Organic Coatings **31** (1997) 147.
65. Y. Korai, Y-G. Wang, S-H. Yoon, S. Ishida, I. Mochida, Y. Nakagawa, Y. Matsumura, Carbon **35** (1997) 875.
66. L. Ding, S.V. Olesik, Chem. Mater. **17** (2005) 2353.

67. (a) S-I. Lee, S. Mitani, C.W. Park, S-H Yoon, Y. Korai, I. Mochida, Carbon **411** (2002) 1652. (b) S-I. Lee, S. Mitani, C.W. Park, S-H. Yoon, Y. Korai, I. Mochida, J. Power Sources **139** (2003) 379. (c) Y-G. Wang, Y-C. Chang, S. Ishida, Y. Korai, I. Machida, Carbon **37** (1999) 969.
68. K. Esumi, S. Eshima, Y. Murakami, H. Honda, H. Oda, Colloids Surfaces A.: Physicochem. Eng. Aspects **108** (1996) 113.
69. R. Alcántara, F.J.F. Madrigal, P. Lavela, J.L. Tirado, J.M.J. Mateos, C. Gómez de Salazar, R. Stoyanova, E. Zhecheva, Carbon **38** (2000) 1031.
70. S. Yang, H. Song, X. Chen, Carbon **44** (2006) 730.
71. (a) Y-C. Liu, X-P. Qiu, Y-Q. Huang, W-T. Zhu, J. Power Sources **111** (2002) 160; (b) Y-C. Liu, X-P. Qiu, Y-Q. Huang, W-T Zhu, Carbon **40** (2002) 2375.
72. Z. Wang, B. Wu, Q. Gong, H. Song, J. Liang, Mater. Lett. **62** (2008) 3585.
73. K.C. Mondal, N.J. Coville, M.J. Witcomb, G. Tejral, J. Havel, Chem. Phys. Lett., **437** (2007) 87.
74. S.D. Mhlanga, N. Khunjuzwa, N.J. Coville, unpublished data.
75. (a) J.B. Donnet, J. C. Bouland, Carbon **4** (1966) 201; (b) W. Hess, C.R. Herd, *In Carbon Black Science and Technology* (Edited by J. B. Donnet, R. C. Bansal and M. J. Wang). p. 89. Marcel Dekker, New York, 1993.
76. http://www.carbonblack.jp/en/cb/youto.html#top (accessed on 2nd March 2007).
77. H.P. Boehm, Carbon **32** (1994) 759.
78. H.P. Boehm, E. Diehl, W. Heck, R. Sappok, Angew. Chem. Internal. Ed. Engl. **3** (1964) 669.
79. J.B. Donnet, Carbon **6** (1968) 161.
80. D.J. Kohls, G. Beaucage, Current Opinion in Solid State & Mater. Scie. **6** (2002) 183.
81. (a) E. Papirer, R. Lacroix and J-B. Donnet, Carbon **34** (1996)1521; (b) E. Papirer, R. Lacroix, J-B. Donnet, Carbon **32** (1994) 1341.
82. J. Leblane, J. Appl. Poly. Sci. **66** (1997) 2257; A.S. Aricó, V. Antonucci, M. Minutoli, N. Giordano, Carbon **27** (1989) 337.
83. A. S. Aricó, V. Antonucci, L. Pino, P.L. Antonucci, N. Giordano, Carbon **28** (1990) 599.

84. B. Sahouli, S. Blather, F. Brouers, H. Darmstadtt, C. Royt, S. Kaliaguinet, Fuel **75** (1996) 1244.
85. (a) G. Nansé. Papirer, P. Fioux F. Moguet, A. Tressaud, Carbon **35** (1997) 515; (b) G. Nansé, E. Papirer, P. Fioux, F. Moguet, A. Tressaud, Carbon **35** (1997) 175; (c) G. Nansé, E. Papirer, P. Fioux, F. Moguet, A. Tressaud, Carbon **35** (1997) 351.
86. T. Shirasaki, F. Moguet, L. Lozano, A. Tressaud, G. Nansé, E. Papirer, Carbon **37** (1999) 1891.
87. A. Tressaud, T. Shirasakia, G. Nansé, E. Papirer, Carbon **40** (2002) 217.
88. E. Papirer, R. Lacriox, J-B. Donnet, G. Nansé, P. Froux, Carbon **32** (1994) 1341.
89. R.C. Sosa, R.F. Parton, P.E. Neys, O. Lardinois, P.A. Jacobs, P.G. Rouxhet, J. Mol. Catal. A: Chemical **110** (1996) 141.
90. P.E. Fanning, M.A. Vannke, Carbon **31** (1991) 721.
91. F. Rositani, P.L. Antonucci, M. Minutoli, N. Giordano, A. Villari, Carbon **25** (1987) 325.
92. J. Qiu, Y. Li, Y. Wang, C. Liang, T. Wang, D. Wang, Carbon **41** (2003) 767.
93. B. Liu, D. Jia, Q. Meng, J. Rao, Carbon **45** (2007) 668.
94. A. Levesque, Vu Thien Binh, V. Semet, D. Guillot, R. Y. Fillit, M. D. Brookes, T.P. Nguyen, Thin Solid Films **464–465** (2004) 308.
95. (a) J. Jang, J.H. Oh, X.L. Li, J. Mater. Chem. **14** (2004) 2872; (b) Jyongsik Jang, J.H. Oh, Adv. Funct. Mater. **15** (2005) 494.
96. H.W. Kroto, K. McKay, Nature **331** (1988) 328.
97. Z.C. Kang, Z.L. Wang. Philos. Mag. B. **73** (1996) 905.
98. (a) J. Lahaye, F. Ehrburger-Dolle, Carbon **32** (1994) 1319-1324; J. Lahaye, Carbon **30** (1992) 309.
99. C.H. Chang, R.A. Beyerlein, S.S. Chan, Carbon **22** (1984) 393.
100. M. Nakamizo, Carbon **29** (1991) 757.
101. (a) F. Ehrburger-Dolle, S. Misono, Carbon **30** (1992) 31; (b) F. Ehrburger-Dolle, S. Misono, J. Lahaye, Science **135** (1990) 468; (c) M.R. Landry, Thermochimica Acta **433** (2005) 27; (d) M. Brun, A. Lallemand, J.-F. Quinson, C. Eyraud, Thermochim. Acta **21** (1977) 59.

102. R.S. Sokhi, C. Gray, K. Gardiner, L.G. Earwaker, Nuclear Instr. Method. Phys. Res. B **49** (1990) 414.
103. H.B. Palmer, A. Voet , J. Lahaye, Carbon **6** (1968) 65.
104. C.M. Tu, H. Davis, H.C. Hotel, Int. Comm. Heat Mass Transfer **11** (1984) 15.
105. P.A. Libby, T.R. Blake, Combustion and Flame **36** (1979) 139.
106. (a) M. C. Daniel D. Astruc, Chem. Rev. **104** (2004) 293; (b) C. Burda, X. Chen, R. Narayanan, M. A. El-Sayed, Chem. Rev. **105** (2005) 1025; (c) S. Laurent, D. Forge, M. Port, A. Roch, C. Robic, L. Vander Elst, R. N. Muller, Chem. Rev. **108** (2008) 2064; (d) S.J. Son, X. Bai, S.B. Lee, Drug Discovery Today **12** (2007) 650.
107. S. Han, Y. Yun, K. Park, Y-E. Sung, T. Hyeon, Adv. Mater. **15** (2003) 1922.
108. Z-X. Liu, J-N. Park, S.H.R. Abdi, S-K. Park, Y-K. Park, W. Lee, Topics Catal. **39** (2006) 221.
109. Y.Z. Jin, Y.J. Kim, C. Gao, Y.Q. Zhu, A. Huczko, M. Endo, H.W. Kroto, Carbon **44** (2006) 724.
110. R. Mouton, V. Semet, D. Guillot, V.T. Binh, J. Vac. Sci. Technol. B **24** (2006) 993.
111. W. Li, D. Chen, Z. Li, Y. Shi, Y. Wan, J. Huang, J. Yang, D. Zhao, Z. Jiang, Electrochem. Commun. **9** (2007) 569.
112. H. Yoon, S. Ko, J. Jang, Chem. Commun. (2007) 1468.
113. S. Pathak, M.T. Greci, R.C. Kwong, K. Mercado, G. K. Surya Prakash, G.A. Olah, M.E. Thompson, Chem. Mater. **12** (2000**)** 1985.
114. A. Deshmukh, R. Islam, N. Tyagi, N.J. Coville, unpublished data.
115. (a) W.B. Wiegand, C.R. Bog and D.W. Kitchina, Industr. Eng. Chem. **23** (1931) 273; (b) W.B. Wiegand, J.W. Snyde, Ind. Eng. Chem. **26** (1934) 413; (c) K.J. Notz, J. Phys. Chem. **71** (1967) 1965; (d) P.L. Walker, Jr. Carbon **10** (1972) 369; (e) M. Marscini, A. Liberti, C. Morgia, Analytica Chimica Acta **173** (1985) 157; (f) P.L. Walker, Jr. Carbon **28** (1990) 261. (g) F. Mangani, G. Crescentini, P. Palma, F. Bruner, J. Chromatography **452** (1988) 527. (h) A.I. Medalia, L.W. Richards, J. Colloid Interface Science **40** (1972) 233; (i) F. Bruner, P. Ciccioli, F. D. Nardo, J. Chromatography **99** (1974) 661; (j) J.M. Martin-Martinez, M.A. Vannice, Industr. Eng. Chem. Res. **30** (1991) 2263; (k) J-S. Chang, L.L. Lauderback, J.L. Falconer, J. Catal. **122** (1990) 10.

Chapter 10

Synthesis and study of carbon microspheres for use as catalyst support for cobalt[#]

10.1 Introduction

Carbon is considered to be a versatile element because it can be a useful building block to form a wide range of structures. The unique ability of carbon to form complexes in which the carbon atom has sp, sp^2 and sp^3 electronic configurations results in a wide range of structures and morphologies with widespread applications [1]. The successful growth of diamond films, the fullerene molecule C_{60} and its family members C_n e.g. C_{70} and C_{80}, and carbon nanotubes (CNTs) have attracted much attention [2]. In particular, an enormous amount of research has to date focused on the synthesis and applications of CNTs.

Another form of carbon, which is graphitic in nature, has been described in the literature. Earlier studies referred to this material as nanosized carbon spheres [2] or carbon nanobeads while more recent studies have called them carbon spherules [3-5], nanoballs [6], carbon pearls [7] or carbon microspheres [8]. These are all spherical in shape. This form of carbon has received less interest in recent years. In recent years it was also discovered accidentally as a by-product in the synthesis of CNTs by chemical vapor deposition (CVD) methods. However, some work has been carried out on these carbon spheres (CSs) focusing on their fabrication using catalytic synthesis as well as direct pyrolysis of hydrocarbons [9,10].

[#]*Sabelo D. Mhlanga, Kartick C. Mondal, Nerona Naidoo, Nikiwe Kunjuzwa, Michael J. Witcomb, Neil J. Coville, partly taken from S. Afr. J. Scie., accepted for publication.*

Interestingly, CSs have been known for many decades and have been made by procedures similar to the procedure described herein. These materials, referred to as carbon black particles [11,12], have been produced from a carbon source such as oil or natural gas, typically in the presence of small amounts of oxygen. For example, when acetylene is used under a reduced presence of oxygen the process is called the acetylene black process [13-15].

Different processes have been used to synthesize the sphere like forms of carbon and these have been discussed in the previous chapter. Carbon onions (named so because of the shape of their microstructure) were observed to be formed from soot that contains polyhedral carbon particles under electron-beam irradiation in a high-resolution transmission electron microscope (HRTEM) [16]. These highly graphitic structures were found to be stable only under irradiation conditions. Mono-dispersed nanosize carbon spheres were synthesized by Wang *et al.*, using a mixed-valent oxide catalytic carbonization process [2]. Solid carbon nanospheres (210 nm diameter) were also synthesized by Kang and Wang, by the thermal decomposition of methane (CH_4) in the presence of a metal oxide catalyst [17]. Solid and hollow nanospheres with diameters in the range 250 - 850 nm were obtained using a catalytic process by Sharon *et al.* from camphor vapour at 1000°C using ferrocene as the catalyst precursor [18]. All the above processes are reported to require a catalyst. More recently, large-scale production of pure carbon spheres, with diameters from 50 nm to 1 μm, has also been achieved through direct pyrolysis of a wide range of hydrocarbons in the absence of a catalyst. These include styrene, toluene, benzene, hexane, cyclohexane and ethane [9,10]. In this study we report on the synthesis of CSs using ethylene or acetylene as carbon source in the absence of a catalyst.

The search for new synthetic strategies for generating nanostructured carbon or carbon-hybrid materials is topical in materials chemistry, motivated by the natural abundance of carbon and therefore the cost effectiveness of carbon precursors and the promising applications of the resulting materials. Due to the intrinsic properties of the carbon materials such as their high strength, high thermal resistance and light weight, CMSs can

be used as high strength composites, catalyst support, lubricants and as wear-resistant materials [10]. An alternative is to use these materials as catalyst supports. Finally, Wang *et al.* have also reported the production of carbon microbeads (2 mm) from a synthetic naphthalene isotropic pitch by simple heating at 420°C under nitrogen [19].

Catalytic hydrogenation is one of the most simple as well as a common application of a heterogeneous catalyst. The usefulness of this reaction has been well covered by texts and reviews [20]. Although, such work has been done on amorphous carbon as a catalyst support in hydrogenation reactions, similar work on new forms of carbon such as the CSs remains to be explored. Mondal *et al.* [21] recently reported that carbon microspheres could be used as a catalyst support for palladium (Pd) for the hydrogenation reaction of ethylene to ethane. The study showed that better ethylene hydrogenation activity and mechanical stability against deactivation were achieved when compared to an activated amorphous carbon supported Pd catalyst. This was suggested to be due to the stronger metal-support interaction between the Pd and the carbon, even though some sintering was noted [21]. The use of CSs as support for Co catalysts, for the hydrogenation reaction of ethylene to ethane had not previously been reported. Less sintering issues were expected with Co than with Pd. Some results on the use of Co/CS in the above reaction are presented.

10.2 Experimental

10.2.1 Synthesis of carbon spheres by non-catalytic CVD

The direct pyrolysis of a pure hydrocarbon source was carried out to synthesize CSs. The experiment was carried out at atmospheric pressure in a fixed-bed reactor made of a quartz tube (having dimensions 51 cm x 1.9 cm). The reactor was placed horizontally into an electronically controlled furnace. The front end of the tube was connected to a glass manifold which allowed for the free flow of gases (i.e. hydrocarbon feedstock gas, N_2 inert gas) into the reactor. The rear end of the tube was closed with a quartz glass plug, thus ensuring that the reaction took place in the absence of oxygen.

The temperature in the furnace was then raised at a constant heating rate of 20°C/min under a constant flow of N_2 (40 ml/min). Once the desired temperature was reached the N_2 gas was replaced with the hydrocarbon source (i.e. C_2H_2 or C_2H_4) at a total constant flow rate of 100 ml/min. The carbon source was converted into the desired activated carbon species which diffused into the quartz tube while the temperature was held constant. After a certain time, the carbon source was replaced by the inert gas (N_2, 40 ml/min), and the system was allowed to cool to room temperature at which time the product was collected. Since no catalyst was required in the synthesis of the CSs, the materials produced were very pure and no removal of catalyst was required in the post-synthesis process. The type of feedstock gas, reaction temperature, reaction time and flow rate of the carbon source were varied in order to study their effect on the structure and yields of CSs obtained.

10.2.2 Synthesis of carbon spheres using alcohols

The synthesis of CSs was carried out by direct pyrolysis of alcohols (ethanol, 1-butanol, 1-hexanol, 1-octanol and 1-dodecanol). This was carried out using a chemical vapor deposition (CVD) procedure without using a catalyst. A high temperature horizontal furnace with an *injector* was used for this purpose. The synthesis conditions were maintained at atmospheric pressure, with a reactor temperature of 1000°C and a 0.4 ml/min injection flow rate. Before synthesis, the system was flushed with N_2 gas. The alcohol (10 ml) was then injected into the heated quartz tube inside the furnace using a *syringe* where the carbon spheres (black soot) were formed. The front of the tube was connected to a glass manifold which allowed for free flow of gases. The temperature in the furnace was raised at a constant heating rate of 10°C/min. Once the desired temperature was reached the injector motor was turned on. The reaction was complete after 10 - 20 min and the system was left to cool to room temperature before collecting the product.

10.2.3 Characterization of the CSs

The collected black soot was weighed and characterized using transmission electron microscopy (TEM) (JEOL 100S Electron Microscope), thermogravimetric analysis (TGA) (Perkin Elmer Pyris 1 TGA Anaylzer) and powder X-ray diffraction (PXRD) techniques (Bruker axs D8 Advance PXRD).

10.2.4 Preparation of CS supported cobalt catalysts (Co/CS)

The CS supported Co catalysts were prepared by the wet impregnation method. Cobalt (II) nitrate [$Co(NO_3)_2{\cdot}6H_2O$] was used as a source of Co. Typically 1.24 g of $Co(NO_3)_2{\cdot}6H_2O$ dissolved in 20 ml distilled water and the solution stirred to make it homogenous. The Co containing solution was then added dropwise to 5 g of dry CSs previously oxidized in 30% HNO_3 solution to make it more hydrophobic. The Co/CS mixture was stirred for another 15 min and the resulting slurry, which contained 5 wt% Co on the CSs was dried in a static air oven at 120°C for 30 min. The catalysts were then calcined in a static air calcination oven for 4 h at 400°C (heating rate = 5^oC/min) and ground to a fine powder using a 150 µm sieve. Other catalysts containing 10 wt% and 20 wt%Co were also prepared as described above. Temperature programmed reduction (TPR) studies were done to determine the reduction temperature of cobalt oxide species under hydrogen and indicated that a temperature of 400^oC would be sufficient for catalyst reduction. The catalysts were reduced under a continuous flow of 5 %H_2/Ar (30 ml/min).

10.2.5 Catalytic hydrogenation reaction

The catalytic hydrogenation reactions were performed at atmospheric pressure by passing continuously, a gaseous feed containing pure ethylene and hydrogen (H_2/C_2H_4 mol ratio = 3.05, total flow of feed gas = 77 ml/min) over the catalyst (50 mg) packed in a fixed bed quartz microreactor, provided with a thermocouple in the catalyst. After attaining reaction steady state, the reaction products were analyzed by using gas chromatograph with a flame ionization detector (FID) and a Porapak Q column. The catalyst was studied

in its prepared state. Only hydrocarbon products are detected by the FID and hence selectivity and conversion data were based only on analysis of the hydrocarbon species. The gas hourly space velocity (GHSV) was measured at 0°C and 1 atm pressure. The experimental setup is shown in Fig. 10.1.

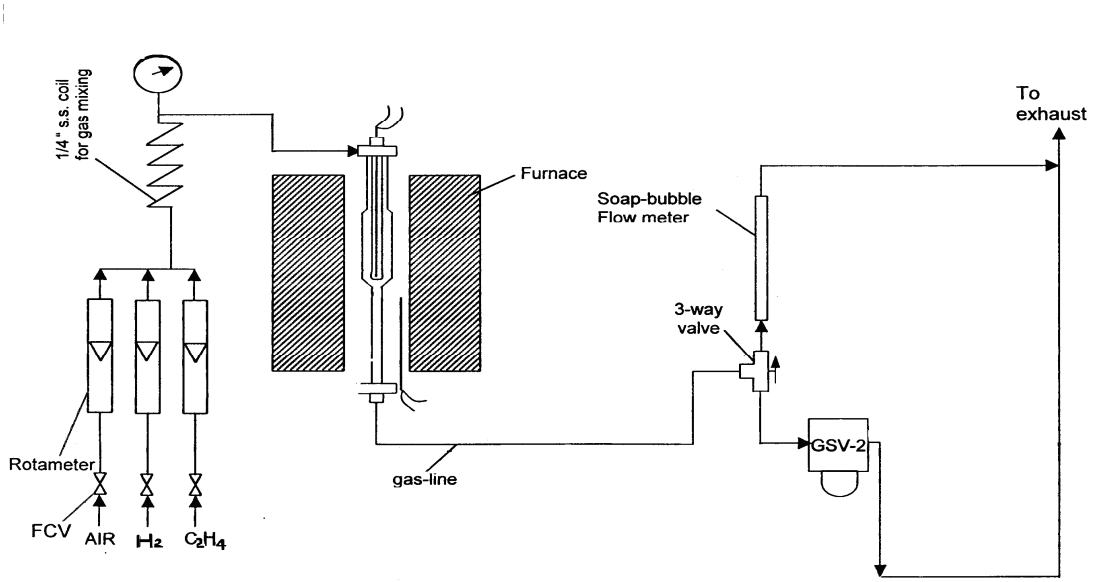

Fig. 10.1: Experimental setup used for the catalytic ethylene pyrolysis reaction [GHSV 2 = gas sampling valve, FCV = flow control valve].

10.3 Results and Discussion

10.3.1 Effect of carbon source

The direct hydrocarbon pyrolysis experiments using C_2H_2 and C_2H_4 as the carbon source were performed over a wide temperature range (600 - 950°C). C_2H_4 gave no CS formation at 600 - 850°C. Low yields were obtained at 900°C (0.2 g in 2 h). The maximum yield attainable was ~ 1.4 g at 950°C in 2 h and the CSs formed had a wide size distribution range (350 - 650 nm).

With C_2H_2, CSs were observed at all the temperatures used and very high yields were obtained at 900°C (> 10 g). The size distribution was also much narrower than that observed with C_2H_4. As a result, C_2H_2 was used as the source of carbon to make CSs in this study. It may be noted that the yields reported above, and others to follow, relate to the mass of the CSs. No other carbonaceous materials were observed in the products. Our method of CS production results to > 99% purity of the carbon.

10.3.2 Effect of temperature

The effect of the reaction temperature on the yield, size and morphology of the CSs was investigated. Experiments were carried out in a temperature range of 600 - 1000°C. At each experimental temperature, the carbon deposit was removed from the reactor and weighed. TEM studies of the products enabled the measurement of their diameters as well as their distribution. The acetylene gas flow rate was kept at 100 ml/min and a reaction time of 2 h was used unless otherwise stated. The effect of temperature on the yield is represented graphically in Fig. 10.2.

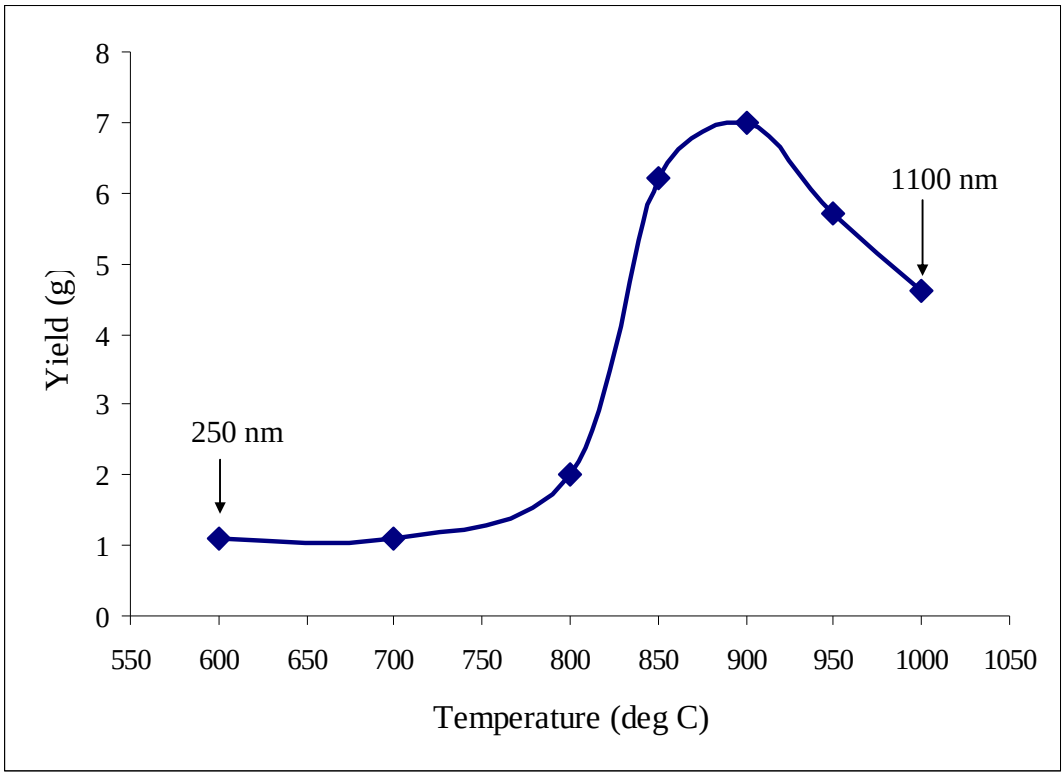

Fig. 10.2: A graph showing the amount of CSs produced as a function of temperature (reaction time = 2 h; C_2H_2 gas flow rate = 100 ml/min).

The yield of CSs produced when C_2H_2 was used as the feedstock gas increased with temperature from 600 (~ 0.2 g) to 900°C (~ 7.0 g). Thereafter, the yield decreased with further increase in temperature from 900 to 1000°C. After a series of experiments (not shown) it could be concluded that the optimum temperature for the production of carbon microspheres is 900°C under the reaction conditions used. The size and diameter distribution of the carbon spheres became larger with an increase in temperature as shown in Fig. 10.3. At 600°C, the average diameter of the spheres was 250 nm with uniform distribution (Fig. 10.3a). At 950°C (Fig. 10.3b) and 1000°C (Fig. 10.3c), the average diameter size increased to 1000 nm and 1300 nm respectively with a broader diameter distribution. Thus higher temperatures produced CSs with larger sizes. It is speculated that the carbon precursor undergoes pyrolysis at a faster rate at higher temperatures, which allows for more carbon deposition on the spheres resulting in larger sizes.

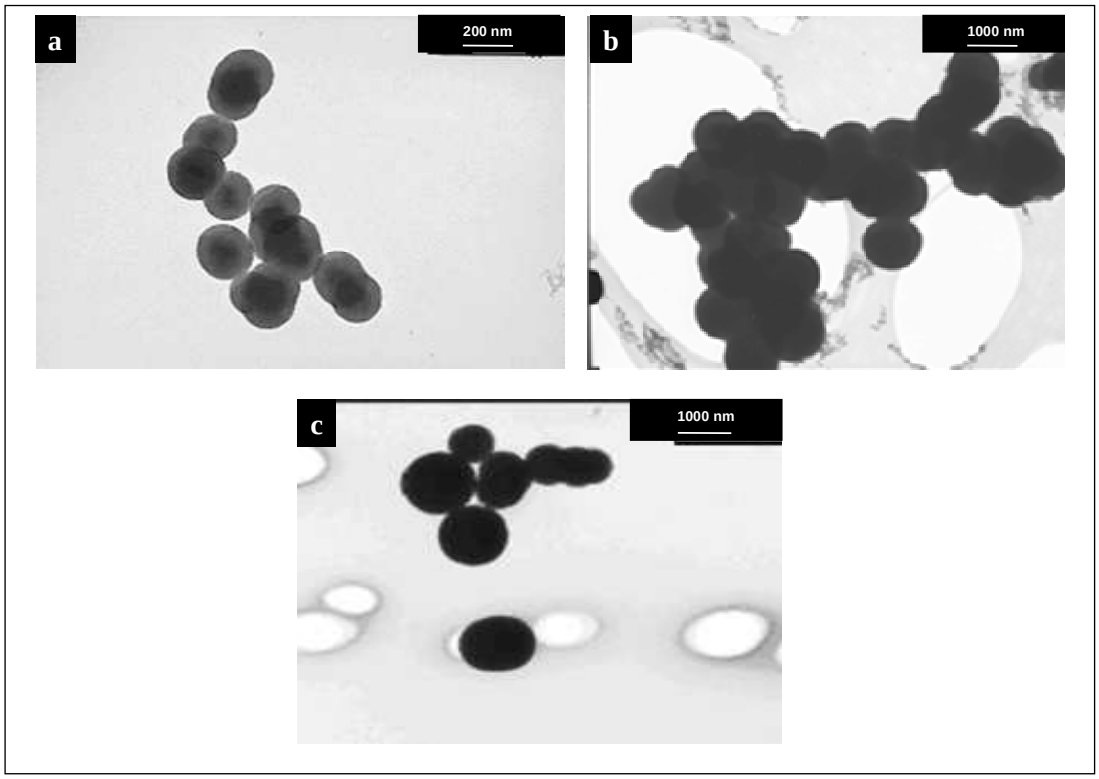

Fig. 10.3: TEM images of CSs synthesized at (a) 600°C, (b) 950°C and (c) 1000°C using C_2H_2 as a carbon source (100 ml/min) and a deposition time of 2 h.

The diameter distribution graph of CSs obtained at a temperature of 900°C with a C_2H_2 flow rate of 100 ml/min is shown in Fig. 10.4. It can be seen that the diameters of carbon spheres obtained lies in the range of 300 - 1900 nm, of which about 90% lie in the range 800 - 1000 nm. This shows that the carbon spheres obtained at 900°C are reasonably uniform in size.

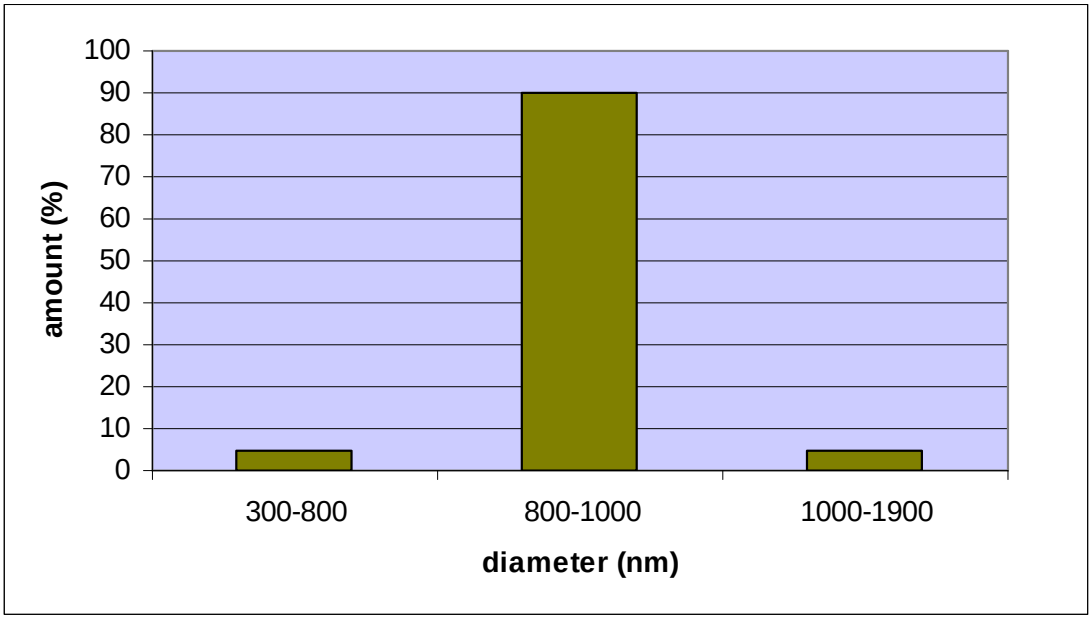

Fig. 10.4: Diameter distribution of CSs obtained at a temperature of 900°C, C_2H_2 flow rate of 100 ml/min and deposition time of 2 h.

10.3.3 Effect of reaction time

The C_2H_2 pyrolysis time was varied from 5 to 300 min at 900°C. The yield of CSs generally increased almost linearly with increase in pyrolysis time (Fig. 10.5). The products however changed from being soft and powdery to hard solid products at times > 150 min. It appears the hardness is related to the core-shell structure formation [21]. With time the shell forms and this makes the spheres 'harder'. An increase in the diameters of the spheres was observed with increase in the reaction time. However a huge variation in the size distribution within the same batch was also observed. This varied size distribution is a challenge, particularly if using the horizontal CVD to produce CSs.

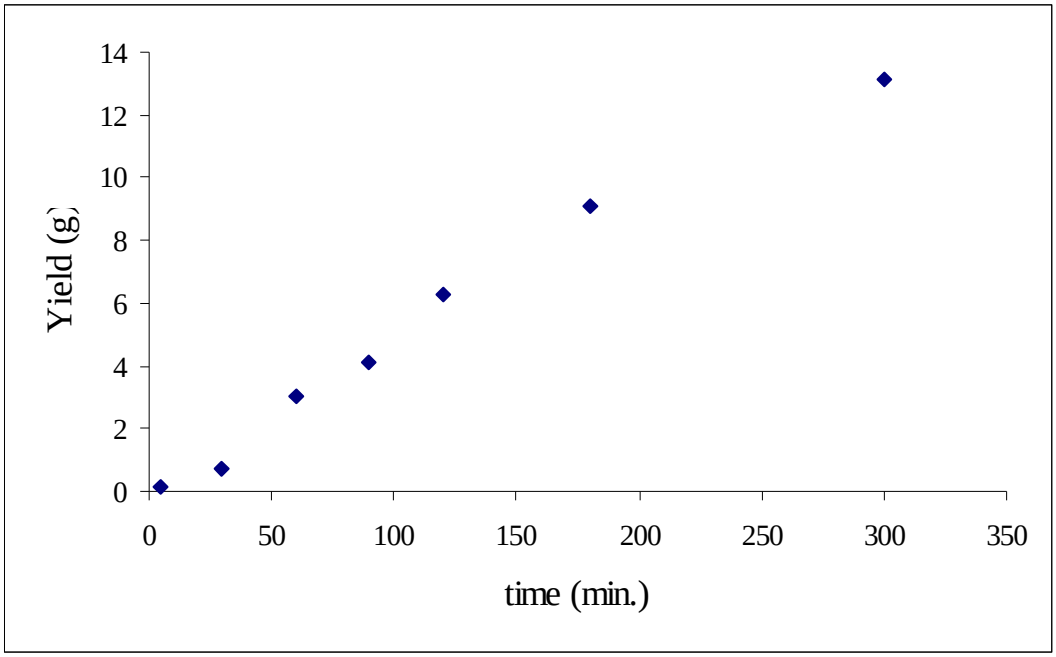

Fig. 10.5: Graph of yield of CSs against the pyrolysis time performed at 900°C using C_2H_2 (100 ml/min).

The observed variation of the diameters of the CSs within a unique experiment prompted the investigation of the effect of the temperature gradient inside the reactor. A series of experiments were performed at an acetylene flow rate of 100 ml/min; pyrolysis time of 2 h and T = 900°C and the set up illustrated in Fig. 10.6.

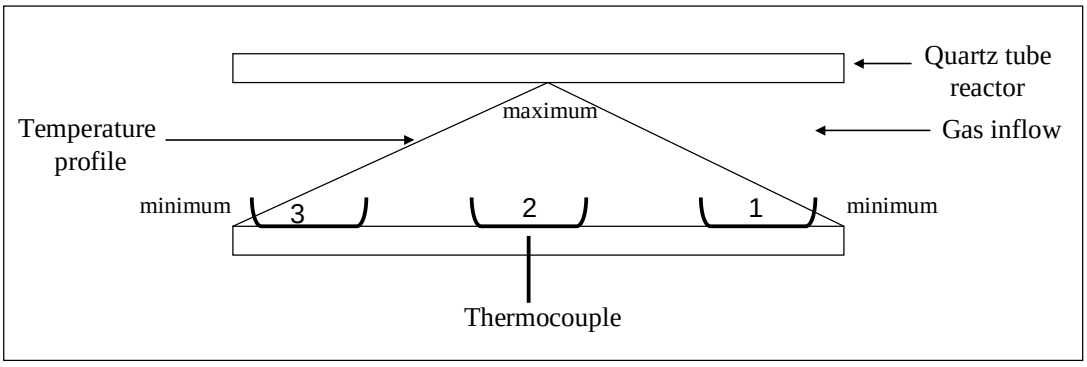

Fig. 10.6: Schematic diagram of the furnace with three quartz boats to collect the CSs.

By analyzing samples collected in the three different boats used in each experiment, it was observed that the CSs in each boat contained material with uniform diameters. However, the boats contained different sizes of microspheres. Generally, the boat placed at the centre of the tube, closest to the thermocouple i.e. boat 2 (Fig. 10.7), contained spheres with larger diameters.

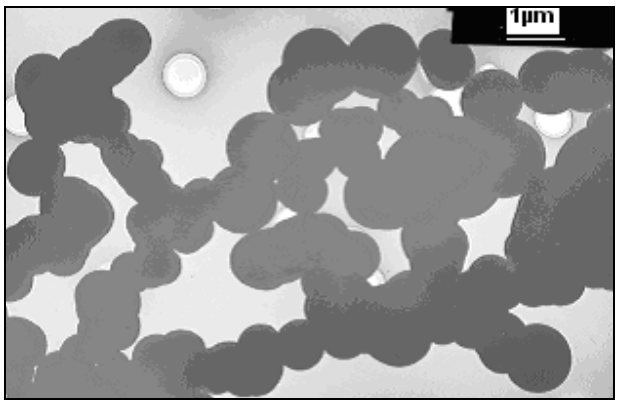

Fig 10.7: TEM image of CSs in boat 2 (T = 900°C, C_2H_2 flow rate = 100 ml/min, t = 2 h).

This observation was attributed to the fact that the temperature in the reactor is highest at this point. Also these results agree with those obtained earlier, that at higher temperatures, the diameters of the CSs also increase. Multiple conglomerates of the carbon spheres were abundant in most cases, even with experiments conducted at a pyrolysis time of 5 min (Fig. 10.8).

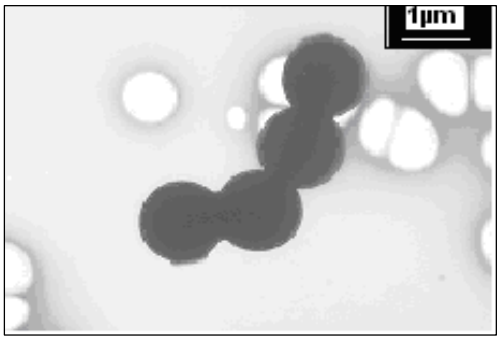

Fig 10.8: TEM image of agglomerated and chain-like CSs obtained at a pyrolysis time of 5 min (T = 900°C, C_2H_2 flow rate = 100 ml/min).

10.3.4 Effect of oxygenates (alcohol C:O ratio dependence) on the CS morphology

There are several studies in the literature that have reported the synthesis of carbon spheres from various hydrocarbons including methane, acetylene, toluene, benzene and anthracene [9,10,18,25-31]. To our knowledge no equivalent studies have been reported using alcohols as carbon sources for the synthesis of CSs. In this study, the synthesis of pure CSs from various *n*-alcohols (ethanol, 1-butanol, 1-hexanol, 1-octanol and 1-dodecanol) without the use of a catalyst was achieved *via* a horizontal injection CVD reactor. All products from the different alcohols appeared black, light weight soot, and some contained a grease-like oil; the yield was less than 1 g for every 10 ml of alcohol used. **Table 10.1** shows the experimental conditions used and corresponding diameters of the CSs obtained.

Table 10.1: The size and distribution of spheres formed from different alcohols.

Carbon Source	Boiling point (^{o}C)	Reactor temperature (^{o}C)	Injection flow rate (ml/min)	Sphere distribution (nm)	Number of moles (mol)
ethanol	78	1000	0.4	540 - 700	0.171
1-butanol	116 - 118	1000	0.4	200 - 500	0.109
1-hexanol	155 - 158	1000	0.4	280 - 700	0.0801
1-octanol	177 - 180	1000	0.4	380 - 700	0.0629
1-decanol	260 - 262	1000	0.4	200 - 600	0.0447

Characterization of the carbon soot by TEM gave evidence that the materials were all spherical and in most cases formed beaded necklace-like arrangements. Fig. 10.9 shows the spheres obtained from the various alcohols as seen under TEM. The TEM images also show the variation in sphere size and the distribution of the CSs for each alcohol used. The diameter distribution was determined in not less than 25 TEM images of each sample. These results give evidence that CSs were readily prepared from the various alcohol sources under the experimental conditions mentioned above.

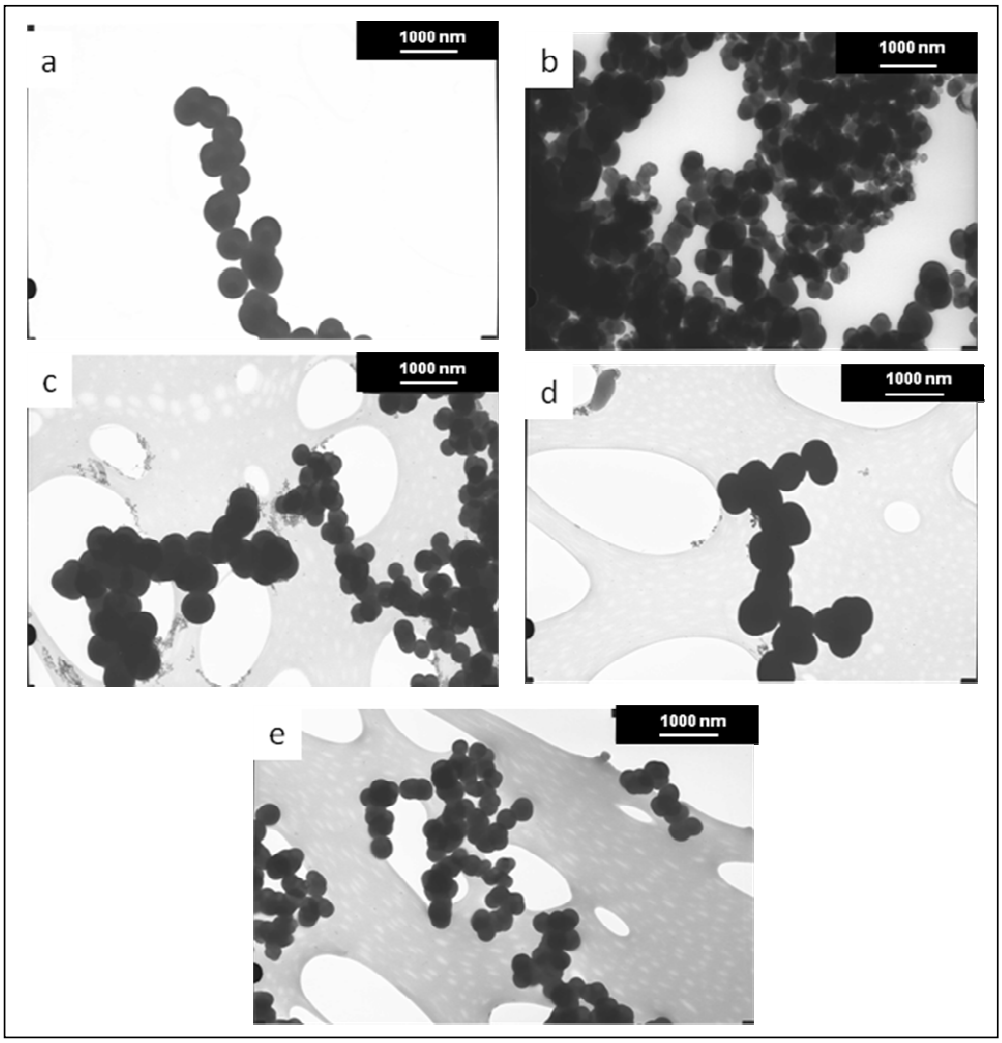

Fig. 10.9: TEM images of CSs synthesized from various alcohols, at 1000°C and an injection flow rate of 0.4 ml/min: (a) ethanol, (b) 1-butanol, (c) 1-hexanol, (d) 1-octanol and (e) 1-dodecanol.

There was no correlation observed between the alcohol used and the *size* of spheres obtained under the same experimental conditions. It was speculated that the size of the spheres would increase with an increase in the chain length of the alcohol. However this was not observed (**Table 10.1**). It was observed that the yield of the synthesized CSs was influenced by the chain length of the precursor (Fig. 10.10). Thus the yield increased from ethanol (C_1) to decanol (C_{10}). The boiling point of the alcohols increases from C_2 to C_{10}. It was speculated that due to the increase in the boiling point, the thermal

decomposition of the materials would require more energy and less products would be formed. However, the observation was the opposite; the yield increased with chain length.

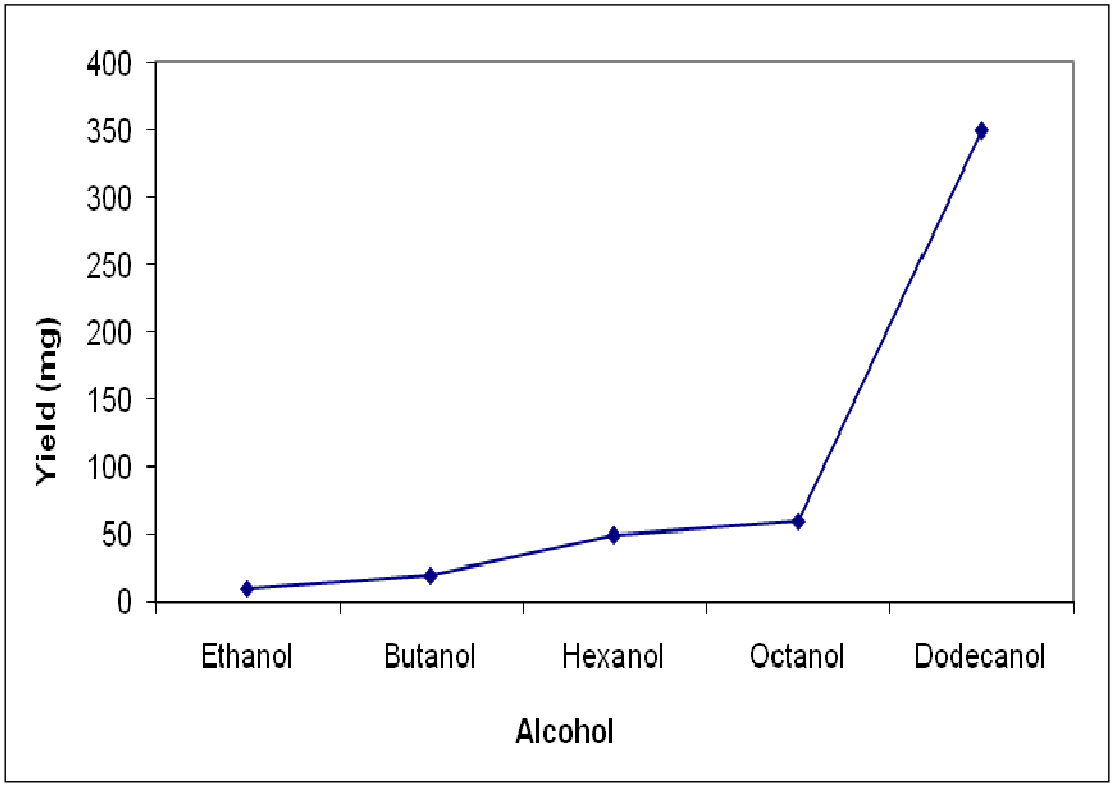

Fig. 10.10: The amount of CSs produced for each alcohol used (T = 1000°C, volume of alcohol = 10 ml, injection flow rate = 0.4 ml/min).

To explain this observation, the ratio of carbon to oxygen (C:O) was considered. **Table 10.2** gives the C:O ratios for each of the alcohols used and the corresponding yields of the CSs. As already mentioned, the yield increased with increase in the amount of carbon with respect to oxygen. This was explained as follows: In the presence of oxygen, graphitic carbon oxidizes to form carbon dioxide at temperatures greater than 550°C. The amount of oxygen present determines the degree of decomposition. For this reason ethanol, which has higher oxygen content with respect to carbon, will be consumed and hence less material would be collected. As the amount of O becomes less and the amount

of C increased, the amount of material collected is expected to increase since there is less oxygen to react with the carbon. This was observed.

It was also observed that a slow injection flow rate (0.2 ml/min) resulted in increase in the yield, while a faster rate (0.4 ml/min) resulted in low yields. At the higher flow rates (0.4 and 0.8 ml/min), no product was obtained from ethanol and only a small amount of product was obtained with 1-dodecanol. Therefore the expected inverse relationship between the flow rate and the yield was observed in the synthesis of CSs from alcohols.

The CS yield also increased with increase in temperature (900 - 1100°C). It has also been established (see Chapter 11 for data) that under controlled experimental parameters, sphere size is regulated by the structural and bonding properties of the hydrocarbons, and is independent of hydrocarbon vapour concentration.

Table 10.2: Carbon/oxygen ratios of the alcohols used and the corresponding yield for every 10 ml of alcohol injected at 1000°C.

Alcohol	C/O ratio	CS yield (mg)
ethanol	2:1	10
1-butanol	4:1	20
1-hexanol	6:1	50
1-octanol	8:1	60
1-decanol	10:1	350

The other important aspect of this study was to illustrate the effect of the oxygenates on the *sphere morphology*. In a separate study, various alkanes (pentane, hexane, and heptane) without any oxygen in their structure were used to make spheres. The results were compared to the data obtained in this study. Our findings revealed that the use of oxygenates readily removed amorphous material from the CS perimeter resulting in a smoother surface. Spheres synthesized from the alkanes contained some amorphous material as observed under TEM (Fig. 10.11b). Thus, this procedure for CS synthesis

results in cleaner materials and hence there would be no need post-treatment of the spheres as done with the spheres synthesized using alkanes.

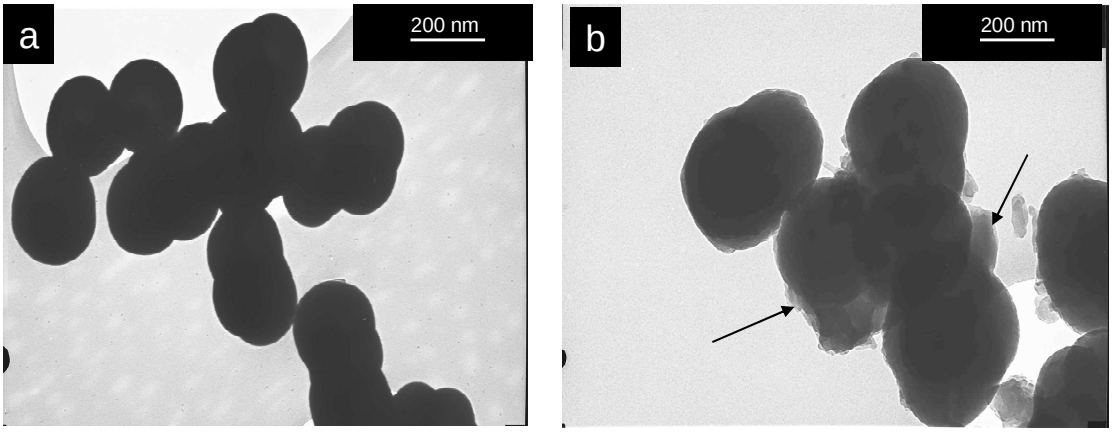

Fig. 10.11: TEM images of (a) CSs synthesized using 1-hexanol as carbon source and (b) CSs synthesized in the absence of oxygenates (hexane) showing some amorphous material on surface.

The results clearly show the importance of having small amounts of oxygen during the synthesis of CSs. Indeed, it is to be noted that industrially synthesized CSs (or carbon blacks) are produced by the reaction of a hydrocarbon fuel such as oil or gas with a limited supply of *combustion air* at temperatures of 1320 to 1540°C. The oxygen burns off some PAHs and amorphous carbon and it is the *unburnt carbon* that is collected as extremely fine black fluffy particles [32]. Thus the effect of using alcohols has similar consequences for the spheres produced in this study. Generally, yields are highest for large spheres and lowest for small spheres [32]. Our data is in agreement with the literature. We obtained higher yields at higher temperatures as well as larger sphere sizes compared with the use of lower temperatures.

10.3.5 Characterization of CSs

A growth mechanism for the graphitic CSs has been proposed based on the microstructural information obtained by high resolution transmission electron microscopy

(HRTEM) [2]. Our study is in agreement with previous studies and reveals that the carbon spheres are perfectly round, clean, solid and do not contain any large porosity (surface area 10 m^2/g). The structure is composed of graphitic flakes and the flakes are in the size range of 1 - 30 nm, with a partial order, similar to earlier reports [21]. The flake-like nature of the CSs implies that the surface structure is defective [1,2]. This suggests that functionalization of the spheres should be possible and that if metals are attached to the surface they should bind with ease. Indeed it is this feature that suggested that the Co/CSs materials should be excellent catalysts.

TGA was used to study the thermal stability of the CSs. The TGA profile of the CSs under air was compared to that of multi-walled carbon nanotubes (MWCNTs) that were synthesized in our laboratory. It was anticipated that if the spheres are graphitic, they should be stable up to about 600°C after which they would begin to gradually loose weight as they decompose to CO_2 (g). The differences observed between the profiles in N_2 and air are shown in Fig. 10.12. A comparison with the TGA of MWCNTs produced with an Fe-Co catalyst is also shown. It may be noted that the TGA profile of the CNTs contained residual metal oxide (3%) associated with the catalyst used to make the CNTs. This can be contrasted with CSs which contained only carbon and no deposit was left at T > 800°C. Also, the CSs decomposed over a wider temperature range suggesting that these materials were more stable and their solid graphitic carbon structure does not allow oxygen to permeate into the structure. Thus the CSs need to be oxidized layer by layer from the surface to the core. In contrast, the fast decomposition of the MWCNTs suggests that pores within and in-between the tubes allows oxygen to diffuse into the graphitic carbon structure with ease. The CSs were found to be stable when heated under N_2 and that was associated with the high stability of the materials under inert conditions; which is typical for the graphite form of carbon.

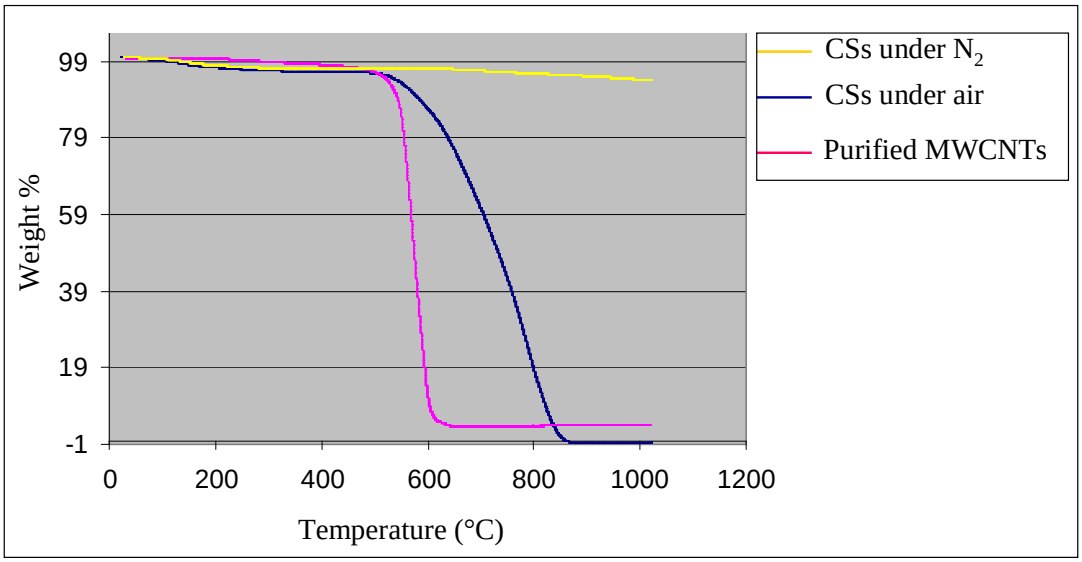

Fig. 10.12: TGA plots of CSs heated under N_2 and CSs heated under air as well purified MWCNTs.

10.3.5 The effect of temperature on performance of Co/CS catalyst

The CSs were synthesized from the pyrolysis of C_2H_2 as described earlier. Co was added to the CSs as described in the experimental section. The activity of as-synthesized (without any reduction pretreatment) as well as pre-reduced 5 wt%-, 10 wt%- and 20 wt%Co/CS catalysts was investigated for the ethylene hydrogenation reaction. The unreduced catalysts as expected were less active and no further information on these unreduced materials will be reported here.

The order of activity for the reduced catalysts was 10 wt% >> 20 wt% > 5 wt%. This effect relates to the exposed surface Co atoms and suggests that if the metal particles are too large, then catalytic activity is lowered. This issue will need to be explored further in later studies. The optimum temperature for the conversion of the ethylene was found to be 100°C for all three catalysts. The conversion of C_2H_4 with the 10 wt% Co/CS catalyst was *ca* 100% at 100°C. However at higher temperatures (T > 100°C), the activity of all three catalysts decreased significantly (Fig. 10.13). This decrease could arise from

catalyst deactivation by sintering or by deposition of carbonaceous deposits on the Co. As discussed below the latter explanation can explain the data.

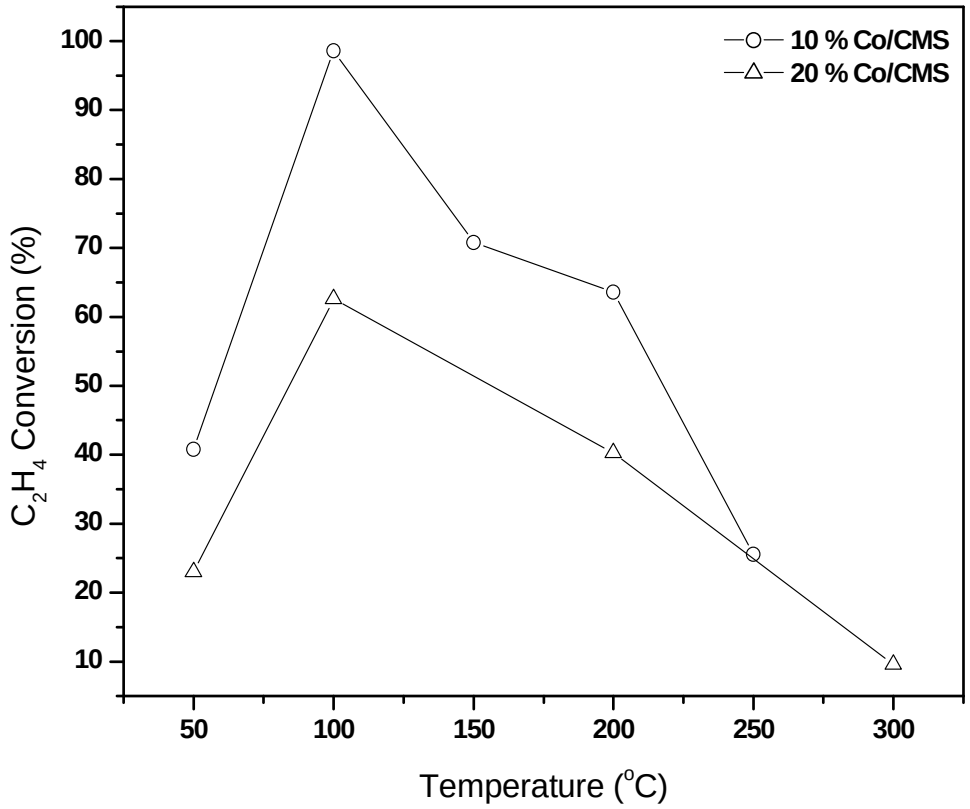

Fig. 10.13: C_2H_4 conversion using catalysts pre-reduced by H_2 at 400^oC for 4 h; H_2/C_2H_4 = 3.05, Catalyst = 0.05 g, GHSV = 71000 $cm^3g^{-1}h^{-1}$.

10.3.7 Time on stream (TOS) studies using pre-reduced catalyst

The pre-reduced catalysts were tested for activity by performing reactions for 16 h. The C_2H_4 conversion was monitored at regular time intervals. It was observed that the catalysts maintained a markedly high percentage conversion throughout the reaction (Fig. 10.14). Such activity is not always observed with many commonly used hydrogenation catalysts (e.g. Pt, Pd and Ni), which are usually supported on silica, activated carbon and γ-alumina [22-24]. The data suggests that no sintering of the catalyst particles is taking

place and that no poisoning due to coverage of the Co by carbonaceous material is taking place at this temperature.

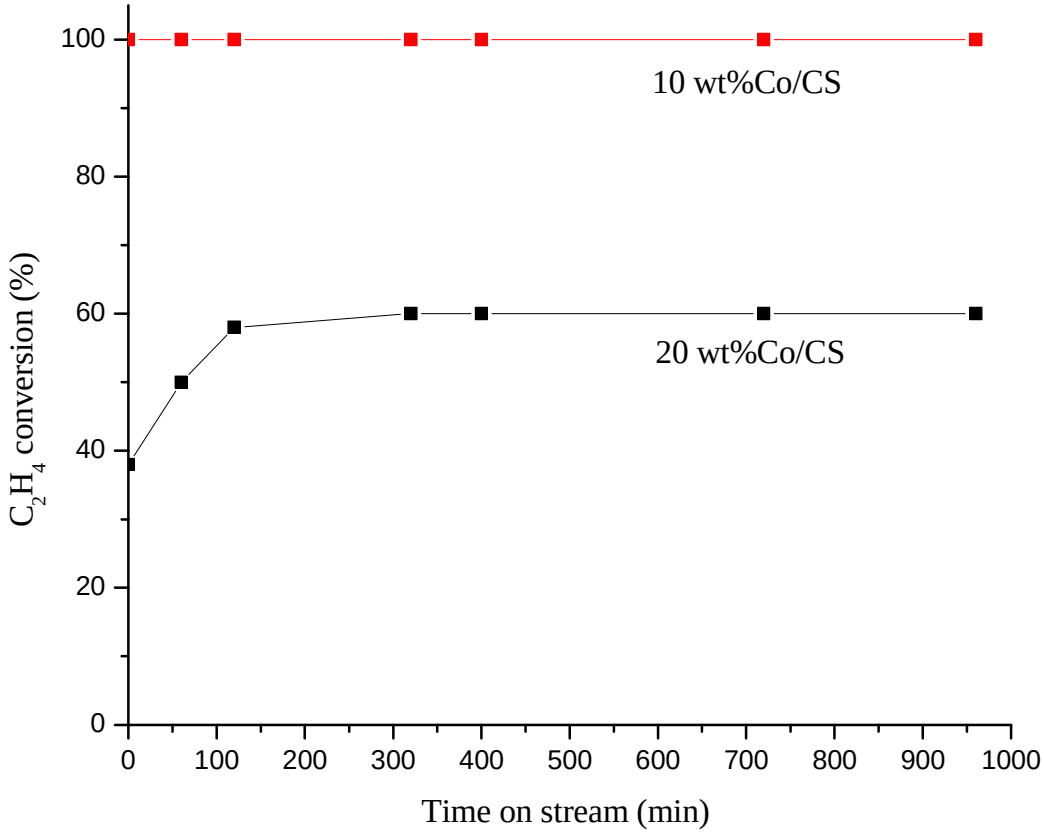

Fig. 10.14: Time on stream over 10- and 20 wt %Co/CMS catalysts (after pre-reduction by H_2 at 400°C for 4 h) in the hydrogenation of ethylene [H_2/C_2H_4 = 3.05, catalyst used = 0.05 g, GHSV = 71000 $cm^3g^{-1}h^{-1}$], T = 100°C.

The Co/CS catalyst showed good activity and chemical stability against deactivation in the time-on-stream study. These results indicate that this catalyst gives better activity and stability when compared with an activated carbon supported Co catalyst [21]. The carbon microspheres have been shown to be a promising support for metal catalysts, in particular for the hydrogenation of ethylene in the presence of Co. Future studies will establish generality and limits of this new catalyst.

10.4 Conclusions

We have demonstrated the direct pyrolysis of C_2H_2 in the absence of a catalyst is an efficient method to produce CSs in large quantities. Different pyrolysis conditions were used to study the size and morphology as well as the distribution of the resulting CSs. The effect of pyrolysis temperature played an important role and influenced both the size and yield of the product. The experiments performed showed that at 900°C, the resulting spheres were prepared in high yield and were of large size (~ 1 μm) and had uniform distribution. The detailed experiments conducted with C_2H_2 as a precursor indicates that the diameters of the carbon spheres can be controlled by varying the pyrolysis conditions (e.g. temperature and synthesis time) and that the process could readily be scaled up for commercial production. It is a variant of the carbon black synthesis procedure.

Another interesting feature explored is the use of oxygenates to make CSs. The yields were generally lower with the alcohols and this was ascribed to the presence of the O atoms in the alcohol. However the oxygenates readily remove amorphous material from the surface of the CSs resulting in the formation of a smooth clean surface. This finding is important and suggests that this is still an interesting area to explore.

CSs have been shown to be a promising support for metal catalysts. The percentage of catalyst loading greatly affects the activity of the CS supported catalysts. The CS supported catalysts showed remarkable stable activity for a long period of time on stream. The abundance of defects in the CSs makes them highly reactive and is consistent with their catalytic support applications. The possibilities of further surface chemical modification of the CSs to produce modified catalyst supports is to be explored.

10.5 References

1. Z.C. Kang, Z.L. Wang, J. Mol. Catal. A: Chemical **118** (1997) 215.
2. Z.C. Kang, Z.L. Wang, J. Phys. Chem. **100** (1996) 5163.
3. Q. Wang, H. Li, L. Chen, X. Huang, Carbon, **39** (2001) 2211.

4. V.G. Pol, M. Motiei, A. Gedanken, J. Calderon-Moreno, M. Yoshimura, Carbon **42** (2004) 111.
5. F. Li, Q. Qian, F. Yan, G. Yuan, Carbon **44** (2006) 128.
6. X. Liu, B. Huang, N.J. Coville, Carbon **40** (2002) 2791.
7. L.P. Biró, G.I. Márk, Z.E. Horváth, K. Kertész, J. Gyulai, J.B. Nagy, Ph. Lambin Carbon **42** (2004) 2561.
8. A. Ma, X. Wang, T. Li, X. Liu, B. Xu, Mat. Sci. and Eng. A **443** (2007) 54.
9. H. Qian, F. Han, B. Zhang, Y. Guo, J. Yue, B. Peng. Carbon **42** (2004) 761.
10. Y.Z. Jin, C. Gao, W.K. Hsu, Y. Zhu, A. Huczko, M. Bystrzejewski, M. Roe, C.Y. Lee, S. Acquah, H. Kroto, D.R.M. Walton, Carbon **43** (2005) 1944.
11. M. Wissler, J. Power Sources **156** (2006) 142.
12. http://www.carbonblack.jp/en/cb/youto.html#top (accessed 4th December 2006).
13. J. Lahaye, Carbon **30** (1992) 309.
14. F. Fallcheri, Y. Schwob, J. Hydrogen Energy **20** (1995) 197.
15. D.B. Scully, R.A. Davies, *Carbon from aromatic hydrocarbons*, Manchester, Vol. 9, pp. 185-189, (1965).
16. D. Ugarte, Nature **359** (1992) 707.
17. Z.L. Wang, Z.C. Kang, Phil. Mag. B **74** (1996) 51.
18. M. Sharon, K. Mukhopadhyay, K. Yase, S. Ijima, Y. Ando, X. Zhao, Carbon **36** (1998) 507.
19. Y-G. Wang, Y-C. Chang, S. Ishida, Y. Korai, I. Mochida, Carbon **37** (1999) 969.
20. B.C. Gates, *Catalytic chemistry*, John Wiley and Sons, Inc. New York, (1992).
21. K.C. Mondal, L.M. Cele, M.J. Witcomb, N.J. Coville. Cat. Comm. **9** (2008) 494.
22. C. Park, R.T.K. Baker, J. Phys. Chem. B **103** (1999) 2453.
23. A. Chambers, T. Nemes, N.M. Rodriguez, R.T.K. Baker, J. Phys. Chem. B **102** (1998) 2251.
24. C. Park, R.T.K. Baker, J. Phys. Chem. B **102** (1998) 5168.
25. P. Serp, R. Feurer, P. Kalck, Y. Kihn, J.L. Faria, J.L. Figueiredo., Carbon **39** (2001) 621.
26. A.L. Ma, X.M. Wang, T.B. Li, Carbon **443** (2007) 54.

27. L.Q. Xu, W.Q. Zhang, Q. Yang, Y.W. Ding, W.C. Yu and Y.T. Qian, Carbon **43** (2005) 1084.
28. D. Pradhan, M. Sharon, Mater. Scie. Engin. B **96** (2002) 24.
29. Q. Wang, F.Y. Cao, Q.W. Chen, Mater. Lett. **59** (2005) 3738.
30. V.G. Pol, S.V. Pol, J.M.C. Moreno, Carbon **44** (2006) 385.
31. X.C. Ma, F. Xu, L.Y. Chen, Carbon **44** (2006) 2861.
32. http://www.epa.gov/ttn/chief/ap42/ch06/final/c06s01.pdf, Chemical organic process industry, accessed on 16th February 2009.

Chapter 11

Controlled syntheses of carbon spheres in a swirled floating catalytic chemical vapour deposition (SFCCVD) vertical reactor[#]

11.1 Introduction

Spherical carbon structures have been receiving interest since their discovery in the 1940s [1] and especially since the discovery of the fullerenes in 1985 [2]. Indeed, in the last two decades many different types of spherical carbons have been reported, both hollow and solid, and these include carbon onions [3,4], carbon microspheres [5-9], carbon beads [10-12] and carbon pearls [13]. The type of spherical particle produced is dependant on the method of preparation, carbon source and the reaction conditions used [5-12]. These spherical materials have many potential applications such as use as absorbents [14,15], as catalyst supports [16] or as anodes for use in lithium ion batteries [9,17].

In this publication carbon spheres (CSs), both carbon microspheres (CMSs) and carbon nanospheres (CNSs), have been produced in a vertical reactor using a vertical mixer i.e. using a vertical swirled floating catalyst (SFC) reactor. The method provides a means for the continuous production of high purity carbon spheres with uniform diameter in the absence of a catalyst. Previously other methods such as chemical vapour deposition [18], pyrolysis of carbon sources and catalysts [19], an arc plasma technique [20], mixed-valence oxide-catalytic carbonization [6], and reduction of carbides with metal catalysts [21] have been reported for the synthesis of carbon spheres.

Interestingly, CSs have been known for many decades and have been made by procedures similar to the procedure described herein.

[#]*Sabelo D. Mhlanga, Neil J. Coville, Sunny E. Iyuke, Ayo S. Afolabi, Saka A. Abdulkareem, Nikiwe Kunjuzwa, to be submitted, 2009.*

These materials, referred to as carbon black particles [22,23], have been produced from a carbon source such as oil or natural gas, typically in the presence of small amounts of oxygen. For example, when acetylene is used under a reduced presence of oxygen the process is called the acetylene black process [24-26]. While much information has been generated in this area, to our knowledge, no report has appeared that systematically relates CS particle size (as determined by electron microscope studies) to reaction conditions as described in this study.

11.2 Experimental

The synthesis of carbon spheres was carried out in a swirled floating catalytic chemical vapour deposition reactor developed by Iyuke *et al.* and presented schematically in Fig. 11.1 [27,28]. Briefly, it consists of a vertical quartz (fluidized bed) reactor loaded in a tubular furnace. Gases (argon, nitrogen and acetylene) flow, with the aid of a system of valves and rotameters, through a swirled coiled passage that enables mixing of the gases before they enter the reactor (Fig. 11.1). While the reactor was designed for using catalysts, hence called catalytic reactor, the same system was used without introducing a catalyst in this study.

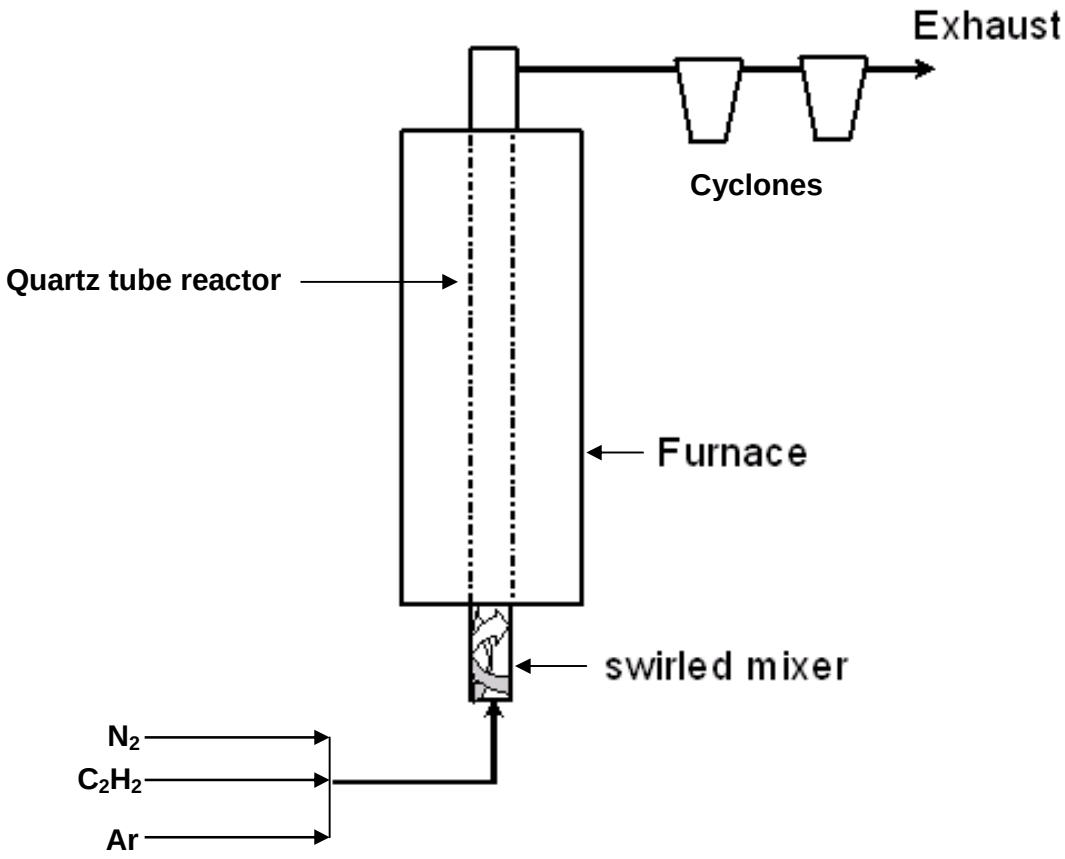

Fig. 11.1: Schematic representation of the swirled floating catalytic chemical vapour deposition reactor.

The furnace was set to a desired temperature under a nitrogen flow (30 ml/min), which was then stopped and acetylene (C_2H_2) together with an inert gas (argon) was fed through the reactor at specified flow rates. A smoky carbon vapour together with black soot from the direct pyrolysis of C_2H_2 was generated and carried to the upper end of the reactor where it was cooled in a condenser (room temperature) and collected in two cyclones. The product from the cyclones was analyzed using Transmission Electron Microscopy (TEM) (JEOL 100S Electron Microscope and a Philips CM200 High Resolution TEM), Thermogravimetric Analysis (TGA) (Perkin Elmer Pyris 1 TGA Anaylzer), Raman Spectroscopy (Jobin-Yvon T64000 micro-Raman spectrometer equipped with a liquid nitrogen cooled charge coupled device detector and excitation laser wavelength of 514.5 nm), BET surface area analysis (Micromeritics TriStar Surface Area and Porosity

Analyzer) and Powder X-ray diffractometry (PXRD) (Bruker axs D8 Advance PXRD). The carbon, hydrogen and nitrogen (CHN) content was performed at the Institute for Soil, Climate and Water (Pretoria). The reaction temperature (900 - 1000°C), acetylene (70 - 370 ml/min) and argon (70 - 480 ml/min) gas flow rates were varied in order to study their effect on the structure and yields of the CSs obtained.

11.3 Results and Discussion

11.3.1 Characterization of carbon spheres

No catalyst was used for the synthesis of the CSs. The materials produced were very pure and unlike products obtained during synthesis in the presence of a catalyst; the CSs contained no amorphous material and did not require removal of catalyst in a post-synthesis process. The yield and sizes (50 - 250 nm) of the spheres formed could be controlled by changing the reaction conditions.

A typical example is described below.

C_2H_2 (118 ml/min) was passed through the reactor at 900°C. The reaction was stopped after 4 min (gas flow changed to argon) and 1.4 g of soot was collected from both the reactor and the cyclones. The synthesis time was determined by the maximum amount of carbon soot deposited in the reactor and cyclones. TEM analysis of the soot from both the reactor and the cyclone appeared to be identical. A TEM image of the soot (Fig. 11.2a) reveals that only spherical nanoparticles of carbon (> 99%) were formed and that these spheres have an average diameter of 100 nm and show a narrow distribution range. The time that the acetylene spends in the reactor is estimated to be 33 seconds and within this short time frame the spheres are already accreted [7].

It is clear that at the high temperature used, the carbon radicals formed in the gas phase under these conditions nucleate and rapidly form the solid spheres [6-8]. The current mechanism for sphere growth is consistent with the results found in earlier studies [7,29].

What is unusual is that the sizes of the spheres are so uniform in diameter. This would suggest that nucleation must commence at the reactor inlet and that once nucleation has commenced deposition of further carbon onto the sphere must be more rapid than further nucleation in the upper end of the reactor. It would appear that once nuclei are formed, the rate of sphere formation will then be determined by the C_2H_2 concentration and the reactor length. However, it also appears that once the sphere has reached an optimum size then little further growth of the sphere takes place.

The spheres form a light and fluffy material, quite different in texture from spheres that we have obtained from similar studies performed in a horizontal reactor [30]. In the horizontal reactor the spheres are left in the reactor at high temperature for a much longer time (15 - 120 min) resulting in secondary reactions occurring on the sphere perimeter. HRTEM analysis of the two types of spheres also reflects this difference (Fig. 11.2b). Spheres obtained from a horizontal reactor have a distinctive core/shell structure whereas the spheres synthesized in the vertical reactor do not show this phenomenon (Fig. 11.2c). As seen in the HRTEM image the spheres show a poorly graphitic structure with short (wavy) carbon layers next to and on top of each other. The surface area analysis of the spheres gave a value of 7 m^2/g indicating that the spheres had little or no porosity. CHN analysis of the spheres revealed that the materials contained carbon (~ 98%) and the remaining 2% comprising hydrogen and some oxygen.

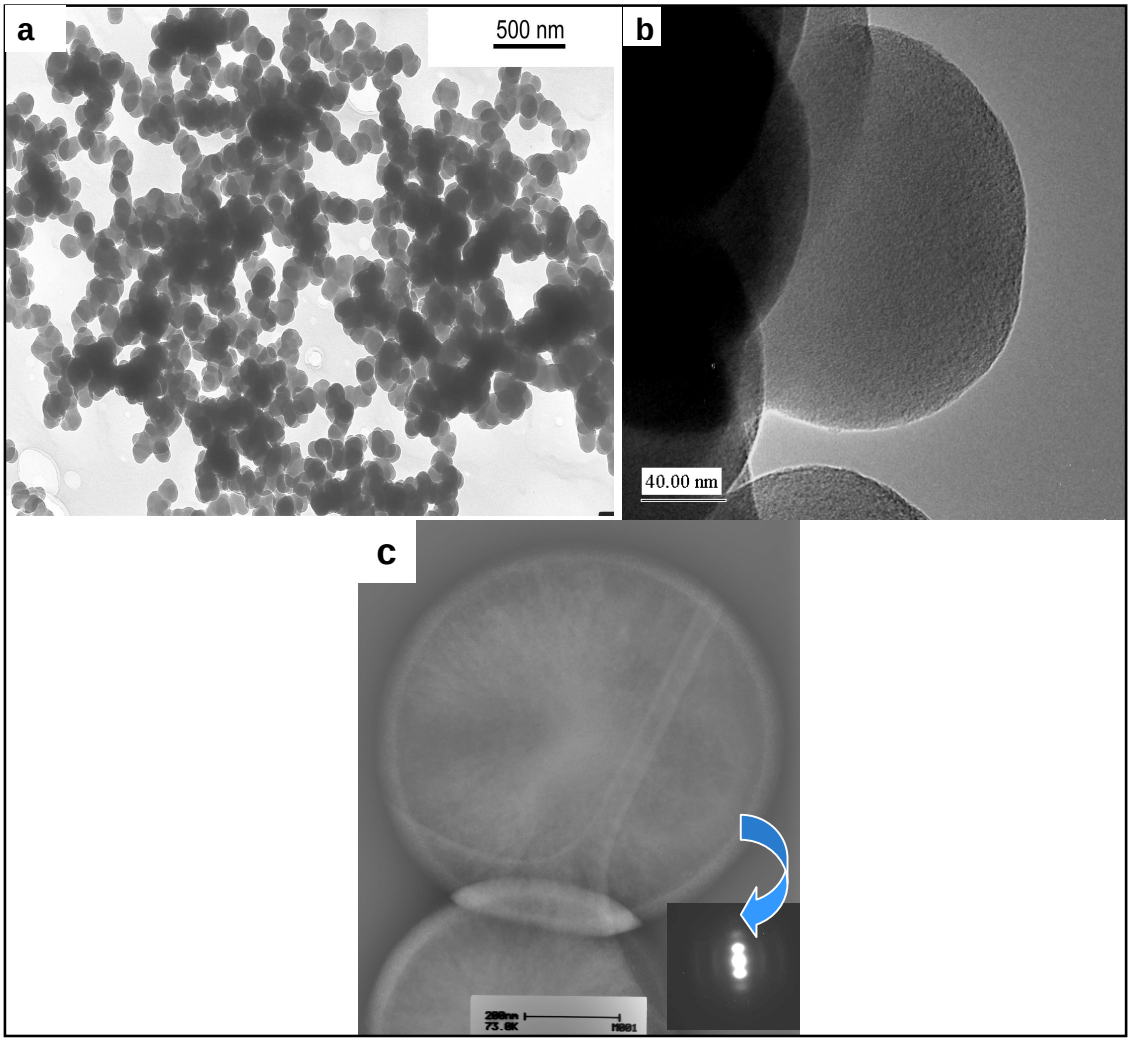

Fig. 11.2: (a) TEM image of CSs produced by the SFCCVD technique at 900°C with C_2H_2 gas flow rate of 118 ml/min, (b) Corresponding HRTEM image of the CSs and (c) HRTEM image of CSs synthesized in a horizontal furnace with the diffraction pattern of the shell of the CS [Inset].

The effect of heat treatment on the CS morphology was investigated. The CSs were placed in a quartz boat in a horizontal furnace and heated under a continuous flow of nitrogen (40 ml/min) at 800°C for 1 h. Upon heating, the surface area of the CSs increased to 15 m^2/g. A TGA analysis of both the as-prepared and post-heated samples is shown in Fig. 11.3. The TGA data indicates an approximately 20% mass loss between 100 and 400°C for the as-prepared spheres, which is not observed after post treatment heating. The results are consistent with the surface area data and suggest that the spheres

prepared in the vertical reactor contain readily removed species (either covalently or physically attached). When the CSs were heated in the reactor under a continuous flow of argon, a black oily substance was generated inside the reactor. It is presumed that this oil may be associated with the 20% material lost in the TGA experiment. This grease was also formed when the CSs were synthesized in a horizontal furnace. However in the horizontal CVD reactor, the grease is found at the exit end of the reactor [30]. While this material found in both the horizontal and vertical reactors it must be a precursor to the solid spheres. The material lost is associated with polycylic aromatic hydrocarbons (PAHs), which have been identified in carbon black extracts in earlier studies [31-33].

Lee and Hites [31] analysed the organic extracts of several carbon blacks which were manufactured under varying conditions. Interestingly they first reported identification of sulfur-containing polycyclics in carbon black. In addition, the detection of high-boiling PAHs was extended to include compounds of molecular weights up to 376 ($C_{30}H_{16}$). Capillary column gas chromatography combined with mass spectrometry (GC/MS) was used for the positive identification of 21 compounds, including naphthalene, pyrene, anthracene, phenanthrene, acenaphthylene, dibenzothiophene, benzo(a)pyrene, benz(a)anthracene etc. [31]. Indeed, the presence of PAHs was identified in earlier studies which also identified the presence of oxygenated polycyclics in the carbon black extracts [32,33].

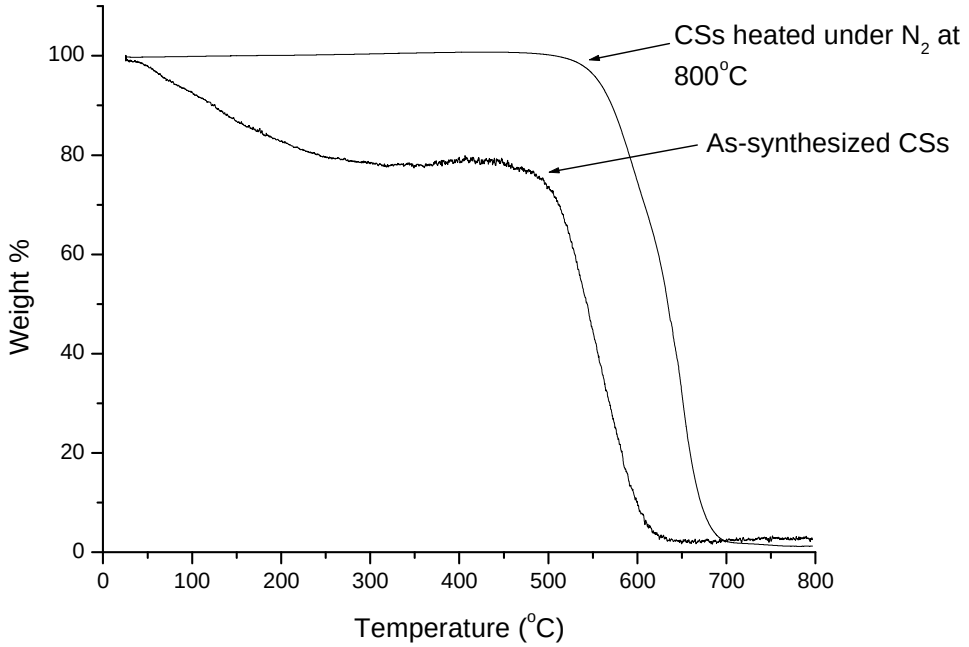

Fig. 11.3: TGA profile of CSs in an oxidizing (air) atmosphere.

TEM analysis of the post heated material is shown in Fig. 11.4. The image reveals that the CSs are made up of disordered arrays of graphene sheets of carbon. These layers are estimated to be 3 Angstroms apart and they form a spherical shape that typifies the CSs. It can be observed that some of the spheres are linked together (accreted) (see arrows indicating the region where two spheres have coalesced in Fig. 11.4b. No outer core shell is again observed for the CSs produced even after the post heating process at 800°C for 3 h [30]. Thus no significant change in the sphere morphology occurs in the post-heating process.

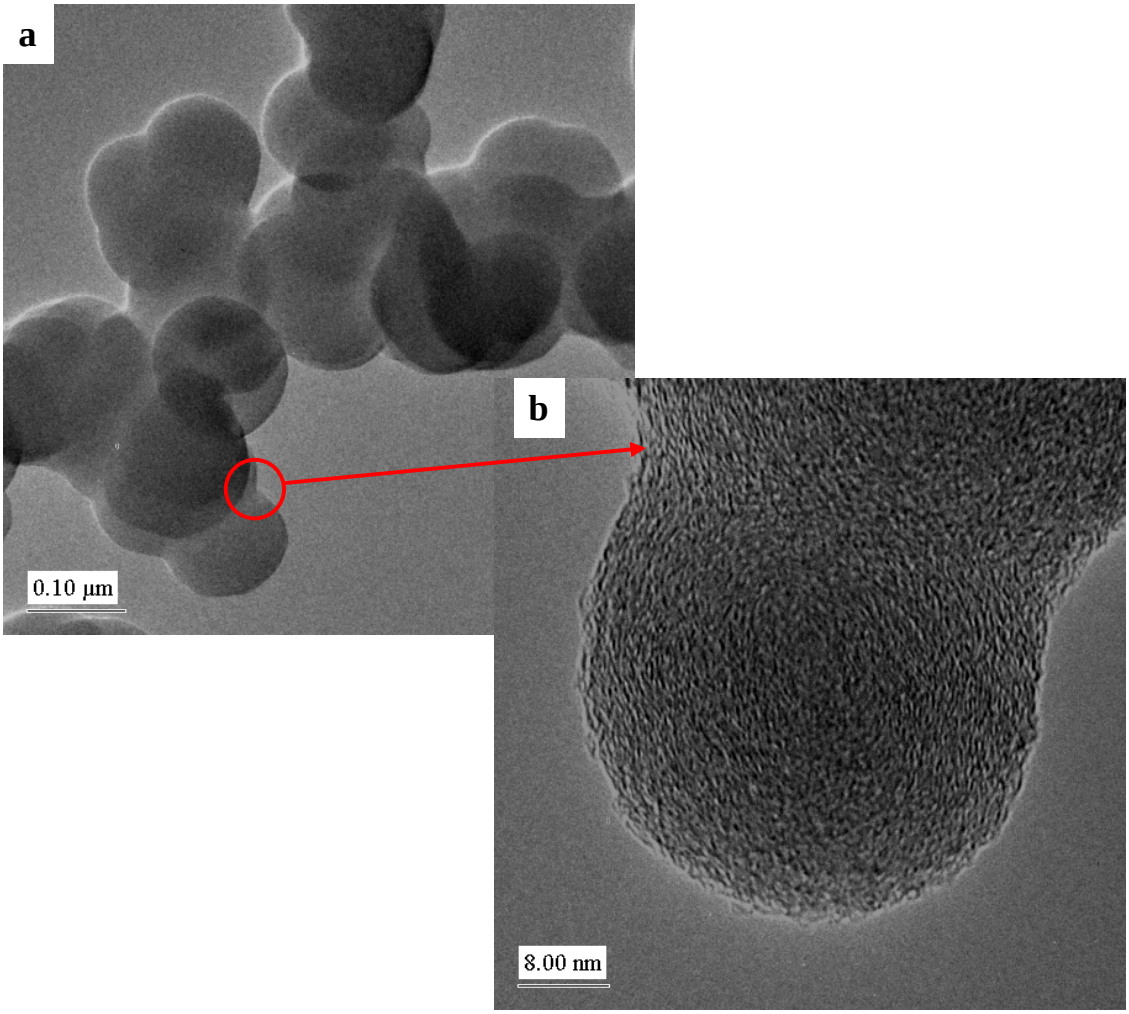

Fig. 11.4: TEM image of CSs after heating at 800°C under nitrogen flow.

11.3.2 Effect of C_2H_2 flow rate and temperature

A series of experiments were carried out to study the effect of acetylene flow rate and temperature on the production rate, size and structural morphology of the CSs. The acetylene gas flow rate was varied from 70 - 370 ml/min while the pyrolysis temperatures used were 900, 950 and 1000°C respectively. The rate of production of CSs increased with increase in the feedstock flow rate at all pyrolysis temperatures. In general, a higher temperature results in a modest increase in yield (Fig. 11.5). A maximum production rate of ~ 0.35 g/min was obtained using an acetylene flow rate of 370 ml/min and a pyrolysis

temperature of 1000°C. The small effect of temperature suggests that above a certain minimum temperature that the carbon species required to form the spheres are available in sufficient concentration and do not limit sphere formation.

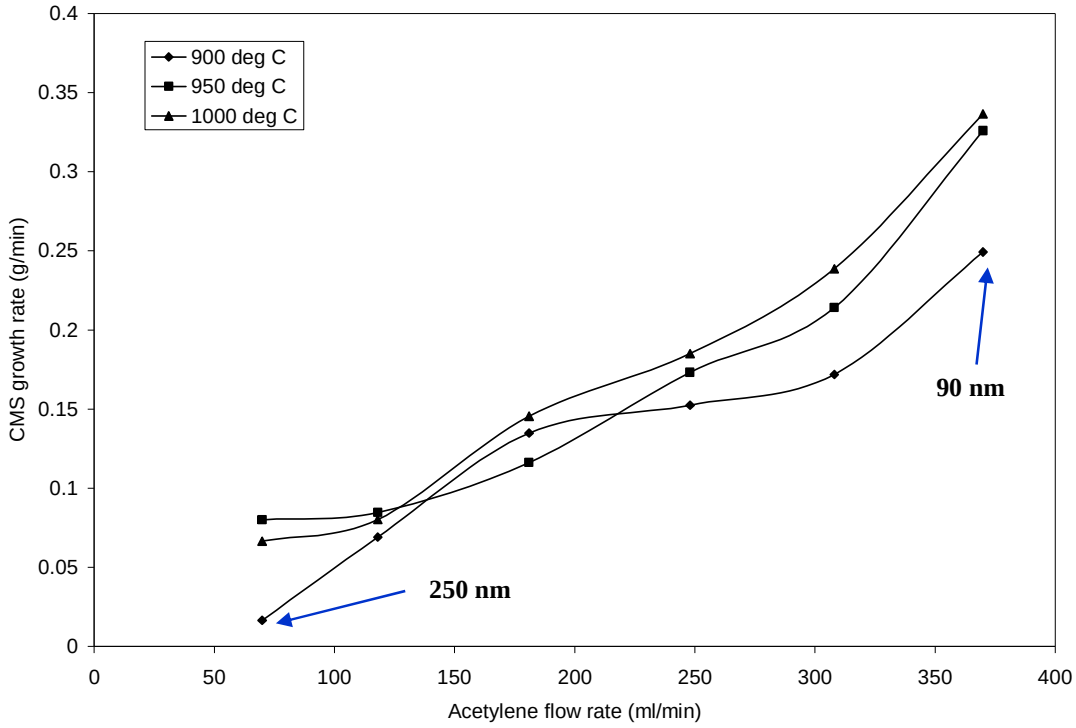

Fig. 11.5: Rate of CS production at different temperatures and flow rate of acetylene.

Table 11.1 shows the sizes of CSs obtained with different C_2H_2 gas flow rates and at different pyrolysis temperatures. The results show that at 900°C and as the flow rate of C_2H_2 increases, the size of the CSs decreases. This observation relates to the residence time of C_2H_2 in the reactor. The residence time of the C_2H_2 will be higher at the lower flow rate of C_2H_2 and this will allow the products to further accumulate reactants before exiting into the cyclones. Results also show that the CS size increases as the pyrolysis temperature increases. At a fixed C_2H_2 flow rate of 118 ml/min, the size of the CSs increases from 120 nm to 150 nm as the pyrolysis temperature increases from 900 - 1000°C.

Table 11.1: Diameters of CSs produced at different temperatures and C_2H_2 gas flow rates.

Temperature (°C)	C_2H_2 flow rate (ml/min)	Av. diameter (nm)
900	70	250
900	118	120
900	181	100
900	248	90
950	118	100
1000	118	150

The effect of C_2H_2 dilution, with carrier gas (Ar), on the production rate of the CSs was also investigated at 1000°C. The Ar flow rate was varied from 70 - 370 ml/min while the C_2H_2 flow rate was fixed at 181 ml/min. In general, at the same flow rate, dilution of the C_2H_2 with argon at the same total flow rate is expected to lead to lowered yields of soot. However, at the increased total flow rate the data (Fig. 11.6) show that the rate of formation increases with dilution. Furthermore, the effect is not linear and a drop in sphere formation rate is to be noted between argon flow rates of 250 and 350 ml/min. This result is reproducible. As the flow rate of the carrier gas increased beyond 310 ml/min, the production rate of CSs increased again.

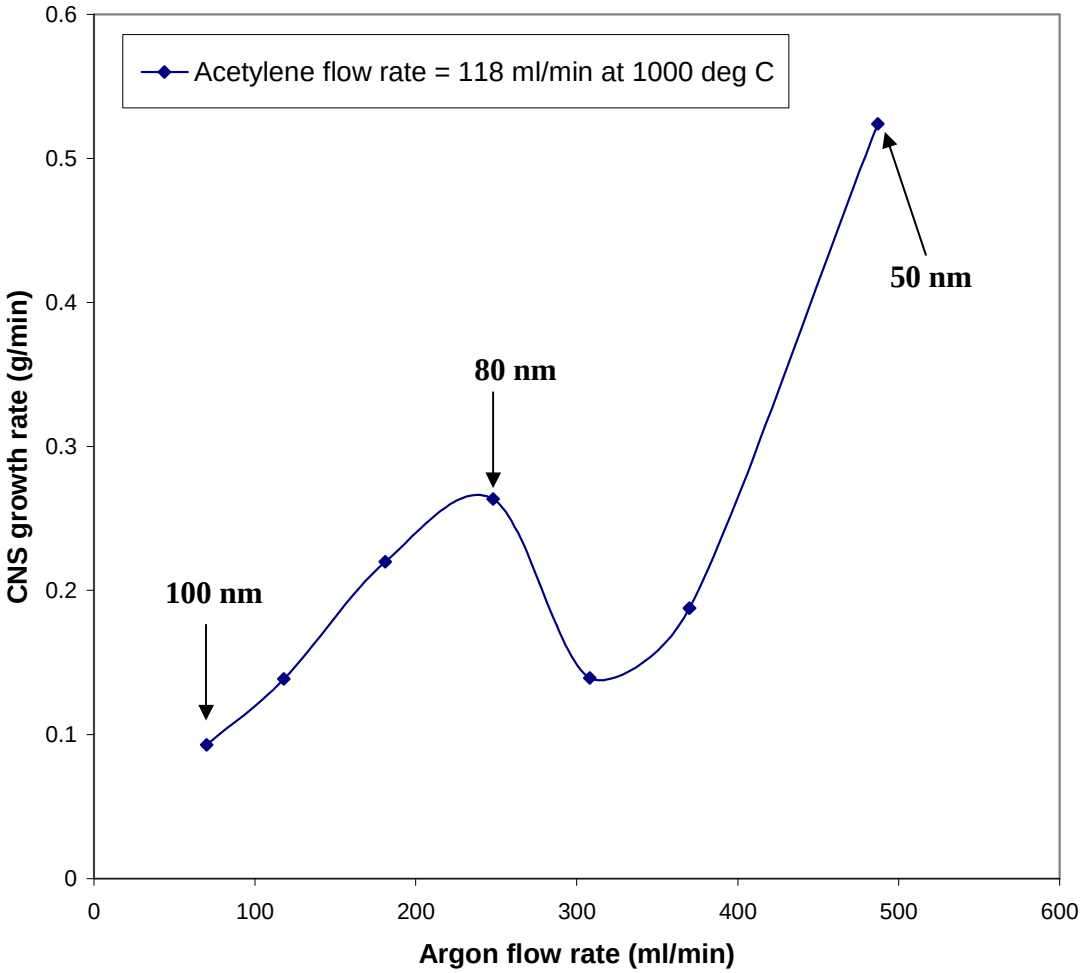

Fig. 11.6: Effects of carrier gas on rate of CS production at constant flow rate of acetylene and temperature.

The size distributions of the CS products are shown Fig. 11.7. The spheres are quite uniform in size (> 80%) and possess similar features to the CSs produced without Ar as a carrier gas.

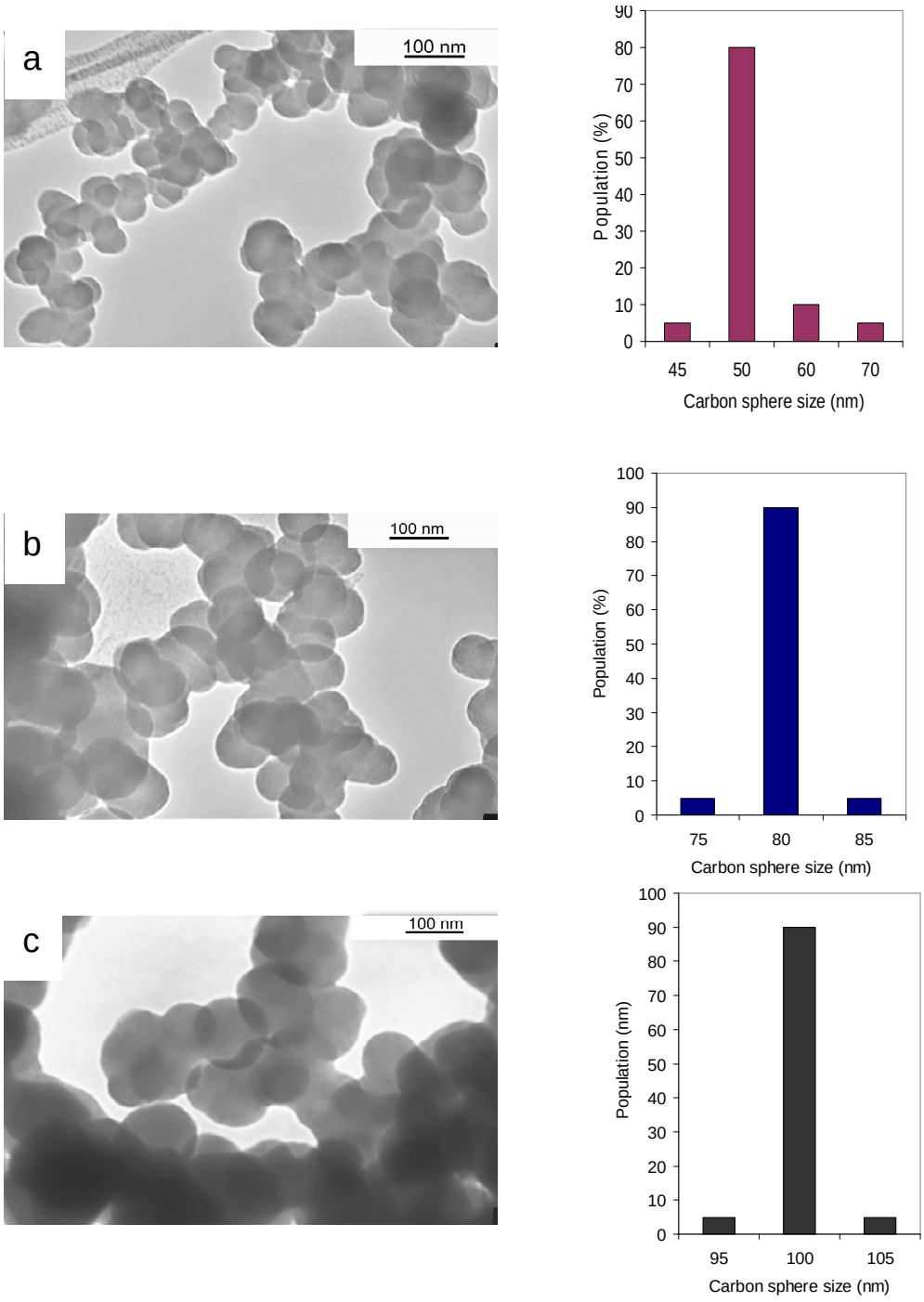

Fig. 11.7: TEM images of CSs synthesized with Ar as carrier gas at (a) 487 ml/min, (b) 248 ml/min, and (c) 70 ml/min. Histograms for the corresponding size distributions of the CSs are shown on the right of the TEM images.

PXRD patterns of CSs synthesized with and without carrier gas are shown in Fig. 11.8. The pattern shows two peak at 26° and 45° corresponding to carbon peaks. The PXRD of both samples show that the peaks are broad; an observation that is attributed to low graphitization of the sample [34]. No differences were noted between the two PXRD patterns indicating that the Ar had no impact on the CS structure.

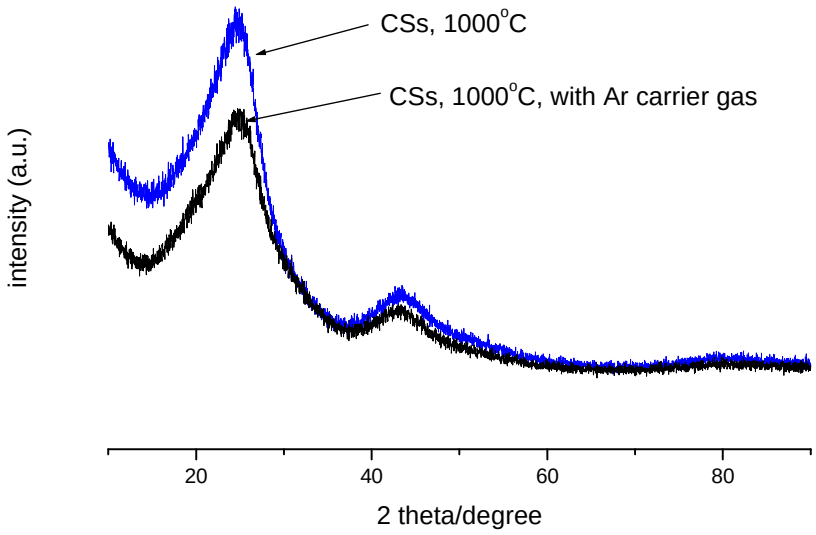

Fig. 11.8: PXRD patterns of CSs synthesized using the SFCCVD technique.

The Raman spectra (Fig. 11.9) of CSs produced at different temperatures (900, 950, 1000°C) and constant C_2H_2 flow rate (118 ml/min) show the presence of two broad peaks at about 1350 cm^{-1} and 1580 cm^{-1} corresponding to the D- and G-bands of graphite respectively. The I_D/I_G ratios (derived from the peak areas) were ~ 4.73, 3.23 and 1.22 at 900, 950 and 1000°C respectively. Appearance of the bands is consistent with the presence of defects and disorder in the samples [34]. Raman spectra also reveal that the intensity ratio of the two bands i.e. I_D/I_G decreases with increase in pyrolysis temperature. The value of I_D/I_G at 1000°C (~ 1.22) indicates that the degree of graphitization of the samples at this temperature has improved suggesting that at higher temperatures the graphitic layers become more ordered.

The defectiveness of the samples produced at 900 and 950°C, associated with the high values of I_D/I_G, suggest that the chemical reactivity of the samples should readily lead to surface modification of the CSs. This in turn could lead to the use of CSs in various applications (e.g. catalysis) as suggested by Jin *et al.* [34] and Xu *et al.* [35].

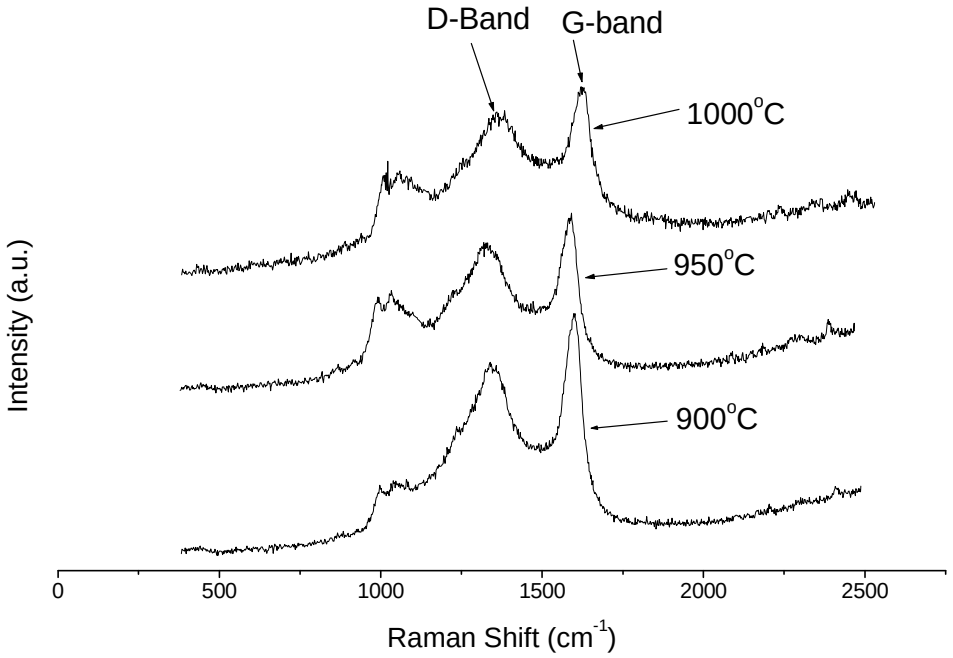

Fig. 11.9: Raman spectra of CSs.

A broad peak at ~ 1000 cm^{-1} was also observed in the Raman spectra of the CSs. This peak was found to be present even after post heating of the CSs. At this stage the origin of this absorption is unknown and instrumental issues are suspected [29].

11.3.3 Effect of hydrocarbon structure on CS morphology

(i) Effect of carbon/hydrogen (C:H) content

This study sought to evaluate the effect of different precursors on sphere morphology. In these experiments we analyzed the effect that the carbon/hydrogen ratio would have on the CS morphology, by considering the carbon deposits formed from pentane, hexane and

heptane as well as in branched molecules (isooctane). To understand the effects that precursors with the same carbon content, but different structures would have on sphere formation, benzene, hexane and cyclohexane where also studied as precursors. These precursors permitted us to verify the effect of C:H dependence on the reactions. To understand the effects that precursors with the same carbon content but different hybridization would have, ethylene and acetylene, with sp^2 and sp hybridization respectively were studied.

Many of the listed carbon precursors have been used by other authors in horizontal reactors. In our study we hoped to evaluate the effect of a vertical CVD setup (described in the experimental section).

TEM characterization (Fig. 11.10) indicates that the carbon deposits contain spheres, with the occurrence of amorphous material around the spheres. TEM also points towards the variation in sphere size and distribution of carbon spheres for each hydrocarbon source. The results indicate that at given experimental conditions, besides the commonly used hydrocarbon source (C_2H_2), CSs can be readily prepared from a variety of hydrocarbon sources, and that while shape appears independent of precursor structure; the size and size distribution do not show such independence (**Table 11.2**).

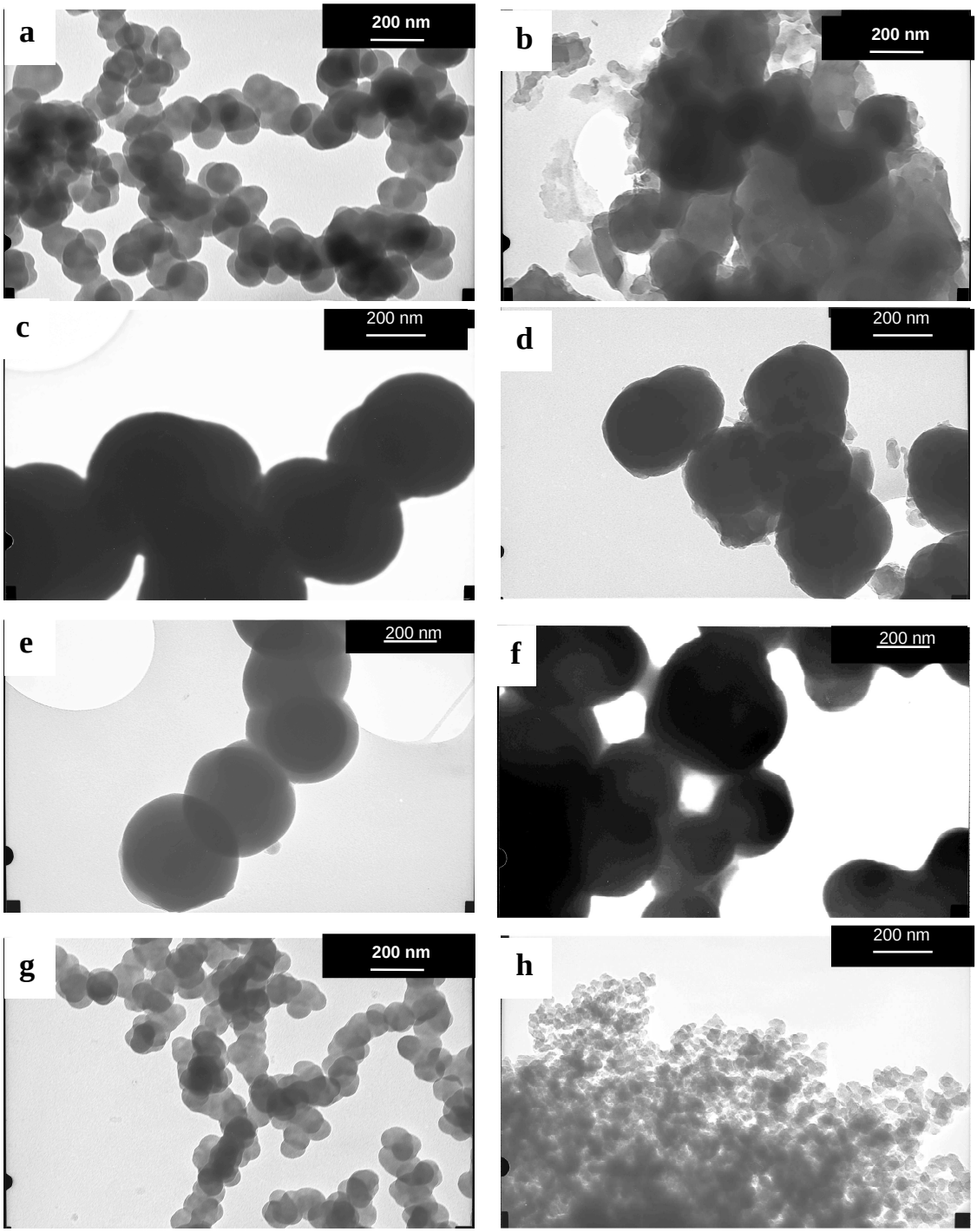

Fig. 11.10: TEM images of CSs synthesized from several hydrocarbons, at 1000°C and flow rate 100 ml/min: (a) acetylene, (b) ethylene, (c) pentane, (d) hexane, (e) toluene (f) isooctane, (g) benzene, and (f) heptane (amorphous material).

Table 11.2: Size and distribution of CSs formed from different hydrocarbon sources at 1000°C.

Carbon source	Liquid Temperature (^{o}C)	Flow Rate (ml/min)	Sphere size Distribution (nm)	CSs size (nm)*
ethylene (horizontal)	-	100	520 - 1200	600
ethylene (vertical)	-	100	150 - 250	200
acetylene (vertical)	-	100	60 - 120	100
pentane	22	100	250 - 625	250
isooctane	50	100	220 - 650	300
hexane	34	100	90 - 360	320
cyclohexane	40	100	240 - 760	260
benzene	40	100	80 - 1000	100
toluene	55	50	150 - 400	300
toluene	55	100	150 - 467	250
toluene	55	200	150 - 480	200
toluene	55	300	160 - 250	180
heptane	49	100	240 - 400	360

* Sphere size that is at least 80% to the total sphere size distribution. Size refers to the diameter of the sphere.

The difference in sphere size and distribution as the hydrocarbon source is varied can clearly be observed (**Table 11.2**). This has led to the understanding that the structural and bonding properties of hydrocarbons play an important role in sphere morphology. In this regard, C:H ratio dependence (**Table 11.3**), hybridization, carbon content and isomerization have been investigated and several trends identified.

Table 11.3: Comparative studies on C:H dependence for various sources under same experimental conditions i.e. T = 1000°C and flow rate = 100 ml/min.

Carbon source	C/H ratio	Sphere size (nm)*	Sphere size Distribution (nm)	Molecular structure
hexane	0.43	320	90 - 360	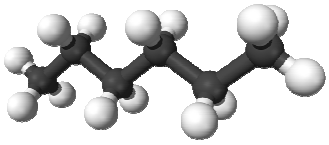
cyclohexane	0.50	260	240 - 760	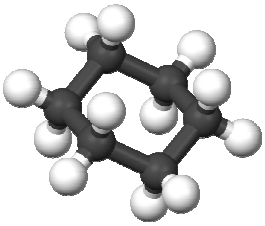
benzene	1.0	100	80 – 1000	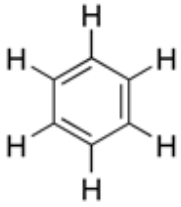

* Sphere size that is at least 80% to the total sphere size distribution. Size refers to the diameter of the sphere.

It can be inferred from **Table 11.3** that as the C:H hydrocarbon ratio increases, there is a decrease in the mean diameter of the spheres. Benzene which has the highest C:H ratio shows spheres with a diameter of 100 nm, whereas hexane with the lowest C:H ratio shows the largest diameter at 320 nm. According to the mechanism of sphere formation, it is understood that spheres grow in size by the addition of graphitic flakes to the growing sphere (nucleation embryo). From observations by Pol *et al*. [29], it can be reasoned that benzene forms a lower number of flakes relative to hexane which allows for the formation of a larger number of flakes. Therefore as C:H ratio decreases the ratio of nucleation embryos to flakes decreases. There are more flakes present for addition to a growing sphere and this causes spheres to become larger. While alternatively as the C:H

ratio increases the ratio of nucleation embryos to flakes increase, causing a decrease in sphere size.

(ii) Effect of hybridization

The effect of hydrocarbon hybridization on sphere morphology was studied by comparing the pyrolysis products from acetylene and ethylene. **Table 11.4** reveals that acetylene shows a narrower size distribution and smaller sphere diameter than ethylene. While the comparison in sphere size is in accordance with C:H ratio dependence as shown earlier, it does not however explain the narrowing of size distribution as shown in **Table 11.3**. A possible explanation is the greater reactivity of acetylene as compared to ethylene caused by the sp and sp^2 hybridization respectively. It can be concluded that as bonding goes from sp to sp^2 to sp^3 we expect a broadening in size distribution. However it must be noted that according to this premise, we would expect benzene to have a narrower distribution as compared to hexane, due to sp^2 hybridization present in benzene. On the contrary this is not the case and may be due to the relative stabilities of the structures as a whole.

Table 11.4: The effect of hybridization on the size of the CSs.

Carbon source	**hybridization**	**Sphere size (nm)**	**Sphere size Distribution (nm)**	**Molecular structure**
acetylene	sp	100	60 - 120	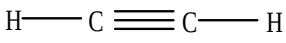
ethylene	sp^2	200	150 - 250	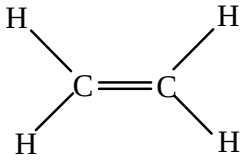

(iii) Carbon content and structural isomers

As mentioned previously it is accepted that hydrocarbons thermally decompose to carbon atoms followed by precipitation of the carbon deposits. This would suggest that any hydrocarbon under standard conditions should result in the formation of similar sized spheres with a similar size distribution. However, this was not observed [29]. Ziegler *et al*. [36] concluded from the experimental pyrolysis of propane that one may obtain not just single carbon atoms in the gas phase, but also large amounts of C2 and C3 species by propagation reactions. They observed that the gas phase species may be anything from methane to cyclopentadiene, benzene as well as various radical species [36].

It can be seen from **Table 11.2** that as the carbon content increases (pentane → heptane), the sphere size increases. It can be stated that as the 'chain' gets longer, the diversity of Cn species (where n = 1, 2, …) gets larger. This increase in Cn species may cause an increase in the number of disordered flakes and reduction of nucleation embryos; thus spheres would get larger as there would be more flakes to accommodate the curvature of the growing sphere. It can be said that as carbon content increases so does the size of the carbon sphere. This argument however, is limited to *straight chain hydrocarbons*, as isooctane (with eight carbon atoms) does not show such an increase in sphere size; a decrease in sphere size is observed for isooctane compared to heptane. If carbon content and C:H dependence were the only factors that determine the sphere size, it would be expected that isooctane should have a larger sphere size. Instead it was observed that structural isomerism is an important factor as well, in limiting sphere size. This observation can be compared to the results obtained with hexane and cyclohexane. It can thus be concluded that straight chain hydrocarbons tend to favour larger spheres as compared to their more branched structural isomers.

(iv) Characterization of the CSs

Characterization of the various hydrocarbon gases and liquids by TGA revealed that when heated in air, an ~ 20% loss of sample can be observed at ~ 200°C for all deposits

and is most likely related to the loss of PAHs and amorphous material (Fig. 11.11). The sample thereafter remains stable below 550°C and is completely oxidised by 650°C. This is in accordance with carbon deposits possessing graphitic nature. The extent of the steepness of the slope is usually indicative of lattice defects which enable oxygen to permeate the carbon structure with greater ease, facilitating rapid oxidation as proposed by Jin *et al.* [34]. Here we see the decomposition of a temperature range indicate the resistance of these materials to decompose.

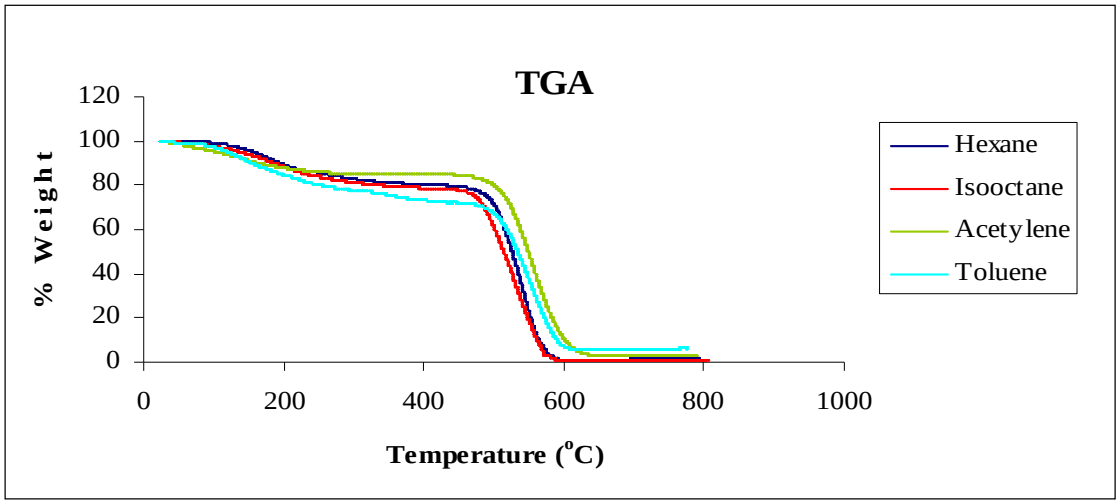

Fig. 11.11: Selected TGA profiles of CSs obtained from the various hydrocarbon precursors used.

Fig. 11.12a shows part of a typical Raman spectrum that was observed for the various hydrocarbons formed by vertical CVD synthesis, in this case toluene. A strong peak at 1591.1 cm^{-1} and a slightly weaker peak at 1356.8 cm^{-1} can be clearly identified. The peak at 1591.1 cm^{-1} (G band) is attributed to the stretching modes of C-C bonds of typical graphite, while the peak at 1356.8 cm^{-1} (D band) is related to the defects and disorders of structure in carbonaceous solids. The value of I_D/I_G is about 0.85, implying that the degree of graphitization of the carbon spheres is not high. The IR spectrum (Fig. 11.12b) shows relatively strong peaks at 1560 cm^{-1} and 1070 cm^{-1} which are indicative of C=C and C-C bond stretching modes, confirming expected bonding which is consistent with graphitic lattices. The strong peak at 3300 cm^{-1} is mostly likely due to moisture.

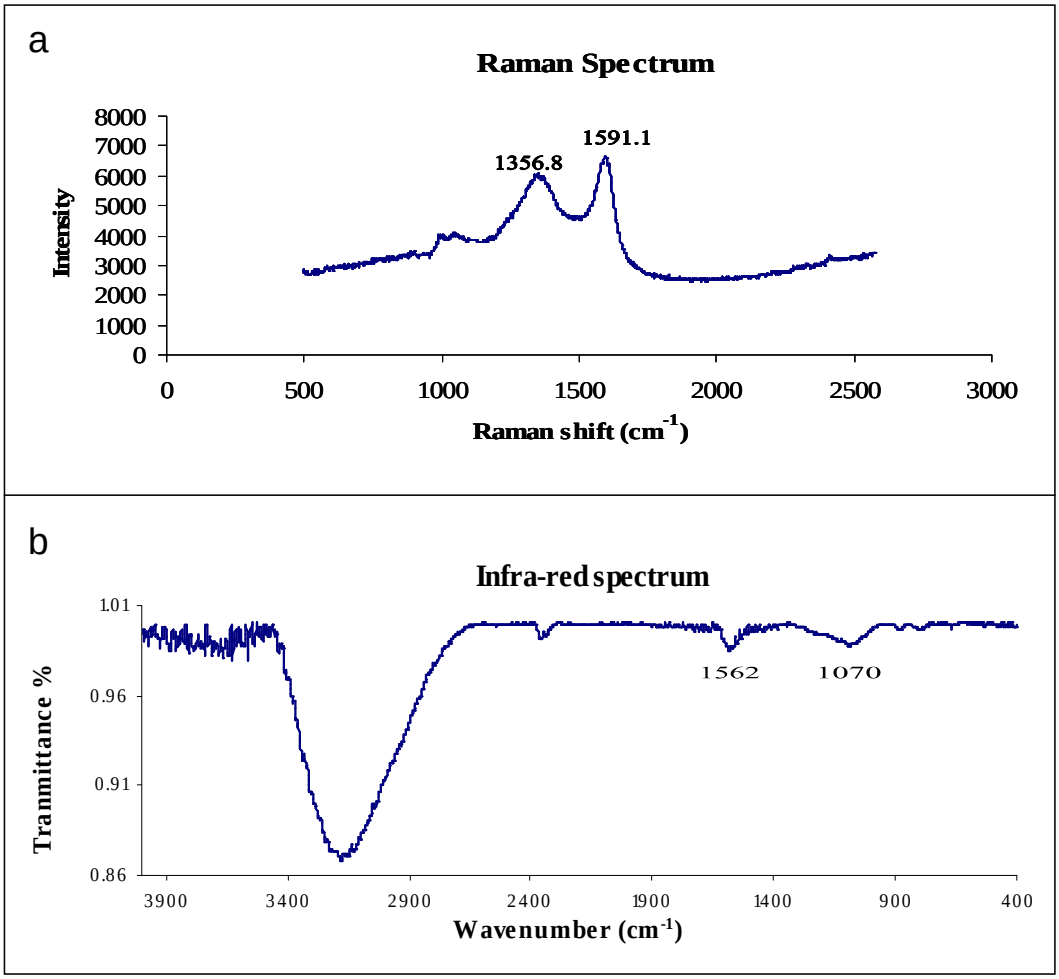

Fig. 11.12: (a) A Raman spectrum of as-synthesized CSs and (b) an infrared spectrum of the carbon soot obtained from toluene as the carbon precursor.

11.4 Conclusions

Carbon spheres of diameters in the range 50 - 250 nm have been synthesized using a vertical swirled floating catalytic chemical vapour deposition reactor. The CSs were produced using direct pyrolysis of acetylene gas without the presence of a catalyst. A maximum production rate of about 0.35 g/min was obtained at an acetylene flow rate of 370 ml/min and a pyrolysis temperature of 1000°C which gives an indication that this process allows for the large scale production of these materials. The produced CSs were

of uniform diameter and the size (nano or micro) could be controlled by changing the pyrolysis temperature as well as gas flow rates of both the acetylene and argon. The effect of gas flow rates displayed a larger impact on the size of the CSs when compared to the temperature effect. As the Ar flow rate increased the amount of material increased and the size of the spheres became smaller.

It was established that under controlled experimental parameters, sphere size is also regulated by the structural and bonding properties of the hydrocarbon source. The results showed that vertical CVD procedures allow for a divergent synthetic route for carbon spheres with different intrinsic properties. This suggests that the potential applications of CSs obtained *via* this process should be unique. Therefore investigations into the reactivity and potential fuctionalization of each are still to be probed.

The study also revealed that the vertical and horizontal CVD (presented in Chapter 10), gives two divergent synthetic routes to CS production. Vertical CVD produces spheres of smaller size, decreased thermal stability and graphitization, as well as increased amorphous material content as compared to spheres prepared by horizontal CVD processes. Vapour flow in vertical CVD tends to be problematic as two distinct peak ranges develop, resulting in broad size distribution range. It could be concluded that the type of precursor and CVD method employed are important factors when considering carbon sphere synthesis.

11.5 References

1. W.R. Smith, *Encyclopaedia of chemical technology,* Interscience: New York, 1949.
2. H.W. Kroto, J.R. Heath, S.C. O'Brien, R.F. Curl, R.E. Smalley, Nature **318** (1985) 162.
3. D. Ugarte, Nature **359** (1992) 707.
4. F. Banhart, M. Ajayan, Adv. Mater. **9** (2004) 261.
5. Z.C. Kang, Z.L. Wang, Philos. Mag. B **73** (1996) 905.
6. Z.L. Wang, Z.C. Kang, J. Phys. Chem. **100** (1996) 17725.

7. Z.C. Kang, Z.L. Wang, J. Phys. Chem. **100** (1996) 5163.
8. Z.L. Wang, Z.C. Kang, Carbon **35** (1997) 419.
9. M. Sharon, K. Mukhopadhyay, K. Yase, S.X. Iijima, Carbon **36** (1998) 507.
10. M. Inagaki, M. Washiyama, M. Sakai, Carbon **26** (1988) 169.
11. K. Kamegawa, H. Yoshida, Carbon **35** (1997) 631.
12. Y.G. Wang, Y.C. Chang, S. Ishida, Y. Korai, I. Mochida, Carbon **37** (1999) 969.
13. L.P. Biró, G.I. Márk, Z.E. Horváth, K. Kertész, J. Gyulai, J.B. Nagy, Ph. Lambin, Carbon **42** (2004) 2561.
14. V. Vignal, A.W. Morawski, H. Konno, M.J. Inagaki, Mater. Res. **14** (1999) 1102.
15. M. Inagaki, V. Vignal, H.J. Konno, Mater. Res. **14** (1999) 3152.
16. E. Auer, A. Freund, J. Pietsch, T. Tacke, Appl. Catal. **173** (1998) 259.
17. S. Flandrois, B. Simon, Carbon **37** (1999) 165.
18. Ph. Serp, R. Feurer, Ph. Kalck, Y. Kihn, J.L. Faria, J.L. Figueiredo, Carbon **39** (2001) 621.
19. X.Y. Liu, B.C. Huang, N.J. Coville, Carbon **40** (2002) 2791.
20. J.S. Qiu, Y.F. Li, Y.P. Wang, C.H. Liang, T.H. Wang, D.B. Wang, Carbon **41** (2003) 767.
21. Z.S. Lou, Q.W. Chen, J. Gao, Y.F. Zhang, Carbon **42** (2004) 229.
22. M.J. Wissler, Power Sources **156** (2006) 142.
23. http://www.carbonblack.jp/en/cb/youto.html#top. (accessed on 1st June 2007).
24. J. Lahaye, Carbon **30** (1992) 309.
25. F. Fallcheri, Y.J. Schwob, Hydrogen Energy **20** (1995) 197.
26. D.B. Scully, R.A. Davies, *Carbon from aromatic hydrocarbons*, Manchester, Vol. 9, pp. 185-189, (1965).
27. S.E. Iyuke, University of the Witwatersrand, Johannesburg. SA Patent Appl. No: 2005/03438, (2005).
28. S.E. Iyuke, A.B.M. Danna, J. Microp. Mesop. Mater. **84** (2005) 338.
29. V.G. Pol, M. Motiei, A. Gedanken, J. Calderon-Moreno, Carbon **42** (2004) 111.
30. S. Mhlanga, K. Mondal, N. Naidoo, N. Kunjuzwa, M. Witcomb, N.J. Coville; S. Afr. J. Scie., accepted for publication.
31. M.L. Lee, R.A. Hites, Anal. Chem. **48** (1976) 1890.

32. L. Wallcave, D.L. Nagel, J.W. Smith, R.D. Waniska, Environ. Sci. Technol. **9** (1975) 143.
33. A. Gold, Anal. Chem. **47** (1975) 1469.
34. X.Z. Jin, C. Gao, W.K. Hsu, A. Huczko, M. Bustrzejewski, M. Rue, C.Y. Lee, S. Acquah, H. Kroto, D.R.M. Walton, Carbon **43** (2005) 1944.
35. L. Xu, W. Zhang, Q. Yang, Y. Ding, W. Yu, Carbon **43** (2005) 1084.
36. I. Ziegler, R. Fournet, P.M. Marquaire, J. Anal. Appl. Pyrolysis **73** (2005) 212.

Chapter 12

General Conclusions

The aim of this thesis was to synthesize and study carbon nanotubes (CNTs) and carbon spheres (CSs) using catalytic and non-catalytic chemical vapour deposition processes respectively. The thesis was successful in achieving its goals in many aspects. A comprehensive literature review of carbon nanotechnology, CNTs synthesized from supported catalysts, the use of organometallic transition metal complexes for CNT synthesis as well as a review of the synthesis and applications of CSs is presented. The importance and relevance of these materials in today's world is clearly outlined with various sources of reference including journal articles, books, as well as internet webpages.

A method for the successful production of high quality CNTs using Fe-Co bimetallic catalysts supported on $CaCO_3$ was investigated and optimum conditions were identified. The results were consistent with other reports in the literature. This method has been used reproducibly to make CNTs for various applications such as catalysts support for Fischer-Tropsch and hydrogenation reactions in our laboratories and as catalysts supports for fuels cells by others. It was shown that the yield, diameter and purity of the CNTs were influenced by C_2H_2/N_2 ratios, time and temperature. Specifically it was observed that the influential parameter in controlling the CNT yield, outer diameter and length was the synthesis time. The CNT purity and selectivity was largely influenced by the synthesis temperature and C_2H_2/N_2 ratios. The use of a bimetallic system was found to produce better yields and quality materials compared to the individual metal particles. A reverse micelle method displayed the ability to prepare nanoparticles of controlled size and consequently the inner diamters of the nanotubes could be tailored. Hence we have presented a comprehensive way of controlling the dimensions of the CNTs. The CNTs could be tailored to suit a specific application.

A novel $Ca_3(PO_4)_2$-$CaCO_3$ support mixture for the CVD synthesis of roughened multiwalled carbon nanotubes was synthesized. This $Ca_3(PO_4)_2$-$CaCO_3$ support gave MWCNTs that possessed very *rough surfaces* that were not seen previously. The nature of these CNTs should provide interesting results especially when the CNTs are used as a catalyst support. Indeed, the idea of CNT surface roughness has been shown to be a new concept in heterogenous catalysis. The rough surfaces (pits) of the CNTs have been shown to serve as *'docking stations'* for metal particles in catalytic reactions such as the Fischer-Tropsch synthesis, thus reducing deactivation of catalyst through sintering of the metal particles. However, while these CNTs possess a rough surface, TEM analysis revealed that the CNT inner walls possess a regular array of crystalline graphite sheets (typically 3 - 5 nm in length). It may be worthwhile to investigate further what could explain the observed dramatic change in CNT structure with incrasing time using a 50wt%$CaCO_3$/50wt%$Ca_3(PO_4)_2$ catalyst support.

The effect of synthesis time on the CNT widths was studied in detail. The study revealed that MWCNTs could be broken into *short fragments* by the deposition of carbon on the tubes. The effect of deposited reactant material on CNT products was examined by performing 'heat treatment experiments' on several carbon materials under the CNT synthesis conditions described (Chapter 8) but over extended reaction times (1 to 12 h). Since Ca, CaO, O_2 and Co-Fe oxides were identified in the final product of the CNTs, by various elemental analysis techniques, their effect on CNT morphology was investigated. It was observed that these reagent residues from the CNT synthesis procedure did not cause the fragmentation of the CNTs. Different CNTs (straight, coiled and randomly oriented) that were synthesized via different methods were all broken by the deposition of excess carbon. A common mechanism for CNT fragmentation was noted. The addition of the carbon causes strain on the underlying tube. If the tube has defects, the defects then provide a point of tube rupture. This rupture then leads to tube fragmentation.

The direct pyrolysis of C_2H_2 in the absence of a catalyst was demonstrated is an efficient method to produce CSs in large quantities. Different pyrolysis conditions were used to study the size and morphology as well as the size variation within each sample batch of

the resulting CSs. The effect of pyrolysis temperature played an important role and influenced both the size and yield of the product. The experiments performed showed that at 900°C, the resulting spheres were prepared in high yield and were of large size (~ 1 µm) and had uniform size. The detailed experiments conducted with C_2H_2 as a carbon precursor indicates that the diameters of the CSs can be controlled by varying the pyrolysis conditions (e.g. temperature and synthesis time) and that the process could readily be scaled up for commercial production. The CSs were used as a support for the hydrogenation of ethylene and they were shown to be a promising support for metal catalysts, in particular for the hydrogenation of ethylene in the presence of Co. The catalyst showed good activity and chemical stability against deactivation in the time-on-stream study.

Another interesting feature that was explored is the use of alcohols (oxygenates) to make CSs. The CSs produced from the alcohols were compared to those produced using alkanes as the carbon source. The yields were generally lower with the alcohols and this was ascribed to the presence of the O atoms in the alcohol. However the advantage of using oxygenates was that they readily removed PAHs and amorphous material from the surface of the CSs resulting in the formation of a smooth clean surface. The results showed the importance of having small amounts of oxygen during the synthesis of CSs. The CSs were shown to be a good support for Co catalysts. The percentage (5, 10 and 20%) of catalyst loading greatly affected the activity of the CS supported catalysts. The CS supported catalysts showed remarkable stable activity for a long period of time on stream.

Finally, CSs of diameters in the range 50 - 250 nm were synthesized using a vertical swirled floating catalytic chemical vapour deposition reactor. The CSs were produced using direct pyrolysis of acetylene gas without the presence of a catalyst. A maximum production rate of about 0.35 g/min was obtained at an acetylene flow rate of 370 ml/min and a pyrolysis temperature of 1000°C which gives an indication that this process allows for the large scale production of these materials. The produced CSs were of uniform diameter and the size (nano or micro) could be controlled by changing the pyrolysis

temperature as well as gas flow rates of both the acetylene and Ar. The effect of gas flow rates displayed a larger impact on the size of the CSs when compared with the temperature effect. As the Ar flow rate increased the amount of material increased and the size of the spheres became smaller.

It was established that under controlled experimental parameters, sphere size is also regulated by the structural and bonding properties of the hydrocarbon source. The results showed that vertical CVD procedures allow for a divergent synthetic route for CSs with different intrinsic properties. This suggests that the potential applications of CSs obtained *via* this process should be unique. The study also revealed that the vertical and horizontal CVD processes result in two different synthetic routes. Vertical CVD produces spheres of smaller size, decreased thermal stability and graphitization, as well as increased amorphous material content when compared with spheres prepared by horizontal CVD processes. It could be concluded that the type of precursor and CVD method employed are important factors when considering carbon sphere synthesis.

The CNTs and CSs were fully characterized to establish their physico-chemical properties using a range of techniques such as transmission electron microscopy (TEM), scanning electron microscopy (SEM), energy dispersive X-ray (EDX) spectroscopy, thermogravimetric analysis (TGA), Raman spectroscopy, powder X-ray diffraction (PXRD), BET surface area and porosity analysis, X-ray photoelectron spectroscopy (XPS) and high resolution scanning tunnelling electron microscopy (HRSTEM).

The range of materials produced in this study should provide a variety of materials to choose from, for application in the area of catalysis. The thesis itself should provide recipes for the controlled synthesis of these materials accompanied by a description of their physico-chemical properties. This has an important bearing for the future of these materials. The various publications stemming from this thesis will ensure a worldwide dissemination of the information to various researchers and scientists.

Future studies in this area may entail the use of various types of CNTs and CSs as discussed in this thesis as supports for various catalytic reactions. This should enable the determination of the most suitable materials in relation to their microstructure and surface areas. In particular the effect of properties such as diameters, lengths, and surface morphology would be necessary for future investigations. These materials can be studied in other applications such as drug delivery, nanotube reinforced composites, as tansport for bisphosphonates, in fuel cell applications etc. where size is an important issue.

Note

It should be noted that the selectivity defined on page 123 is not customary, based on qualitative analysis of TEM images and differs significantly from definition used in conventional catalysis.